# Electronic energy transfer processes in π-conjugated polymers

Dissertation

Zur Erlangerung des Grades

"Doktor der Naturwissenschaften"

am Fachbereich Chemie und Pharmazie

der Johannes-Gutenberg-Universität Mainz

Vor- und Zunahme des Doktoranden

**Panagiotis E. Keivanidis**

geboren in Pireas, Attika

Mainz, 2004

To Venetia and Stathis

¨ Άν είσαι σοφός, πολέμα στο κρανίο, σκότωνε τις ιδέες , δημιούργα καινούριες. Ο Θεός κρύβεται μέσα σε κάθε ιδέα, όπως μέσα σε σάρκα. Σύντριψε την ιδέα, λευτέρωσέ τον! Δώσε του μιαν άλλη ιδέα, πιό απλόχωρη, να κατοικήσει.¨

Nikos Kazantzakis

Currently π-conjugated polymers are considered as technologically interesting materials to be used as functional building elements for the development of the new generation of optoelectronic devices. More specifically during the last few years, poly-*p*-phenylene materials have attracted considerable attention for their blue photoluminescence properties. This Thesis deals with the optical properties of the most representative blue light poly-*p*-phenylene emitters such as poly(fluorene), oligo(fluorene), poly(indenofluorene) and ladder-type penta(phenylene) derivatives. In the present work, laser induced photoluminescence spectroscopy is used as a major tool for the study of the interdependence between the dynamics of the probed photoluminescence, the molecular structures of the prepared polymeric films and the presence of chemical defects. Complementary results obtained by two-dimensional wide-angle X-ray diffraction are reported. These findings show that the different optical properties observed are influenced by the intermolecular solid-state interactions that in turn are controlled by the pendant groups of the polymer backbone. A significant feedback is delivered regarding the positive impact of a new synthetic route for the preparation of a poly(indenofluorene) derivative on the spectral purity of the compound. The energy transfer mechanisms that operate in the studied systems are addressed by doping experiments. After the evaluation of the structure/property interdependence, a new optical excitation pathway is presented. An efficient photon low-energy up-conversion that sensitises the blue emission of poly(fluorene) is demonstrated. The observed phenomenon takes place in poly(fluorene) derivatives hosts doped with metallated octaethyl porphyrins, after quasi-CW photoexcitation of intensities in the order of kW/cm$^2$. The up-conversion process is parameterised in terms of temperature, wavelength excitation and central metal cation in the porphyrin ring. Additionally the observation of the up-conversion is extended in a broad range of poly-*p*-phenylene blue light-emitting hosts. The dependence of the detected up-conversion intensity on the excitation intensity and doping concentration is reported. Furthermore the dynamics of the up-conversion intensity are monitored as a function of the doping concentration. These experimental results strongly suggest the existence of triplet-triplet annihilation events into the porphyrin molecules that are subsequently followed by energy transfer to the host. After confirming the occurrence of the up-conversion in solutions, cyclic voltammetry is used in order to show that the up-conversion efficiency is partially determined from the energetic alignment between the HOMO levels of the host and the dopant.

# Outline of this Thesis

This Thesis deals with the optical properties of phenylene-based π-conjugated polymers. Currently these organic materials constitute an active field of research due to their optoelectronic characteristics. The major experimental tool that was used for this Thesis was the laser induced fluorescence spectroscopy. Both steady-state and time-resolved photoluminescence techniques have been exploited.

The general principles of molecular spectroscopy and their applications in the field of π-conjugated polymers are presented in Chapter 1. Particularly for this section of the Thesis, a specialized bibliography has been used as a pool of figures and as a guideline of the presented concepts. The reader may like to gain further details from the recommended literature that is given at the end of this section.

Chapter 2 deals with the photophysical properties of poly- and oligo(fluorene) derivatives. The importance of these compounds for their exploitation as potential blue light-emitting materials is emphasized. Our results demonstrate the significant influence of the solid-state properties on the optical properties of the studied compounds. We present two alternative approaches that aim in the achievement of stable blue emission of fluorene derivatives; in the polymer regime we explore the effect of dendron substitution onto the polymer backbone. By complementing our results with previously measured X-ray data, we conclude that dendron substitution does not hinder effectively the intermolecular interactions, as it was initially expected. Additionally we show the positive impact of the thermal annealing on the spectral properties of an alkyl derivatized poly(fluorene). The particular result becomes a representative example of how positional disorder in a film influences the photophysical performance of a light-emitting material. In the oligomer regime, the effect of pendant group that is attached onto the oligomer backbone is addressed. More specifically, the photophysical performance of pentafluorenes as films and as dilute solutions is evaluated as a function of the length of the side chain. After concluding on the unique chemical purity of the studied oligo(fluorene)s, we discriminate two different species to be responsible for the reduction of the blue light emissive performance: an inherently driven excimer formation and an extrinsically driven fluorenone creation. The short linear butyl side chain favors the former while the latter is found in all oligomers films after thermal oxidation in air.

Chapter 3 introduces poly(indenofluorene)s, the successor molecules of poly(fluorene)s, in terms of molecular architecture. Our interest in these materials arose due to technologically attractive emission wavelength that is positioned in the blue spectral region where the human eye has higher sensitivity. Four different poly(indenofluorene)s derivatives are studied. The structure-

property relationship is evaluated by complementing our experimental results that were obtained by means of 2-dimensional wide-angle X-ray scattering of powder and oriented filaments and optical spectroscopy. Through this work the positive impact of a new synthetic route on the spectral stability of these materials is identified. Moreover, we exploit two different methods of polymer doping: an extrinsic one and an intrinsic one. The former is based on mixing our host polymer with a model monoindenofluorene-ketone that acts as photoluminescence quencher whereas the latter one is achieved by endcapping the host polymer with a thiophene moiety. Based on these results conclusions are drawn regarding the nature of photoluminescence quenching of the host polymers and the mechanisms that are involved in this process. Finally delayed fluorescence and phosphorescence are reported for the one of the four poly(indenofluorene)s derivatives studied.

In Chapter 4 we present results of energy transfer in blends of poly(fluorene) and metal(II)-octaethyl porphyrin (MeOEP). In the studied systems two alternative pathways of energy transfer processes are investigated. Firstly an ordinary energy transfer that takes place upon direct excitation of the polymer at 405 nm and leads to excitation energy transfer to MeOEP. Secondly, for the first time an extraordinary energy transfer channel is identified. Upon quasi-cw laser excitation of MeOEP at 532 nm the up-converted characteristic blue emission of PF2/6 is detected, for excitation intensities in the order of kW/cm$^2$. We further demonstrate that this phenomenon occurs in a broad range of blue light-emitting polymers that are doped with PtOEP. The photoluminescence dynamics of the up-converted host emission and PtOEP emission are studied. We show that up-conversion takes place also in dilute solutions. By exploiting cyclic voltammetry we deduce the HOMO and LUMO energy levels of polymer and MeOEP components. This information in combination with our spectroscopic results enables a discussion on the alternative mechanisms that may lead to the observed up-conversion process.

# Table of contents

# 1 THEORETICAL BACKGROUND

## 1.1  LIGHT ABSORPTION

Light is an electromagnetic wave that can be described as the combination of two oscillating fields, an electric and a magnetic field, that are perpendicular to each other and to the direction of propagation. In the special case of linearly polarised light, according to the classical description of the electromagnetic radiation, the spatial position of the electromagnetic wave along the propagation axis is mathematically expressed from the wave equation:

$$\vec{E}(x,t) = E_0 * \sin\left[2*\pi\left(v*t - \frac{x}{\lambda}\right) + \theta\right] \qquad \text{(eq. 1.1)}$$

where $E_0$ is the magnitude of the vector in a plane perpendicular to the direction of propagation, $2*\pi*\left(v*t - \frac{x}{\lambda}\right)$ is the phase at time t in position x, $\theta$ is the phase at time t=0, x=0 and $v$ is the frequency in Hz. The direction of E is referred to as the polarisation direction of the light. In eq. 1.1 $\lambda = \frac{c}{v}$ denotes the wavelength that corresponds to the light wave while c is the speed of light in vacuum.

The quantum mechanical description of light exhibits the quantised nature of light. Hence a medium can absorb or emit electromagnetic radiation in quasi particles known as photons, with energy of

$$E = h*v = h*\left(\frac{c}{\lambda}\right) \qquad \text{(eq. 1.2)}$$

Absorption and emission of electromagnetic radiation from molecules are processes that correspond to electronic transitions occurring within the energy levels of the molecules. Especially in the case of UV-Vis regime of the electromagnetic spectrum, these transitions correspond to promotion of electrons at different electronic states. That is the electronic transitions occur within different molecular orbitals of inequivalent energies.

Macroscopically, the absorption of an incident light beam from a medium is observed as attenuation of the beam. Lambert-Beer law correlates the extent of this attenuation to the concentration *C* of the absorbing species in the light-absorbing medium:

$$I(v) = I_0(v) * \exp[-a(v)*d] \Leftrightarrow \log\left(\frac{I_0}{I}\right) = \varepsilon(v)*C*d \qquad \text{(eq. 1.3)}$$

where $a(v) = 2.303 * \varepsilon(v) * C$ is the absorption coefficient of the medium for light of frequency v and d is the path length that light travels in the medium. When the concentration of the absorbing

species in the medium is expressed in molarity units the molar extinction coefficient $\varepsilon(v)$ is in use and absorptivity is measured as absorbance A, or optical density:

$$A = \varepsilon(v) * C * d \qquad \text{(eq. 1.4)}$$

The overall absorbing ability of a medium in the range of a given frequencies of electromagnetic radiation is represented from the integrated absorption coefficient or alternatively oscillator strength $f$:

$$f \propto \int \varepsilon(v) * dv = N * \sigma(v) \qquad \text{(eq. 1.5)}$$

Here N denotes the number of absorbing species and $\sigma(v)$ is the absorption cross-section of the transitions in question. In the thermodynamic description of Einstein for excitation of atomic systems, the absorption cross-section is related to the Einstein coefficient for spontaneous emission. Further theoretical treatment of this model from Strickler and Berg exhibited the modified relationship for strongly allowed transitions in organic molecules, where the absorption cross-section and the time $\tau_0$ that the excited level remains activated are related as:

$$\frac{1}{\tau_0} \propto \int \varepsilon(v) * dv \qquad \text{(eq. 1.6)}$$

## 1.2   ELECTRONIC TRANSITIONS OF ISOLATED ORGANIC MOLECULES

### 1.2.1 The transient dipole moment

For an organic molecule the interaction with UV-Vis light results in electronic transitions that occur in a relatively broad range of energies. In the particular case of light absorption, the spectral intensity distribution is the pictorial representation for the absorbed intensity of incident radiation as a function of radiation's wavelength. The observed bands that differ in intensity are interpreted as results of different strength of coupling between the electronic states that participate in the electronic transitions. This strength of coupling is inherently determined from the quantum mechanical nature of the electronic transitions and the corresponding electronic wavefunctions. In principle, electronic transitions are governed by rigorous selection rules that arise from the fundamental laws of energy and momentum conservation. Electric dipole electronic transitions are considered as interaction of the electromagnetic field with an inherent

molecular transient dipole. Quantum mechanically this is expressed as the transient dipole moment

$$\vec{M}_{f \leftarrow i} = \left\langle \Psi_f^T \left| \hat{M} \right| \Psi_i^T \right\rangle \qquad \text{(eq. 1.7)}$$

which is related to the transition of the electron from the initial molecular eigenstate $\Psi_i^T$ to the final molecular eigenstate $\Psi_f^T$.

The term T in $\Psi^T$ in eq. 1.7 declares that these eigen states represent the total wavefunction of a molecular electronic state. The latter is defined as a vibronic state and it reflects the sum of the vibrational and electronic energy in the system. The contribution of motion to the overall energy due rotations is considered to be relatively small and it becomes important only in the case that the fine structure of a vibrational line is monitored. Therefore, the vibronic state $\Psi^T$ reflects the parameterisation of the electronic energy on the corresponding spatial nuclear coordinates of the system. According to the approximation of Born and Oppenheimer a vibronic wavefunction $\Psi^T$ can be expresses as the product of its corresponding spatial electronic $\Psi_f$ and vibrational $X_f$ wavefunctions. Moreover, the spatial electronic wavefunction corresponds to two different spin-state electronic wavefunctions known as spin-orbital functions. Taken all these into account, the expression for the transition dipole moment becomes:

$$\vec{M}_{(f \leftarrow i)} = \left\langle \Psi_f \left| \hat{M} \right| \Psi_i \right\rangle * \left\langle X_f \left| X_i \right\rangle * \left\langle S_f \left| S_i \right\rangle \qquad \text{(eq. 1.9)}$$

which consists of the product of the respective electronic $\Psi_f$, vibrational $X_f$ and electron spin wavefunctions $S_f$ that correspond to the given molecular configuration that participate in the transition. The dipole moment operator $\hat{M}$ operates on those wavefunctions that contain variables, which correspond to electron coordinates. It remains inert for the wavefunctions that correspond to vibrational or electron-spin coordinates.

Here $\hat{M}$ refers to the electric dipole moment operator, which in the case of allowed transition in the UV regime is the most important operator in comparison with the magnetic dipole or electric quadrupole operators.

The probability for occurrence of an electric dipole transition is proportional to the square of the scalar product between the inherent molecular transition moment vector and the electric field vector of linearly polarised light:

$$P = \left( \vec{M}_{(f \leftarrow i)} * \vec{E}(x,t) \right)^2 = \left| \vec{M}_{(f \leftarrow i)} \right|^2 * \left| \vec{E}(x,t) \right|^2 * \cos^2 \varphi \qquad \text{(eq. 1.8)}$$

Therefore an orientational dependence results for the absorption of linearly polarised light.

The probability of a transition between two electronic states theoretically stems from the squared magnitude of the transition dipole moment $\left|\vec{M}_{(f \leftarrow i)}\right|^2$. Alternatively, the strength of an electronic transition is expressed as the observed absorption intensity of the transition. The magnitude of this strength is enclosed physically in the oscillator strength $f$, that eq. 1.6 describes. The latter is a ratio of the observed integrated absorption coefficient to that calculated classically for a single electron in a three dimensional harmonic potential well. As a ratio, the maximum value of $f$ of a fully allowed transition is of the order of unity. For a transition that corresponds to energy $E(\tilde{\nu})$:

$$f \propto E(\tilde{\nu}) * \left|\vec{M}_{(f \leftarrow i)}\right|^2 \quad \text{(eq. 1.10)}$$

After implementing the Born-Oppenheimer approximation the oscillator strength of a transition is directly proportional to:

$$\left|\vec{M}_{(f \leftarrow i)}\right|^2 = \left|\left\langle \Psi_f \left| \hat{M} \right| \Psi_i \right\rangle\right|^2 * \left|\left\langle X_f \middle| X_i \right\rangle\right|^2 * \left|\left\langle S_f \middle| S_i \right\rangle\right|^2 \qquad \text{(eq. 1.11)}$$

The intensity of an electronic transition is determined from the $\left|\left\langle \Psi_f \left| \hat{M} \right| \Psi_i \right\rangle\right|^2$ term whereas the spectral shape of the transition band is determined from the term $\left|\left\langle X_f \middle| X_i \right\rangle\right|^2$ in eq. 1.11.

## 1.2.2 Electronic transitions

Based on the model of the harmonic oscillator, the vibrational energy levels of a certain electronic state correspond to distinct harmonic oscillations of the nuclei around an equilibrium point that reflects the bond length. In polyatomic molecules the nuclear cordinates correspond to more than two atomic centres and a variety of vibrational modes exists. Hence, the visualisation of this oscilating process is achieved by the use of the potential energy hypersurfaces. However it has been shown that even in a a large molecule like MEH-PPV the consideration for electronic coupling to a single vibrational mode is possible. Even more simple, the description of different electronic states $\Psi$ can be visualised by using parabolas that depict the vibrational energy of a given electronic state, as a function of the configurational coordinates in the given electronic state.
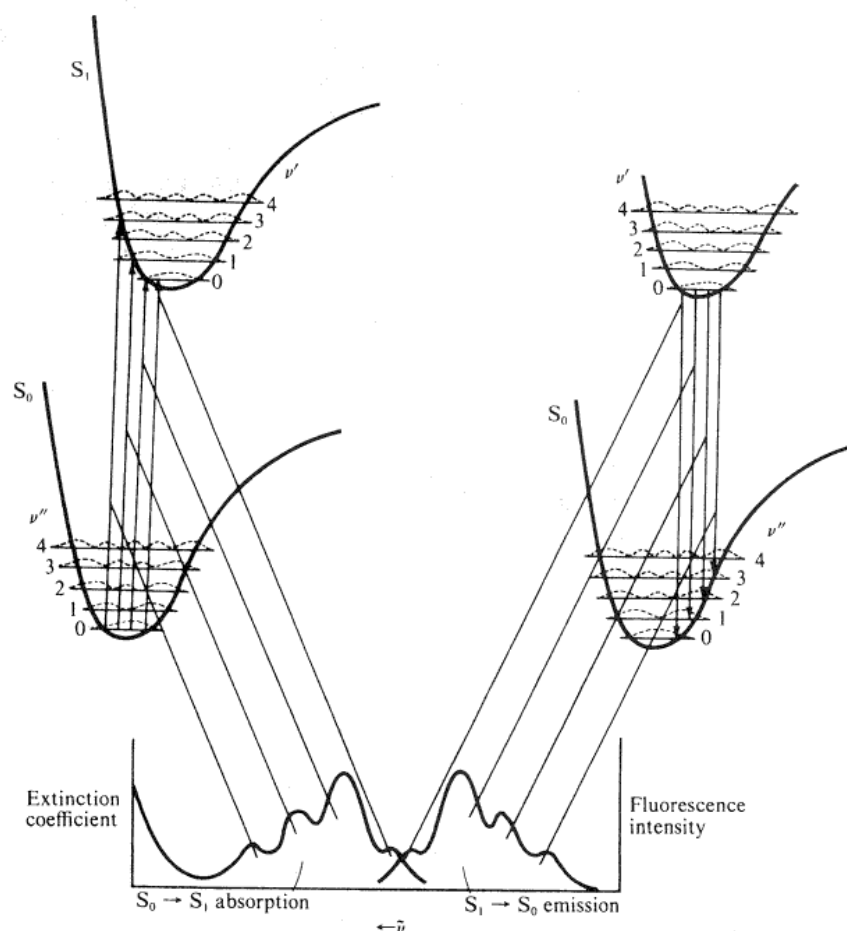
Figure 1.1: Absorption of a photon results in an electronic transition from the ground state to a vibrational level of the excited state (left-side potential energy curves). After relaxation of the excited state to the lowest vibrational level, emission of a photon occurs upon the transition to the vibrational levels of the ground electronic state (right-side potential energy curves). Note the mirror-image relationship of the corresponding absorption and emission spectra. From Pope & Swenberg.

The overlap integral of the vibrational wave functions $\langle X_f | X_i \rangle$ is termed Franck-Condon factor and determine the intensity of vibrational components in the absorption or the emission band. In principle the observation of of vibronic structure in the spectra is an indication for the existence of electron-phonon coupling. The latter reflects the displacement of the bond equilibrium minima in the configurational nuclear coordinates upon the transition from an initial to a final vibronic state. Qualitatevely the magnitude of this displacement is expressed from the dimensionless Huang-Rhys parameters. In principle the lager is the displacement the broader is the spectrum of the transition.

## 1.2.3 Visualising the photophysical processes: The Jablonski Diagram

The emission intensity of light that is emitted from an optical centre after the interaction with an electromagnetic radiation field can be correlated with the emitting wavelengths. The resultant spectrum is a photoluminescence spectrum that like in the case of absorption, is characteristic of the emissive molecule. The efficiency of the photoluminescence process is measured from the quantum efficiency $\Phi$ of this luminescence, that is the ratio of the emitted photons over the total amount of the absorbed photons:

The intensity of the emission is then expressed as:

$$I_{em}(v) = k * I_0(v) * \Phi * \left(1 - 10^{-\varepsilon(v)*C*d}\right) \qquad \text{(eq. 1.12)}$$

According to this expression, the intensity of the emitted light is proportional to to the quantum efficiency $\Phi$ of the compound and to the magnitude of the absorption of the excitation radiant power $I_0(v) * \left(1 - 10^{-\varepsilon(v)*C*d}\right)$. The proportionality constant $k$ refers to the experimental conditions of the measurement.

The visualisation of the electronic transitions and of their relative magnitude can be achieved by use of a Jablonski diagram. In such a diagram the energy levels are hierarchically positioned according to their energy values. It is important to clarify that a Jablosnski diagram represents a different configuration of the electrons in a given set of molecular orbitals and not molecular orbitals. Therefore different orientations of the angular momentum of electronic spin result in different Jablonski states. Hence a Jablonski diagram is appropriate for the visualisation electronic processes that take place between states of different spin multiplicity.

Electronic configurations in a given set of molecular orbitals where the electrons have their spin vectors parallel are represented by singlet states, while triplet states reflect electronic configurations in a given set of molecular orbitals where the electrons have their spin vectors anti-parallel. In that way, the main processes that may take place when an organic molecule absorbs a photon are depicted in Figure 1.2.
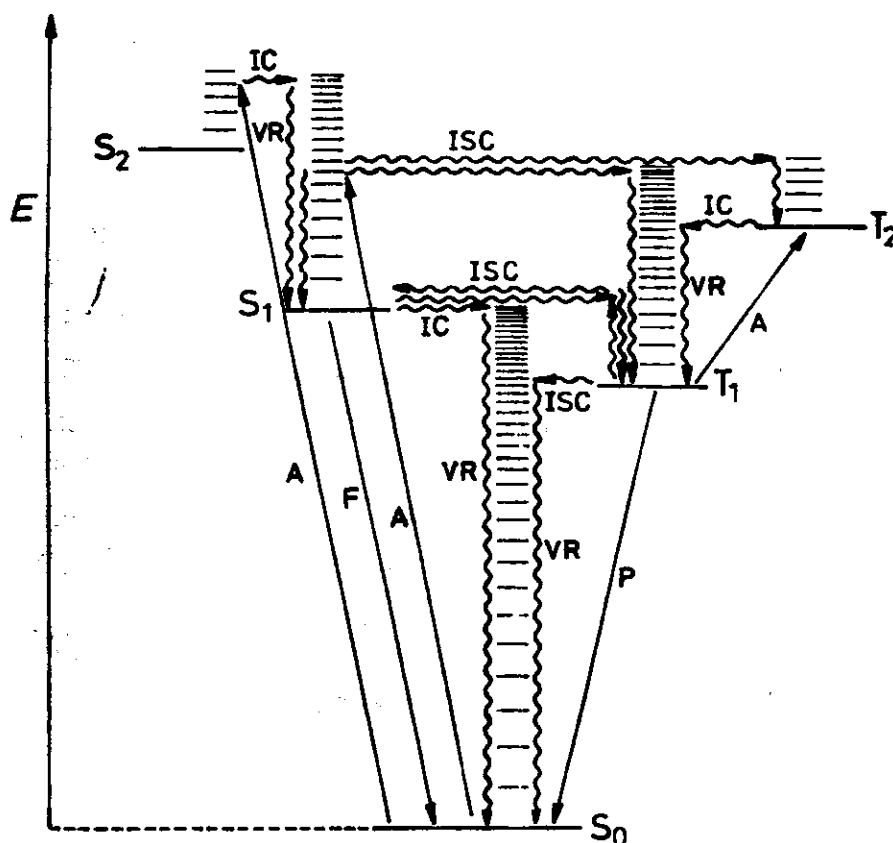
Figure 1.2: A Jablonski diagram visualising the photophysical processes that may take place after the absorption (A) of a photon from a molecule. Straight arrows indicate radiative processes (F=fluorescence, P=phosphorescence) wheras wavy arrows indicate non-radoative processes (IC=internal conversion, ISC=intersustem crossing, VR=vibrational relaxation). From McGlynn, Azumi & Kinoshita.

Given that the ground state $S_0$ of the organic molecule is of single spin-multiplicity, absorption of a photon results in the promotion of an electron to a vibrational level of an upper single excited state via an allowed electronic transition. Subsequently, in the presence of an isoenergetic high vibrational level of a lower singlet excited state, excitation is transferred to the vibrational manifold of this state. This process is termed as internal conversion (IC) and it reflects a radiationless passage between two different electronic states of the same multiplicity. It is assisted by the effective overlap of the vibrational wavefunctions that participate in the process. Finally, according to the rule of Vavilov and Kasha, the system rapidly relaxes to the lowest vibrational level of the first excited singlet state $S_1$ state via fast vibronic relaxation (VR). This step takes place with the parallel emission of heat to the sourroundings via the activation of molecular vibrations known as phonons until a thermally equilibrated ensemble of molecules in $S_1$ nuclear configuration is produced. Alternatively, the system can relax to a manifold of triplet states. This transition is termed as intersystem crossing (ISC) and it reflects a radiationless passage from an electronic state in the singlet manifold to an electronic state in the triplet

manifold or vice versa. Thus ISC may take place either from the lowest singlet excited to vibrational levels of the lowest triplet excited state or it may occur between the vibrational levels of higher excited states of singlet and triplet multiplicities. The major difference between in IC and ISC processes is related to the demand for spin-axis reorientation for the latter.

Once the zero vibrational level of the first excited singlet state $S_1$ or triplet $T_1$ has been reached, the system can relax to the ground state radiatively via the emission of a photon or non-radiatively. Emission originating from a singlet state is termed as fluorescence (F) and from a triplet state as phosphorescence (P). The difference of these types of transitions lie in their coupling strength to the ground state. As transitions between different spin-state multiplicities are forbidden, a triplet state is longer lived than a singlet state and hence P is a slower radiative process than F. Excited states can return to the ground state via non-radiative transitions and under this circumstances the quantum efficiency of photoluminescence is found decreased.

It should be mentioned that as a triplet is longer lived than a singlet state, it is plausible that during the triplet excited state lifetime several processes may take place.

Upon the absorption of a second photon the population of a higher triplet excited state can be achieved. This effect is termed as photo-induced absorption.

Alternatively, thermalisation of an excited triplet can result in a backtransfer process from a vibrational level of the lower triplet state to an equienergetic vibrational level of a singlet electronic state, via a ISC step. This process results in emission from a singlet state that exhibits kinetic characteristics of a triplet state. Since it was first observed in the molecules of Eosin, this fluorescence is alternatively termed E-type fluorescence.

Finally, a bimolecular event may occur if collision events take place between two excited molecules that are in the triplet state. This is a fusion process, which is termed as triplet triplet annihilation and its kinetics exhibit those of a triplet state. As Figure 1.3 shows, triplet-triplet annihilation results in the simultaneous population of the vibrational level in the ground state configuration of the one molecule and a vibrational level of a singlet excited state of the second molecule.
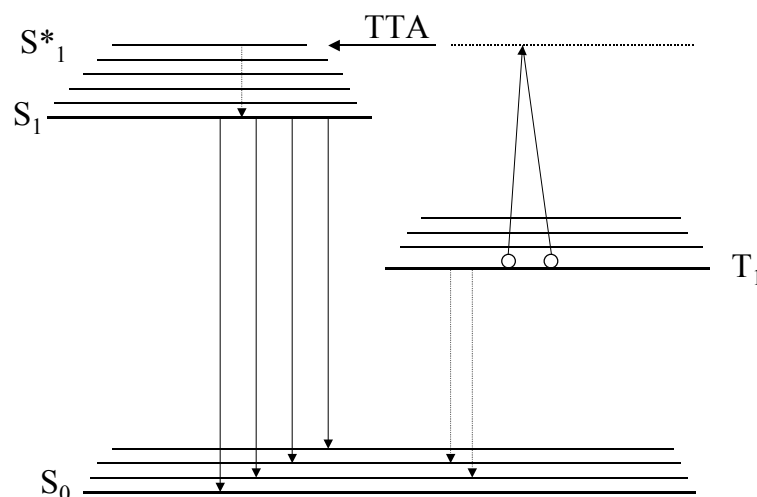
Figure 1.3: A schematic represenation for the generation of delayed fluorescence via triplet-triplet annihilation. From Ern.

This process requires that the energy of the singlet state that is reached is equal to the double of the energy of the triplet state that participates in this photophysical process. Subsequently after relaxation of the reached singlet excited state to its zero vibronic level a radiative transition occurs back to the ground state and thus delayed fluorescence can be observed. The first observation of this delayed fluorescence was for the Pyrene molecules thus the term P-type fluorescence is used.

The importance of the triplet state and the alternative channels of triplet level deactivation are discussed again in Chapters 3 and 4.

## 1.3 INTERMOLECULAR COUPLING

### 1.3.1 Aggregation

In many cases the absorption spectra of dye aggregates such as dimers or polymers show distinct differences from the spectra of their monomeric analogues. According to Kasha et al., aggregation effects impose alterations of the emission properties as well. Aggregation implies the interaction of two monomers either via a physical dimerisation process or via a chemical dimerisation process. Nonetheless, the term aggregation refers to a ground state interaction of the monomers that comprise the aggregate.
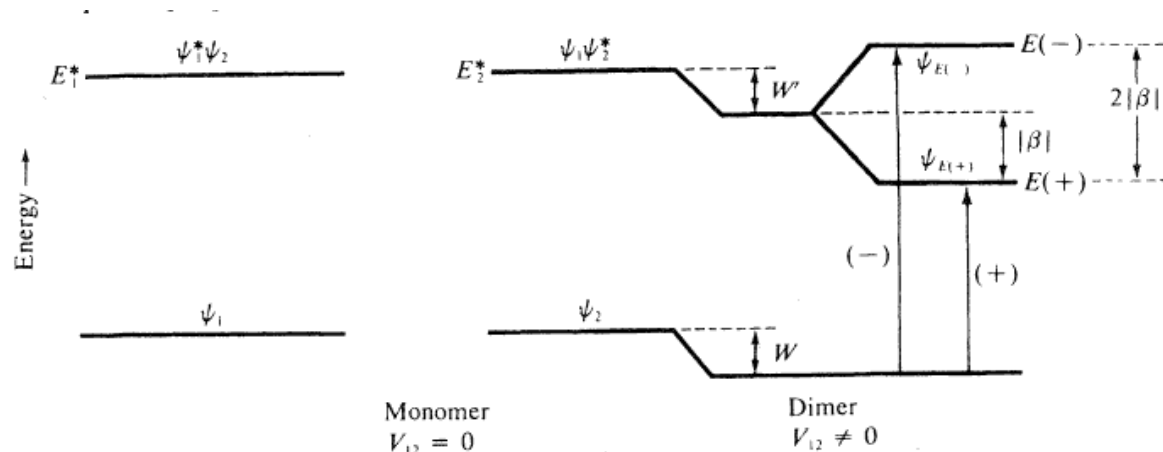
Figure 1.4: The splitting of the excited stae of a monomer into two levels upon the presence of the interaction potential $V_{12}$ caused by the presence of an adjacent monomer. Dimerisation induces a stabilisation of the ground and the excited state by W and W', respectively, due to the coulombic energy interaction of the two units. The splitting of the excited state into two levels of E(+) and E(-) energy depends on the magnitude of the resonance interaction energy β of the excited states. The latter is influenced by the relative orientation of the monomers. From Pope & Swenberg.

As Figure 1.4 shows, ground state aggregation creates an interaction potential that induces a splitting of the initial excited state of the monomers to two distinct excited levels of different symmetry. The extent at which the new emerged levels are radiatively coupled to the ground state is determined from the relative orientation of the transition dipole moment of each monomer. In the special case where the transition dipoles of the monomers are not parallel or antiparallel, both of the levels are radiatively coupled to ground state. Alternatively when the transition dipole moments are parallel or antiparallel, only one of the new levels is radiatively coupled to the ground state.

## 1.3.2 Excited state interaction

In the case where one of the monomers is in a higher excited state the intermolecular interaction gives rise to an entity described as an excimer. Excimers are well known species in the field of conjugated polymers and their influence on the optical properties has been widely investigated both from an experimental and theoretical point of view. In the case where intermolecular interactions take place between two different molecules the term exciplex is in use. Both excimers and exciplexes are transient moieties that exhibit appreciable stability in their excited state, that is they live only during the time interval in which one of the participating components exists in an excited state configuration. Hence these transient species can not be detected by absorptpion spectroscopy due to the fact that they do not exist in the ground state. In contrast they

are characterised by a broad red shifted emission peak that the individual components do not have.
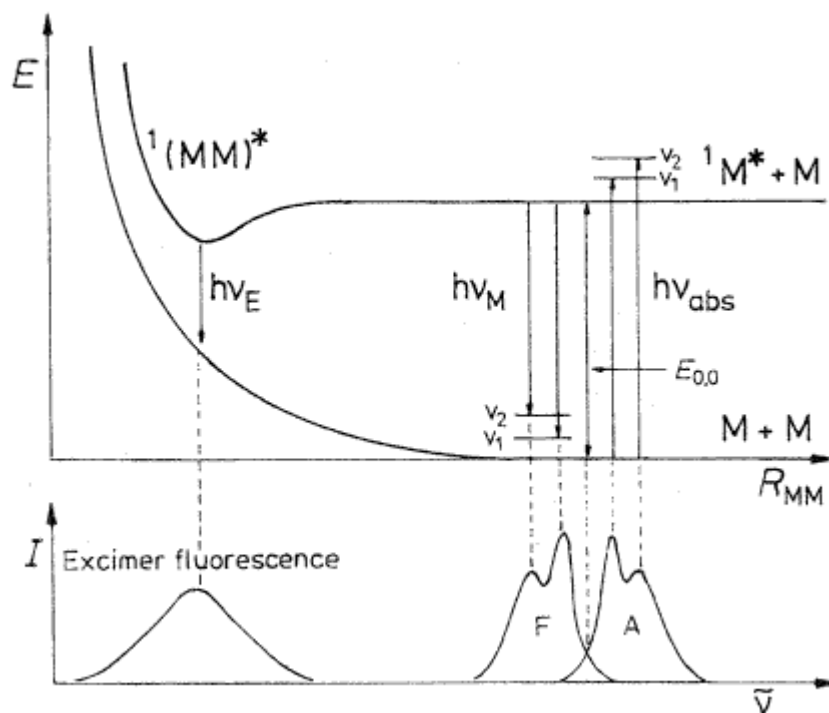


Figure 1.5: Schematic representation of the potential energy curves for excimer formation. Note the difference between monomer fluorescence and excimer fluorescence. From Klessinger & Michl.

As Figure 1.5 shows, after the absorption of light and in a given intermolecular distance between an excited and a grounde state molecule, excimer formation occurs due to the energy stabilisation that accounts for the delocalisation of the photoexcitation at the entire dimer. Subsequently the return to the ground state will result in the excimer characteristic emission and the rapid excimer discossiation due to the repulsive forces that will dominate.

Excimer or exciplex formation depends on the concentration of the participant molecules in the formation of the excited dimer. Figure 1.6 shows two characterristic examples of exicmer (I) and exciplex (II) spectra, as a function of concentration. For high concenrations the distance bewteen the molecules is decreased, thus the strenght of  intermolecular interactions is increased and the consequently the excimer or exciplex spectral feature is intensified.
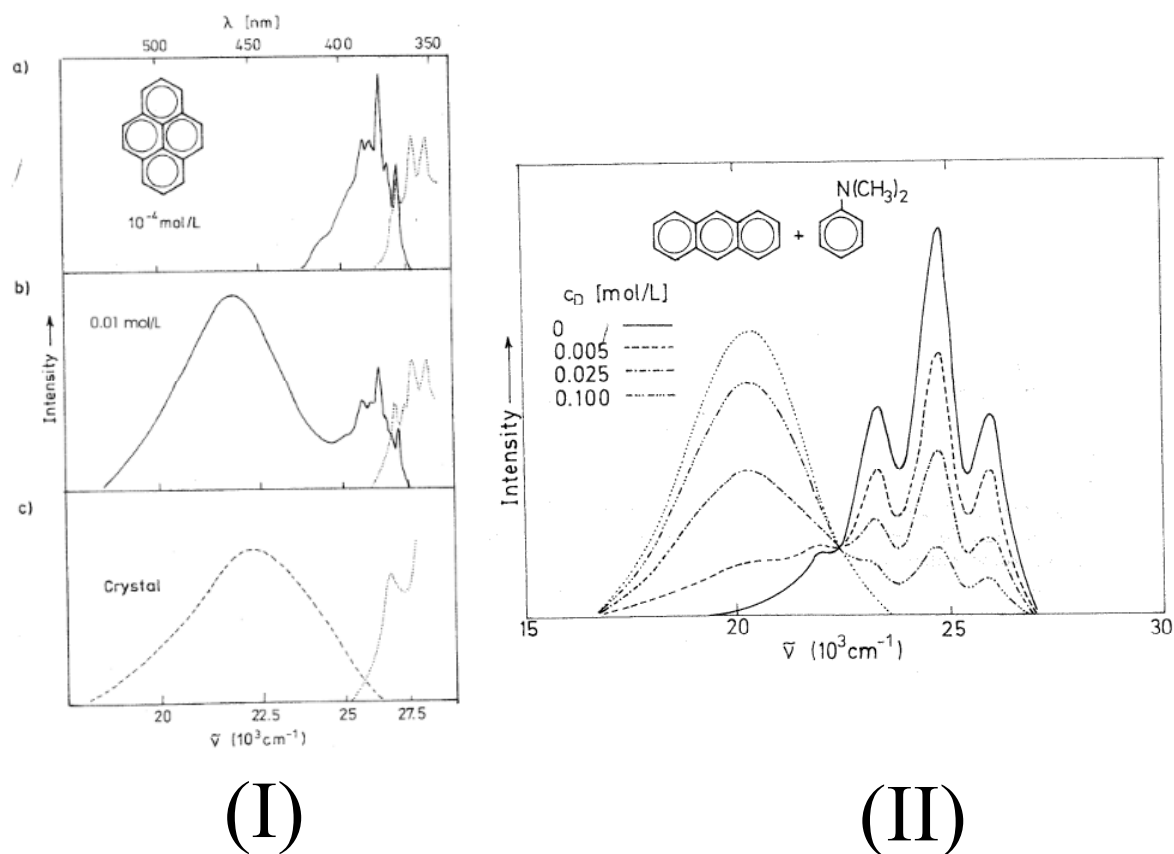
Figure 1.6: Examples of an excited state dimer between (I): excimer formation by two identical molecules of pyrene and (II) exciplex formation by two different molecules, anthracene and dimethylaniline. For (II) various concentrations of dimethylaniline in solution of toluene are shown. From Klessinger & Michl.

## 1.4 ELECTRONIC ENERGY TRANSFER

In many systems that are composed of two different chemical species, photo excitation of one of the components is followed from an unexpected reduction of the photoluminescence that was anticipated for this component. Moreover the characteristic emission of the second component is observed, even in the case that absorption of the incident photoexcitation from this component is not probable. Such systems are best described as systems of a donor (D) and an acceptor (A) molecule and the process of energy transfer is referred to as electronic energy transfer. During this process the excited donor molecule $D^*$ returns to its ground state with the simultaneous transfer of its electronic energy to the acceptor molecule A:

$$D^* + A \rightarrow D + A^*$$
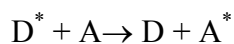
Under these conditions D molecules are termed as sensitizers and A molecules as activators. Subsequently, the photoexcited molecules $A^*$ may proceed in either giving a sensitised photochemical reaction or exhibit sensitised photoluminescence.

23

The electronic energy transfer can be described further according to the photophysical processes that are involved in it. If energy transfer consists of a two-step scheme that is emission from the excited donor and subsequent absorption from the ground state acceptor, the transfer mechanism is based on a radiative step and it reflects the so-called trivial case of electronic energy transfer. In this case the dependence of energy transfer efficiency on the separation distance of donor and acceptor molecules is weak and the only important factor that influences the process is the quantum efficiency of the donor in the spectral region in which the light-absorbing power of the acceptor is appreciable.
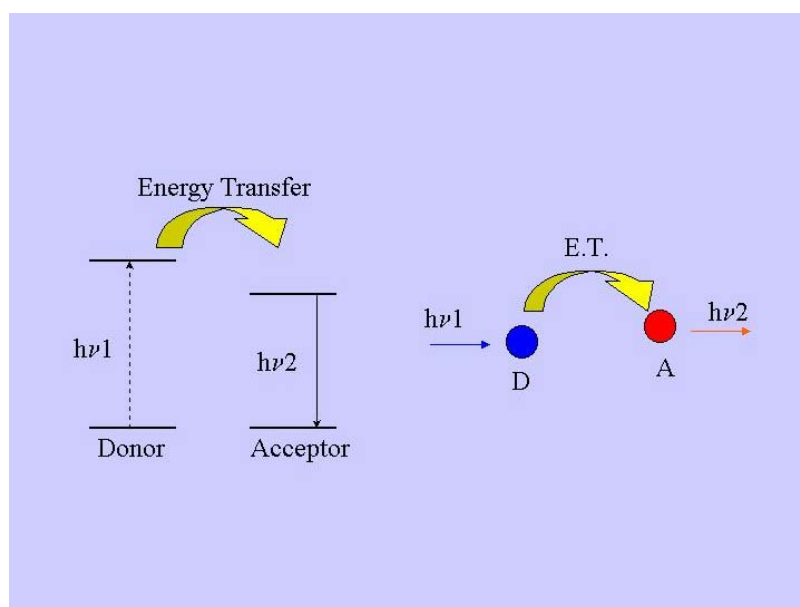


Figure 1.7: A schematic illustration of electronic energy transfer from the optically excited level of a donor (D) to an Acceptor (A), that results in emission of a photon from A.

When electronic energy transfer takes place in one single step via a non-radiative process, two alternative photophysical mechanism need to be considered. That is the Coulombic energy transfer mechanism mostly known as Förster-type energy transfer and the exchange energy transfer mechanism. For these two types of transfer the term resonance enery transfer (RET) can be alternatively used in order to declare the non-participation of a photon in the transfer process. Both mechanism of nonradiative transfer require spectral overlap of the electronic transitions

$$D^* \rightarrow D \text{ and}$$

$$A \rightarrow A^*$$
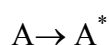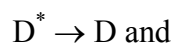
which implies that the overlap between excited state donor's emission spectrum and ground state acceptor's absorption spectrum should be considerable. Under conditions of rapid excited-state vibrational relaxation and Franck-Condon principle validity for energy transfer, the spectral overlap is defined as:

$$J = \int_0^\infty I_D\left(\tilde{\nu}\right) * \varepsilon\left(\tilde{\nu}\right) * d\tilde{\nu} \qquad \text{(eq. 1.13)}$$

where $\int_0^\infty I_D\left(\tilde{\nu}\right) * d\tilde{\nu} = \int_0^\infty \varepsilon\left(\tilde{\nu}\right) * d\tilde{\nu} = 1$ are the emission spectral distribution of donor and the

absorption spectral distribution of the acceptor, respectively, after normalisation to a unit area on the wavenumber scale. According to these required spectral overlap condition for normalised spectra it is evident that the magnitude of the spectral overlap is not subject to the absolute values of the oscillator strengths of the transitions that are involved in the process.

The main important difference that exist in the two alternative resonance RET mechanisms is the dependence of the rate of the transfer constants on the separation distance between donor and acceptor molecules.

Coulomb type of transfer is based on classical dipole-dipole interactions and is significant at distances up to the order of 10 nm. The dependence of the rate constant on distance is:

$$k_{ET} \sim \frac{f_D * f_A}{R_{DA}^6 * \tilde{\nu}^2} . J \qquad \text{(eq. 1.14)}$$

where $f_D$ and $f_A$ are the oscillator strength values for donor and acceptor transition respectively and $R_{DA}$ the distance between donor and acceptor molecules.

The dependence of the rate constant on distance for the case of exchange type of transfer as has been expressed from Dexter is

$$k_{ET} \sim J * e^{-2*R_{AD}/L} \qquad \text{(eq. 1.15)}$$

where again $R_{DA}$ represents the distance between donor and acceptor molecules and L is a constant related to an effective average orbital radius of the electronic donor and acceptor states that are involved in the process.

Initially the Förster theory that expressed the Coulombic RET mechanism was based on the assumption that a fixed distance separated the donor-acceptor pair. In reality this assumption may be incorrect and in that case more sophisticated models for the analysis of energy transfer mechanism should be applied. This issue will be addressed again in Chapter 3 and Chapter 4.

## 1.5   SPECTROSCOPY OF CONJUGATED POLYMERS

Theoretically the energy levels of small organic molecules reflect the interactions of the electrons that are positioned in the molecular orbitals that comprise the molecular framework. Therefore the calculation of the energy for these levels requires detailed knowledge of the number of atomic orbitals that constitute the base for each of the molecular orbital and the level of electron-electron interaction between these orbitals.

## 1.5.1 Energy levels of a single polymer chain: The Hückel approximation

In the case of a linear $\pi$-conjugated polyene that is comprised of $n$ carbon atoms of $sp^2$ hybridization, the energetic position of the lowest lying electronically excited state, can be calculated according to the Hückel approximation:

$$E_k = \alpha - 2*|\beta|*\cos(\frac{k*\pi}{n+1}), k = 1,2,..,n \qquad \text{(eq. 1.16)}$$

In eq. 1.16 the terms $\alpha$ and $\beta$ represent the overlap and exchange integrals, respectively, of the wavefunctions that are chosen as the basis of the electronic wavefunction for the studied system. Especially in the case of a linear $\pi$-conjugated polyene the Hückel approximation choses these wavefunctions to be the $p_z$ orbitals of the carbon atoms in the molecule, that build up the $\pi$-electronic system.

The number of energy levels in a given energetic interval E to E+dE , is termed density of states (DOS) and is described by the general expression:

$$N(E) = \frac{1}{E_{n+1} - E_n} \qquad \text{(eq. 1.17)}$$

where $E_r$ is given by eq. 1.16. However, the Hückel approximation is only a semi-empirical approach on the energies of the excited states in infinite conjugated systems and $E_r$ can be alternatively expressed differently.

For example, in the case of a cyclic conjugated system such as poly($p$-phenylene) that is comprised of $n$ benzene rings that are covalently linked in $p$-position units, the dependence of the lowest electronically excited state on $n$, has been described by Davydov as:

$$E_n = A - 2*|M|*\cos\left(\frac{k*\pi}{n+1}\right), k = 1,2...,n \qquad \text{(eq. 1.18)}$$

where A reflects the energy of the monomer unit and M the interaction between adjacent units. Independently from the theory that is used for the energy determination of the electronic states,

the lowest energetic transition is reffered to as the HOMO-LUMO transition that corresponds to a promotion of an electron from the Highest Occupied Molecular Orbitals to the Lowest Unoccupied Molecular Orbitals of the system.

## 1.5.2 Solid State interactions: The tight-binding approximation

Upon shifting to the solid state, the electronic properties of molecules are strongly affected due to the rise of the electronic interactions that are born from the enhance intermolecular interactions. Under conditions of a periodical structure in a solid, discrete energy levels of isolated molecules are transformed to broad bands.

Upon increasing the number of the atoms that comprise one single molecule, the calculation of the representative molecular wavefunctions becomes a complicated mathematical task. The degree of complexity is further increased in the case of intermolecular couplings of these large molecular systems. Many times several assumptions reduce the degree of difficulties in calculating the appropriate field in which electrons are placed. For instance in an independent electron model, electron-electron interactions can be approximated by some average effective periodic potential that interacts with an electron. Additionally, the existence of molecular symmetry reduces to some extend the difficulties in the calculation of wavefunctions and the corresponding energies of a system in the solid state.

The method that makes use of the aforementioned approximations is termed the tight-binding approximation. It is a modified Linear Combination of Atomic Orbital-Molecular Orbital (LCAO-MO) method applied on a translationally periodic structure. The electronic state keeps the atomic-like properties because of the assumption that the overlap of an electronic state of one atom with that of its neighbours is relatively small.

In the ideal case of one-dimensional structure composed of N atoms that are separated with a lattice constant $\alpha$, LCAO scheme would suggest that the general form of the wavefunction, which describes the system corresponds to:

$$\psi_k(x) = \sum_{j=1}^{N} C_j * \phi(x - X_j) \qquad \text{(eq. 1.19)}$$

where $\phi(x - X_j)$ is the normalised atomic orbital centred around the $j^{th}$ atom with energy $E_a$. Here $X_j = n_j \alpha$ where $n_j$ is an integer and N is the total number of atoms that comprise the studied system. In terms of LCAO method, $\{\phi(x - X_j)\}$ is the basis needed for the calculation of $\psi_k(x)$ wavefunction.

 Due to the fact that the wavefunction can not be discontinued at the transition from atom j=1 to atom j=N , cyclic boundary conditions are applied to the infinite periodic structure of N atoms. The general condition for the preservation of continuity of a wavefunction in a periodic structure such as a lattice, is expressed from the Bloch theorem. The cyclic conditions that the Bloch theorem introduces result in that $C_j = N^{-\frac{1}{2}} * e^{i*k*X_j}$ therefore

$$\psi_k(x) = N^{-\frac{1}{2}} * \sum_{j=1}^{N} e^{i*k*X_j} * \phi(x - X_j) \qquad \text{(eq. 1.20)}$$

The wavefunction $\psi_k(x)$ is alternatively termed Bloch sum and it represents states that are analogues of molecular orbitals embedded in periodic structures. In terms of solid-state physics, the Bloch theorem reflects a status in which the lattice periodicity modulates the wavefunction of electrons.

The corresponding energies $E_k$ of $\psi_k(x)$ can be calculated as:

$$E_k = \langle \psi_k(x) | \hat{H} | \psi_k(x) \rangle \qquad \text{(eq. 1.21)}$$

which after assumptions within the tight-binding approximation results in:

$$E_k = E_\alpha - W * \cos(k * \alpha) \qquad \text{(eq. 1.22)}$$

where $-W$ corresponds to stabilisation energy due to nearest-neighbours electronic interactions.

 For the characteristic values of $k = 0$ and $k = \pm\dfrac{\pi}{\alpha}$ the corresponding $E_k$ values are $E_k = E_\alpha - 2 * W$ and $E_k = E_\alpha + 2 * W$. By plotting the energy levels of the $\psi_k(x)$ states as a function of $k$ the formation of an energy band arises, which is centred at $E_\alpha$ and has a width of 4W. Such a plot of E as function of the k-space, reflects the DOS of the structure. The values of k in such a E(k) diagram may be interpreted as a node counter of the corresponding $\psi_k(x)$ state. A restricted interval of k values is termed as Brillouin zone.

 Not always a unit cell of a lattice consists of only one type of molecular orbitals. If more type of atomic orbitals co-exist, Bloch sums must be set-up for each of these orbitals. Therefore the eigenstates of the $\psi_k(x)$ states that represent the studied periodic structure will result from linear combinations of these Bloch sums.

 The distance that separates the individual atoms within the unit cell of the lattice determines the width of the energy band, which is referred to as dispersion. Therefore the closer the atoms are positioned the stronger the band is dispersed. The number of the discrete levels that an energy band occupies is determined from the number of atoms that compose the system. Therefore N atoms will result in N energy levels. The energy of the highest occupied level is called the Fermi

energy and at a given temperature, is determined from the total electron number present in the system.

## 1.6 THE ELECTRONIC PROPERTIES OF CONJUGATED POLYMERS: THEORETICAL CONTEXT

### 1.6.1 *Trans*-polyacetylene: An ideal case

Since the establishment of the materials science field as an independent scientific branch of the general scientific family, a meddling of scientific nomenclature took place due to the interdisciplinary character, which was demanded for such an attempt of scientific research.

Especially in the case of conjugated polymers, the postulates regarding charge transport phenomena within these materials should be expressed mainly via the terminology of mechanistic organic chemistry yet combined with the symbology developed by solid-state physics.

For organic chemists and solid-state physicists, the main difference in addressing questions regarding phenomena such as charge transport in organic molecules was the direction followed in the size-scale of the studied materials. In contrast to the chemical bottom-up approach where the examination traditionally starts from discrete organic molecules and it is extrapolated towards the expansion to an infinite polymeric domain, solid-state physics choose the imposition of boundary conditions to an initially infinite bulk material.

Such an approach was used in the case of *trans*-polyacetylene. This system is the most closest one to the consideration of one-dimensionality and thus an analogue treatment was used for its theoretical modeling. *Trans*-polyacetylene is envisaged as an infinite chain consisting of carbon units of $sp^2$ hybridization that are linked subsequently with double bonds. This is the simplest visualization of a polymer that exhibits an infinite $\pi$-conjugation system, a set of $p_z$-orbitals that are positioned vertically on the molecular plane defined from the carbon atoms of the molecule. Electrons placed in these $p_z$ orbitals are delocalized and the electronic interactions of these electrons result in the $\pi$ molecular orbitals of the system.

The ground state of polyacetylene can be represented from two different chemical structures that are of equivalent energy. Therefore *trans*-polyacetylene is defined as a degenerate polymer. Yet this degeneracy is vanishing when a change in the bond length alternation along the polymer chain occurs. This effect was suggested first by Peierls and its consequence for degenerated polymers, is the lifting of degeneracy for the two alternative structures.
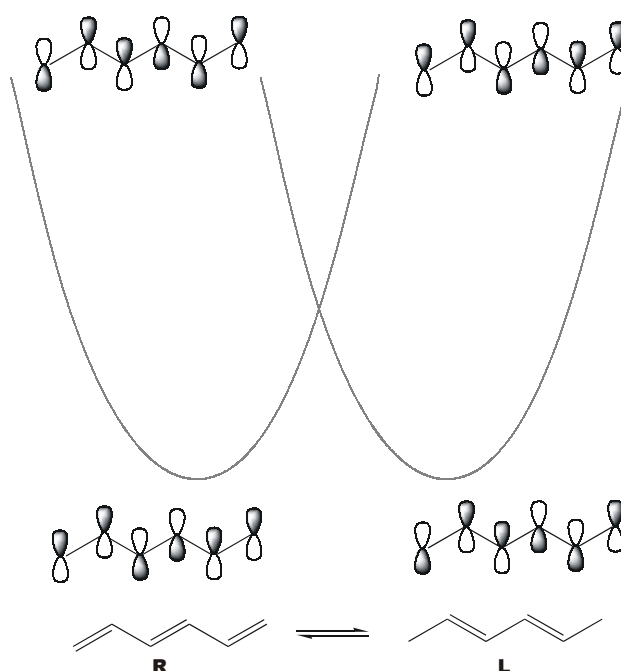
Figure 1.8: The two inequivalent ground state isomers R and L of polyacetylene and the corresponding Woodward-Hoffmann representation of the molecular orbitals for their ground and first excited levels. Ground state isomerisation between these two structures reflects the Peierls distortion ans it reflects a forbidden reaction. From Tolbert.

An energy gap thus is formed in the dispersion curve at $k = \pi/2\alpha$, where $\alpha$ is the unit cell length before bond alternation. The physical interpretation of Peierls consequence can be expressed as the response of the system on the excess of the elastic strain energy required distorting the chain, by the lowering of the occupied energy levels on the proximity of $k = \pi/2\alpha$.

The established method for the development of a theoretical model on trans-polyacetylene has been presented from Su, Schrieffer and Heeger (SSH). The approach of this team was based on the tight-binding calculations by neglecting electron-electron correlations and by assuming cyclic boundary conditions. The application of the latter assumption on a polymer chain consisted of odd number of carbons gave rise to soliton concept. The requirement of a soliton presence in a polymer chain of odd number of carbons that is expected to fulfill the cyclic boundary conditions is inevitable as it explains the coexistence of two ground state configurations in *trans*-polyacetylene. In terms of spatial cordinates, soliton extends over a large polymeric segment, which intermediates between these two configurations. In terms of energy, the existence of a soliton allows an energetically forbidden interconversion of the two alternative equivalent ground state configurations R and L (Figure 1.8).

In mechanistic organic chemistry terminology, a neutral soliton corresponds to a radical, an unpaired valence electron that is localized onto a carbon atom of the polyacetylene chain. The hybridization of such a 'kink' defect point is considered to be of $sp^3$ nature. It was suggested that this kink was the reason why a one dimensional ideal all-*trans* polyacetylene chain is divided into two topologically different chain segments.
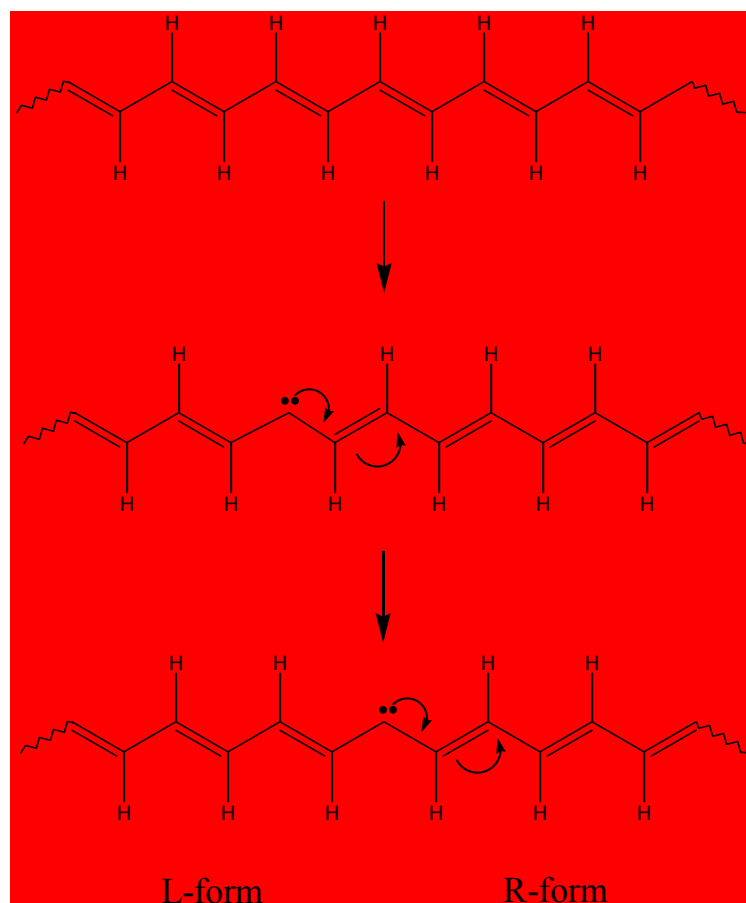


Figure 1.9: The soliton and the proposed mechanism for polyacetylene conduction. From Tolbert.

In examining the optical properties of a conjugated polymer such as polyacetylene, the band-to-band transition notion has been applied to the ideal case of one dimensional, single chain semiconductor in which the potential interactions are attributed to one-electron considerations. In this framework of understanding, the existence of a solitonic center implies the introduction of a mid-gap localized state originating from a non-bonding molecular orbital. Population of this mid-gap state by the unpaired electron corresponds to a radical, which in terms of spin multiplicity description is referred to as a doublet. Manipulation of the population in this mid-gap state and all the possible interactions of these states with other similar states in the vicinity of the molecule, result in a group of novel mid-gap states such as solitons, positive solitons and

negative solitons. It should be noted that so far the character of this mid-gap state is considered to be spatially localised however at the same time the theory that was developed for explaining polyacetylene conductivity, considered that solitons could delocalise over a large number of carbon atom units in the polyacetylene lattice. In other words they anticipated that a soliton would have considerable mobility in order to freely move along the polymer chain. The latter consideration is in accord with the mechanistic point of view in organic chemistry, where radicals may be delocalized via resonance effects. Heeger et al. have reviewed extensively on the theoretical and experimental investigation applied to solitons and other excited states in *trans*-polyacetylene. However experimentally this concept is by no means clear.

## 1.6.2 Experimental reality: Major deviations from the ideal case

Not all the class of conjugated polymers can be categorized as degenerated polymers. There are many examples of π-conjugated structures that correspond to a unique ground state configuration. Representative examples are poly(-p-phenylene-vinylene)s, poly(-p-phenylene)s, poly(fluorene)s, poly(indenofluorenes) and ladder type poly(-p-phenylene)s. From all these types of π-conjugated molecules, PPV has been extensively studied with respect to its charge transporting and photophysical properties. In this type of polymer, Peierls disortion effect is not important. However, two ground state configurations of different energy exist due to the absence of symmetry in the chemical structure of these polymers. These inequivalent ground state configurations correspond to bond alternation patterns that arise before and after the introduction of charge onto the molecular orbital framework that represents the electronic properties of the system. In chemical terminology the aforementioned ground state configurations are reflecting the benzenoid and the quinoid isomer of the molecule, respectively.
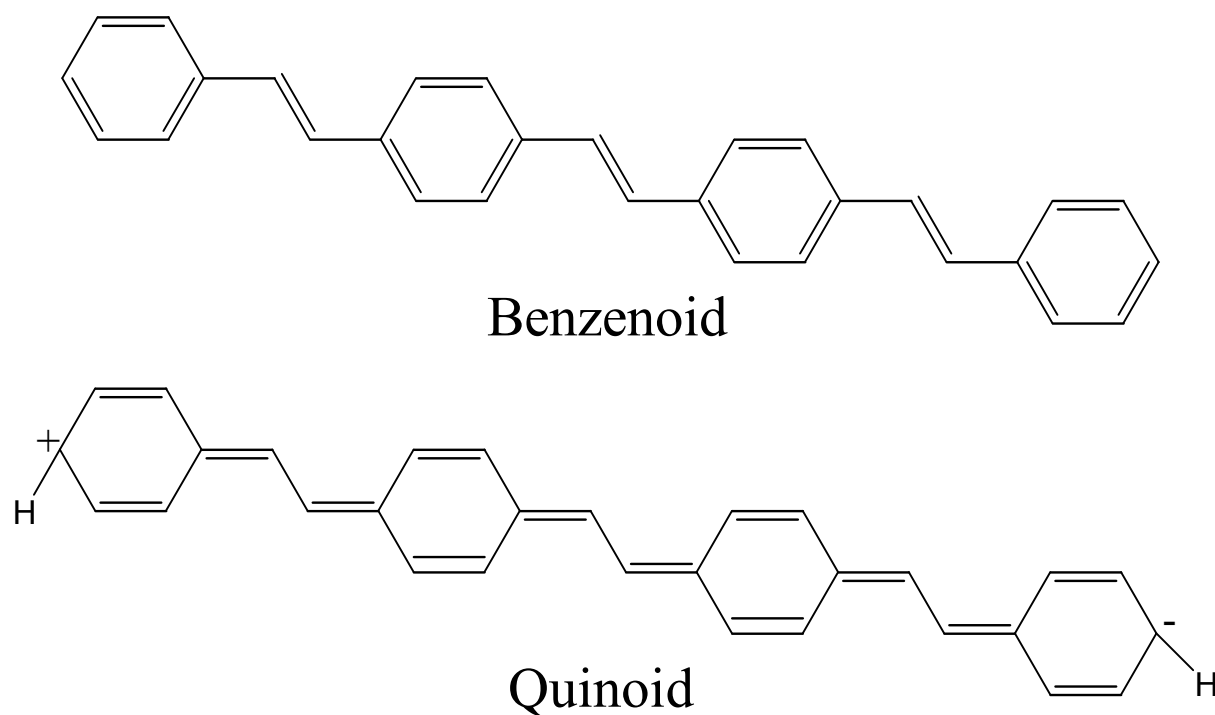
Figure 1.10: The two alternative non energetically degenerated isomeric forms of phenylene-vinylene polymer (PPV).

Hence a different ground state configuration of these polymers can be obtained only after the interaction with oxidizing or reductive agents. The charged ground state configuration (quinoid) will be of higher energy than the neutral one (benzenoid).

The analogue of a soliton in non-degenerated polymers is the polaron, a term actually borrowed from the nomenclature of solid-state physics. For non-degenerated polymers, polarons are envisaged as charges localized onto the polymeric chain that cause local rearrangement of bond alternation. They are defects originating from the presence of a unpaired electron which subsequently delocalizes via resonance effects within the $\pi$ orbital framework of the molecule.

The role of polarons in the electronic properties of non-degenerated conjugated polymers has been theoretically predicted from modified SSH models derived by Brazovski and Kirova (BK). Additional theoretical improvements that brought closer agreement between theory and experiment came from Choi and Rice. The presence of an unpaired electron onto the molecular backbone of a non-degenerate polymer, results in the appearance of novel states within the gap, that are positioned symmetrically in respect to the midgap. Therefore, four different novel electronic configurations can be deduced once these states are formed that correspond to the occupation with 0, 1, 2, 3, 4 electrons. Accordingly, the obtained new subgap electronic states are termed positive bipolaron ($bp^{2+}$), positive polaron ($bp^{+}$), polaron exciton (p), negative polaron ($p^{-}$) and negative bipolaron ($bp^{2-}$).

So far the discussion of the electronic properties of conjugated polymers was based on SSH model where electron-electron interactions have been neglected by virtue of the tight-binding approximation where one-electron considerations are valid. This approach is applicable in a satisfactory degree only for the case of degenerate polymers such as *trans*-polyacetylene. More importantly, SSH theory is based on the major assumption that a polymeric chain may be considered as infinite, one-dimensional, isolated chain where tight-binding model is in action. In reality, not all polymers are of degenerate ground state configuration. In addition to that, even if isolated, a polymeric chain may be not one-dimensional due to conformational effects that force the chain to fold in such a way that will break the continuum of electronic π-system, resulting in a distribution of conjugated segments. Finally, the individuality of a polymeric chain in the solid state cannot be guaranteed due to the enhanced interchain interactions that arise due to packing phenomena. Under these conditions, the one-electron consideration that the tight-binding model demands is not longer applicable.

The thermodynamic state of a conjugated polymer as a thin film is dependent from the glass transition temperature of the polymer. Given that $T_g$ is significantly higher than room temperature, a thin film prepared from spin coating of a concentrated solution is comprised of a conformational distribution of the polymer chains onto the substrate, frozen in a glassy state. Since spin coating is a process by which no control on the orientational adsorption is operative, a distribution of conjugational lengths randomly oriented in respect with a virtual axis will be collected onto the substrate surface. This positional disorder will result in an energetic disorder in the electronic levels of the film as a whole.

The active electronic features of a conjugated polymeric chain are a consequence of the π-conjugation in the chain. As it has been discussed in paragraph 1.5.1, the energy levels of conjugated polyenes, were initially deduced from the quantum mechanical description given by Hückel. Within this context, the observed energy gap of an individual chain is directly related to the distribution of the conjugated segments that are not necessarily comprised of the same number of carbon atoms. Hence for the case of conjugated polymers, the distribution of conjugational lengths in a thin spin-coated film will result in an analogues distribution of energy gaps. In addition to these single-chain parameters, under conditions of the strong interchain interactions in the film, the electronic characteristics of the individual chains are altered and the new energy levels will exhibit the phenomenon of dispersion, as discussed in paragraph 1.5.2. A pristine spin-coated film is comprised of closely stacked polymer molecules that are interacting with each other. This chain interaction results in a vectorial interaction of the transition moments that each polymeric chain carries. Especially in the case of rigid-rod molecules, the main

component of the transition dipole moment of each chain lies along the long molecular axis. The extent of the interchain interaction is dependent on the relative orientation of the polymeric chains and consequently of the relative orientations of the transition moment dipoles. Eventually in the strong regime of interaction, the discrete energy levels are replaced from a broad band that is a common feature in solid-state spectroscopy. This band is consisted of many discrete energy levels whose energetic difference is of the order of meVs.

When a chain in a film of a polymer such as PPV, absorbs a photon, a photoexcited state is created during the lowest $\pi$-$\pi^*$ electronic HOMO-LUMO transition on the polymeric chain. However, as the polymeric chain is composed of a series of segments of varying length the $\pi$-conjugation can not be represented as continuum along the whole polymeric chain. It is more correctly assumed that a distribution of conjugated segments build up the polymeric chain. In this picture the active chromophores that participate in the absorption of light are these oligomer-like segments. The average conjugated length of these segments is termed as effective conjugation length $L_{eff}$ of the polymeric chain.

Since the energy of a $\pi$-$\pi^*$ electronic transition reflects the degree of $\pi$-conjugation, the presence of a distribution in conjugated segments will result in a distribution of their corresponding energy levels. Therefore upon shifting from a monomer to its polymeric analogue, the narrow absorption line of a singlet electronic state is replaced by an inhomogeneously broadened absorption band, which reflects a distribution of electronically excited states.
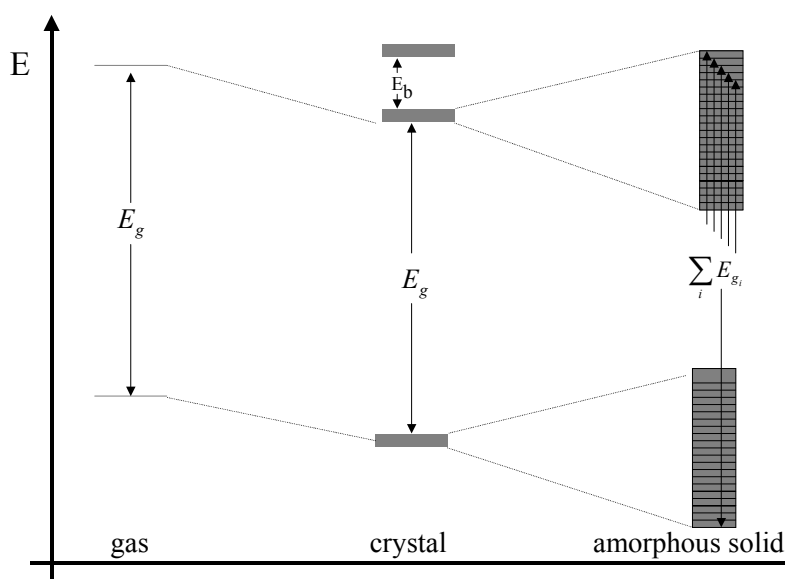
Figure 1.11: A schematic representation for the energy levels of a molecule upon the decrease in the intermolecular distance. The energy gap $E_g$ obtains a statistical character when the coulombic interaction of adjacent monomers is a subject to positional disorder like that of an amorphous solid. The term $E_b$ accounts for the exciton binding energy in the crystal.

## 1.7 EXCITON MODELS APPLIED IN CONJUGATED POLYMERS

Absorption of light results in a transition from the HOMO to the LUMO of the polymer and a primary photoexcited state is formed into the DOS. This excitation is consisted of a correlated pair of an electron and a hole that in the case of condensed matter, have the ability for transport. In the following the main theoretical concepts for the description of this electron-hole pair will be briefly presented.

### 1.7.1 Wannier-Mott model

By keeping the concept of tight-binding approximation valid, one comes to the conclusion that the nature of an optical excitation in a conjugated polymer should be described within the one-electron band picture that tight-binding approximation demands. This way of description has been expressed initially from Wannier and Mott.

In this point of view, electronic transitions are considered to take place in between states that originate from the weak electron-electron correlations that have been assumed due to the tight-binding approximation. When a photon is absorbed, an electron is promoted to an electronically

excited state leaving a hole behind. This electron-hole pair is coulombically bound and has a characteristic energy that depends on the electron-hole distance.

 In the field of solid-state physics this coulombic pair corresponds to a new electronic state and it is termed exciton. Although it is an abstract term, an exciton is better treated as a quasi-particle that is characterized from the value of the electron-hole distance, which is referred to as the exciton radius.  In terms of real space, for Mott-Wannier excitons the electron and the hole may be placed far apart from each other, thus they are considered to be largely delocalized over different molecular sites of the lattice. The energies that correspond to Mott-Wannier excitons can be derived from the degree of interaction between two oppositely charged species, the electron and the hole, that are separated by an intervening medium which has the characteristics of a dielectric continuum. The energy of a Mott-Wannier exciton is expressed in terms of Rydberg formalism that describes the hydrogenoic (hydrogen analogues) molecules:

$$E = E_G - \frac{G}{n^2}, n = 1,2,3,..., \qquad \text{(eq. 1.20)}$$

where $E_G$ is the ionization energy in the solid and G is the energy that keeps the electron-hole pair stabilized at a given *n* number.
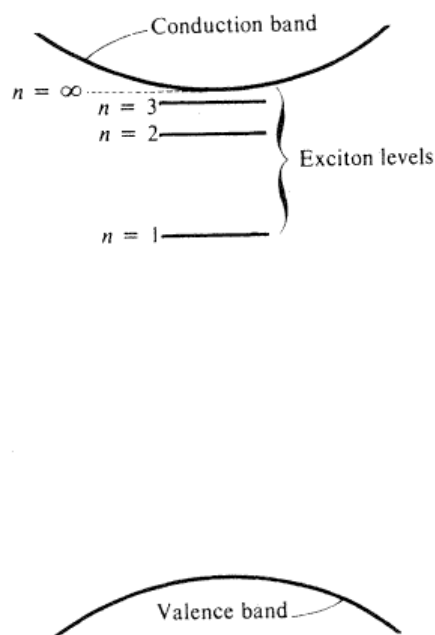


Figure 1.12: The exciton levels according the Wannier-Mott exciton model. Only a fracttion of the valence and conduction bands are shown, in the region of k=0 (see eq. 1.22). From Pope & Swenberg.

In the case of π-conjugated polymers and in particular for PPV polymer, comparison of the above mentioned theoretical analysis with the experiments, results in that the Wannier-Mott model is not appropriate for describing the lowest electronically excited states. It seems that the magnitude of electron-electron correlation is far more important than it was assumed initially when the SSH model had been suggested. In the presence of strong electron-electron correlation the model that appeals the most for describing the neutral photoexcitations in PPV is a modified Frenkel model.

## 1.7.2 Frenkel model

Davydov initially applied the Frenkel model for molecular crystals, for the interpretation of the obtained optical spectra. The driving force for the formation of a Frenkel state in a molecular crystal is the presence of many translationally inequivalent molecules in a unit cell. Splitting of a molecular level is anticipated in as many components as the number of inequivalent molecules in a unit cell. Therefore the energy level of an excited state that corresponds to an isolated molecule will be split into two components in a molecular crystal composed of unit cells that enclose two translationally inequivalent molecules per cell. The ground state of a molecular crystal will be stabilized depending on the degree of interaction between equivalent molecules in the bulk of the crystal. However, the splitting of the excited state, known as Davydov splitting, will vary depending on the degree of interaction between inequivalent molecules in the unit cell. The new energy levels, the Davydov components, correspond to energies of the new electronic states in the molecular crystal termed as Frenkel excitons.
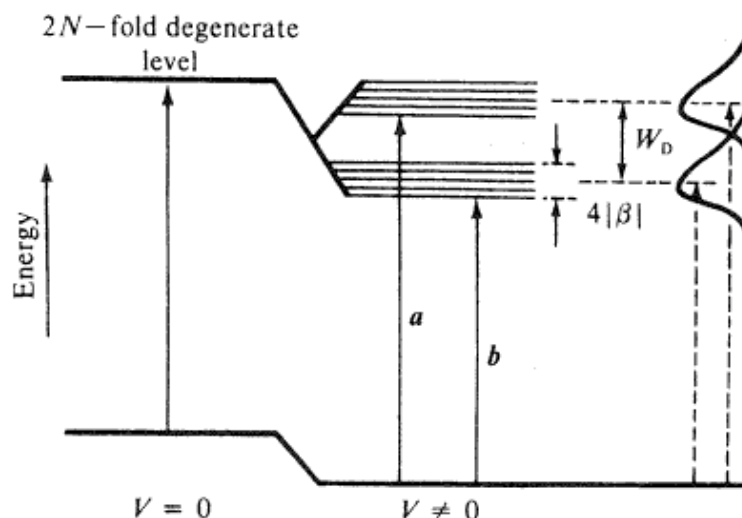
Figure 1.13: The characteristic energy splitting of the 2-N fold degenerate level for a crystal with two translationally inequivalent molecules per unit cell into two distinct Davydov bands. The width β of each Davydov component reflect the total intermolecular interactions between neighboring molecules. The energetic distance $W_D$, of the exciton bands is defined as the Davydov splitting and its magnitude arises only from inequivalent intermolecular interactions. From Pope & Swenberg.

In comparison with a Mott-Wannier exciton, the delocalisation of a Frenkel exciton wavefunction over the lattice takes place in less extent. This limited delocalisation range is imposed by the significance of the electron-electron correlation. The total amount of intermolecular interactions in the solid state can be represented by the energetic term J. Similarly the electron phonon interactions can be described from the term *b*. For a pure Frenkel state $b/J \rightarrow 0$.

In order to include this enhanced electron-electron correlation into the SSH model originally developed for *trans*-polyacetylene, features of the Frenkel model were implanted in the SSH Hamiltonian. This was achieved by considering the first-order effects of interelectronic interactions. A repulsion energy term U which describes on-site electronic interactions was taken into account and it was compared the long-range Coulombic interaction as expressed from the energetic term J. Variation of the calculations dependent on the U/J ratio was performed by Abe et. al., when the SSH Hamiltonial for a non-degenerate polyene was numerically diagonalised. It was found that electron-electron correlation is becoming significant when U/J>2. This was evidenced from the clear separation of a singlet state from a lower lying triplet state, that indicates enhanced exchange energy of the electrons. The resultant model is considered as a meddling of Wannier and Frenkel characteristics and it is termed as intermediate exciton model or charge-transfer (CT) exciton model. An early expression of the CT model was presented from Phillpott for describing the electronic properties of polydiacetylenes.

The intermediate exciton model envisages a neutral exciton as an electronic photoexcited neutral state that is represented by a wavefunction that can be delocalized over distances corresponding to maximum twice the nearest-neighbor intermolecular distance. Figure 1.14 depicts the three different types of excitons.
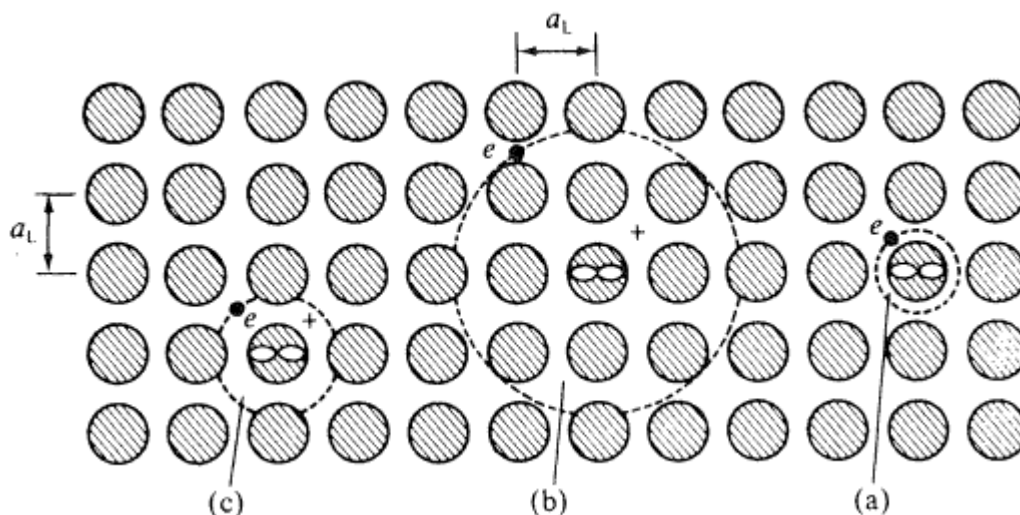


Figure 1. 14: A schematic representation for the three different types of excitons discussed in this Chapter. a) a Frenkel exciton the radius of which is small in comparison with the lattice contant $a_L$, b) a Wannier-Mott exciton the radius of which is large in comparison with the lattice contant $a_L$ and c) a charge transfer exciton the radius of which in the presented case is equali to the lattice contant $a_L$. From Pope & Swenberg.

## 1.8   EXCITON MIGRATION

Exciton motion is a known process in organic crystals. Energy transfer processes occurring between donors and acceptors may take place in molecular crystals, giving rise to exciton motion phenomena. In this case, excitations in the lattice of the molecular crystals are described according to the exciton concept formalisms that were introduced earlier. In the special occasion where energy transfers steps are taking place subsequently in between an array of molecules with the same chemical composition, the term exciton migration is used.

Exciton migration is a transport process that is characterized energetically from the motion of the exciton within in the density of states, in the k-space. In terms of real space, an exciton diffuses among the sites of the lattice, during its lifetime. The magnitude of the average distance that the exciton travels is given from the exciton diffusion length:

$$l = \sqrt{Z.D\tau} \qquad \text{(eq. 1.21)}$$

where D is the isotropic diffusion coefficient of the exciton, $\tau$ is the exciton lifetime and Z may vary depending on the dimensionality of the diffusion process. However, in most of the cases, Z is taken to be unity. For the case of three-dimensional diffusion, sensitized fluorescence studies

in anthracene-tetracene systems showed that diffusion coefficient was approximately equal to the number sites that the exciton was visiting during its lifetime.

So far its has been stated that the neutral photoexcitations of a polymeric chains are best described as charge-transfer excitons with energy levels dispersed into a broad band of excited states, due a the distribution of segments with different conjugation length. The effective conjugation length $L_{eff}$ that corresponds to the average value of the distributed conjugated segments represents the electronic properties of the chain. These oligomer-like segments act like chromophores that absorb light, which is resonant to their corresponding $\pi$-$\pi^*$ transition. As charge transfer excitons are considered to delocalize over a small extent onto the polymeric chain, it has been proposed that the effective conjugation length can represent the length at which the wavefunction of the charge-transfer exciton remains coherent. This assumption is still under investigation and there is not any clear-cut evidence for its validity. The term hoping has been used for describing the step at which the exciton loses its coherency. Therefore exciton diffusion in a conjugated chain is depicted as a hoping process of the exciton along polymeric segments that preserve the exciton coherency. The driving force of the hoping process has a dual origin. Mainly it is an inherent characteristic of the charge-transfer excitonic nature, which exhibits an enhanced strength of the exciton-phonon coupling. Upon encounter with phonons an exciton is disturbed and it looses its memory. Encounters may also take place with impurities embedded in the lattice. Destructive exciton interference is a result of the inevitable presence of structural and chemical defects in the polymeric chain. Hence, the hoping process of an exciton is a consequence of exciton's coherency destruction due to the exciton interaction with phonons or defects present in the polymer chain.

Exciton migration is an important process in the case of $\pi$-conjugated polymers, however the interpretation of its physical origins still remains a subject of controversy. There is an open issue regarding the fate of these primary photoexcitations. Given the fact that the length of these segments is a multiple of the monomer unit length, Förster formalism is operative for explaining the process of energy migration between polymeric segments as the distances involved lie in within the Förster range. However upon considering that energy migration may take place within the monomer units themselves, the Förster dipole approximation is not applicable due to the short distances that separate the monomer units. It is expected that the emerging field of single molecule spectroscopy will elucidate many of these doubts, by focusing into transfer processes of individual monomer units of a polymeric segment.

Within the context of this Thesis, energy migration will be treated as taking place from units that are of oligomeric nature and are the building blocks of a polymeric chain. After absorption of a

photon, a primary neutral photoexcitation of intermediate excitonic nature is formed in the density of states. This exciton will diffuse towards lower lying energy levels that correspond to longer conjugated segments and it will decay radiatively or non-radiatively. This type of exciton migration is termed spectral diffusion and it is characterized from a dynamic red shift of the photoluminescence that occurs in the order of hundreds of *ps*. Alternatively this process has been described as dispersive relaxation due to the random character of the exciton migration within its DOS. Spectral diffusion leads to an equilibrated state that lies in the tail of density of states and that reflects the localization threshold. This state has been experimentally determined for PPV and PFO via site-selective exitation within the DOS of these polymers.
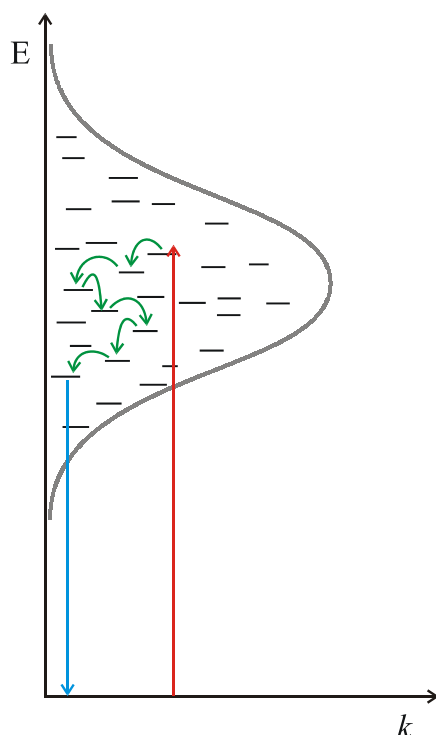


Figure 1. 15: A schematic illustration of the disoreder energetic nature of the excited states of a conjugated polymer. Optical excitation into the inhomogenous DOS is followed by dispersive relaxation within the DOS via incoherent hopping steps. When a certain energetic relaxation has taken place, emission is more probable than further energy migration.

The exciton migration takes place within the energy transfer mechanism of the dipole-dipole approximation. In the presence of a neighboring polymeric chain or in the presence of an agent that will favour exciton dissociation by virtue of electronegativity arguments, this neutral exciton may split into oppositely charged carriers. These charge carriers can subsequently give rise to observation of conductivity. The excitonic nature of the excited states was determined from exciton quenching upon the application of an electric field. The determination of exciton binding energy magnitude in PPV initiated a long discussion in the community of conjugated polymers. Currently, the accepted value is in the order of 0.1 eV.

 When polymeric chains are closely spaced with each other, the intermolecular interactions are strongly enhanced. This tight packing may alter the nature of the spatial character of the CT exciton. It is possible that the charge carriers will be located in different segments that are not part of the same polymeric chains. According to Rothberg this excitations are termed spatially indirect excitons and are considered to be results of strong interchain interactions. Alternatively, this correlated ion pair of oppositely charged carries has been described as a geminate pair. Geminate pairs are depicting electron-hole pairs that are loosely bound via coulombic interactions and located on different polymeric chains. Hence, geminate pairs or spatially indirect excitons are characteristics of polymers in solid state, e.g. as thin films.

 In the presence of molecules of different chemical composition, intermolecular energy transfer may take place if the energy levels of the system are appropriately set. Acceptor molecules that have energy level values equal or lower than the average DOS will act as extrinsic energy trap sites for the migrating exciton.

 Although in the case where spectral overlap of allowed transitions of the polymer-donor and acceptor molecules exists, Förster formalism is partially valid. The determined Förster radius should be larger than the one that eq.1.14 gives. A discussion on this aspect is presented in Chapters 3 and 4.


## 1.9  ENERGY GAPS

 The difference of the lowest electronically excited state that is coupled radiatively to the ground state is termed optical energy gap. Energy gap value is an important parameter for $\pi$-conjugated polymers. This class of chromophoric compounds is very promising for the development of polymer-based display devices. Therefore the color gamut that can be obtained from these materials is of strong importance for the realization of full color displays.

As it has been discussed the electronic description of the lower electronic excited states is better recovered by usage of the molecular exciton model. The latter description is favored in account of the importance of the electron-electron correlation along the conjugated chain. Consequently, the validity of this assumption should be reflected on the distinct discrimination of a singlet and a triplet excited state in a polymeric chain. In the presence of enhanced electron-electron correlation, the exchange energy of electrons should be significantly pronounced. Therefore a triplet excited state should be identifiable and different in energy than the corresponding singlet excited state. Indeed this is the case for a large variety of conjugated polymers. A firmly established relationship between the energetic difference of singlet-triplet levels and the number of monomer units in a polymeric chain has been obtained experimentally. Chapter 3 includes a

detailed discussion on the triplet states in π-conjugated polymers. Hence, the term band gap is rather erroneous as it reflects the concept of the one-electron model, which is better applicable in inorganic semiconductors but not in non-degenerate conjugated polymers.

The potential ability of observing efficient charge carrier photoconductivity in these conjugated polymers should be better interpreted as a result of competition between autoionisation of neutral bound states and internal conversion processes, rather than direct carrier photogeneration occurring in band-like energy structures. In terms of molecular organic chemistry, the ground electronic level and the lowest lying electronically excited level are represented by the HOMO and the LUMO levels, respectively. Both HOMO and LUMO levels are referred to as frontier orbitals of the studied system. In the case of a conjugated polymeric chain the HOMO-LUMO energetic gap corresponds to the energy of a $\pi$-$\pi^*$ electronic transition. Therefore the determination of the energy gap is potentially possible by means of optical spectroscopy. An absorption spectrum can be used for the extraction of the HOMO-LUMO energy gap. The energetic difference of the $S_{0-0} \rightarrow S_{1-0}$ transition corresponds to the energy where the onset of absorption occurs. Alternatively, if a photoluminescence spectrum is available, the $S_{0-0} \leftarrow S_{1-0}$ transition corresponds to the energetic gap. In the same way the triplet energy gap may be determined, if a phosphorescence spectrum is available the $S_{0-0} \leftarrow T_{1-0}$ transition can be identified. Usually, the values obtained from optical spectroscopy for polymeric films, are slightly lower in energy than the real HOMO-LUMO energetic gap. The observed energy reduction is attributed to reflection processes and to re-absorption effects, for absorption and PL spectra, respectively. These problems are resolved with rigorous calibration of the optical set up and careful experimentation.

As it is described in Chapter 2, the emission of light from polymer-based display devices is preferably achieved by exploiting the phenomenon of electroluminescence. Electroluminescence results in by the recombination of charge carriers that have been injected in the polymer material. Therefore, the efficiency of EL is partially determined from the efficiency of the charge carrier injection. The latter is better accomplished when the frontier levels of the polymer are appropriately balanced to the energy levels of the used electrodes. Hence, except the knowledge for the energy gap value, the absolute energy values of the frontier orbitals, in respect to vacuum level are of great significance. Tuning of the energy gap is a relatively easy task in the field of conjugated polymers. Experimentally, the determination of absolute values of the frontier orbitals can be achieved by using Ultraviolet Photoemission Spectroscopy (UPS) and Inverse Photoemission Spectroscopy (IPES). Having as reference the Fermi level of the material studied,

the former determines the density of states of the HOMO level and the latter determines the density of states of the LUMO.

It may be argued that UPS and IPES experimental methodologies are not widely spread and they include a high degree of difficulty. An alternative approach to the estimation of the HOMO-LUMO energy gap of a conjugated polymer relies on electrochemistry methodology. More specifically, cyclic voltammetry can be used for the determination of the working function and the electron affinity of the conjugated chain/film. Working function corresponds to the ionization potential measured in the experimental temperature. A discussion on the utilization of electrochemistry for the determination of energy gaps in a polymer is presented in Chapter 4.

# 1.10 CHARGE CARRIER MOBILITY

Current reflects the transport of charges between two spatially different locations. The motion of a charged particle in a solid such as a metal can be described by the contribution of two different types of motion.

In the absence of an electric field, the free electrons of the metal perform a random motion that has been described as the motion of an electron gas. The electrons that make up this gas have a mass $m$, posses a velocity $\vec{u}_m$ and they exist in a thermal equilibrium due to collisions with neighboring electrons. The overall kinetic energy of the gas is smaller than the average potential energy of the attractive field of nuclei therefore no ionization effects take place. The scattering time of the electrons is considered vanishing in comparison with the average time interval $\tau$, between each scattering event. The mean free path $l = \tau * |\vec{u}_m|$ is the average distance between collisions of the electrons in the metal.

Upon the application of an electric field to the metal, a field force is applied on each of the randomly moving electrons, in the direction of the applied field. This force imparts directionality on the motion of electrons by developing a velocity that is opposite to the vector of the applied field. This is the drift velocity $\vec{u}_d$.

The application of an electric field on material results in current. For a material that obeys the Ohm law, this transport of charges is expressed from the current density J which is the number $n$ of charges $q$ that pass through a cross section $A$ of the material, per unit time. Current density $J$ is related to the drift velocity $\vec{u}_d$ by:

$$\vec{J} = n * q * \vec{u}_d \quad \text{eq. 1.22}$$

The dependence of drift velocity $u_d$ on the strength of the applied electric field E is expressed from:

$$\vec{u}_d = \mu * \vec{E} \quad \text{eq. 1.23}$$

where $\mu$ is termed carrier mobility and is the proportionality constant in the relationship of drift velocity and the electric field,

$$\mu = \frac{q * \tau}{m} \quad \text{eq. 1.24}$$

Charge carrier mobility $\mu$ is measured in $m^2*(V*sec)^{-1}$. The sign of q could be either positive or negative depending on whether the charge that is monitored is a hole or an electron, respectively. As it has been shown above, the description of the energy levels of molecules in the solid state can be done by the utilisation of Mott-Wannier or Frenkel approach in the excited states. Similarly the rationalisation of electrical conductivity in solids is achieved by the discrimination of charge carrier mobility in these two different concepts that have been presented. In the validity of a wide band-like structure of the energy levels, charge carrier mobility is $\mu$ $>>1cm*(V*sec)^{-1}$ and its temperature dependence exhibits the type of $\mu \propto T^{-n}$ with n>1. In the other extreme case that the charge carriers are strongly localised on molecular sites, conductivity is mediated by hopping of the carrier between the molecular sites and the carrier mobility is $\mu$ $<<1cm*(V*sec)^{-1}$ with a temperature dependence that includes an activation energy term that corresponds to the occurence of hopping $\mu \propto e^{-E/k*T}$. Like in the case of the electronic excitations, the band model corresponds to the collectivistic nature of the conduction state whereas the hopping model reflects the individualistic nature of the conduction state that is consisted of many molecular sites. Alternatively, the former model is reffered to as non-dispersive and the latter as dispersive.

## 1.11 PHOTOLUMINESCENCE DYNAMICS

The physical processes that can eventually lead to the emission of light from an optically active material such as a conjugated polymer are via optical or electrical excitation. Therefore, photoluminescence (PL) and electroluminescence (EL) are used respectively. Although the mechanisms of these two processes are different, PL as a result is not differing from EL and therefore PL spectroscopic studies can contribute valuable information regarding the behaviour of the studied material as an EL component. Apart from the fact that different routes to the excited state exist, the methods of studying this excited state once it is reached are also different. Time integrated techniques can be applied if the equilibrated nature of the excited state is the

object under study. Otherwise, time resolved methods should be used in order to clarify the dynamics of the excited state. Especially in the case of conjugated polymers where disorder is contributing significantly to the macroscopic properties of the material, dynamic phenomena such as energy transport are relevant to time resolved studies. Furthermore since the optical performance of a conjugated polymer is largely dependent on the existence of quenching centres, time resolved techniques can be applied if the nature of the quenching centres and the photoluminescence quenching rates are to be revealed.

## 1.11.1 Single exponential decay transient

Once an electronically excited state has been reached, a temporal change in the population distribution is taking place in the total system. This disturbance of the equilibrated system is gradually restored in a transient fashion. The excess of the energy given to the system is dissipated through the pathways that have been described in paragraph 1.2.3. Figure 1.15 present an ideal three level system together with the most representative photophysical processes that take place after the absorption of a photon. According to the Einstein thermodynamic description for the radiative transitions in an atomic two-level system, there is a constant probability in which the excited level will emit a photon, with energy equal to the energy gap that will lead the system back to its ground state:

$$w' = \beta \Leftrightarrow \frac{dn_t}{dt} = -\beta * n_t \Leftrightarrow ... \Leftrightarrow n_t = n_0 * \exp(-\beta * t) \Leftrightarrow I_t = I_0 * \exp(-\beta * t) \quad \text{(eq. 1.25)}$$

where $\beta$ is the probability for emission and, $w'$ is the depopulation rate of the excited state, whereas $n(t)$ and $n_0$ is the population of this state at time t and t=0, respectively, after the absorption of the photon. Since, population of the excited state is proportional to the intensity of the emitted light, $n_0 = I_0$ and $n(t) = I(t)$.
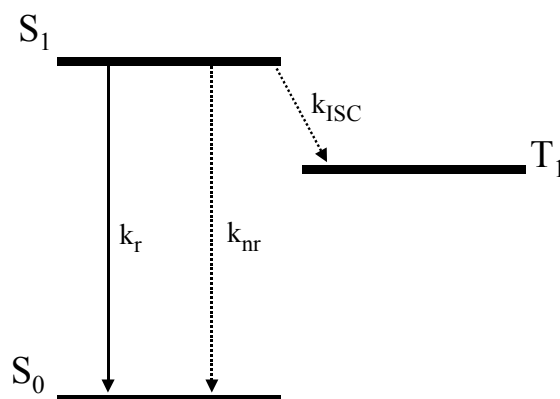
Figure 1. 16: The possible deactivation pathways of an excited state and their corresponding relaxation rates: $k_r$ for radiative relaxation, $k_{nr}$ for non-radiative relaxation and $k_{ISC}$ for intersystem crossing (see paragraph 1.2.3).

Based on the last term of eq. 1.25 it becomes evident that the transient intensity of the photoluminescence, which originates from a two-level system should follow an monoexponential decay law with a characteristic time constant $\beta$. This time-constant reflects the probability for the occurrence of relaxation. Therefore the higher the probability for deactivation, the faster the observable deactivation rate $k_{obs}$ and thus, the shorter is the lifetime $\tau_{obs}$ of the excited state:

$$\beta_{10} \propto \left(k_{r.} + k_{nr}\right) = k_{obs} = \frac{1}{\tau_{obs}} \qquad \text{(eq. 1.26)}$$

From the combination of eq. 1.25 and 1.26, the expression for the monoexponential decay of an excited state population is :

$$I(t) = I_0 . e^{-t/\tau_{obs}} \qquad \text{(eq. 1.27)}$$

As Figure 1.16 shows, in the presence of additional decay pathways such as intersystem crossing or a significant vibrational coupling between e.g. C-H oscillators and the electronically excited energy level, the deactivation rate is further enhanced:

$$k_{obs} = k_r + k_{nr} + k_{ISC} = k_r + \sum_i k_i \qquad \text{(eq. 1.28)}$$

where $k_i$ represents the monomolecular deactivation rate of the upper excited state due to any non-radiative channel. By using these expressions, the quantum yield of fluorescence can alternatively be defined as:

$$\Phi = \frac{k_r}{k_r + \sum_i k_i} = \frac{k_r}{k_r + \sum_i k_i} = \frac{\tau_{obs}}{\tau_r} \qquad \text{(eq. 1.29)}$$

According to Stricler-Berg relationship (eq. 1.6), the raditive lifetime of an excited state is reciprocally related to the oscillator strength of the involved transition. The physical interpretation that underlies in the Stricler-Berg expression is based on the fact that the more allowed is a transition, the less time will spend on the excited level involved.

## 1.11.2 Multiexponential decay transients

In many cases the transient decay curve of an excited state deviates from the monoexponential decay and follows decay kinetics similar to these of Figure 1.17. In this case the obtained transients are better described by a multiexponential decay equation of the type:

$$I(t) = \sum_{i=1}^{n} a_i * e^{-t/\tau_i} \qquad \text{(eq. 1.30)}$$

where $a_i$ and $\tau_i$ reflect the amplitude and the corresponding lifetime, respectively. The emerging complication that arises from the mathematical expression of eq. 1.30, is the relationship of $a_i$ and $\tau_i$ parameters. These two factors are strongly correlated and therefore, in the presence of a series of ($a_i, \tau_i$) pairs, a careful interpretation of the obtained fitting parameters should be performed.
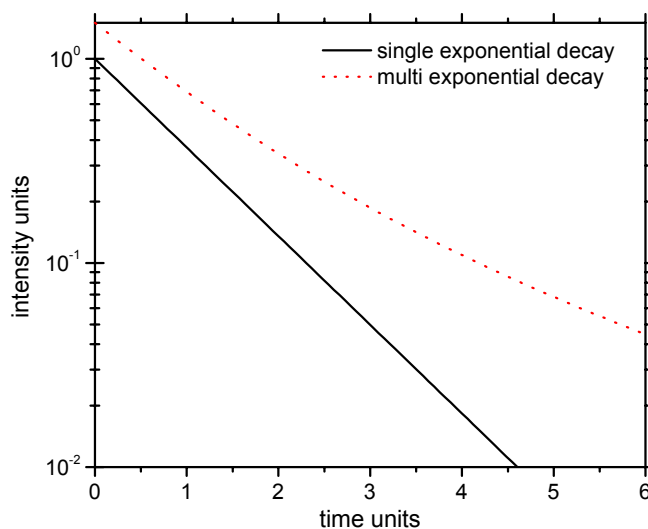
Figure 1. 17: A schematic illustration for the function type of the decay transient of a monitored emission intensity: single exponential decay (solid line) and multiexponential decay (dotted line), depicted in a semilogarithmic plot.

The presence of more than one observable lifetime co-existing with their corresponding amplitudes indicates the existence of a complex decay law. This complexixity can be attributed to different chromophores that emit in the same monitored spectral region or of one chromophore that is distributed into different molecular environments. The latter case can also be attributed to a distribution of different conformations of the molecular unit in which the chromophore is attached or embedded into. Finally the deviation of a decay transient of a monitored excited state from the monoexponential decay, is many times related to the existence of bimolecular events such as energy transfer to a different optical centre. The presence of an optical centre, which fulfils the requirements for energy transfer, will open up an additional depopulation channel of the excited state. This new optical centre will act as a acceptor that will collect the excitation energy of the donor by means of resonance energy transfer. If alternatively the depopulation of the donor is induced by the acceptor by means of colissional processes, the deactivation of donor's excited state can be described as simple colissional quenching. Chapter 3 presents the Stern-Volmer formalism according to which a collisional quenching process can be treated.

 Especially for the case of $\pi$-conjugated polymers, where the ensemble of excited states is subject of the statistical distribution of the conjugation length, another model has been suggested for the interpretating the deviation of the decay from the monoexponential behavior. As the distribution of conjugation length will result a distribution of the relaxation times the stretched

exponential decay function of Kohlrausch-Williams-Watts (KWW), that eq. 1.31 describes, has been used:

$$I(t) = I_0 * \exp\left[(-t/\tau)^\beta\right] \quad \text{eq. 1.31}$$

where $\beta$ is related to the distribution of decay times and $0 \leq \beta \leq 1$.

In the case of chromophores that are embedded in film geometries, the determination of emission quantum yield is a relatively complicated procedure. Quantum efficiencies of thin films mostly refer to the quantum efficiency of the sample studied and not to the inherent material that makes up the film. This peculiarity on the quantum yield determination in thin films arises from the dependence of the quantum efficiency on structural parameters of the films that are not always accurately, reproducible (film thickness, nature of the substrate, etc). In the case that time resolved photoluminescence experiments are available, they may provide information regarding the lifetime-weighted quantum yield values. These values might be more easily obtained than those from the usage of an integrating sphere. Lifetime-weighted quantum yield values can be obtained via the average lifetime $\langle \tau \rangle$ given by:

$$\langle \tau \rangle = \sum_i \alpha_i . \tau_i = \int_0^\infty I(t) . dt \qquad (\text{eq. 1.32})$$

## 1.12 REFERENCES

1.      McGlynn S.P.& Azumi T. & Kinoshita M., *Molecular Spectroscopy of THE TRIPLET STATE*. 1969, Englewood Cliffs, New Jersey: Prentice-Hall, Inc.
2.      Guillet J., *Polymer Photophysics and Photochemistry , An Introduction to the Study of Photoprocesses in Macromolecules*. 1985, Cambridge, New York: Cambridge Univ. Press.
3.      Klessinger M. & Michl J., *Excited States and Photochemistry of Organic Molecules*. 1995, New York, Weinheim, Cambridge: VCH Publishers, Inc.
4.      Lakowicz J.R., *Principles of Fluorescence Spectroscopy*. 2nd ed. 1999, New York, Boston, Dordrecht, London, Moscow: Kluwer Academic/Plenum Publishers.
5.      Pope M. & Swenberg C.E., *Electronic Processes In Organic Crystals and Polymers*. Second ed. 1999, New York, Oxford: Oxford University Press.
6.      Sariciftci N.S., ed. *Primary Photoexcitations in Conjugated Polymers: Molecular Excitation versus Semiconductor Band Model*. 1997, World Scientific, Singapore.
7.      Hoffmann R., Janiak C., Kollmar C., *A Chemical Approach to the Orbitals of Organic Polymers*. Macromolecules, 1991. **24**(13): p. 3725.
8.      Kohler B.E., *A simple model for linear polyene electronic structure*. J. Chem. Phys., 1990. **93**(8): p. 5838.
9.      Tolbert L.M., *Solitons in a Box: The Organic Chemistry of Electrically Conducting Polymers*. Acc. Chem. Res., 1992. **25**(1992): p. 561.
10.     Choi H.-Y., Rice M.J., *Excited polarons in poly(phenylene vinylene) and poly(diacetylene)*. Phys. Rev. B, 1991. **44**(19): p. 10521.
11.     Basescu N., Liu Z.-X., Moses D., Heeger A.J., Naarmann H., Theophilou N., *High electrical conductivity in doped polyacetylene*. Nature, 1987. **327**: p. 403.
12.     Philpott M.R., *Excitons in Polymerised Diacetylenes*. Chem. Phys. Lett., 1977. **50**(1): p. 18.
13.     Movaghar B., Grünewald M., Ries B., Bässler H., Würtz D., *Diffusion and relaxation of energy in disordered organic and inorganic materials*. Phys. Rev. B, 1986. **33**(8): p. 5545.
14.     Hagler T.W., Pakbaz K., Voss K.F., Heeger A.J., *Enhanced order and electronic delocalization in conjugated polymers oriented by gel processing in polyethylene*. Phys. Rev. B, 1991. **44**(16): p. 8652.
15.     Mollay B., Lemmer U., Kersting R., Mahrt R.F., Kurz H., Kauffmann H.F., Bässler H., *Dynamics of singlet excitations in conjugated polymers: Poly(phenylenevinylene) and poly(phenylphenylenevinylene)*. Phys. Rev. B, 1994. **50**(15): p. 10769.
16.     Rothberg L.J., Yan M., Papadimitrakopoulos F., Galvin M.E., Kwock E.W., Miller T.M., *Photophysics of phenylenevinylene polymers*. Synth. Met., 1996. **80**: p. 41.
17.     Kersting R., Mollay B., Rusch M., Wenisch J., Leising G., Kauffmann H.F., *Femtosecond site-selective probing of energy relaxing excitons in poly(phenylenevinylene): Luminescence dynamics and lifetime spectra*. J. Chem. Phys., 1997. **106**(7): p. 2850.
18.     Ern J., Bock A., Lionel O.-M., Heiko R., Wegner G., Trommsdorff H.P., Kryschi C., *Femtosecond Study of Exciton Transport Dynamics in (Phthalocyanninato)polysiloxane*. J. Phys. Chem. A, 1999. **103**: p. 2446.
19.     Karaburnarliev S., Bittner E.R., Baumgarten M., *Franck-Condon spectra and electron-libration coupling in para-polyphenyls*. J. Chem. Phys., 2001. **114**(13): p. 5863.
20.     Wong K.F., Bagchi B., Rossky P.J., *Distance and Orientation Dependence of Excitation Transfer Rates in Conjugated Systems: Beyond the Förster Theory*. J. Phys. Chem. A, 2004. **108**: p. 5752.

21.     Dimitrakopoulos C.D., Malefant P.R.L., *Organic Thin Film Transistors For Large Area Electronics.* Adv. Mater., 1999. **14**(2): p. 99.

22.     Nelson J., *Diffusion-limited recombination in polymer-fullerene blends and its influence on photocurrent collection.* Phys. Rev. B, 2003. **67**: p. 155209.

23.     Nelson J., Choulis A.S., Durrant J.R., *Charge recombination in polymer/fullerene photovoltaic devices.* Thin Solid Films, 2004. **451-452**: p. 508.

24.     Moses D., Dogariu A., Heeger A.J., *Ultrafast detection of charged photocarriers in conjugated polymers.* Phys. Rev. B, 2000. **61**: p. 9373.

25.     Moses D., Dogariu A., Heeger A.J., *Ultrafast photoinduced charge generation in conjugated polymers.* Chem. Phys. Lett., 2000. **316**: p. 356.

26.     Miranda P.B., Moses D., Heeger A.J., *Ultrafast photogeneration of charged polarons in conjugated polymers.* Phys. Rev. B., 2001. **64**: p. 081201.

27.     Schindler F., Jacob J., Grimsdale A.C., Lupton J.M., Scherf U., Müllen K., Feldmann J., *Counting chromophores in conjugated polymers.* Angewandte Chemie Int. Ed., 2004. **44**(10): p. 1520.

28.      V. Ern in *Energy Transfer Processes In Condensed Matter*, (Di Bartolo B. ed.)  1983, New York, London , Plenum Publishing Corporation,  NATO series, Vol. 114, B: Physics.

# 2 PHOTOPHYSICAL PROPERTIES OF POLY- AND OLIGO-(FLUORENE) DERIVATIVES

## 2.1 LIGHT-EMITTING POLYMERS

In the advent of developing novel organic functional materials, conjugated polymers have attracted a significant degree of attention for their implementation in the emerging area of molecular optoelectronics. Since the realisation that certain polymers can be conductive, a vast research effort has opened up the prospects of using conjugated polymers in such a way that it is set to change everyday life. Polymers have already started to revolutionise electronics and it is expected that they will contribute further to the general trend of miniaturisation technology.

Especially in the field of optoelectronics, the scientific community has focused upon the electronic properties of $\pi$-conjugated polymers as the latter can potentially be used as chromogenic materials, able to be incorporated in devices that are meant to be for the emission of light. Furthermore, there are also technological applications where the polarisation of the emitted light is of great importance. This is why in the context of light-emitting polymers, polarised light emitters have attracted a special attention of the material scientists.

Of great significance both scientifically and commercially is the technology of flat, flexible plastic screens and polymer light-emitting diodes (PLEDs). These devices have their operative principle based on the property of semiconducting polymers to emit light upon excitation with an applied voltage. This phenonomenon known as electroluminescence can be achieved if a layer of semiconducting polymer is placed in between oppositely charged electrodes. Injection of charge carriers from the electrodes into the polymer layer is subsequently followed by charge recombination that gives rise to emission of the desired light. There are currently important drawbacks in the aforementioned process. The electrochemical stability of the active polymer layer is a major issue that needs to be optimised in order the desired spectral stability of the device to be obtained. Moreover a balancing of the negatively and positively charged carriers that are injected must be accomplished. This issue is related to the charge carrier mobility, which for electrons and holes is not the same.
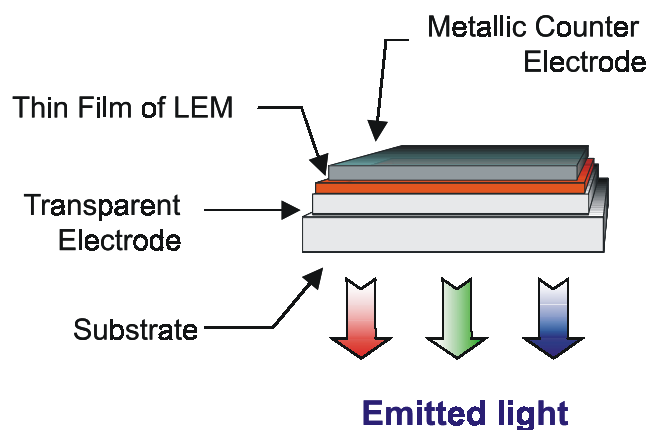
Scheme 2.1: A typical structure of a polymer based light-emitting diode. Upon applying voltage on the two electrodes that sandwich the thin film of the active light-emitting polymer, electroluminescence is observed.

Although the field of optoelectronics is traditionally saturated by the exploitation of inorganic assemblies, there are several reasons for justifying the use of polymers as building blocks of optoelectronic devices. Even if comparison of performance is still tilting the balance towards the side of inorganics, there are a few attracting arguments regarding polymers that are worth considering with the most significant of them to be the good processabilty, low operating voltage and fast response time of polymers. More importantly, the tunability of the emission profile via chemical substitution onto the polymer framework gives to the polymers an extra degree of freedom regarding material selection and device fabrication. Additionally the appropriate colour gamut, which is needed for the realisation of a full colour display, can be in principle obtained from the combination of a central polymeric high-energy emitting host and other incorporated low-energy emitting guests. Such a utilisation of energy transfer phenomena is a well-known method for the development of photonic materials based on host/guest systems of inorganic lattices (mostly those composed of the rare-earth transition elements) or small organic molecules.

## 2.2 POLY(FLUORENE) AS A BLUE LIGHT-EMITTING POLYMER

In principle for a light-emitting polymeric material that is to be incorporated in a optoelectronic device such as light-emitting display the basic requirements contain issues of stability (photochemical, thermal and electrochemical), carrier-injection and transport ability, excellent film forming capability that includes high solubility of the active polymer. Beginning from the early studies of poly(p-phenylene)s (PPPs), progress in synthetic approaches led to the more easily processable poly(fluorene)s (PFs), as materials of interest for optical applications [1], [2],

[3]. PFs are comprised of alternate phenylene rings that are linked by the C-9 carbon atom bridge of $sp^3$ hybridization (the so-called ladder type bond). In comparison with the case of PPPs, PFs have a more planar geometry due to the rotational hindrance that the C-9 atom introduces between the two benzene rings.  Particularly for the C-9 carbon atom of the monomer unit, the ability for functionalisation with appropriate side-chains that increases the solubility of the polymer, consequently to better processing. As the need for large energy gap emitting organic materials of high efficiency, aiming to serve both as blue emitters or as energy transfer donors, is still unsatisfied, a great body of data is currently collected aiming for the correlation of the mechanical and structural features of PFs with their corresponding optical properties. PF has high photoluminescence (PL) quantum efficiency and in combination with its high-energy optical gap of (absorption peak ~3.2 eV, emission peak ~2.95 eV [2]), PF can serve as a donor (sensitiser) for electronic energy transfer to a lower energy acceptor (activator). In that way colour tuning can be achieved by the energy transfer from the host (sensitiser) to the guest (activator) moiety. Particularly for PF such systems have been demonstrated by blending of the two components [4], [5] or by their covalent linkage [6] (via co-copolymerisation [7], [8] ,[9], [10] or/and side chain substitution [11], [12]).
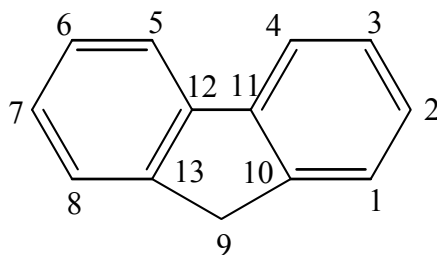


Scheme 2.2: The chemical structure of the fluorene unit.

The internalisation of light-emitting polymers in structures of confined geometry can potentially lead to the development of polymer based optolelectronic devices e.g. polymer based lasers [13]. Within this context, studies on the light amplification in poly(fluorene) waveguides have been presented [14]. Further more due to the broken centrosymmetry in PF derivatives the non-linear optical properties of PFs have also been investigated [15]. Apart from the scientific interest for the determination of the two-photon absorption (TPA) cross-sections, non-linear studies PFs aim to the development of translucent polymer based displays that could be written via TPA with a red/near infra-red laser [15]. Due to their shape persistent macromolecular nature, PF derivatives have also stimulated the interest for chain conformation studies [16], [17].

## 2.2.1 Polymer based optoelectronics: Charge carrier mobility

The phenonomenon of electroluminescence is in principle based on the recombination of oppositely charged carriers that are transported within the optoelectronic material, after charge injection. Electroluminescence occurs after a series of steps. Following charge carrier recombination, formation of an exciton takes place, which subsequently diffuses within the recombination zone of the active material. Finally the formed exciton returns to the ground state via radiative and/or non-radiative processes. Therefore it becomes clear that in order to optimise the electroluminescence efficiency of a light-emitting diode, one has to take care of the important parameters related to each of the steps of the electroluminescence process.

Long after the demonstration of efficient electroluminescence emission from an organic-based device [18], a π-conjugated polymer based LED was realised [19]. The active material was a PPV derivative and the observed electroluminescence was centred in the orange region of the spectrum (~ 565 nm).
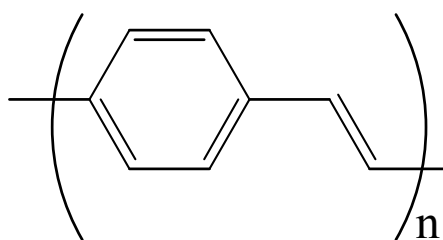


Scheme 2.3: The chemical structure of poly(phenylenevinylene) (PPV) unit.

Later on a PF derivative was used as the active electroluminescent polymer, thus resulting in blue emission [20]. Since then various works have been reported regarding electroluminescence of π-conjugated polymers [21], [22], [23].

Practically the conditions of preparation and the film morphology are crucial factors for the device efficiency. Additionally, the harvesting of all the generated excitons that are produced and the activation of their radiative relaxation channels, is another active field of scientific and industrial research [24].While the absorption and photoluminescence characteristics have been found to be slightly affected from the film thickness, in the case of electroluminesecence this dependence is more pronounced [25]. In order to explain this influence, optical interference effects have been invoked [25]. The rationalisation of these affects have been based on the solution of the one-dimensional inhomogeneous Helmholtz equation, from which the transmission and reflection Fresnel coefficients have been derived. In this theoretical approach [25], the polymer based-LED has been visualised as a multilayer stack whose emission spectra are dependent on the thickness and the refractive indices of the individual layers. By assuming a source consisting of an oscillating point dipole placed within this layered medium, the Helmholtz

equation has been solved. Although the theoretical results did not agree well with the experimental data, the influence of the optical interference effects on the emissive properties of LEDs has been shown.

Even more important though, is the establishment of a balanced ratio of oppositely charged carriers that reach the recombination zone of the material prior to exciton formation. Due to the significant differences in the mobility of the oppositely charged carriers, it turns out that within the recombination zone of almost all polymer materials, the number of holes is higher than that of electrons. Practically the field of polymer based optoelectronic devices such as thin-film-transistors and displays, required charge carrier mobility in the order of 0.1 $cm^2*V^{-1}*s^{-1}$. As it has been described in Chapter 1, charge carrier mobility can be described by to distinct temperature dependence algorithms, depending on the nature of the mechanism of charge transport. Particularly for PF, the hole mobility has been determined to be non-dispersive both for isotropic [26] and oriented films [27]. Moreover a group of phenylenediamine PF-copolymers has been found to exhibit non-dispersive hole transport [28]. These conclusions have been extracted from results of time-of-flight measurements, however no temperature dependence measurements have been performed.

For PF-based LEDs, it has been shown that incorporation of hole trapping molecules, such as aromatic amines, results in an increase of electroluminescence yield and an improvement in the colour stability [29], [30]. Moreover, the brightness of an electroluminescence device is another important parameter to be optimised. In the case of passive matrix displays where each of the pixels is activated only for a fraction of time, the targeted peak brightness has a level higher than $10^5$ cd/$m^2$ [28]. A typical averaged luminescence value is 100 cd/$m^2$, which corresponds to the brightness a computer monitor [22]. Adding to that the fact that such brightness values should be achieved at low bias voltages for reaching acceptable power efficiencies, it is clear that charge carrier mobility is a key-parameter in the development of light-emitting devices. In practice, conjugated polymers have shown to have a range of hole mobility values between $10^{-5}$ and $10^{-4}$ $cm^2*V^{-1}*sec^{-1}$. In the case of poly(fluorene)-copolymer an even more promising hole mobility value was reported in the order of $3*10^{-3}$ $cm^2*V^{-1}*sec^{-1}$ at a bias field of $2.5*10^5$ V/cm [28]. This experimental value was deduced via time-of-flight current measurements. Alternatively, the time-resolved microwave conductivity technique has been exploited for the determination of hole mobility [31]. The generation of positive charge carriers in a PF derivative and the subsequent hole transfer to hole transport functional groups has also been studied by pulse radiolysis [32].

By exploiting the liquid-crystalline nature of PF, homogeneously aligned films of a PF derivatitive were prepared on rubbed polyimide and a hole mobility value of $8.5*10^{-3}$ cm$^2$*V$^{-1}$*sec$^{-1}$ at a bias field of $10^4$ V/cm was observed, normal to the alignment direction [33]. Furthermore, the construction of a thin-film-transistor has been realised based on an oriented monodomain for a PF copolymer deposited on an alignment layer. This device exhibited a mobility anisotropy of 5-8 for current flow parallel and perpendicular to the alignment direction [34].

## 2.2.2 Physicochemical states: Liquid Crystallinity

An extra advantage of PFs is their liquid crystaline character. PFs can in general be categorised into the class of calamitic liquid crystals [35] and in principle, many different phases can be expected from these materials. The further assignment of those mesophases that can be obtained from fluid PFs is still under discussion.

In principle, for a liquid crystalline material several intermediate phases can be obtained by temperature adjustment during heating, before the material reaches the melting point where it is transformed to an isotropic liquid. In particular, the nature and perfection of the liquid crystalline phase of PFs can be manipulated either by means of thermal treatment (thermotropic liquid crystal phases) or by selection of a specific solvent (lyotropic liquid crystal phases).

Due to the rigid-rod shape of the PF molecules, their backbone provides an anisotropy to one of the inherent molecular axes. The existence of structures corresponding to both nematic and smectic liquid crystal phases has been postulated in order to explain the experimental results obtained from structural studies performed for PFs by means of X-ray experiments (see paragraph 2.2.3). In a nematic mesophase the individual molecules are uncorrelated except that one of the molecular axes is preferentially oriented along an imaginary axis, the director *n* [35]. In contrast to the nematic phase, the smectic mesophase is more ordered and the formation of layers is observed. The director *n* is in this case considered as a vector that indicates the average orientation of the long molecular axis in each layer [36]. In addition the smectic mesophase exhibits polymorphism; more than one smectic mesophase has been idientified [35]. Figure 2.1 shows the different liquid crystal phases that a rigid-rod molecule can adapt to.
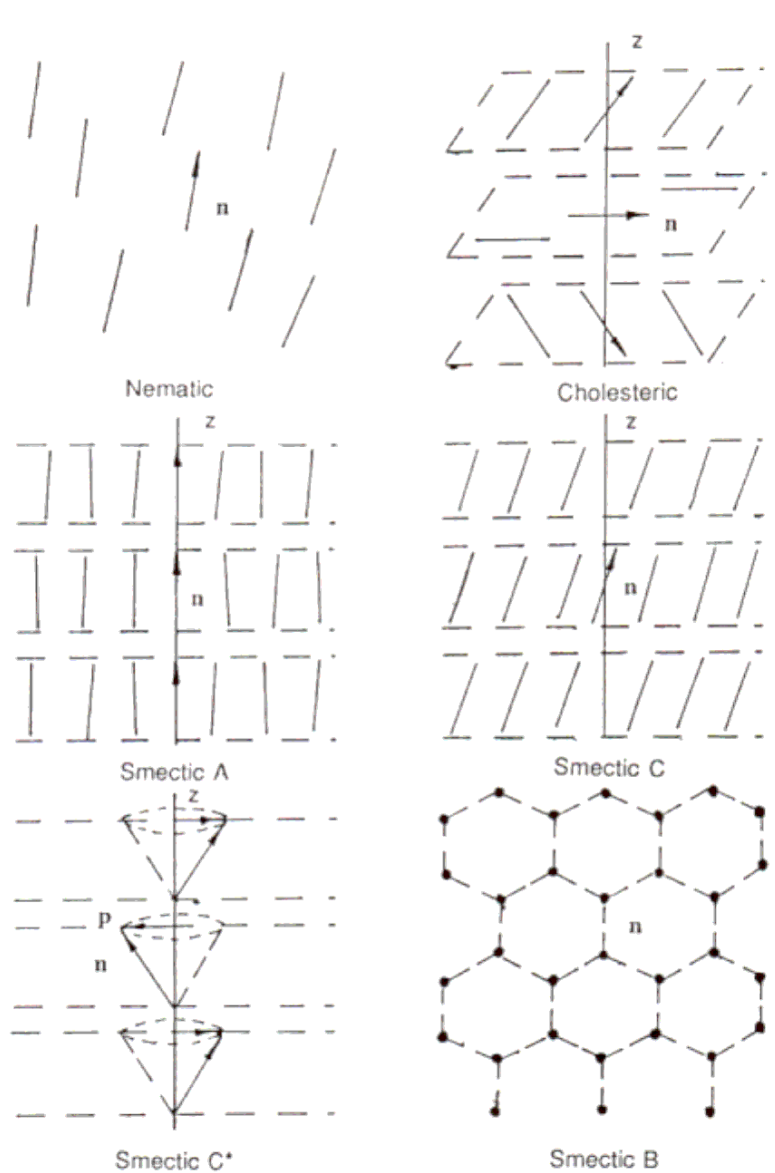
Figure 2. 1:The different liquid crystal phases that a rigid-rod molecule can adapt (from [36]).

 The impact of the liquid crystalinity of PFs to their optical properties is reflected in the optical anisotropy that can be reached when films of PFs have been oriented [2],[37], [38], [39]. A direct measure of such an anisotropy is obtained by the dichroic ratio or polarisation ratio, depending on the type of optical data that were used (absorption or luminescence profiles, respectively). Several methods for orienting a liquid crystalline material exist such as stretching-induced alignment, rubbing-induced alignment, Langmuir-Blodgett-induced alignment or liquid-crystalline self-organisation [40]. More recently alignment of poly(fluorene)s on photo-addressable polymers has been reported [39].

 The first example of an oriented PF derivative, bearing linear octyl side chains, was given after the alignment of the material into a monodomain on rubbed polyimide [37]. After reaching the liquid crystalline mesophase of the polymer, rapid cooling of the system forced the polymer to

solidify in form of a glass with the structure of well-defined liquid crystalline phase. Great improvement has been achieved in the increase of dichroic ratio and polarisation ratio values for light-emitting diodes that were both based on poly(fluorene)s and oligo(fluorene)s [2], [38], [41]. An additional advantage is given in the case of oligomers since the film forming properties and the optical characteristics are maintained with simultaneous increase of chemical purity. This aspect is discussed in more detail in paragraph 2.4.2.

## 2.2.3 Structural investigation

PF derivatives exhibit a variety of liquid crystalline mesophases. The thermotropic liquid crystalline ordering in PF is mainly related to the nature of the side chains of the polymer backbone. Hence, the  molecular packing that the different observed structural patterns reflect will be strongly affected by the nature of the pendant groups. X-ray studies provide information on the spatial arrangement of the atoms that comprise the studied molecular structure. Therefore, X-ray and electron diffraction studies have suggested that different molecular arrangements exist dependent on the whether the side chain is of linear or branched alkyl character [38], [42], [43], [44] .

The first report on X-ray investigations of a PF derivative was based on data collected for extruded filaments that had been subjected to different treatment protocols [38]. Due to the linear octyl pendant chains of the studied PF derivative (PFO), the polymeric backbone adapted an extended planarisation that led to a much longer effective conjugation length than the one observed in the PF derivatives bearing branched side chains. The fully extended planarised chain segment was described as a 'planar zigzag' or $2_1$ conformation. Alternatively, this structural characteristic has been referred to as the 'β-phase'. Although the term 'phase' should be correlated with a distinct thermodynamic parameter, in the present case the authors used this term as an empirical expression rather than as a thermodynamic description of the material. This unique order characteristic, results in the appearance of specific spectroscopic changes in thin films, such as a new low-energy absorption band and a red-shift of the PL maximum. The impact of the 'β-phase' presence on exciton migration in PFO films has recently been reported [45], [46]. Rigorous photophysical investigation was based on site-selective excitation of the 'β-phase'absorption peak.

Complementary Raman spectroscopy investigations on the different phases of the PF derivatives bearing linear alkyl side chains, have correlated the obtained thermodynamic phases with the corresponding conformations of the polymer [47]. The order-disorder transition of PFO derivative has been studied [46]. Alternatively, the presence of branched alkyl groups as

substituents forces the PF derivative to adapt   a of $5_2$ helical conformation [42]. Grazing-incidence X-ray diffraction measurements have been performed both for linear and branched alkyl-derivatised PFs [43], [44]. In the case of the linear alkyl derivatives the polymer backbone was found to lie in the plane of the substrate surface, while the spacing between polymer chains normal to the surface was found to be influenced from the length of the side chains [43].

As it has been described in paragraph 1.6.2, for rigid rod-polymers such as PFs, the intermolecular interactions can be mainly represented by the dipole-dipole moment interactions. Moreover, in the solid state where positional disorder prevails, the intermolecular interactions might be better represented by the Van der Waals or London dispersion interactions. In principle, the nature of the side chain will affect the status of the interchain interactions in the solid state. Due to the presence of the linear side chains, side chain crystallisation occurs and results the formation of crystalline islands distributed in between amorphous regions. Very recently transmission electron microscopy has been applied for studying the molecular packing of crystalline PFO [48]. In contrast to that, branched side-chains will tend to surround the main polymeric backbone and result in supramolecular cylindrical objects.

## 2.2.4 Photoluminescence dynamics

The blue emission of poly(fluorene) is a consequence of an electronic $\pi$-$\pi^*$ transition that results in an intrachain singlet exciton which participates in the radiative transition [2]. The variety of film morphologies that films of PF derivatives may posses influence strongly their photophysical properties [49], [50]. The radiative quantum yields of the prompt photoluminescence in PFs were studied as a function of pressure at room temperature and at 20 K [51]. The authors presented results where the pressure regime reached was lower than that of one bar. Unfortunately, they presented a comparison between fresh PF films under pressure and old PF films at room pressure. This fact makes their conclusion unclear as far as the origins of the spectral differences that they observe we concern. It was not clarified whether the differences they observed where due to ageing of the studied films or due to the high pressure that their samples had experienced.

In Chapter 1 it has been discussed that that the electronic levels of a $\pi$-conjugated polymer are significantly influenced from the distribution of effective conjugation lengths of the polymeric chains that the film is comprised of. Photoexcitations are considered to relax within the density of states (DOS) of the polymer via a *ps* hopping mechanism [52]. Especially for a representative PF derivative, the relaxation dynamics of the photoexcitations in a film have been extensively studied by means of ultra fast time resolved fluorescence spectroscopy [53], [54]. A similar experiment was presented for a monodomain of the same PF derivative  that had been aligned on

rubbed polyimide [55]. In this work time dependent photoluminescence spectroscopy was utilised in order to study the molecular anisotropy by means of time resolved depolarisation. Through these experiments the molecular excitonic character of the excited states in $\pi$-conjugated polymers was confirmed, as proposed earlier for the case PPV [56].

In practice, the photoluminescence transients of PF derivatives are found to depart from the monoexponential decay patterns [45], [57]. A biexponential function was used to fit the singlet emission transients of poly(fluorene) in solution [57]. The existence of two emission lifetimes was attributed to two main relaxation processes that were arising from poly(fluorene) segments with different degree of chain-relaxation after the absorption of the excitation pulse. In another work regarding the dynamics of exciton migration in a poly(fluorene) derivative as film, a biexponential emission decay, after laser excitation, was reported [45]. This experiment gave evidence for the existence of a fast and a slow decay component in the collected decay transients. The fast decay component ( 25 *ps* ) was interpreted as indication of rapid energy transfer of the photoexcitation from high-energy sites towards lower-energy sites of the density of states (DOS) whereas the relatively slower decay component ( 150 *ps* ) was attributed to radiative excitations that became localised in the DOS, unable to undergo further migration to lower-lying energy sites. The determined relaxation times were far shorter than the times corresponding to segmental relaxation of PF and oligo(fluorene) derivatives [58]. Therefore, after optical excitation and during the dissipation of the given excitation energy, PFs in the solid state are considered immobilised systems, with regard to segmental motion.

In cases where electronic energy takes place from poly(fluorene) to other acceptor groups, the observable fluorescence lifetime of PF is found significantly reduced [59], [60]. The acceptor groups were intentionally chosen e.g. in order to enhance the electron transport properties of PFs [61]. However energy transfer from PFs to acceptor groups is not always deliberately chosen. In many cases chemical defects exist in the polymer backbone that lead to the so-called spectral contamination of the PF blue emission.

## 2.2.5 Spectral purity

Polymer-based displays and light-emitting diodes should render emission of light in a controlled manner. For this reason the optical active polymers should exhibit narrow, if not monochromatic, luminescence of long operating time.

Especially in light-emitting devices based on polymer films, the thermal stability of the material is a crucial parameter that will determine the device performance [62]. Under conditions of applied bias a thermal stress is delivered in the polymeric film. Consequently the thermal

stability of the polymer will determine also the efficiency of the electroluminescence process [63]. In many cases a light-emitting device is comprised of more than one light-emitting component. In this case, the glass transition temperature $T_g$ of the polymer is a relevant parameter. If the thermal stress given to the device is such that the $T_g$ of one of the components is reached, phase separation may occur in the blend and lead to aggregation phenomena that will negatively affect the optical performance of the device.

In the presence of air, molecular oxygen may react with the polymeric segments and photo-oxidation of the polymeric film may take place. In the case of PPV derivatives, photo-oxidation was found to strongly affect the electronic properties of the polymer.

Apart from the reduced photoluminescence lifetime due to photo-oxidation in PPV, the most characteristic feature was the presence of an unwanted broad red-shifted emission band. The origin of this emissive signature was concluded to be keto sites that were incorporated into the polymer backbone via a photo-oxidative process. The photochemical reaction resulted in breaking of the vinylic double bond in favour of the formation of a carbonyl group [64]. The presence of keto defects was confirmed by their characteristic IR spectroscopic signature in PPV [64]. Additionally, it was found that photoconductivity for steady-state measurements of PPV-based devices showed an order of magnitude increase after the deliberate photo-oxidation of the PPV layer of the device [65]. Therefore it was suggested that keto sites due to their high electron affinity [66] could act as traps that would capture the emissive excitons and result in dissociation of the coulombically bound electron-hole pair that was formed in device after the absorption of light [65].

As poly(fluorene) derivatives are considered potential blue emitters in the field of polymer based displays, the spectral purity of poly(fluorene) luminescence is a major issue for further improvement. Like in PPV, PF derivatives exhibit a red-shifted emission located in the region of 530 nm. In comparison with PL, the defect emission signature was found to be much more pronounced in electroluminescence [50], [67]. The origin of this green spectral contamination in poly(fluorene)s was assigned to a combination of processes [68], [69], [70], [71]. An early report had argued for aggregation effects that lead to excimer formation that was followed by the production of photo-oxidation. This photochemical reaction eventually leads to the formation of fluorenone defects on the PF backbone [69]. The same spectral red-shifted feature was observed in the electroluminescence of a PF-based LED. In this report the green emission was interpreted as a result of the low molecular weight ($M_w$) segments of PF that due to their high chain mobility could aggregate. The authors separated the low $M_w$ part in a GPC column. By using the fraction of the polymer with $M_w$ higher than 10000 they observed the absence of the green spectral

feature in EL. However no proof for the colour stability of the high $M_w$ based device was presented and therefore, their making their hypothesis shows lack of convincing evidence [72].

Like in the case of PPV, the presence of fluorenone defects was confirmed by their characteristic IR spectroscopic signature in films of poly(fluorene) [69]. A mechanism of introducing a keto defect site on the poly(fluorene) backbone was formulated [70]. According to this suggestion, the formation of fluorenone sites on the polymeric backbone of PF occurs on repeating units that are only partially substituted. Further support for this notion came from studies on the optical properties of monoalkylated and dialkylated PFs [73]. Efforts for the fluorene monomer purification and the removal of monoalkylated sites resulted in improved colour purity and stability of blue emission [71]. Time-resolved PL studies also detected fluorenone defects in dilute solutions of poly(fluorene)s where interchain interactions are vanishing small [74]. The polarization of fluorenone emission has been addressed in photo-oxidized aligned PF layers [75]. Fluorene-fluorenone copolymers were used as model systems for unravelling the nature of the observed red-shifted emission in PFs [76], [77]. These studies concluded that the fluorenone sites are the reason for the observed red-shifted PL band. The existence of fluorenone groups in copolymers of fluorene-fluorenone blended with an Iridium(III) complex lead to the observation of white light electro-phosphorescence from a light-emitting device based on poly(fluorene) [77]. The use of fluorene-fluorenone-fluorene trimer as a model compound for investigating the origin of this spectral feature, gave further supporting evidence for the importance of on-chain fluorenone defects on the spectral purity of PFs [78]. It was only very recently that another report argued for the notion that fluorenone itself could not be the reason for spectral impurity of PF, but a combination of interchain/intersegmental interactions with fluorenone defected sites was postulated as the origin of the unwanted band [79]. A crosslinking process induced by thermal oxidation in adjacent PF chains has been supported [80].

As it was mentioned in 2.2.3, a variety of structural patterns could be obtained in films of different PF derivatives. The issue of morphology in polymers relates to phenomena in which crystalline and non-crystalline regions of the polymer build a superstructure. Therefore the different side chain substitution of PFs consequently results in different film morphologies. This variety of mesoscopic order may affect significantly the optical properties of poly(fluorene) films due to enhanced interchain interactions. It was already described in Chapter 1, that aggregation of chromophores can result in either charge-transfer complexes or excimer moieties that will largely determine the optical properties of the bulk. It was experimentally demonstrated [81] that aggregation of poly(fluorene) derivatives induced by hydrogen bonding, gives rise to a

red-shifted emission band both in solution and in the solid state. The selection of side-chains to be attached on the C-9 carbon of the monomer fluorene unit seems to be of crucial importance for the morphology of the film and thus the type of aggregation in the obtained films. The correlation of the side-chain length in different PF derivatives with the extend of the observed interchain interactions, as probed by photophysical characterisation methods, has been reported [82]. The impact of obtained film morphology of a certain PF derivative on the PL quantum efficiency has also been addressed [49]. For reducing the effect of chain aggregation in PFs block-co-polymerisation of oligo(fluorene) segments with inert polymers has been reported. Block-copolymers with poly(ethylene-oxide) have been reported [83], [84]. More recently PF copolymerised with styrene and *tert*-butyl acrylate have been synthesised [85]. This type of rigid-rod-coil copolymers of PF seems to offer opportunities for further understanding of the impact of interchain interactions on the film morphology and spectral purity of PF [86]. However the issue of efficient charge transport in the films of these systems needs additional investigation, as it is a key-point for their implementation in a light-emitting device. Other synthetic attempts for the shielding of the PF backbone in order to prevent extended interchain interactions in the solid state are presented in paragraph 2.2.7.

## 2.2.6 Quantum-chemical studies and experiment

 The photophysics of conjugated polymers has been widely studied experimentally [87]. Since these materials are to be utilised as functional elements of optoelectronic devices, it is of paramount importance to explore their photophysical properties not only as single chains in dilute solution but also as bulk media e.g. as thin films [54], [88]. This condensed state brings difficulties since the degree of complexity is high due to unpredictable intermolecular interactions that arise from the relative positioning of the polymer chains in a film, resulting in so-called positional disorder. Such a state of interaction is far more complicated than the case of small molecules that are traditionally the field of molecular spectroscopy. Since the photophysics of polymers mainly deals with photoexcited species that are subject to strong intermolecular interactions [89], it is very likely that excited state interactions will dominate the photophysical landscape in the condensed state . This leads the discussion towards the area of excimers and/or exciplexes that potentially could be mediated by charge transfer processes. The main interest on the potential capability of conjugated polymers to form excimers/exciplexes is due to the strong impact of excimer formation on the photoluminescence quantum yields of excimer/exciplex containing films [90]. From small aromatic organic molecules it is known that the formation of excimers or exciplexes is essentially based on co-facial sandwich-type topologies (see Chapter

1). For example, the interplanar distance of the naphthalene excimer, as determined from pressure dependent measurements, has been found to be 0.3 nm [91].

Especially in the field of conjugated polymers the molecules are comprised of covalently linked aromatic rings that form stiff chains. The films obtained by spin coating of these systems are of disordered positional nature, and therefore the term excimer could as well represent entanglements consisting of more than two different chains. This type of configuration should mostly reflect an interchain geometry that has been kinetically locked in a solidified glass in the solid state, rather than an equilibrated co-facial dimer aggregate. The influence of interchain interactions on the photophysical properties of conjugated oligomers and polymers has been questioned by computational methods of correlated quantum-chemical calculations [92]. Similarly as in the case of small organic molecules, $\pi$-conjugated polymers may adapt a cofacial chain packing in the solid state. Both X-ray diffraction and computational modeling have concluded on the existence of supramolecular structures. These structures were of sandwiched-type and X-ray diffraction experiments have determined their interplanar distances to be in the order of 0.33 to 0.36 nm [90].

The effect of interchain separation between two cofacial segments on the electronic properties has been addressed by theoretical calculations [92]. For the particular case of interchain coupling of two stilbene units where one was superimposed on top of the other, it was predicted that the interplanar distance of the two interacting chains has a small effect on the photophysical properties of the single chain, when the value ranges between 3 and 0.8 nm. Within this range of interchain distances, even if there is interchain coupling, the optical properties of the resulting aggregate maintain the individual single chain character. In this weak coupling regime the electronic properties are still explainable via the dipole-dipole interaction model, as the Kasha model for aggregates describes (see also Chapter 1). Although it is equally probable to find the created photo excitation on each of the two chains of which the aggregate consists, the excitation transfer rate between the two units is low so as at any time the excitation is localised on a single chain. At a closer interchain distance of 0.7 nm the molecular orbitals of the interacting chains begin to delocalise on the entire dimer. These molecular orbital interactions give rise to the formation of a new set of frontier orbitals of the complex. Four new not degenerated levels are created with parity character different than the original orbitals of the isolated system. As a result of energy level mixing, parity allowed and forbidden transitions occur to the first excited state and to the second excited state, respectively. The energy splitting of these two excited states tends to increase as the interchain distance is decreased. The regime of strong interchain interactions was found to have an upper boundary limit of 0.5 nm.

Given a constant value of inter-planar distance, the role of positional disorder in the optical properties of an interacting system was investigated [92] (see Figure 2.2). The interacting system was studied in this literature was a highly symmetric complex of a co-facial dimer of two stilbene molecules separated by 0.4 nm. For this complex, the basic relative positions of the interacting units were selected by basic operations of translation and rotation performed in one of the units.
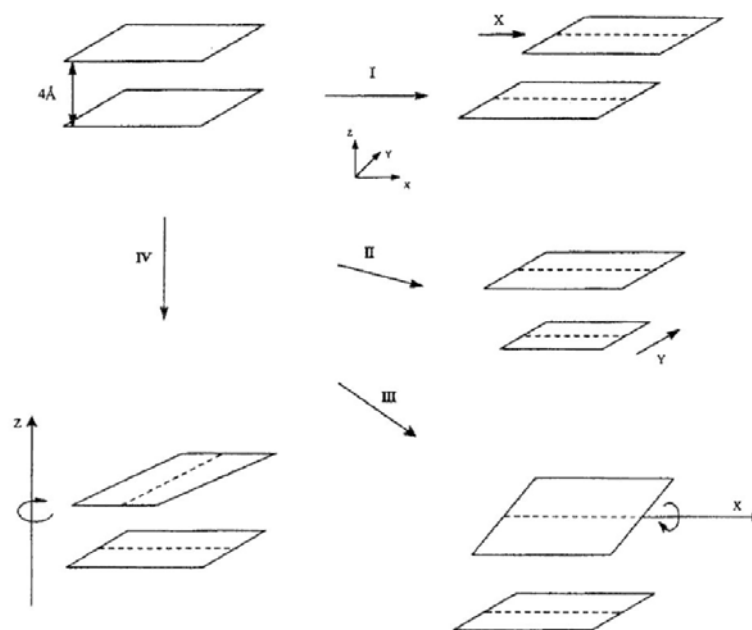


Figure 2.2: The operations applied to a cofacial dimer formed by two stilbene molecules separated by 0.4 nm. (I): the translation of one molecule along the chain-axis direction, (II):the translation of one molecule along the in-plane transverse axis, (III): the rotation of one stilbene molecule around the stacking axis and (IV): the rotation of one stilbene molecule around the stacking axis while keeping the parallelism between the planes. From [92].

The influence of all the operations performed on the oscillator strength and thus on the luminescence efficiency of the systems was evaluated [92].

As it was described in the previous paragraph, a keto defect can be introduced in the bridged PPP derivatives, leading to spectral contamination of these materials. The photophysical properties of molecular fluorenone have been investigated experimentally [93], [94]. More recently, some reports have been focused on the photophysical studies of poly- and oligo-fluorene from a theoretical point of view [95], [96], [97]. The studied systems were both defect free and fluorenone containing. The comparison of the reported conclusions with the experimental results that have been discussed in paragraph 2.2.5 could shed light on some still controversial subjects of oligo- and poly(fluorene) emission photophysics.

It is very useful to exploit the predicted geometrical parameters of the studied system on the excited state such as torsional angles and bond lengths, in order to rationalise the photophysical observables that are extracted experimentally from the time resolved photoluminescence measurements. In the case where the subject of study was focused on oligo(fluorene) derivatives [95], the studied systems were of three types pentamers, all of them without side chain pendant groups on the C9-position. One pentafluorene was fluorenone free, from now on described as pristine [FL5], the second pentafluorene had a fluorenone unit in the middle of the oligomer [FL2(FLO)FL2] while the third one had the fluorenone moiety as end group [FL4(FLO)]. The calculated excited state energies were restricted only to the extent that singlet manifolds were concerned. No quantum-chemical calculations have addressed the prediction of the lowest lying triplet state, although there are several reports that dealt with the experimental determination of the first triplet electronic state in poly- and oligo- fluorenes (for a discussion on the triplet state, see Section 3.4). For the pristine oligomer, it was predicted that the first lowest lying excited state was of $\pi$-$\pi^*$ character that in terms of spin multiplicity corresponds to the $S_1$ singlet excited state. The case of the fluorenone-containing oligomers was however different. Only the third singlet excited $S_3$ state was found to lie closest in the energy of the $S_1$ excited state of the pristine oligomer. The lowest two lying excited states $S_1$ and $S_2$ were arising due to the heterogroup within the oligomeric backbone. More specifically, $S_1$ excitation energy level was related with excitations of electrons belonging to $\sigma$-orbitals of the C=O functional group and therefore it was described as an n-$\pi^*$ state. The energy level $S_2$ was found to have contributions from several occupied $\pi$-orbitals and to be associated with significant charge redistribution in the fluorenone unit. For this reason the $S_2$ energy level was classified as a charge-transfer (CT) energetic state. For all the transitions within the calculated energetic levels of the studied oligomers the oscillator strengths were found to be negligible, except those related to the highest energy level of each system. This is consistent with the notion that n-$\pi^*$ transitions have weak oscillator strength due to the orthogonality of the involved molecular orbitals (see Figure 2.3) which eventually lead to vanishing overlap of electronic wavefunctions integral in the transition dipole moment modulus (see Chapter 1). Such low-lying n-$\pi^*$ states are common in the spectroscopy of small aromatic molecules such as aromatic ketones. As it was already mentioned above, after absorption of a photon and the subsequent population of an excited state, the occurrence of lattice relaxation tends to shift the emitted energy to lower values. The impact of lattice relaxation phenomena that occur in the lowest lying singlet state was explored for all three oligo(fluorene)s. Surprisingly it was predicted that when geometrical relaxation phenomena were taken into account, a reversal in the ordering of the lowest two excited states was taking place,

with the first excited state becoming the CT π-π* excitation. The calculated values of all determined energy levels of the three model oligomeric systems studied, are given in the Table 2.1, together with the corresponding oscillator strenght. Both CT π-π* states in the fluorenone-containing oligomers, have a not vanishing albeit weak, oscillator strength. This implies that oligomers with fluorenone moieties are expected to be emissive. A first look in these energy level values implies that after excited state relaxation in the two different fluorenone-containing systems, the emission of the oligomer, which has the fluorenone as a central unit of the chain, will fluoresce at lower energies than that which contains the fluorenone as endcapped unit. More specifically the predicted values are 506 nm for FL2(FLO)FL2 and 480 nm for FL4(FLO).
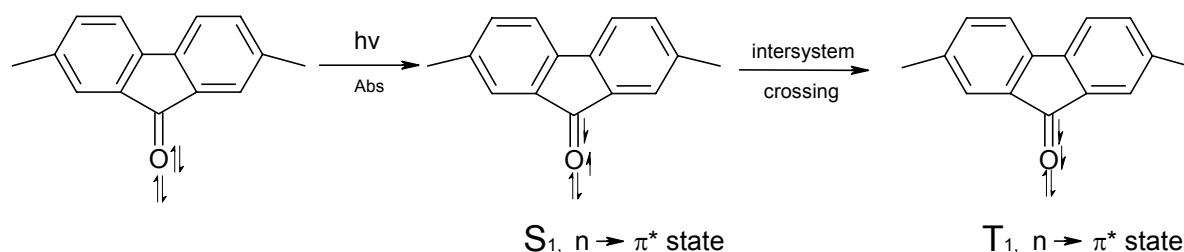


Chart 2.1: The two electronic states of a n-π* transition and the corresponding electron redistribution and spin-flipping, after excitation.

| | (FL)₂(FLO)(FL)₂ | | | (FL)₄(FLO) | | |
|---|---|---|---|---|---|---|
| STATE | Energy (eV) | Wavelength (nm) | Osc. Strength | Energy (eV) | Wavelength (nm) | Osc. Strength |
| CT π-π* | 2.45 | 506 | 0.48 | 2.58 | 480 | 0.26 |
| π-π* | 2.65 | 468 | 0.00 | 2.64 | 470 | 0.00 |
| π-π* | 3.44 | 360 | 3.02 | 3.49 | 355 | 3.45 |

Table 2.1: Energy of the lower electronically excited states of non-substituted fluorenone-free (FL5) and fluorenone-containing pentafluorenes (FL2-FLO-FL2 and FL4-FLO), as predicted from computational calculations in [95]. FL2-FLO-FL2: fluorenone is in the middle of the molecule, FL4-FLO: fluorenone is at the end of the molecule.
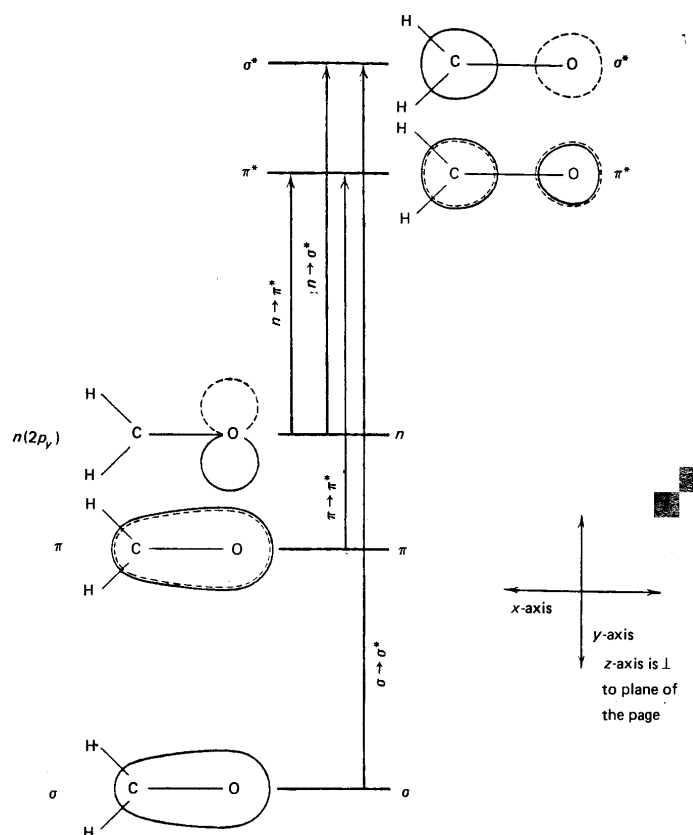
Figure 2.3: The electronic transitions that occur in formaldehyde are a typical example of the electronic transitions of a carbonyl group. The molecular orbitals in which each of the electronic transition takes place are also shown. Note the orthogonality of the n and $\pi^*$ orbitals. From [91].

 Absorption of light leads to the creation of an exciton, by promoting an electron to a higher unoccupied orbital and leaving a hole on the lowest occupied orbital. It is of great interest to clarify the degree of exited-state localisation of the exciton in order to rationalise the different experimental observables that are acquired from ketone-free and ketone-containing poly- and oligo-fluorenes. It is expected that the presence of a fluorenone moiety will impose large variation of the exited-state confinement of the photoinduced electron-hole bound pair and will have a strong impact on the dynamics of the excited state. From the calculated molecular orbitals for the CT state of the fluorenone-containing oligomers, it was predicted that this excited state becomes strongly localised on the central fluorenone unit due to Coulomb interaction between the electron, which is localised in the LUMO and the hole. From quantum-chemical semi empirical investigations the electron-vibrational dynamics of the photoexcitations on model oligo(fluorene)s were investigated [96]. In terms of symmetry, the first excited state of [FL5] is of $1B_u$ character. Due to the strong coupling of this state to the ground state, the corresponding transition is optically allowed and results in emission of light. For excitation at the $1B_u$ level, [FL5] was found to get flattened in the middle of the molecule, in the inner three units. In the

same region of the molecule bond lengths were predicted to be shortened. These effects of dihedral angle reduction and bond length shortening are an indication for exciton self trapping.

## 2.2.7 Dendronised PFs: Attempts for reducing the interchain interactions

 The negative role of interchain interactions for the spectral purity of fluorescent optical centres has been known from earlier studies on several π-conjugated polymers [89], [90], Especially for poly(fluorene)s intermolecular interactions were held responsible for the formation of excimers/aggregates that contaminate the blue emission spectra of these materials with a red-shifted emission band in the green [68], [69], [81]. The isolation of chromophores via dendrimer substituents has been successfully reported for dyes that are used in light-emitting diodes [98]. Therefore attaching bulky side groups at the C-9 carbon of the fluorene unit was considered as an appropriate method for shielding the luminescent polymer backbone, and thus hindering the detrimental π-π stacking of polymer backbones [99], [100], [101], [102], [103]. Bulky functional groups have been found to hamper the formation of excimers in small organic dyes such as a perylene derivative [104]. For the case of polymers, the charge transport properties are likely to be modified in the presence of bulky substituents.

 Several synthetic attempts have been reported for the dendronisation of poly(fluorene) derivatives. A synthetic approach was presented that leads to self-encapsulation of a poly(fluorene) that was symmetrically derivatised with benzyl-ether (Fréchet-type) dendrons [101], (see Chart 2.2). A macomonomer approach was deliberately chosen in order to ensure the complete coverage of the polymer backbone with dendrons, a result that would be less efficient from the alternative graft-onto route. However, the nucleophilic substitution of the dendrons onto the monomer unit had a yield of 84%-91% after purification. This implied that already a minimum level of 9% of the monomer precursors remain unsubstituted or partially substituted, leading to the presence of incomplete derivatised units in the final polymer product.
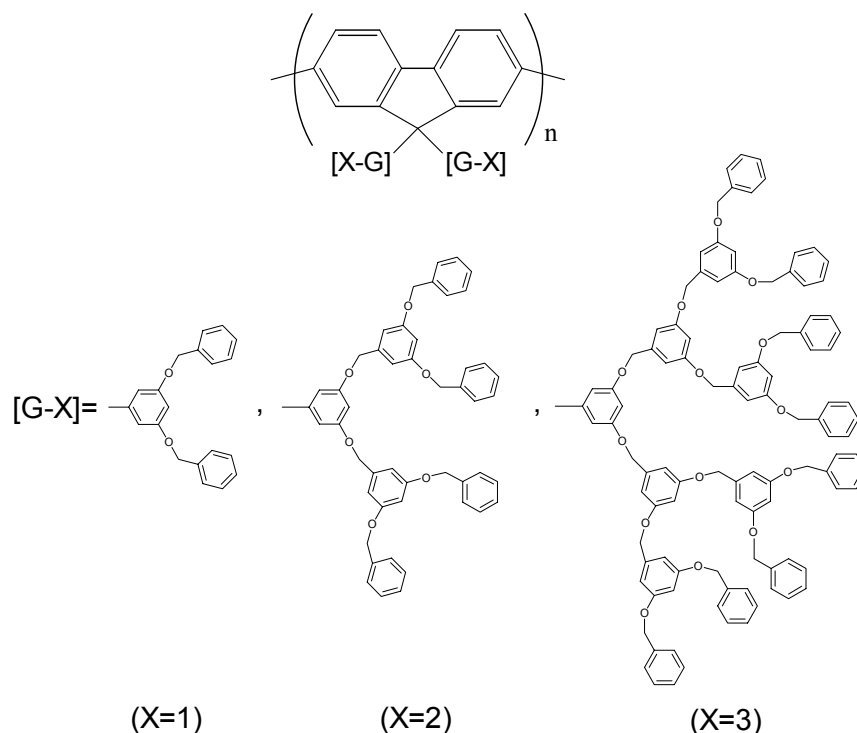
Chart 2.2: Symmetrically derivatised poly(fluorene) with benzyl-ether (Fréchet-type) dendrons. X=1: first generation of dendrons, X=2: second generation of dendrons and X=3: third generation of dendrons (from [101]).

 The symmetric substitution of a poly(fluorene) backbone which bears bulky dendritic side-chains results in high dilution of the luminescent backbones into the dendritic matrix. In that way, the weight-based luminescent efficiency of the material is greatly reduced. Therefore another attempt tried for the synthesis of unsymmetrically substituted poly(fluorene)s [100]. This derivative was bearing poly (benzyl ether) and a less bulky 3,6-dioxaoctyl substituent as side chains and it was found to possess a relatively pure blue luminescence time-integrated spectrum (see chart 2.3).

(1)

(2)

(3)

R-Br
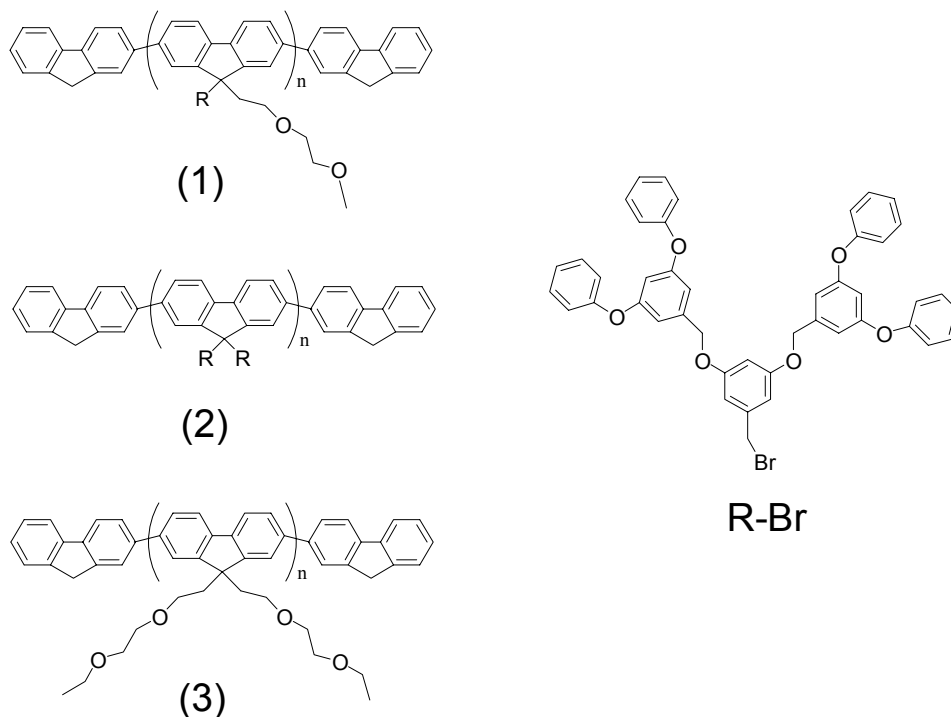
Chart 2.3: Types of unsymmetrically-substituted poly(fluorene)s, as presented in [100].

In contrast to the benzyl-ether dendrons, polyphenylene dendrimers are both shape-persistent and chemically stable. A synthetic effort to derivatise the poly(fluorene) backbone with polyphenylene side-chains has also been reported [99]. The macromonomer approach was again selected for the synthesis of the polymer structure. However two alternative synthetic routes were used for the synthesis of the bis-dendron substituted monomer unit. More specifically, either attachment of the dendrons on to the C-9 position or attachment of the dendron side-chains on to the C-9 position of the fluorene monomer unit prior to ring closing were chosen. The structure of a dendronised poly(fluorene) derivative (PF-D) is depicted in Chart 2.4, together with its alkylated analogue PF-EH.

(PF-EH)                                    (PF-D)
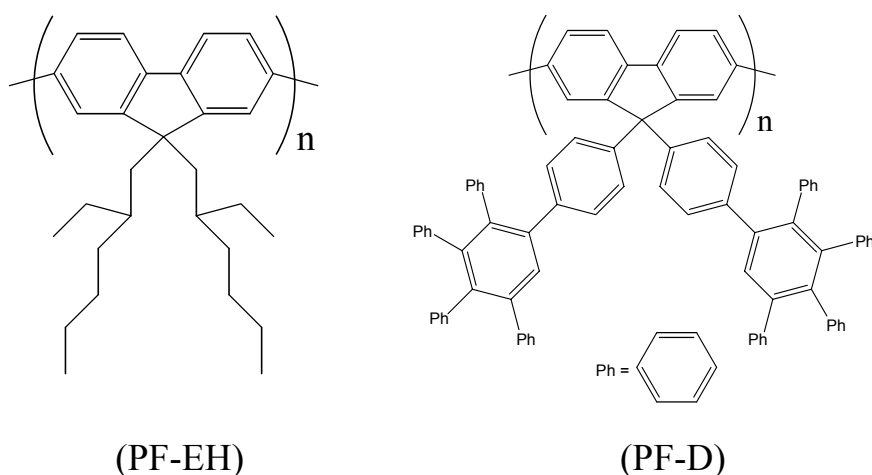
**Chart 2.4:** The monomer units of each of the in here studied poly(fluorene) derivatives. PF-EH: poly(fluorene) ethyl-hexyl, (non-dendronised PF) and PF-D: poly(diarylfluorene), (dendronised PF).

The resultant product was found to be extremely stable at higher temperatures up to 843 K. Moreover the obtained thermograms showed no indication of a phase transition for temperature up to 523 K. X-ray diffraction experiments showed that another polyphenylene-bis-dendronised poly(fluorene) (see inset structure in Figure 2.4) is an amorphous material in the solid state exhibiting two broad correlation peaks related to the average values of interchain and intrachain distances. Low temperature X-ray diffraction measurements on single crystals of this hexaphenyl monomer unit revealed that hexaphenylbenzene groups stand perpendicular to the fluorene unit, thus providing effective shielding of the polymer backbone.
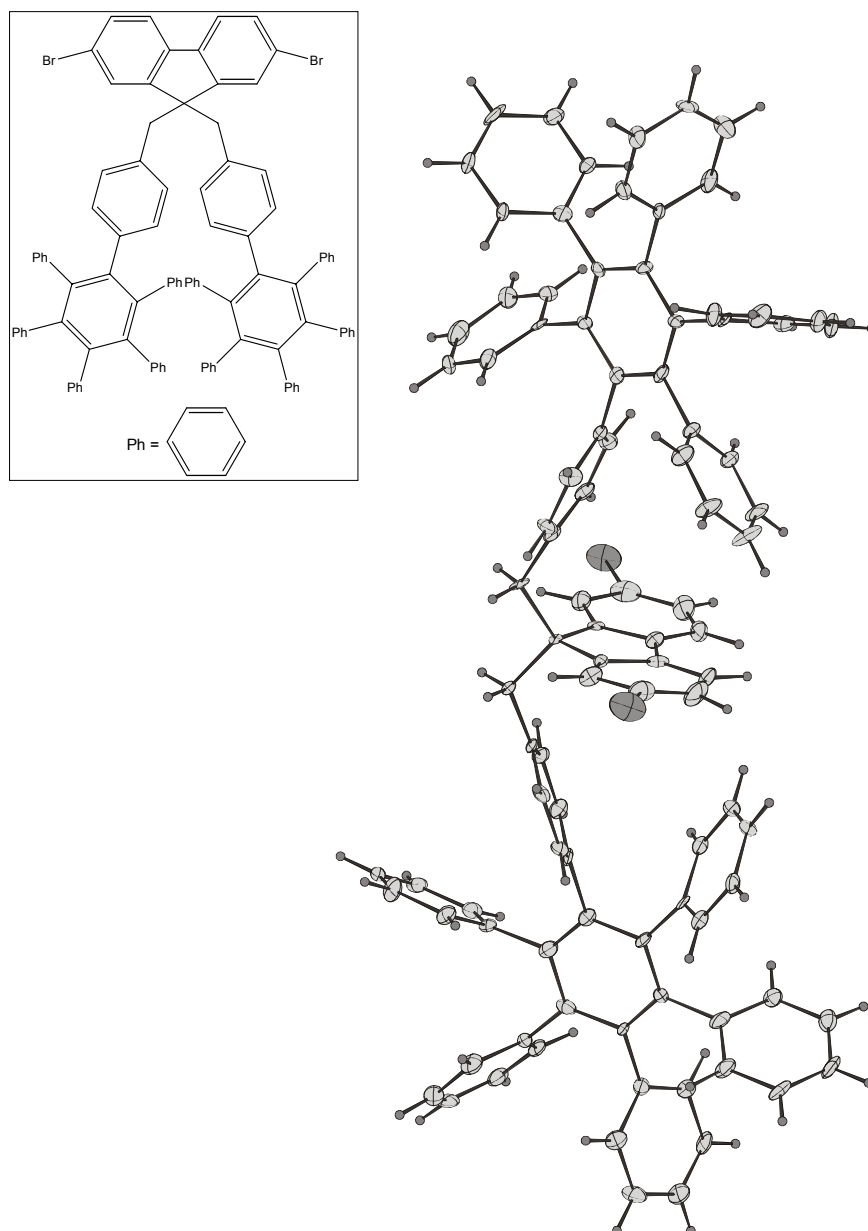
Figure 2.4: ORTEP diagram of the monomer unit of a PF-D derivative as determined by X-ray at 150 K (from [99]). The inset shows the chemical structure of this PF-D derivative.
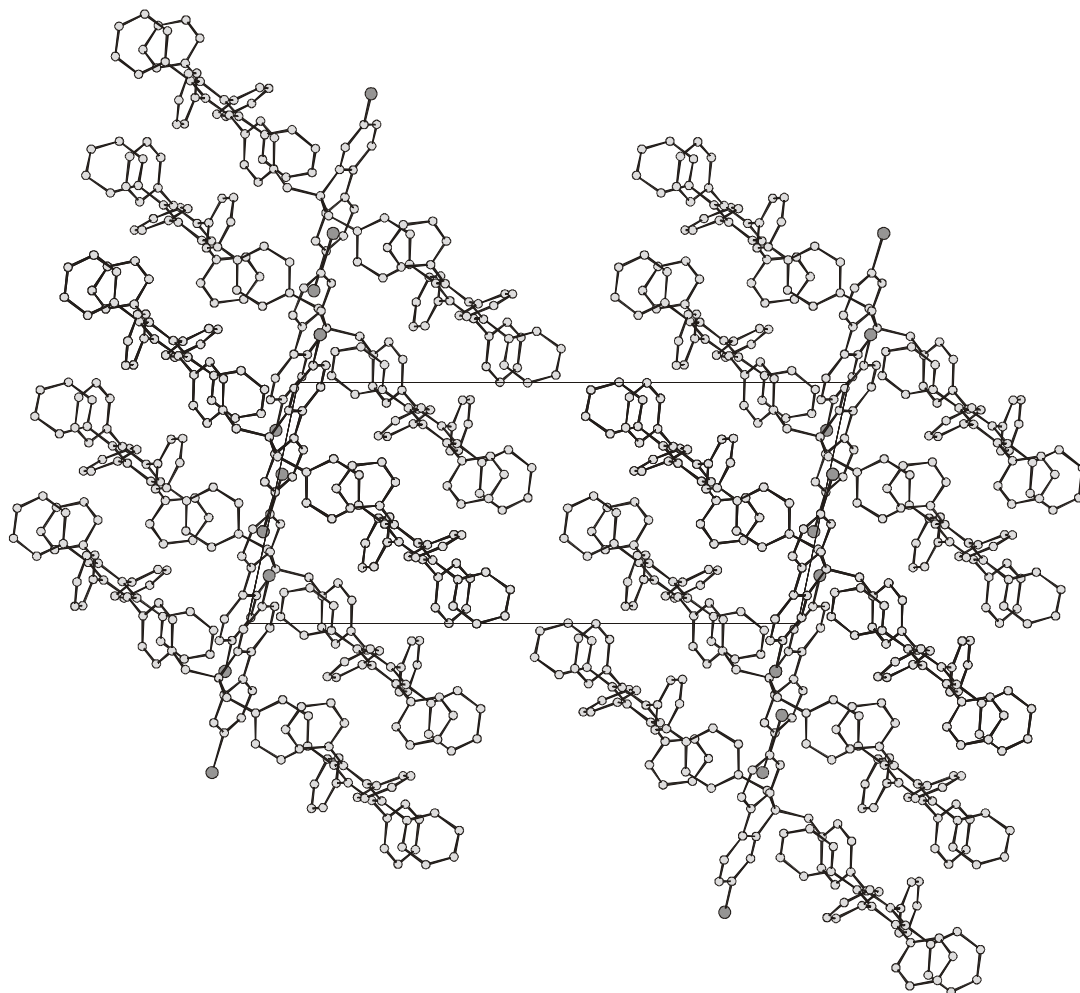
Figure 2.5: Structure of single co-crystal formed by the monomer unit of a PF-D derivative and CHCl$_3$ as determined by X-ray diffraction at 150 K (from [99]).

The influence of dendronisation on the overall energy transfer in films of the dendronised PF derivative has been addressed by means of ultra fast time resolved spectroscopy [102]. In the same study, evidence for PF-D chain aggregation in the solid state was given. The spectral

emissive signature of the interchain aggregate band was identified in time-resolved PL spectra for films of PF-D. Although dendronisation has been found to reduce the rate of excitation migration in the studied system, energy transfer of the singlet states was found to be still operative as the Förster formalism predicts. The impact of dendron shielding was found to retard the energy transfer rate of triplet states [105]. This type of electronic energy transfer is better described by the Dexter theory and it is much more sensitive to distance variation. The observed increase in the triplet lifetime of the dendronised PF derivative is assigned to the increased interchain distances caused by the presence of dendritic side chains onto the polymer backbone. The dendronised PF derivative as an amorphous polymer could be applied as an active electronic component on a polymer based light-emitting diode. A first example of such a device has been already presented and the result was promising for further device optimisation [106].

## 2.2.8 The oligomer approach

In order to overcome the aforementioned problems related to the existence of defects in light-emitting materials that can originate from chemical impurities and/or from intermolecular complex formation, oligomers that still maintain the desired optical characteristics of the polymers can be addressed. After optimising the parameters of length/optical properties, these oligomers can be employed as photonic materials in the fabrication of relevant devices. In order to minimise the disorder complexity and to interpret with higher accuracy the spectroscopic observable, conjugated oligomers of high chemical purity and well-defined thermotropic properties can be used as model compounds. Since in this type of model materials the total number of atoms is significantly reduced, theoretical studies based on quantum-chemical calculations [107] can be also performed the result of which can be directly compared with the experimental ones. Such a theoretical investigation was performed for a terfluorene derivative and its analogue bearing carboxylic acid groups as endcappers [108]. The fully relaxed single-bond torsional potentials of both oligo(fluorene)s were evaluated.

The oligomer approach could eventually lead to significant information regarding the electronic properties of the polymer regime [109], [110]. For instance, by parameterising the optical properties of well-defined oligo(fluorene) derivatives on the number of units of which the oligomeric backbone consists, the effective conjugation length of the polymers could be deduced [109], [111], [112].

Due to their liquid crystal character, polymers such as poly(fluorene) derivatives, have been indicated as key-elements for the construction of uniaxially aligned films of high optical anisotropy that can emit polarised light. The use of PFs as mesogenic material for the fabrication

of highly anisotropic electroluminescence light-emitting diodes has been extensively reported [2], [37], [39], [40]. Hence, it is still crucial to obtain dichroic ratios of higher values. The use of oligomeric analogues has given very positive results, so far, towards this direction [10], [41], [113], [114].

One of the main issues that concern the feasibility of such an attempt is related to the glass transition temperature of the oligomers that should be used. Recently, for the case of fluorene oligomers an attractive synthetic approach gave blue light-emitting fluorene based materials that possessed an emission at ~ 420 nm both for dilute solutions and thin films [115]. Those chromophores were of amorphous nature based on symmetrical molecules with three non-conjugated, covalently linked fluorenyl units. Nevertheless, it is the low $T_g$ values of these neat compounds, close to the room temperature, that only allowed the incorporation of this material as guests in a host polymeric material of a $T_g$ higher than room temperature.

Another attempt for fluorene-based oligomers was more successful regarding the material of macroscopic rigidity at room temperature [113]. In that case, it was pointed out that among other parameters, the aspect ratio was the one that contributes to the material optimisation by means of increasing both the values of photoluminescence quantum yield and dichroic ratio. Novel oligo(fluorene)s of high chemical purity were developed in such a way that they showed interesting thermal properties. By exploiting the thermotropic nature of these materials, glassy-nematic films were obtained. The high values of PL quantum yields were achieved due to the well-defined and uniform molecular structure of these systems. In parallel to this work, another report was made for the synthesis of monodisperse conjugated fluorene oligomers that contained varied segments of other functional groups [10]. This covalent linking was pointing to the creation of chemical systems comprising donor-acceptor pairs. In that way the completion of the colour gamut of light emission was targeted. Encouraging results on these attempts were very recently presented. Strongly polarised and efficient light-emitting diodes were demonstrated by using the specific blue-light-emitting oligo(fluorene)s [41]. Based on this investigation it was determined that the more efficient uniaxial backbone alignment was accomplished for the oligomer comprising twelve monomer units. Integrated dichroic ratios of these materials reached a value of 24.6, much higher than prior reports using poly(fluorene)s. By utilising the Förster transfer process green, red and white LEDs were also fabricated exhibiting green, red and white polarised light [114]. At a current density of 20 mA*cm$^{-2}$, emission integrated polarisation ratio values of up to 19, and a luminance yield of up to 6.4 cd*A$^{-1}$ were obtained. Especially for the white light-emitting LED, the integrated polarisation ratio had a value of 16 and a luminance yield of 4.5 cd*A$^{-1}$.

The photophysical properties of well-defined oligo(fluorene)s comprised of one to six monomer units has been reported [116]. Further more studies on the molecular segmental motion of oligomers as films has been recently presented [58].

## 2.3  EXPERIMENTAL

Dilute solution of the materials were prepared in 2-methyltetrahydrofuran (MTHF) at a concentration of 5 µg/mL. Thin films of the materials were prepared via spin-coating at a rotational speed of 1200 rpm and rotation duration time of 60 sec. Quartz or glass substrates were used for the deposition of the films. Film thickness of the studied films was on average between 60 – 80 nm. The solutions used for spin-coating had a concentration of 10 mg/mL. Annealing of the pristine films took place at $170^0$ C for app. 2 hours. This thermal treatment took place either under ambient conditions or in vacuum. The quality of the vacuum for the annealing process was that of an average vacuum oven. After the end of the annealing, the films were quenched to room temperature.

Absorption spectra were recorded by a UV-VIS Perkin-Elmer spectrometer (Lambda2). A Xe-lamp equipped spectrofluorometer (SPEX FluoroLog II (212)) was used in order to obtain continuous-wave (CW) photoluminescence (PL) and photoluminescence excitation (PLE) spectra of films and dilute solutions.

Time resolved PL spectra were obtained by excitation of the samples with a frequency-doubled mode locked Ti:Saph laser, producing approx. 200 *fs* pulses operating at a repetition rate of 80 MHz at 377 nm or 405 nm. PL of the dilute solutions was recorded by using a home-built glass cell of 4 mm path length. Unless otherwise indicated in the following, no focal lens was used for exciting the samples and the diameter of the laser spot was kept at ~1mm by using an aperture. For the time resolved measurements PL, the signal was dispersed by a 0.25 m monochromator with a 50 lines/mm grating and detected with a Hamamatsu C4742 streak camera. Time-integration of the obtained signals higher than 2 ns exhibit similar spectra to that obtained from the CW measurements.

During the measurement the samples were kept under vacuum in a continuous cold finger liquid $N_2$ cryostat. For room temperature measurements, the thin films were kept under a dynamic vacuum of $10^{-4}$ mbar -$10^{-5}$ mbar, by using a turbo pump.

For low temperature measurements liquid $N_2$ was used for cooling down to 77 K. For the case of low temperature measurements at 4.2 K, experiments were performed in a He atmosphere in a He-flow cryostat. For all time-resolved PL measurements care was taken to avoid *in situ* photo-

oxidation of the samples during measurement time. The maximum average laser power was kept in the order of 500 μW, unless otherwise indicated.

## 2.4  RESULTS

## 2.4.1 Dendronised poly(fluorene)s

In the following we present experimental results obtained on the optical properties of the polyphenylene-bis-dendronised poly(fluorene) (PF-D), prepared as [99] describes. A non-dendronised poly(fluorene) (PF-EH) was used as a reference. From the comparison of the optical properties, conclusions are drawn regarding the impact of dendronisation on the degree of interchain interactions in dilute solutions and in the solid state (thin films).

### *2.4.1.1 CW-spectroscopy*

In principle, the absorption bands of conjugated polymers originate from electronic transitions occurring within the π-π* molecular orbitals. In terms of spin-multiplicity the observed transitions have been assigned as transitions occurring between the singlet manifolds of the ground state and higher excited states. In the case of poly(fluorene), the main absorption band peaks at app. 390 nm and higher energy bands of lower intensity are following which are due to vibronic transitions of the excited state. The line-widths values of the absorption bands of poly(fluorene) are strongly influenced by the physical state in which the molecules exist. The main absorption band of poly(fluorene)s has a typical band width (FWHM) equal to ~0.6 eV [2]. More elaborated spectroscopic studies for dilute solutions of a PF derivative have deduced the excited state inhomogeneous broadening to be in the order of 0.4 eV [117].

The existence of side-bands absorption and emission spectra reflect the vibronic progression of the monitored transitions. However, in the case of a conjugated polymer such as poly(fluorene), at least at room temperature, due the inhomogeneous broadening effect this vibronic progression of the absorption band is masked. The effect of inhomogeneous broadening is caused by the disordered nature of the electronic states of the polymer. Especially for films, this effect contributes largely to the high values of the line widths that are commonly observed in absorption spectra of polymers.

Regarding photoluminescence of the conjugated polymers in the solid state, a red shift of the spectral maxima is observed. Generally speaking in films of polymers, the density is increased and polarity effects are pronounced. The extent of these effects will be determined from the cohesive energy density (cal/cm$^3$) of the polymer and the substrate, as described by the square of

the Hildebrant parameter $\delta$. The squared difference $(\delta_{substrate} - \delta_{polymer})^2$ will determine the degree of polymer adhesion on the surface . This treatment has been applied for solutions of polymers in solvents with different $\delta_{solvent}$ [118]. Within this context, the observation of polymer/solvent gelation and the corresponding red-shift of polymer's absorption band have been explained.

The observed red-shift in PL depends on the degree of order that the film posseses. In the solid state, interchain interactions are enhanced due to local variation of the dispersive forces between the surrounding molecules. Therefore the more pronounced are the order characteristics in the film, the smaller this variation of the dispersive forces will be. Consequently the lowest electronically excited state will be described by less energetic inhomogeneity and the energetic stabilisation of the lowest lying excited state will be observed as bathochromism in the photoluminescence spectra.

In order to identify the spectral maxima of the obtained spectral bands, a deconvolution process must be applied in the obtained spectra. As it is known, photoexcitations in conjugated polymers, such as poly(fluorene) derivatives are dominated by strong coupling with phonons. In this case, a Gaussian fitting for the deconvolution of the absorption bands is more advised than a Lorentzian one. Gaussian deconvolution reflects a statistical nature of events, which is in line with the disordered nature of the electronic states of conjugated polymers, especially if the transport of the excitation takes place at room temperature.

### 2.4.1.1.1 *Spectroscopy of solutions*

Figure 2.6 presents the absorption spectra of PF-EH and PF-D derivatives. Both of the materials exhibit a broad absorption band that seems to be a superposition of two distinct peaks. Additionally, the spectrum of PF-EH is found to be compared to that of the dendronised-PF.
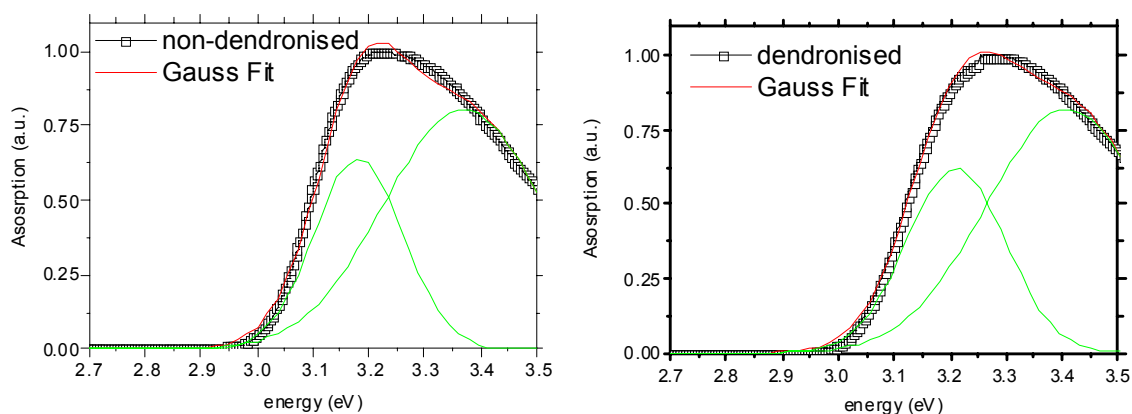
Figure 2.6: Room temperature absorption spectra of PF-EH (left) and PF-D (right), in dilute solution of toluene.

Upon excitation at 3.29 eV (377 nm), the photoluminescence of the poly(fluorene) derivatives was obtained. Figure 2.7 presents the registered time-integrated spectra. The luminescence spectra are assigned to the intrachain singlet emission of poly(fluorene) which is accompanied by their characteristic vibronic progressions. Both of the materials exhibit photoluminescence centred at 3 eV.
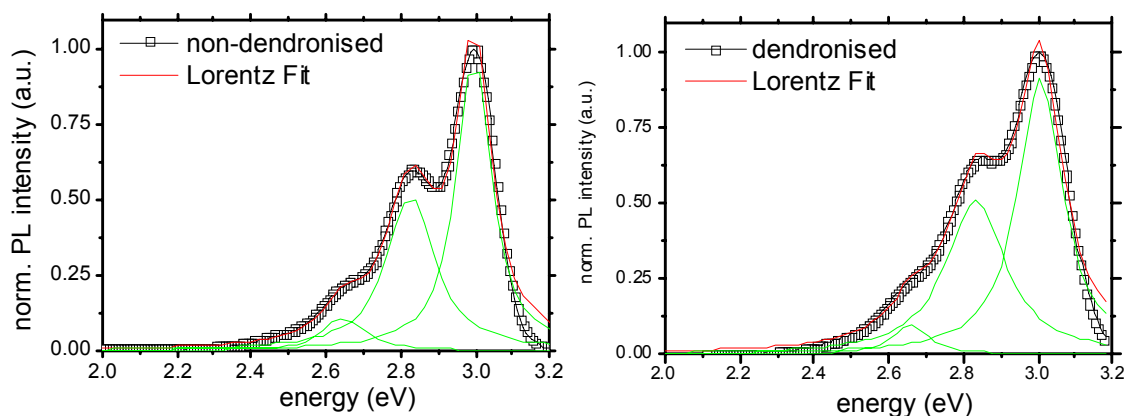


Figure 2.7: Room temperature PL spectra of PF-EH (left) and PF-D (right), in dilute solution of toluene. Excitation upon 377 nm ( 3.29 eV).

Figure 2.8 presents the photoexcitation spectra of the two PF-derivatives, when the low-energy tail of PL emission (2.43 eV) is monitored. No additional intensities in the spectral distribution of photoexcitation spectra were found in comparison with the PLE spectra, that were recorded

when the maxima of the PL spectra were monitored. This indicates that also the low-energy spectral region of the PL emission in the two derivatives, originates from the same levels that are related to the main emission peak.
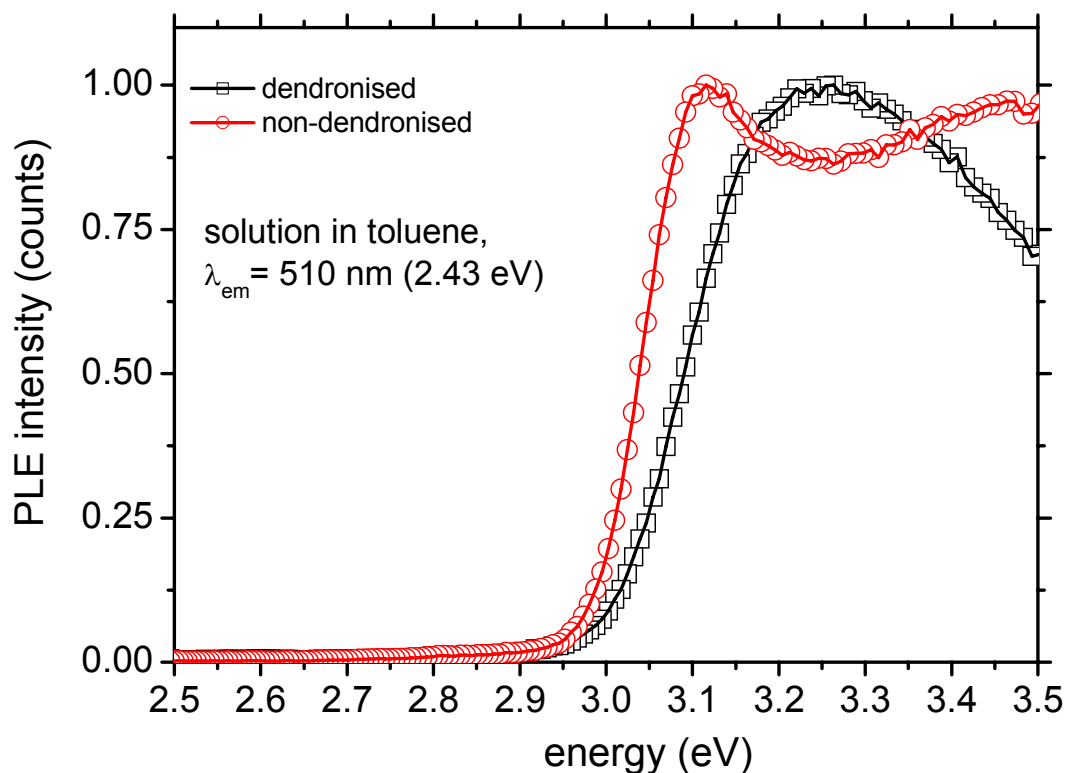


Figure 2.8: Room temperature PLE spectra of PF-EH (circles) and PF-D (squares), in dilute solution of toluene, monitoring $\lambda_{em}$= 510 nm (2.43 eV) emission.

### 2.4.1.1.2 *Spectroscopy of films*

For the case of the two derivatives as thin films on glass substrates, the absorption spectra were found to be similar to that of the corresponding dilute solutions. As Figure 2.9 depicts, in the solid-state the differences that are observed in the degree of broadening are much more pronounced, with PF-D exhibiting substantially more broadened absorption band. Like in the case of dilute solutions, the absorption peak of the alkylated-PF derivative is found to be slightly red-shifted in respect to that of the dendronised-PF by ~90 meV.
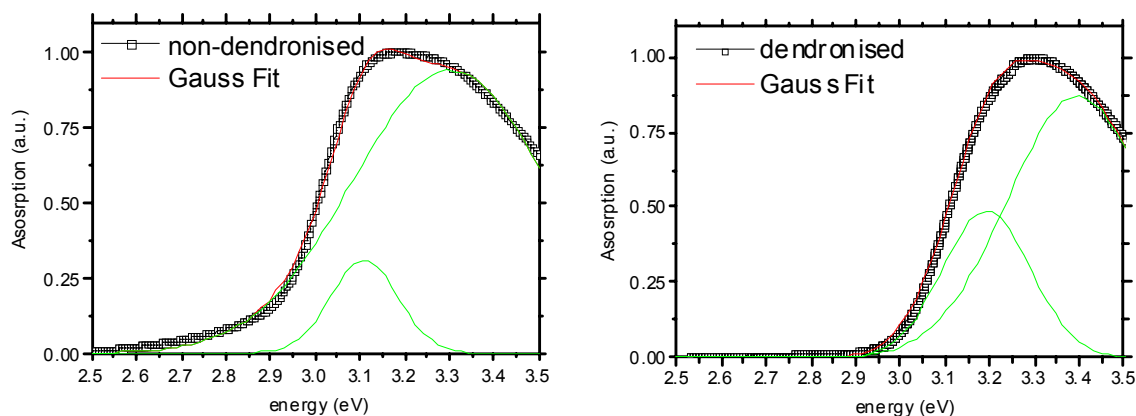
Figure 2.9: Room temperature absorption spectra of PF-EH (left) and PF-D (right), as films on glass substrate.

The photoluminescence spectra of the two materials in the solid-state are presented in Figure 2.10. While the spectral position of the emission maxima is the same, the width of the main singlet emission peak is larger in the case of PF-D. Additionally the intensity of the spectral region centred on 2.6 eV is higher for the PF-D than PF-EH.
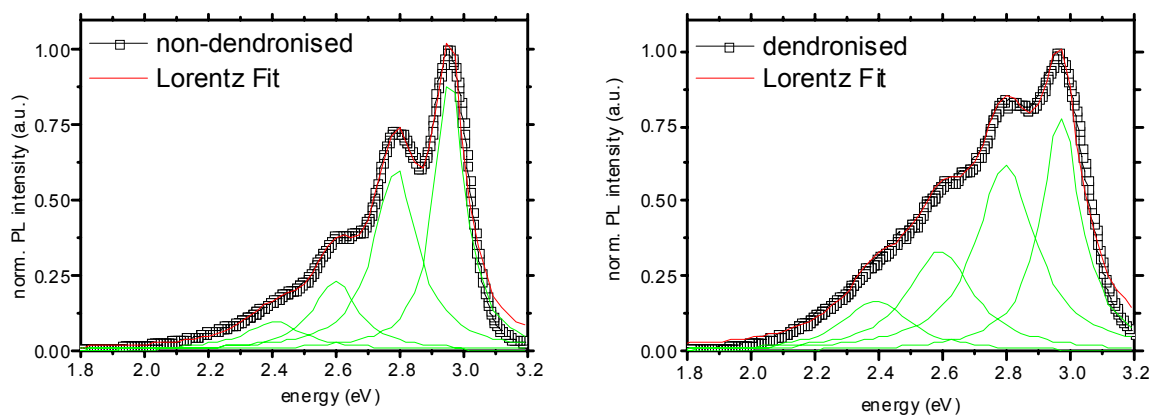


Figure 2.10: Room temperature PL spectra of PF-EH (left) and PF-D (right), as films on glass substrate. Excitation upon 377 nm ( 3.29 eV). Pressure ~$10^{-4}$ mbar.

PLE spectra recorded for the two films, monitoring the low-energy region of 2.3 eV are presented in Figure 2.11. No difference is observed in these spectra with respect with the

corresponding absorption spectra of Figure 2.9, indicating that the whole absorbing spectral region is active in the photoluminescence process in thin films.
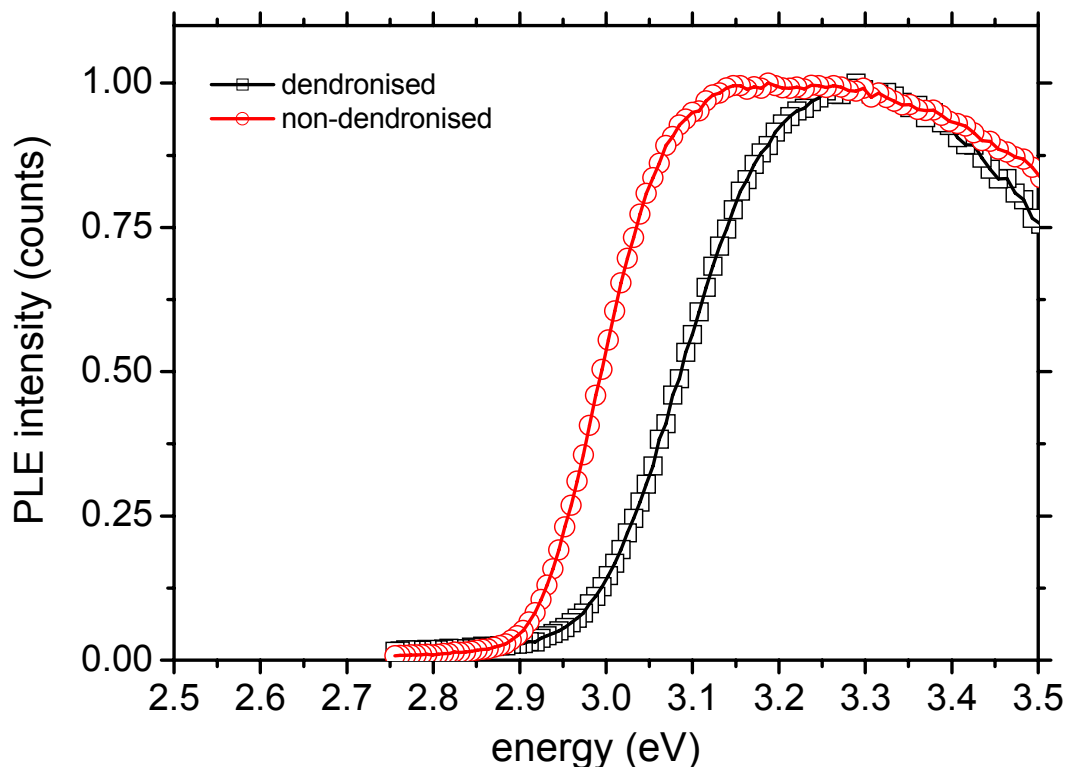


Figure 2.11: Room temperature PLE spectra of PF-EH (circles) and PF-D (squares), as films on glass substrate, monitoring $\lambda_{em}$= 530 nm (2.34 eV) emission.

Finally, low temperature emission spectra at 4.2 K are presented in Figure 2.12. In comparison with the room temperature PL spectra, at low temperatures the $S_{0-0} \leftarrow S_{1-0}$ is found to gain intensity on the expense of the $S_{0-1} \leftarrow S_{1-0}$ component, for both poly(fluorene) derivatives. This difference is related to the different bond equilibrium geometries between the ground state and lowest-lying excited electronic state. A more detailed discussion on this observation is presented in the last part of paragraph 2.4.3.

From the obtained spectra at low temperature, it becomes clear that the degree of spectral broadening is much larger in the case of PF-D than PF-EH. Even at this temperature range, the maximum intensity peak of the PL spectrum for PF-EH is found to be red-shifted in comparison with the corresponding spectrum of PF-D.
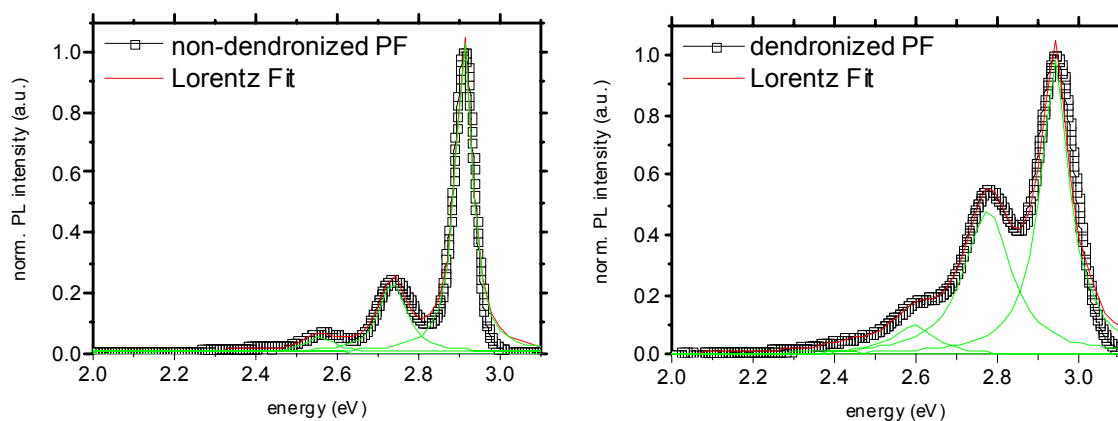
Figure 2.12: Low temperature (4.2 K) PL spectra of PF-EH (left) and PF-D (right), as films on glass substrate. Excitation at 377 nm ( 3.29 eV), pressure p= $10^{-4}$ mbar.

The data obtained from the spectroscopic analysis of the steady-state luminescence spectra of both PF-EH and PF-D derivatives are contained in the Tables 2.2-2.6. In principle, absorption spectra are related to the geometries of the electronically excited states, whereas luminescence spectra contain information related to the ground state conformations. In this context, the similarity of the FWHM of the absorption spectra between PF-EH and PF-D (almost 0.42 eV, see Table 2.2) is assigned to the similar distribution of excited state conformations that both of the materials have in solution. The smaller extend of this conformational distribution in the dendronised PF is attributed to the spatial requirements of the bulkier dendron side-chains. The almost similar spectral widths of the luminescence spectra of the two materials in dilute solution indicate that no important differences exist in the conformational distribution of both materials in the ground state. Consequently, the presence of the dendron-side chains seems not to affect, and if than only slightly, the dihedral angle between the linked fluorene units and thus the ground state average conjugational length, in dilute solutions. This is further supported from the fact that both derivatives emit in the same spectral position and therefore have the same average conjugation length. The influence of dendronised side-chain on the optical properties becomes important in the case of the films both in absorption and emission spectra. The FWHM of the PF-D absorption main peak is larger than the corresponding value of PF-EH (see Table 2.3).

At the temperature of 4.2 K, the spectral width of singlet emission peak is significantly increased for the case of PF-D. This large difference of ~ 50 meV is a further indication for the presence of enhanced intermolecular interactions in the solid state of a dendronised PF derivative. At 4.2 K all thermalised degrees of freedom are expected to vanish. Under these

conditions the assignment of the main vibronic levels of the ground state can be deduced. Both of PF derivatives exhibit a slight bathochromism of their luminescence, interpreted an increased planarisation of the main polymer backbone. This result is in agreement with previously reported temperature-depended PL studied of the same dendronised and non-dendronised PF derivatives [105].

According to Table 2.5, PF-D has its zero-band vibronic component blue-shifted in comparison with the corresponding one of PF-EH. Since blue shift in the emission reflects a smaller average conjugation length, it seems that the existence of bulky dendrons hinders PF-D to adapt the same degree of planarisation as PF-EH did. According to Table 2.6, PF-EH shows emission peaks that are almost equally spaced by 180 meV. This energy difference is very close to the in-plane vibrational mode of octyl derivatised PF (1605 $cm^{-1}$ ), as it has been deduced from Raman spectroscopy [47]. In the case of PF-D this value is met as an average but the assignment is still acceptable with marginal error.

| Compound in solution | Peak 1 (eV) | FWHM$_{Abs}$ (eV) |
|---|---|---|
| Non-dendronised PF | 3.22 | 0.424 |
| Dendronised PF | 3.27 | 0.420 |

Table 2.2: Maxima of the first absorption peak of PF-EH and PF-D, at room temperature, in dilute solution of toluene. The FWHM values are also quoted. All values were obtained after Gaussian fitting of the data (see text).

| Compound in films | Peak 1 (eV) | FWHM$_{Abs}$ (eV) |
|---|---|---|
| Non-dendronised PF | 3.10 | 0.173 |
| Dendronised PF | 3.19 | 0.225 |

Table 2.3: Maxima of the first absorption peak of PF-EH and PF-D, at room temperature, as films on glass substrates. The FWHM values are also quoted. All values were obtained after Gaussian fitting of the data (see text).

| Sol rT | Peak 1 (eV) | Peak 2 (eV) | Peak 3 (eV) | FWHM$_{PL}$ (eV) |
|---|---|---|---|---|
| Non-dendronised PF | 3.00 | 2.84eV | 2.64 eV | 0.098 |
| Dendronised PF | 3.01 | 2.83 eV | 2.66 eV | 0.151 |

Table 2.4: Maxima of the PL peaks of PF-EH and PF-D, at room temperature, in dilute solution of toluene. The FWHM values of the $S_{0-0} \leftarrow S_{1-0}$ band are also quoted. All values were obtained after Lorentzian fitting of the data (see text).

| Film rT | Peak 1 (eV) | Peak 2 (eV) | Peak 3 (eV) | Peak 4 (eV) | FWHM$_{PL}$ (eV) |
|---|---|---|---|---|---|
| Non-dendronised PF | 2.94 | 2.80 | 2.60 | 2.40 | 0.099 |
| Dendronised PF | 2.97 | 2.80 | 2.60 | 2.40 | 0.173 |

Table 2.5: Maxima of the PL peaks of PF-EH and PF-D, at room temperature, in dilute solution of toluene. The FWHM values of the $S_{0-0} \leftarrow S_{1-0}$ band are also quoted. All values were obtained after Lorentzian fitting of the data (see text).

| Film 4K | Peak 1 (eV) | Peak 2 (eV) | Peak 3 (eV) | Peak 4 (eV) | FWHM$_{PL}$ (eV) |
|---|---|---|---|---|---|
| Non-dendronised PF | 2.92 | 2.74 | 2.57 | 2.38 | 0.064 |
| Dendronised PF | 2.94 | 2.76 | 2.59 | 2.42 | 0.107 |

**Table 2.6:** Maxima of the PL peaks of PF-EH and PF-D, at 4.2 K, as films on glass substrates. The FWHM values of the first band are also quoted. All values were obtained after Lorentzian fitting of the data (see text).

## 2.4.2  The influence of thermal treatment

Photoluminescence dynamics are especially informative for polymeric materials such as PF derivatives. As it has been already described in Chapter 1, the energetic inhomogeneity that exists in conjugated polymers emerges from a distribution of effective conjugative length in this materials. This distribution is a consequence of the conformational distribution of the polymer backbones that is dynamic in nature if the material exists in solution, or it has static characteristics, if the polymer exists in the solid state as film. The fate of a primary photoexcitation is strongly dependent on the type of the energetic disorder.

In the following we present a study of the impact that the thermal protocol has, on the photophysics of a poly(fluorene) derivative bearing branched alkyl chains (PF-EH, see Chart 2.4). The photophysical investigation is based on the time-resolved photoluminescence technique. Within the context of keto defect contamination (see paragraph 2.2.5) we combine the thermal treatment followed, with deliberate molecular oxygen contamination of the studied films. In such a way we discriminate the influence of the thermal history on the optical properties of the film from the effect of thermal oxidation that eventually alters the inherent optical characteristics. Subsequently in paragraph 2.4.3, we move on, applying the same experimental method on a set of pentafluorene derivatives bearing different side chains.

### 2.4.2.1 Time-resolved photoluminescence spectroscopy

Our discussion begins with the obvious differences observed in the singlet emission dynamics of three films of polymers, with different thermal history. Figure 2.13 presents the transient curves of the singlet emission of PF-EH films that have been treated with three different thermal

protocols. The studied samples were a pristine spin-coated film, a film annealed in vacuum and a film annealed in air. The thermal treatment was done by heating up to 170 $^{\circ}$C, in both cases.



Figure 2.13: Room temperature PL decay transients of PF-EH as thin film on quartz substrate, after different treatment: pristine film (squares), annealed at 170 $^{\circ}$C in vacuum (circles) and annealed at 170 $^{\circ}$C in air (triangles). Excitation upon 377 nm ( 3.3 eV), with 500 µW average laser power. Pressure was kept at ~$10^{-4}$ mbar. The area of spectral integration was centred at the $S_{0-0} \leftarrow S_{1-0}$ emission ± 20 nm

In all of the cases a biexponential function was found to be the most appropriate recovering function of the recorded transients [45]. Table 2.7 summarises the determined lifetime values of the singlet emission of the films for each of the different physicochemical treatment. The percentage amplitude of each component in these emissions is given as %$A_1$ and %$A_2$ respectively, while $\tau_1$ and $\tau_2$ represent the extracted lifetimes.

| FILMS | PF-EH iso | PF-EH (ann. in vaccuo) | PF-EH (ann. in air) |
|:---:|:---:|:---:|:---:|
| %$A_1$ | 92 | 7 | 42 |
| %$A_2$ | 8 | 93 | 58 |
| $A_1$ | $1814 \pm 14$ | $47 \pm 2$ | $395 \pm 12$ |
| $\tau_1$ (*ps*) | 193 | $76 \pm 5$ | 100 |
| $A_2$ | $150 \pm 14$ | $602 \pm 2.6$ | $283 \pm 13$ |
| $\tau_2$ (*ps*) | $413 \pm 13$ | 292 | $229 \pm 4$ |
| $\tau_{1/e}$ (*ps*) | 207 | 281 | 144 |

Table 2.7: Determined amplitudes and decay constants for the films of PF-EH, after different thermal treatment. Time constants $\tau_{1/e}$ are also quoted.

Surprisingly it turns out that the main emission lifetime component with the higher amplitude increases after annealing of the isotropic film under vacuum conditions. In parallel the second relaxation channel of the singlet manifold shows a sharp decrease in its lifetime value. As it is seen in Figure 2.13, the singlet exciton lifetime is reduced only after heating the annealed polymer film in the presence of oxygen.

In accordance with the decay transients the emission profiles of the samples in Figure 2.14 also differ. This difference in the emission spectral distribution is much more pronounced in the delayed spectra displayed in Figure 2.15.
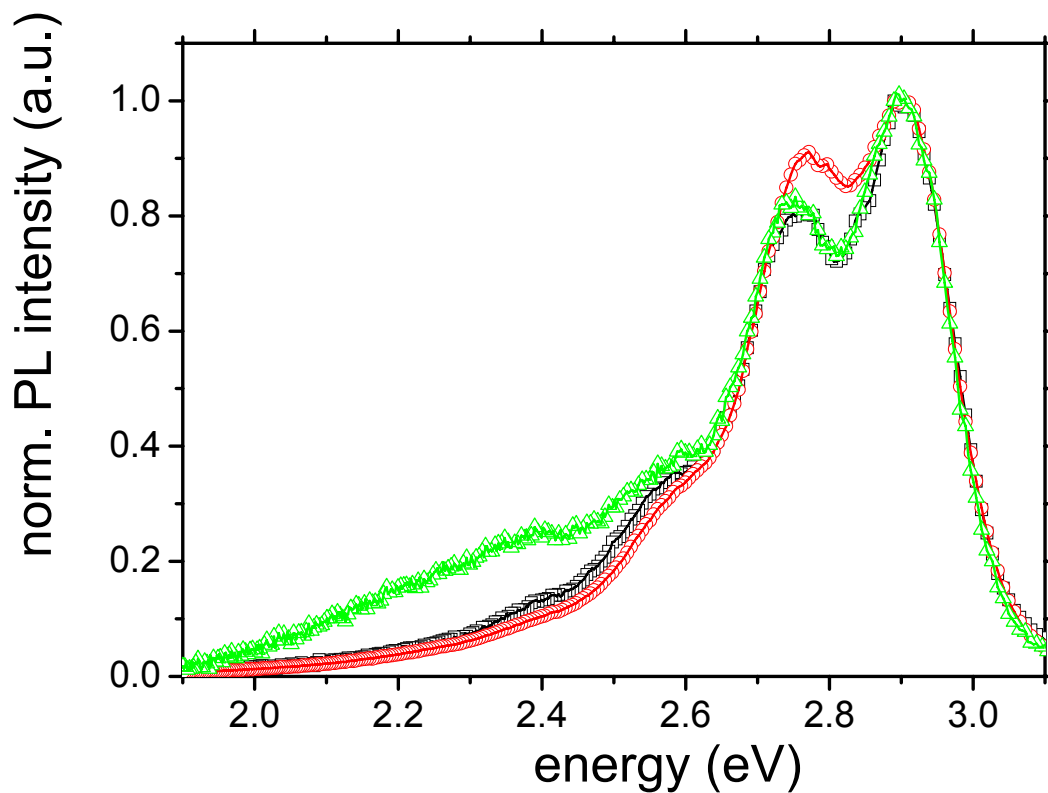
Figure 2.14: Room temperature time-integrated PL spectra of PF-EH as thin film on quartz substrate, after different treatment: pristine film (squares), annealed at 443 K in vacuum (circles) and annealed at 443 K in air (triangles). Time-integration in a 2 *ns* window. Excitation upon 377 nm (3.3 eV), with 500 µW average laser power. Pressure was kept at ~$10^{-4}$ mbar.
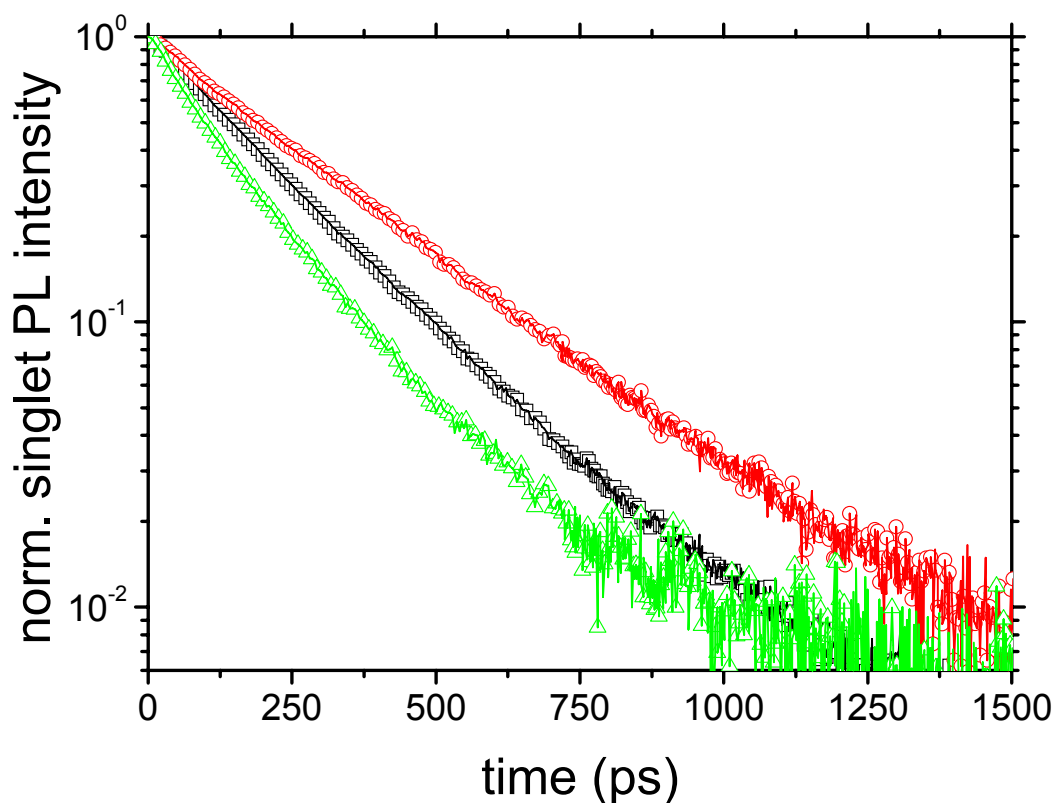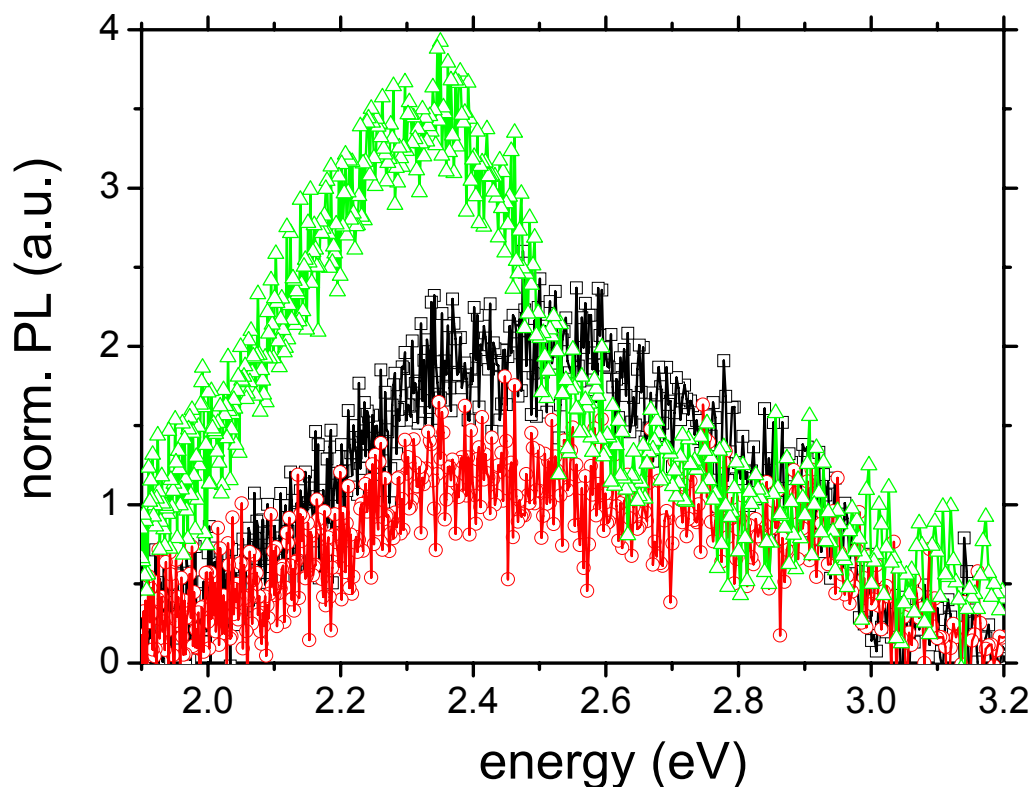
Figure 2.15: Room temperature time-resolved PL spectra of PF-EH as thin film on quartz substrate, after different treatment: pristine film (squares), annealed at 443 K in vacuum (circles) and annealed at 443 K in air (triangles). Detection was app. 2 *ns* after excitation pulse in an integration window of 500 *ps*. Excitation upon 377 nm ( 3.3 eV), with 500 µW average laser power.  Pressure was kept at ~$10^{-4}$ mbar.

## 2.4.3 Oligomers

Here we report on the time-resolved photoluminescence properties of a series of differently derivatised pentafluorenes bearing different pendant groups on the 9-position of monomer units that comprise the oligomer backbone. Chart 2.5 presents the chemical structures of the oligo(fluorene) pentamers (OF5). The influence of side-chain on the optical properties and on the efficiency of solid state packing of oligo(fluorene) derivatives has been previously addressed [110]. However this approach was not performed in a systematic manner. In the following, the experimental results of chemical pure monodisperse pentafluorenes, bearing different pendant chains, will be discussed both in dilute solution and as thin films. A correlation of these results with similarly obtained results of the related polymers will be done. Finally a comparison with theoretical studies for similar compounds that have been discussed in paragraph 2.2.6 will be presented.
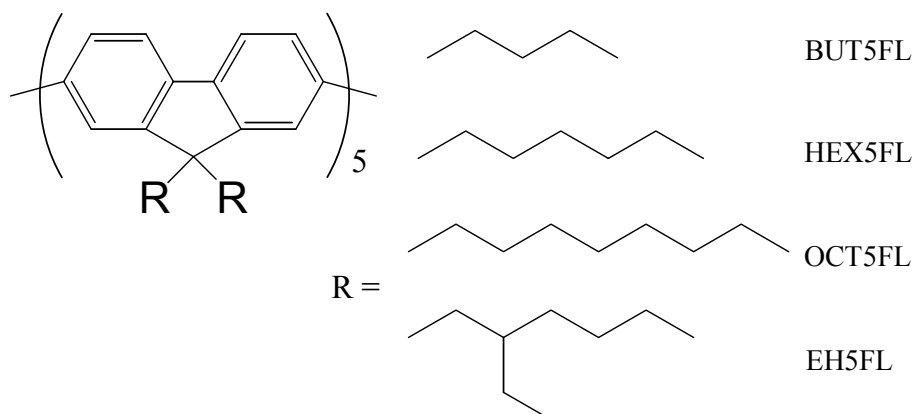
Chart 2.5: The monomer unit of the studied pentamer backbone and the chemical structure of different pendant groups attached to it.

 Although time-resolved PL technique has been widely applied in a series of previous studies on polyfuorenes still a quantitative interpretation of the obtained time-resolved results in the case of thin films was not attempted. Moreover, we emphasize here on the advantage of studying the photo kinetics of oligomer singlet emission. We exploit the oligomeric nature of the studied chromophores, that is the lack of wide spectral inhomogeneous broadening which arises presumably due to the presence of an effective-conjugation-length distribution in the corresponding polymer. Our discussion is centred on the spectral purity of these compounds. It is well known that poly(fluorene)s suffer from spectral instability, which is caused by an unwanted green/yellowish spectral component centred on 530 nm. This spectral feature has been observed numerous times in the case of poly(fluorene)s and a long literature debate has been devoted to the question of whether the nature of this emission is excimer-like or that of a chemical defect (see paragraph 2.2.5).

### *2.4.3.1 CW-spectroscopy of OF5 solutions*
 Figures 2.16 present the UV-Vis absorption and PL spectra of the four different OF5 derivatives, in dilute solutions of MTHF.

Figure 2.16: Room temperature absorption spectra (left) and time-integrated PL spectra for dilute solutions of the oligo(fluorene)s in MTHF: BUT5FL (squares), HEX5FL (circles), OCT5FL (up-triangles) and EH5FL (down-triangels). For PL spectra: excitation took place at 377 nm (3.29 eV), with 500 µW average laser power.

 Regarding absorption, all OF5 derivatives are found to posses a broad absorption band that is centred at 3.35 eV (nm). Only the case of EH5FL is found to be slightly blue shifted with the absorption maximum at 3.41 eV. Similarly the PL spectra of all OF derivatives have peaks in the same spectral region of ~ 2.98 eV. The only differences that could be observed is the one related to the different ratio of the $(S_{0-0} \leftarrow S_{1-0})/(S_{0-0} \leftarrow S_{1-0})$ intensities of the vibronic side-bands in the PL spectra of the derivatives. While the $S_{0-0} \leftarrow S_{1-0}$ transition is found to be the strongest in the three derivatives that bear linear side-chains, this is not the case for the derivative that carries branched side-chain. Therein, the first $(S_{0-1} \leftarrow S_{1-0})$ vibronic band is found to have a stronger intensity than the zero-phonon band $S_{0-0} \leftarrow S_{1-0}$. The observed difference is related with the shift in the minima of the potential energy curves along the configurational axis, upon excitation. This aspect is discussed in more detail below in the last part of this section.

 The different side chains are not affecting importantly the bandwidths of both absorption and photoluminescence spectra. Table 2.8 summarises the absorption and PL bandwidths of OF5s in solution. The positions of the photoluminescence peaks are quoted in Table 2.9. PL bandwidths correspond to the $S_{0-1} \leftarrow S_{1-0}$ vibronic bands of the presented spectra.

### *2.4.3.2 CW-spectroscopy of OF5 films*

Figure 2.17 present the UV-Vis absorption and PL spectra of the four different OF5 derivatives in the solid state, as thin films on quartz substrates. As in the case of the dilute solutions, no significant differences are observed in the peak maxima of the absorption band of each

derivative. As it was described above, in solid state the interchain interactions are enhanced due to local variation of the dispersive forces between the surrounding molecules. Therefore, the absorption bands are found to be broader in comparison with the corresponding ones in dilute solutions. Table 2.10 summarises the absorption and PL bandwidths of OF5s as films.
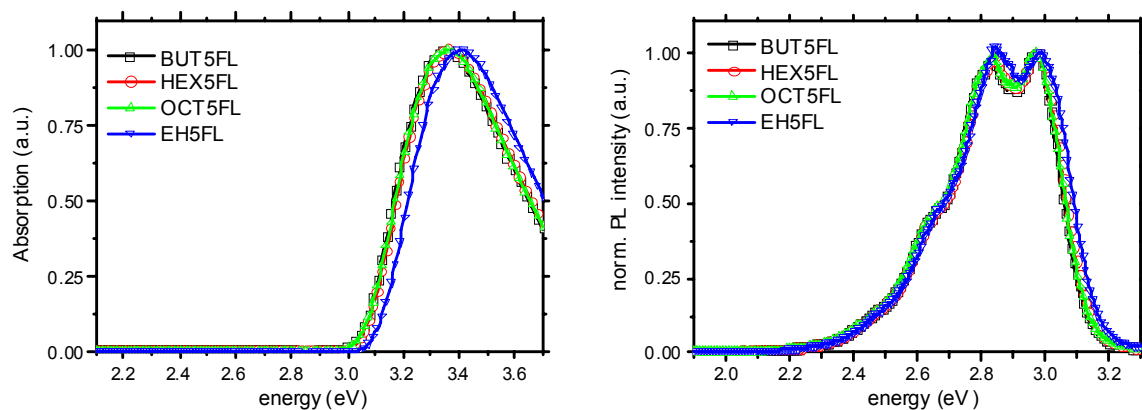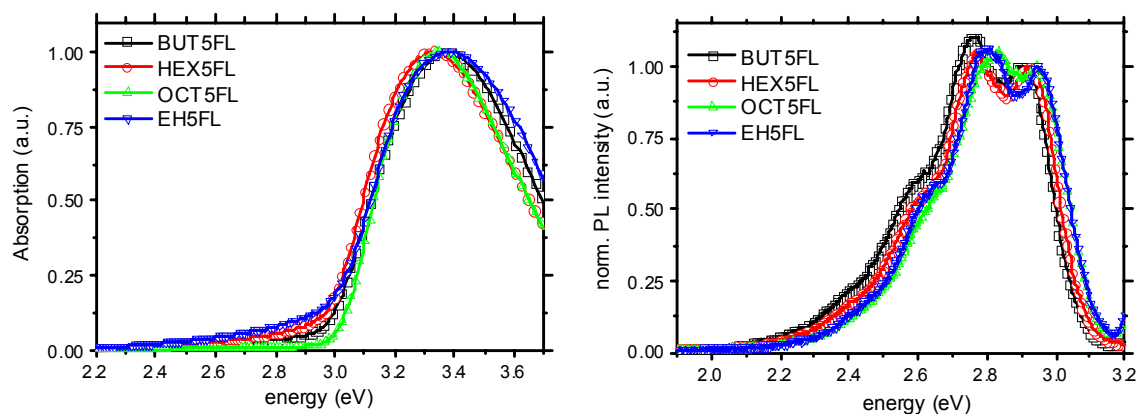


Figure 2.17: Room temperature absorption spectra (left) and time-integrated PL spectra for the oligo(fluorene) derivatives as thin films on quartz substrates:  BUT5FL (squares), HEX5FL (circles), OCT5FL (up-triangles) and EH5FL (down-triangels). For PL spectra: excitation took place at 377 nm (3.29 eV), with 500 µW average laser power. Pressure was kept at ~$10^{-4}$ mbar.

 Regarding photoluminescence the situation accounts as for the case of absorption spectra. All PL spectra are found to be broader with respect to solution, but still having the main $S_{0-0} \leftarrow S_{1-0}$ emission band centred on the same spectral position. The observed difference in the intensity ratios of the $(S_{0-0} \leftarrow S_{1-0})/(S_{0-0} \leftarrow S_{1-0})$ vibronic bands is more pronounced in the solid state PL spectra. All materials are found to possess a more intensive $S_{0-1} \leftarrow S_{1-0}$ vibronic band than the respective $S_{0-0} \leftarrow S_{1-0}$ band. As Table 2.11 quotes, a slight bathochromic shift is observed in the PL maximum, as the side-chain become shorter.

| Compound in solution | $FWHM_{Abs}$ (meV) | $FWHM_{PL}$ (meV) |
|:---:|:---:|:---:|
| BUT5FL | 250 | 200 |
| HEX5FL | 250 | 200 |
| OCT5FL | 280 | 200 |
| EH5FL | 280 | 200 |

Table 2.8: FWHM values of the absorption and PL bands for the oligo(fluorene) derivatives in dilute solution of MTHF, at room temperature. Values for absorption were obtained after Gaussian fitting, while values of PL were obtained after Lorentzian fitting (see text).    The $S_{0-1} \leftarrow S_{1-0}$ band of PL is compared.

| Sol rT | Peak 1 (eV) | Peak 2 (eV) | Peak 3 (eV) |
|--------|-------------|-------------|-------------|
| BUT5FL | 2.97 | 2.82 | 2.62 |
| HEX5FL | 2.99 | 2.82 | 2.65 |
| OCT5FL | 2.99 | 2.82 | 2.65 |
| EH5FL | 2.99 | 2.85 | 2.65 |

Table 2.9: Maxima of the PL peaks for the oligo(fluorene) derivatives, at room temperature, in dilute solution of MTHF. Excitation of the samples took place at 377 nm (3.29 eV).

| Compound in films | $FWHM_{Abs}$ (meV) | $FWHM_{PL}$ (meV) |
|-------------------|--------------------|--------------------|
| BUT5FL | 330 | 200 |
| HEX5FL | 330 | 200 |
| OCT5FL | 280 | 230 |
| EH5FL | 500 | 200 |

Table 2.10: FWHM values of the absorption and PL bands for all the studied oligo(fluorene) derivatives, as pristine films on quartz substrates, at room temperature. Values for absorption were obtained after Gaussian fitting, while values of PL were obtained after Lorentzian fitting (see text). The $S_{0-1} \leftarrow S_{1-0}$ band of PL is compared.

| Film rT | Peak 1 (eV) | Peak 2 (eV) | Peak 3 (eV) | Peak 4 (eV) |
|---------|-------------|-------------|-------------|-------------|
| BUT5FL | 2.91 | 2.75 | 2.57 | 2.41 |
| HEX5FL | 2.93 | 2.78 | 2.59 | 2.41 |
| OCT5FL | 2.96 | 2.82 | 2.64 | 2.55 |
| EH5FL | 2.96 | 2.80 | 2.62 | 2.46 |

Table 2.11:Maxima of the PL peaks for the oligo(fluorene) derivatives, at room temperature, as pristine films on quartz substrates.Excitation of the samples took place at 377 nm (3.29eV).

### 2.4.3.3 Time-resolved photoluminescence spectroscopy in OF5 solutions

Figure 2.18 presents time-resolved spectra of the pentafluorene derivatives in MTHF solution of high dilution after laser excitation with 3.29 eV (377 nm). As it can be seen, the spectral distribution of the presented spectra remains unchanged in time, even for delays up to almost 4 *ns* after excitation pulse.
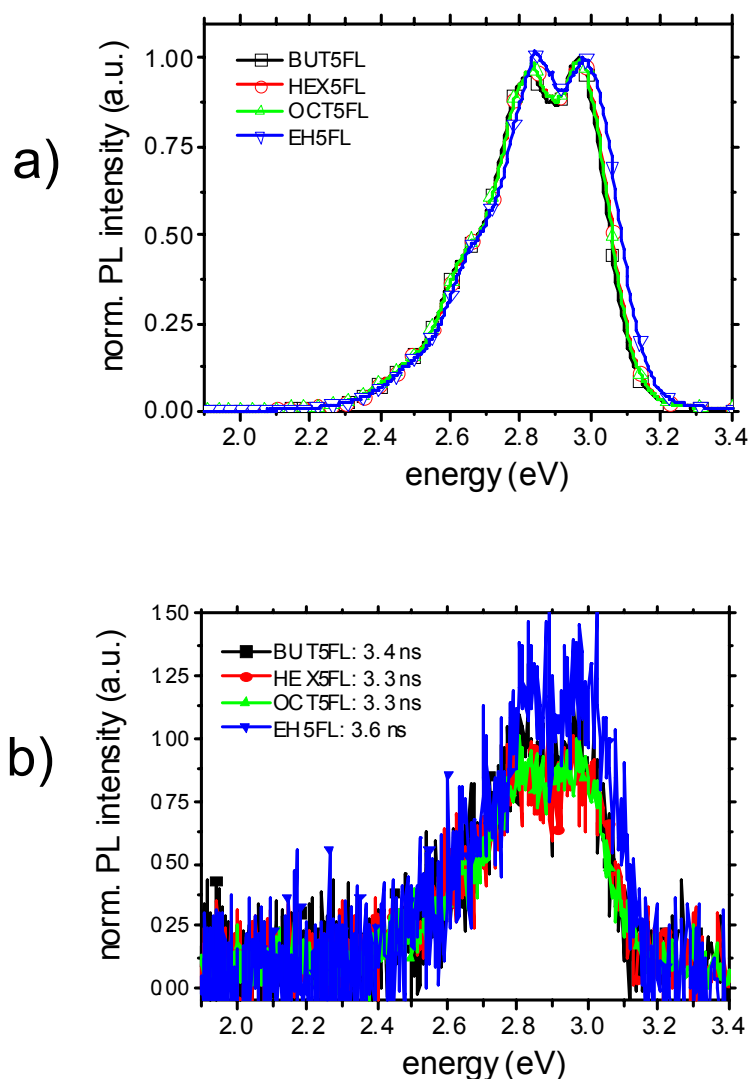
Figure 2.18: Room temperature normalised time-resolved PL spectra for the oligo(fluorene) derivatives, in dilute solutions of toluene: BUT5FL (squares), HEX5FL (circles), OCT5FL (up-triangles) and EH5FL (down-triangels). a) Prompt PL, b) delayed PL ~ 4 *ns* after the excitation pulse. Integration window of 500 *ps*. Excitation took place at 377 nm (3.29 eV ), with 500 µW average laser power.

Evidently, all spectra resemble those obtained from steady-state spectroscopy. By monitoring the decay of the emission intensity, the emission dynamics were recorded for all OF derivatives.
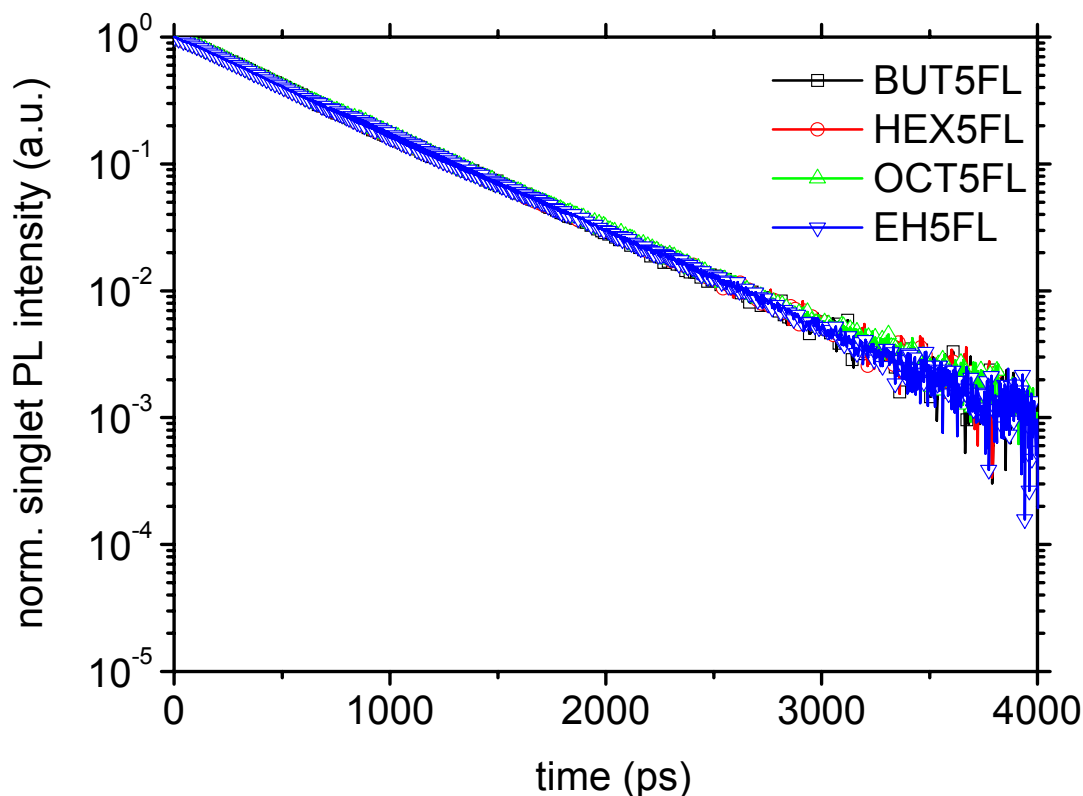
Figure 2.19: Room temperature PL normalised decay transients of all the oligo(fluorene) derivatives in dilute solution of MTHF: BUT5FL (squares), HEX5FL (circles), OCT5FL (up-triangles) and EH5FL (down-triangels). Excitation took place at 377 nm (3.29 eV ). The area of spectral integration was in average centred at the $S_{0-0} \leftarrow S_{1-0}$ singlet emission $\pm$ 20 nm.

Figure 2.19 presents the room temperature singlet emission transients for each of the OF5 derivative in solution, after laser excitation with 3.29 eV (377 nm). The determined fitting parameters of the collected emission decay curves are summarised in Table 2.12. Like previously reported for a set of oligo(fluorene) derivatives, the singlet emission dynamics are found to follow a monoexponential decay pattern [116].

| SOLUTIONS | BUT5FL | HEX5FL | OCT5FL | EH5FL |
|---|---|---|---|---|
| Concentration ($\mu$g/mL) | 5 | 5 | 5 | 5 |
| $A_1$ | 2636 $\pm$ 1.3 | 2331 $\pm$ 1.3 | 4020 $\pm$ 1.9 | 3756 $\pm$ 1.9 |
| $\tau_1$ (*ps*) | 551 | 546 | 555 | 556 |
| $\tau_{1/e}$ (*ps*) | 550 | 550 | 550 | 550 |

Table 2.12: Determined amplitudes and decay constants for the dilute solutions of the oligo(fluorene) derivatives, as measured at room temperature. Time constants $\tau_{1/e}$ are also quoted.

## *2.4.3.4 Time-resolved photoluminescence spectroscopy in OF5 pristine films*

Figure 2.20 presents the time-resolved spectra of pentafluorene films. There are striking differences observed in the case of delayed spectra obtained from films in respect to these obtained from solutions. Although prompt photoluminescence remains nearly unchanged regarding the spectral positioning of the singlet emission, the delayed spectra differ with each other depending on the side chain that is attached on the 9-position of the monomer units. A red-shifted emission with a peak between 480 - 500 nm is detected in the case of the pentamers that bear short linear pendant chains, namely butyl- and hexyl- groups. When the pendant group is the octyl chain, the delayed emission seems to keep its initial singlet character until the complete decay of the detected signal. The same accounts for the case of the branched ethyl-hexyl pendant group.
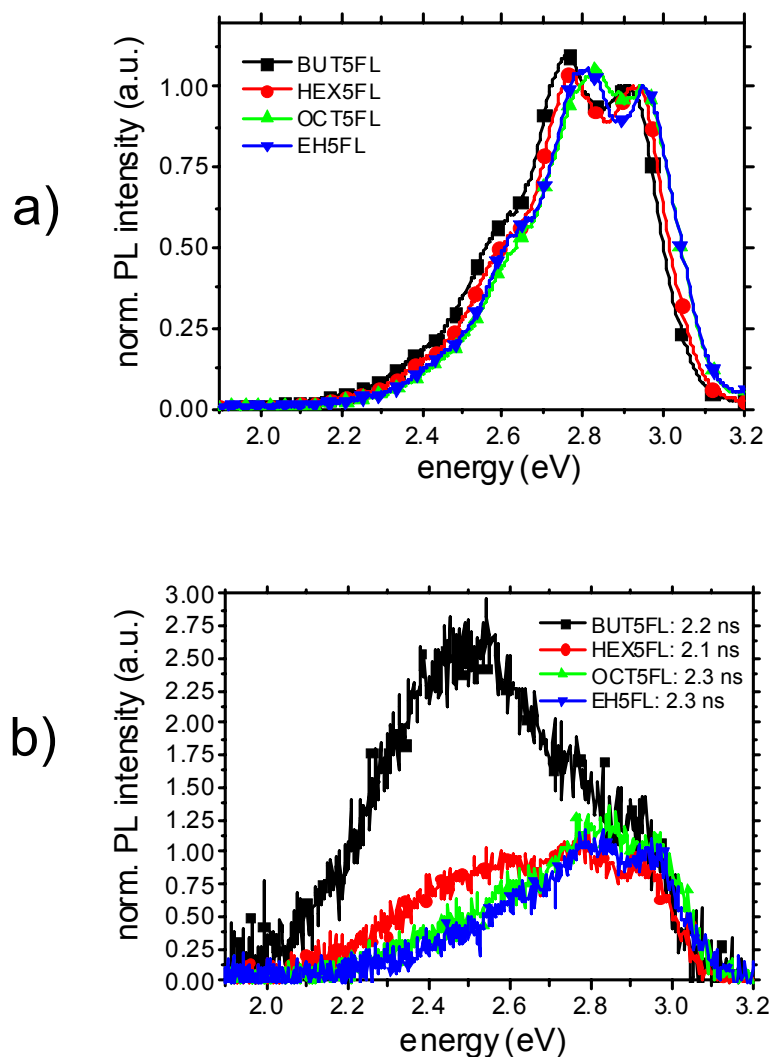
Figure 2.20: Room temperature normalised time-resolved PL spectra for the oligo(fluorene) derivatives as thin pristine films on quartz substrates:  BUT5FL (squares), HEX5FL (circles), OCT5FL (up-triangles) and EH5FL (down-triangels). a) Prompt PL, b) delayed PL ~ 2 *ns* after the excitation pulse. Integration window of 500 *ps*. Excitation took place at 377 nm (3.29 eV, with 500 µW average laser power.  Pressure was kept at ~$10^{-4}$ mbar.

 The emission dynamics of the OF derivatives are also found to differ in the solid state. The analysis of the emission decay transients that are presented in Figure 2.21 results in a biexponential decay function for the cases where the red-shifted emission is detected while a monoexponential function is appropriate for fitting the decay transients of the octyl and ethyl-hexyl pendant groups. The determined fitting parameters are summarised in Table 2.13. It should be noted here that from the data analysis of the transient decays, it is shown that the 1/e emission intensity time-constant, which is commonly used as an empirical parameter in lifetime measurements, is in most of the cases representing the relaxation process with the highest

amplitude that contributes to the overall monitored decay. Hence if the emission transient is a second-order process, the 1/e intensity time-constant will neglect the second process at a degree that will be dependent from the ratio of the amplitudes of the two contributing processes.

 As it has been discussed in paragraph 2.2.4, second-order exponential functions are considered a good tool for recovering the registered transient decays in photoluminescence of polymers like PF. This is clear in Tables 2.13 where the $\tau_{1/e}$ constant values are also quoted together with the values obtained from the fits.



Figure 2.21: Room temperature normalised decay transients of all the oligo(fluorene) derivatives, as pristine films on quartz substrates: BUT5FL (squares), HEX5FL (circles), OCT5FL (up-triangles) and EH5FL (down-triangels). Excitation took place at 377 nm (3.29 eV ), with 500 $\mu$W average laser power.  Pressure was kept at ~$10^{-5}$ mbar. The area of spectral integration was centred at the $S_{0-0} \leftarrow S_{1-0}$ singlet emission $\pm$ 20 nm.

| FILMS | BUT5FL | HEX5FL | OCT5FL | EH5FL |
|---|---|---|---|---|
| $\%A_1$ | 5.2 | 3.3 | 95.7 | 100 |
| $\%A_2$ | 94.8 | 96.7 | 4.3 | - |
| $A_1$ | $33 \pm 1.4$ | $21 \pm 1.2$ | $724 \pm 1.5$ | $420 \pm 0.3$ |
| $\tau_1$ (*ps*) | $53 \pm 5$ | $63 \pm 7$ | 497 | 500 |
| $A_2$ | $609 \pm 1.2$ | $612 \pm 0.9$ | $32 \pm 1.4$ | - |
| $\tau_2$ (*ps*) | 387 | 447 | $105 \pm 8$ | - |
| $\tau_{1/e}$ (*ps*) | 377 | 443 | 485 | 515 |

Table 2.13: Determined amplitudes and decay constants for the pristine thin films of the oligo(fluorene) derivatives, as measured at room temperature. Time constants $\tau_{1/e}$ are also quoted.

Figure 2.22a presents a comparison between the emission decay transients of two different spectral regions for the case of BUT5FL in dilute solution. The fact that these two different spectral positions follow identical photo kinetics decays suggests the singlet manifold $S_1$ of BUT5FL to be the common origin of the monitored emissions. Actually, this is the case for all of the OF5s studied in this degree of dilution in MTHF.

In contrast to the solution case, the same spectral areas are following a different decay pattern in the solid state. As Figure 2.22b presents, for BUT5FL film at room temperature, the decay transients of the singlet emission follow a different decay law than the transients of the spectral position where the red-shifted band is monitored (see spectra in Figure 2.20b), in the range of 460 – 560 nm. The same differences are observed for the case of HEX5FL and slightly in the case of OCT5FL. However in the case of EH5FL (Figure 2.22c) similar kinetics laws were found for the two different spectral positions, suggesting that ethyl-hexyl branched pendant groups are making EH5FL derivative to behave photophysically as it was in solution. Finally, for reasons of comparison similar comparison of the decay transients is shown in Figure 2.22d for the case of a PF-EH film.
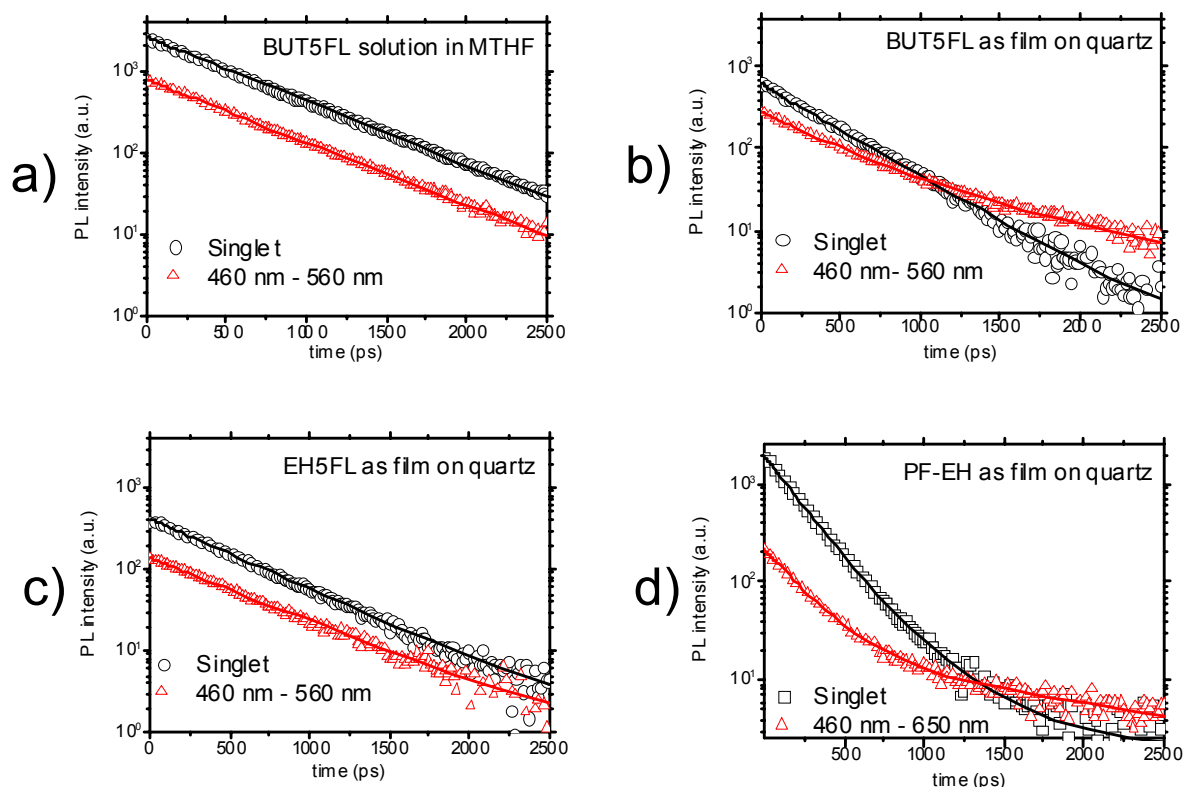
Figure 2.22: Room temperature decay transients of oligo(fluorene) and poly(fluorene) derivatives: a) BUT5FL in dilute solution of MTHF, b) BUT5FL as film on quartz substrate, c) EH5FL as film on quartz substrate and d) PF-EH as film on quartz substrate. Each plot presents the transients for two different spectral areas of the recorded PL: $S_{0-0} \leftarrow S_{1-0}$ emission $\pm$ 20 nm (squares), green spectral region as indicated (triangles). Excitation took place upon 377 nm (3.3 eV), with 500 µW average laser power. For the case of films: pressure was kept at ~$10^{-4}$ mbar.

### *2.4.3.5 Films of OF5: Thermal oxidation*

In order to examine the impact of $O_2$ on the optical properties of the OF5 films, we treated the prepared films thermally at 443 K, in air. Subsequently, the films were quenched back to room temperature and their time-resolved photophysical properties were studied. Figure 2.23 presents the spectral profiles of the OF5s at 2 *ns* delay after the excitation pulse. Therein it is shown that the delayed emission has lost completely all the singlet characteristics and has been transformed into a broad featureless band located around 525 nm. This spectral position is red-shifted even in respect with the delayed emissive component observed in the OF5 films prior to thermal treatment in $O_2$, shown in Figure 2.20b.
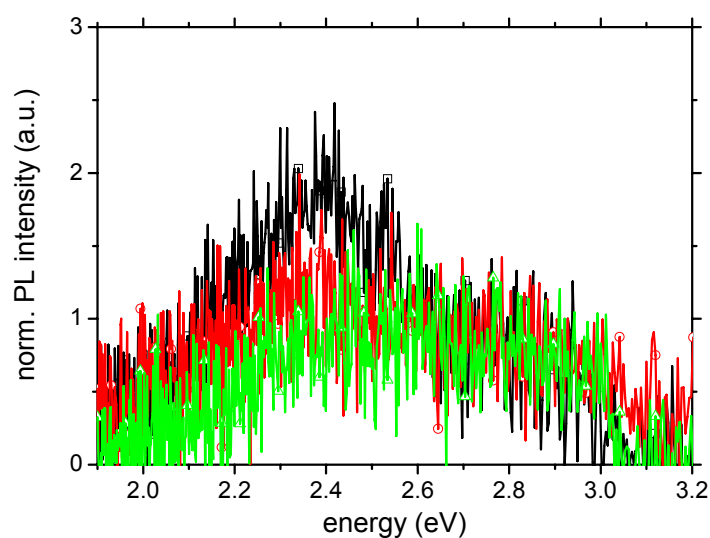
Figure 2.23: Room temperature normalised time-resolved PL spectra for the oligo(fluorene) derivatives as thin films on quartz substrates, annealed in air at 443 K:  BUT5FL (squares), OCT5FL (circles) and EH5FL (triangles). Delay of ~ 2 *ns* after the excitation pulse. Integration window of 500 *ps*. Excitation took place at 377 nm (3.29 eV), with 500 µW average laser power. Pressure was kept at ~$10^{-4}$ mbar.
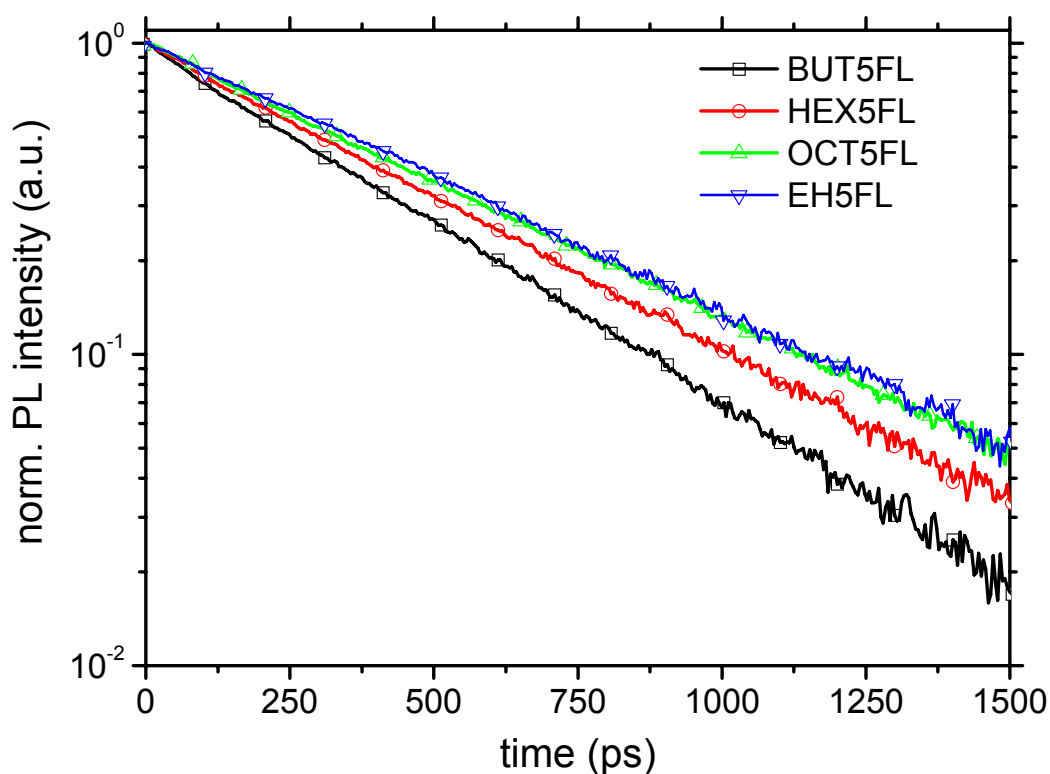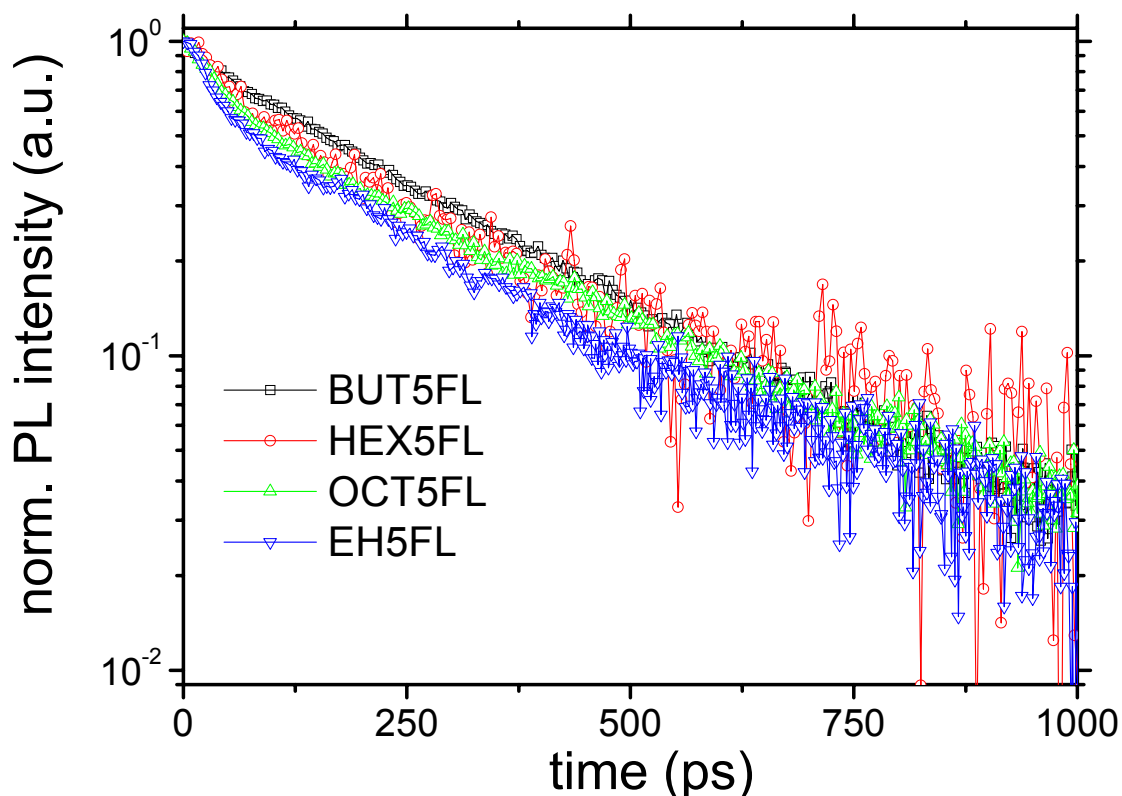
Figure 2.24: Room temperature normalised decay transients of all the oligo(fluorene) derivatives, as films on quartz substrates after annealing at 443 K in air: BUT5FL (squares), HEX5FL (circles), OCT5FL (up-triangles) and EH5FL (down-triangels). Excitation took place took place at 377 nm (3.29 eV), with 500 μW average laser power.  Pressure was kept at ~$10^{-4}$ mbar. The area of spectral integration was centred at the $S_{0-0} \leftarrow S_{1-0}$ singlet emission ± 20 nm.

| FILMS | BUT5FL | HEX5FL | OCT5FL | EH5FL |
|---|---|---|---|---|
| %$A_1$ | 11 | 11 | 39 | 23 |
| %$A_2$ | 89 | 89 | 61 | 77 |
| $A_1$ | $27 \pm 1.5$ | $15.1 \pm 1.8$ | $91 \pm 1.4$ | $70.45 \pm 1.3$ |
| $\tau_1$ (*ps*) | $35 \pm 4$ | $50 \pm 10$ | 46 | 37 |
| $A_2$ | $216 \pm 1$ | $36 \pm 2$ | $140 \pm 1$ | $87 \pm 1$ |
| $\tau_2$ (*ps*) | 271 | $247 \pm 9$ | 307 | 280 |
| $\tau_{1/e}$ (*ps*) | 237 | 194 | 178 | 137 |

Table 2.14: Determined amplitudes and decay constants for the annealed in air thin films of the oligo(fluorene) derivatives, as measured at room temperature. Time constants $\tau_{1/e}$ are also quoted.

According to analysis of the singlet transient decays of Figure 2.24, after heating in air all films of the OF5 are emitting biexponentially. Interestingly it is found that the amplitudes of the

second process related with the monitored decays have increased dramatically at the expense of the main observable radiative rates. Although this increase should be correlated with the concentration of the keto defects in the films, no quantitative interpretation can be done regarding the exact concentration of the keto defects, since no reference sample with a known concentration of keto sites was measured.

### *2.4.3.6  Spectroscopy of OF5 films at low temperature*

As it was shown in the beginning of this section, the intensity ratio ($S_{0-0} \leftarrow S_{1-0}$)/($S_{0-0} \leftarrow S_{1-0}$) was found to be different between the photoluminescence spectra of dilute solution and thin films of the PF derivatives. Differences in this ratio were also observed in paragraph 2.4.1, at low temperatures photoluminescence in the presented PF derivatives.

In principle, the presence of vibronic bands in a PL spectrum of a molecule gives strong evidence of electron-phonon coupling during an electronic transition. Electron-phonon coupling originates from a displacement between the minima of the ground and excited state potential energy curve, along the configurational axis. Such a displacement reflects the different equilibrated bond-geometries that molecules have in their ground state with respect to the corresponding electronically excited state. According to the Franck-Condon principle, the absorption process of a photon is a vertical process (see Chapter 1). Accordingly, the reversed transition of fluorescence process is based on the same principle. In this case the origin of the electronic transition is the zero-vibrational level of the lowest-lying electronic state. Under these conditions, the Franck-Condon factors become significant when a maximum wavefunction overlap exists with the vibrational levels of the ground state. In molecular spectroscopy, the strength of this electron-phonon coupling quantitatively is described by the Huang-Rhys parameter **S** [119]. For the simple case of a single harmonic oscillator of reduced mass M and angular frequency ω:

$$S = \frac{M * \omega}{2 * \hbar} * (\Delta Q)^2 \qquad \text{(eq. 2.1)}$$

where $\Delta Q$ is the above-mentioned displacement. For large values of $\Delta Q$ the vibrational wavefunction overlap becomes dominant for the higher vibrational levels of the ground state. In this case S>1 and the vibrational components of fluorescence carry more intensity than the electronic origin band [119].

 Due to the important band broadening of the emission in solid state, at room temperature, the assignment of the vibronic bands is a complicated task. Therefore low temperature data can be helpful for the identification of the vibronic levels of an electronically excited state. For the case of the here studied OF5 oligomers and the corresponding PF-EH polymer, low temperature (77 K) photoluminescence spectra were recorded.

 As a representative example, the PL spectrum of BUT5FL is presented, for which the increase of the $S_{0-1} \leftarrow S_{1-0}$ band intensity was found to be the most pronounced in the solid state. Figure 2.25 shows the PL spectrum of this derivative both at room temperature and 77 K. Apart from the expected band narrowing that is observed at lower temperature, it seems that the $S_{0-0} \leftarrow S_{1-0}$ emission band gains intensity on the expense of the lower energy vibronic bands.
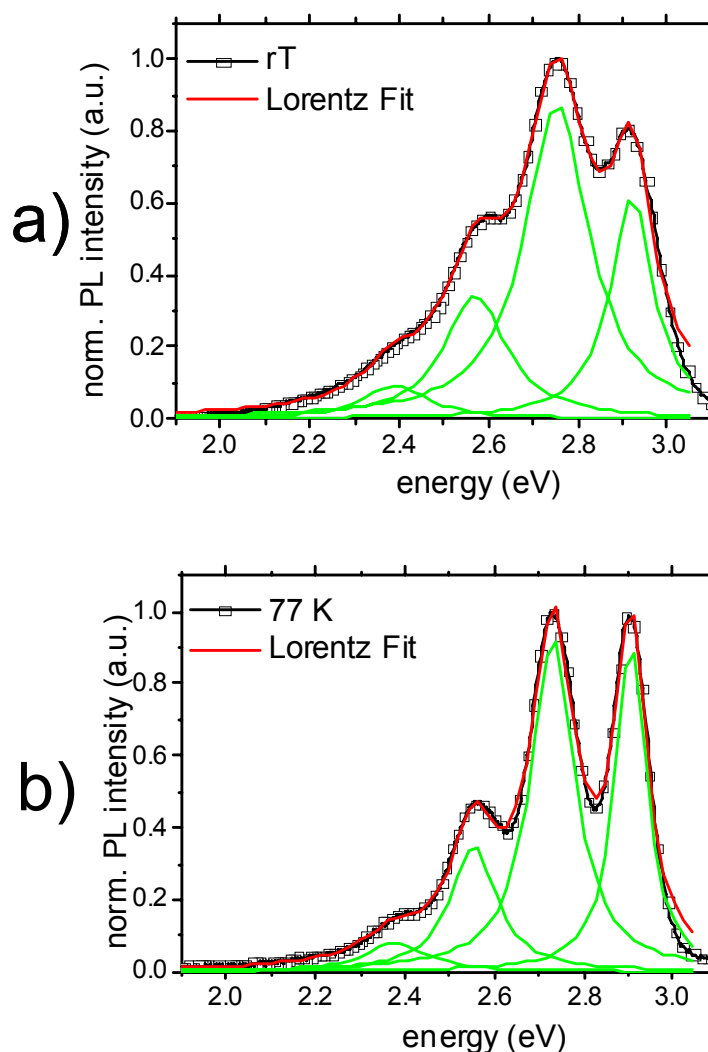


Figure 2.25: Time-integrated PL spectra of BUT5FL as thin film on quartz substrate, at: a) Room temperature and b) Low temperature (77 K). Time-integration in a 2 *ns* window. Excitation upon 405 nm (3.05 eV), with 500 µW average laser power. Pressure was kept at ~$10^{-5}$ mbar.

Table 2.15 and Table 2.16 presents an overview of the $(S_{0-0} \leftarrow S_{1-0})/(S_{0-1} \leftarrow S_{1-0})$ band amplitude ratios of the OF5 derivatives and the PF-EH polymer at room and low temperature.

| Films rT | $S_{0-0} \leftarrow S_{1-0}$ (a.u.) | $S_{0-1} \leftarrow S_{1-0}$ (a.u.) | $S_{0-2} \leftarrow S_{1-0}$ (a.u.) | $S_{0-3} \leftarrow S_{1-0}$ (a.u.) | $(S_{0-0} \leftarrow S_{1-0})/(S_{0-1} \leftarrow S_{1-0})$ |
|---|---|---|---|---|---|
| BUT5FL | 0.60 | 0.87 | 0.34 | 0.09 | 0.69 |
| EH5FL | 0.71 | 0.85 | 0.32 | 0.06 | 0.84 |
| PF-EH | 0.80 | 0.80 | 0.15 | 0.03 | 1 |

Table 2.15: Relative intensities of the time-integrated PL peaks for the systems studied as films on quartz substrate, at room temperature. The $(S_{0-0} \leftarrow S_{1-0})/(S_{0-1} \leftarrow S_{1-0})$ value is also quoted.

| Films 77 K | $S_{0-0} \leftarrow S_{1-0}$ (a.u.) | $S_{0-1} \leftarrow S_{1-0}$ (a.u.) | $S_{0-2} \leftarrow S_{1-0}$ (a.u.) | $S_{0-3} \leftarrow S_{1-0}$ (a.u.) | $(S_{0-0} \leftarrow S_{1-0})/(S_{0-1} \leftarrow S_{1-0})$ |
|---|---|---|---|---|---|
| BUT5FL | 0.89 | 0.92 | 0.35 | 0.08 | 0.98 |
| EH5FL | 0.90 | 0.85 | 0.32 | 0.09 | 1.06 |
| PF-EH | 0.90 | 0.70 | 0.14 | 0.07 | 1.29 |

Table 2.16: Relative intensities of the time-integrated PL peaks for the systems studied as films on quartz substrate, at low temperature (77 K). The $(S_{0-0} \leftarrow S_{1-0})/(S_{0-1} \leftarrow S_{1-0})$ value is also quoted.

## 2.5  DISCUSSION

In section 2.4.1 the optical properties of a dendronised and a non-dendronised PF derivative were compared. For our presented experimental results, it is of importance to remind that PF-D derivatives are amorphous material in the solid state that exhibit a glass transition temperature at ~520 K, whereas the main thermal decomposition of the material occurs at 700 K [99]. According to [99] studies with the polarised optical microscope gave no indication for the existence of a thermotropic liquid crystal phase. More importantly, from the X-ray diffraction experiments on a dendronised PF derivative, two broad correlation peaks were observed with *d*=0.44 nm and *d*=0.73 nm [99]. In contrast, PF-EH is a known thermotropoc liquid crystal [37] that has been described as a worm-like backbone surrounded by a cylindrical shell of disordered side chains [42].

Although in dilute solutions both of dendronised and non-dendronised materials posses similar spectral characteristics, their films exhibited different spectral broadening of the photoluminescence, indicating a different extend of interchain interactions in the solid state. This difference was also manifested in the time-resolved PL spectra of these derivatives where evidence for chain aggregation was given for the case of PF-D [102]. We attribute these observations in the different solid-state packing of the materials. The spectral broadening observed in PF-D, is attributed to the enhanced interactions imposed from the pendant bulky dendritic side-chains. This is in contrast to what was expected for a dendronised PF backbone. Initially dendronisation aimed on the effective shielding of the main polymer backbone. This idea arose from the hypothesis that interaction of polymer backbones is only a consequence of

co-facial π-π stacking. The dendritic side chains of the PF derivative shown in Figure 2.5, were found to stand perpendicular to the fluorene unit, shielding it efficiently [99]. However, as the side chains are comprised of aromatic units, π-π interactions between the pendant groups may take place. The structure of the monomer unit of this particular PF-D, as single crystal, was deduced for the temperature of 150 K (Figure 2.4 and Figure 2.5). At this stage, this experiment gave evidence for the existence of interaction between the terminal positions of each of the monomer molecules. Further analysis of the X-ray data is needed for the confirmation of this hypothesis. Additionally, interchain interaction may be a result of edge-to-edge interaction of two polymer backbones that lie on the same plane (see *Appendix A*). In fact the X-ray diffraction data collected for the same PF-D derivative in solid state [99] support this notion. The $d$=0.44 nm distance, as extracted from the one of the broad correlation peaks for PF-D, is approximately half of the fluorene monomer unit length [46]. Therefore this distance should be attributed to intercalation of side chains between two adjacent polymer backbones. Due to this virtual side chain interdigitation, the two adjacent backbones are closely separated by $d$=0.73 nm, as extracted from the second broad correlation peak for PF-D.

 The strong influence of solid-state packing on the observed optical properties of the studied polymers is pronounced from the experiments presented in 2.4.2. As it has already been mentioned PF-EH is a thermotropic liquid crystal that exhibits mesophase transitions at temperatures of 429 K and 440 K [37]. Comparison of the observed relaxation channels prior and after annealing at 443 K suggests that during annealing the material becomes more ordered. The thermally induced order reflects the transition from the glassy state to the more ordered liquid crystalline state that is trapped by rapid cooling back to room temperature. Consequently in this glassy state, the concentration of photoexcitation quenching traps is decreased in a way that the quenching of the singlet emission is reduced. Hence, this reduction of the photoluminescence is further expressed as an increase of the observable radiative singlet emission lifetime represented by $\tau_{1/e}$. Therefore, thermally induced intermolecular ordering may result in a rearranged exciton density of states in which the singlet exciton can migrate longer prior to radiative emission. Practically, quenching of luminescence occurs from extrinsic chemical defects that act as traps of the excitation energy. These defects usually lie lower in energy. Therefore any rearrangement of the density of states in which the exciton migrates would not importantly affect the quenching process. Hence, in the present case where exciton migration is influenced from the annealing, the PL traps should be related with film morphology rather than with extrinsic chemical impurities. We will refer to these quenching traps as physical defects by implying their interchain/intersegmental character. Although our experiment has not

clarified for the moment the exact nature of these defects, it assists their discrimination from the chemical defects that have been discussed in paragraph 2.2.5.

 The additional thermal treatment in air should have introduced chemical changes on the polymer backbone via formation of keto groups in the 9-position of the monomer units that constitute the polymer backbone. This suggestion is further supported by the comparison of the time delayed photoluminescence spectra of each of the differently treated polymers, presented in Figure 2.10. While in the cases of films isotropic and annealed under vacuum the spectra show a broad band centred at 480 nm, films treated under air show an extra red shifted broad band, with peak at 530 nm, which is the characteristic spectral position of the previously detected fluorenone defect [74].

Based on our observation for the case of polymeric PF derivatives, we make an effort to explain the spectroscopic results that were obtained for the case of fluorene-pentamers. Figure 2.16 shows for dilute solutions that the position of the peak absorption band is virtually independent from the nature of the side-chain attached on the pentamer backbone. According to Table 2.8 it was found that the band-width of the 0-0 absorption is almost the same for all derivatives, indicating a comparable width of excited state energy levels. Upon change of state from dilute solution regime to solid state as thin film, differences arise in the absorption characteristics (Figure 2.17).

 The fact that identical spectral positions of the absorption maxima in the solid-state are found reflects the monodispersed nature of the oligomers. Since no distribution of the effective conjugation length can exist in the oligomer, the electronic excitation during absorption occurs at sites of distinct energy gap. In other words, no inherent disorder effects of the electronic excited states are found when the conjugation length of the chromophore is not subject to statistical distribution. However, energetic disorder in the solid state of the oligomers may arise from the existence of an inhomogeneity in the environment that surrounds the chromophores. Alternatively this can be envisaged as enlargement of the absorption bandwidth in the solid state. This is particularly emphasized for the pentamer that is derivatised with branched side-chains. For this oligomer the band width is 1.5 times broader than in the case of the derivatives with *n*-alkyl pendant groups.

 In principle efficient packing results in a small degree of energetic dispersion in the energy levels of a chromophore in a matrix consisting of the same molecules. As absorption spectra reflect the width of the energy levels in the electronically excited state, small widths of absorption bands suggest narrow energetic widths of the excited state. Therefore *n*-alkyl pendant

groups should induce more ordered molecular arrangement of the oligomer backbones than the case of branched side chains.

Evidence for the existence of efficient packing of the oligomers bearing *n*-alkyl pendant groups comes from the red shift of the photoluminescence, upon shifting from dilute solution to solid state. By comparing the energetic difference in the spectral position of the second PL band between dilute solution and thin films (Table 2.9 and Table 2.11) it seems that the shorter the side chain, the higher is the PL red-shift. In terms of packing this should be interpreted that the more efficient molecular arrangment is achieved for the shortest *n*-alkyl side chain.

As the main backbone of the oligomers is built from repeated monomers that consist of bridged aromatic benzene rings, the origin of the interchain packing could arise from interchain π-π interactions between these aromatic units. Therefore it is conceivable that for the oligomer bearing the shortest *n*-alkyl side chains the degree of π-π interactions has to be highest. Alternatively, the origin of the packing behavior in the solid-state may arise from the different interaction of the side chains. Side-chain crystallization could also induce unique packing effects and this has been demonstrated in the case of a poly(fluorene) with octyl-side chains. In this case the crystallization of the side chains gave rise to a 'planar zigzag' or $2_1$ conformations with longer effective conjugation length (see paragraph 2.2.3). In the case of oligomers with octyl-side chain, no evidence of 'β-phase' formation was found, probably due to the good solvent that was used for the formation of films.

Our fluorescence spectroscopic data are an indirect examination for solid-state effects such as packing efficiency. Further structural investigation by diffraction experiments on oligo(fluorene) derivatives, bearing different side chains, is expected to justify our proposed hypotheses. For the moment the model compound that could elucidate the structural parameters is a pentfluorenone molecule that has been studied by means of X-ray diffraction.
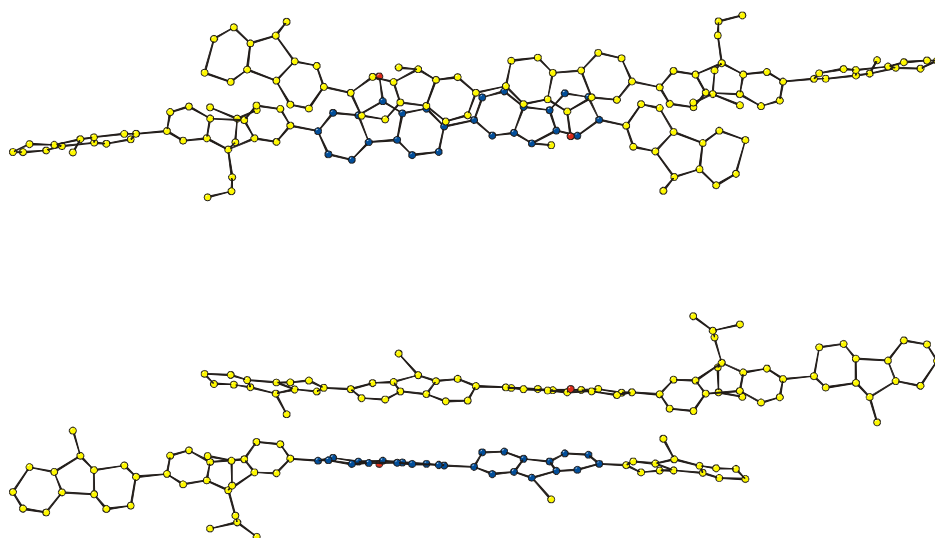
Figure 2.26: X-ray data as obtained for a single crystal structure of a penta(fluorenone) oligomer. The projection of the molecular plane onto the plane of an adjacent molecule is shown (upper structure). The interplanar distance has been found to be in the order of Van der Waals regime (lower structure). The atoms of the molecular segment that participate in the molecular interaction have been coloured differently for reasons of clarity. Note the existing intermolecular dihedral angle of the interacting molecular planes in the lower structure. X-ray data analyses as obtained from Dr. V. Enkellamnn [120].

The presented time-resolved spectroscopic data of the dilute OF5 solutions (Figures 2.18, 2.19) give a strong evidence for the chemical purity of the studied materials. As it has been discussed in paragraph 2.2.5, previous reports on dilute solutions of fluorene derivatives showed that at delayed times of detection, a significant contribution was observed in the spectral area of 530 nm. This emissive feature was assigned to keto defects located onto the backbone of the solutes studied. Our results presented in Figure 2.18b, clearly show that the delayed part of the monitored emission, maintains the singlet character of the prompt emission. In comparison with the prompt spectra (Figure 2.18a), no differences of the spectral position of the emission are observed, besides a reduction in absolute intensity. The postulate regarding chemical purity of the studied samples is further supported by the monoexponential character of the transient decay of the singlet emission up to 4 *ns* after excitation pulse. The fact that no deviation from the monoexponential decay is observed, implies the absence of extra relaxation channels for the dissipation of the initially given excitation energy, e.g. energy transfer to quenching centres that originate from extrinsic contaminants or interchain moieties. The latter are usually responsible for a red-shift of the prompt photoluminescence of isolated chromophores.

Alternatively it could be argued that even in the case where keto defects were present in the materials studied, the energy transfer towards them would be very slow due to the high dilution regime used. Therefore the possibility for the occurrence of excitation migration towards these quenching centres would be plausible only via an intrachain pathway. The time scale of an intrachain energy transfer process is orders of magnitude slower than the interchain energy transfer is [121], [122]. However, for the results presented here the slow transfer rate of intrachain energy migration would not make any major difference. We believe that the activation of on-chain keto defect on the studied pentamer would be instant. This would occur, due to the restricted length of the oligomeric chain that would leave give the opportunity to the primary photo excited state for experiencing the full length of the chain. Intrachain energy transfer has been described as hopping of the photo excitation within energetic sites of the polymer that are reflecting different effective conjugation lengths within the polymer backbone. For poly(fluorene) it has been determined that the effective conjugation length is in the order of 10-12 monomer fluorene units, depending on the optical data that were used, UV-Vis abs. or photoluminescence (see paragraph 2.2.8). Therefore, in the case of the isolated pentafluorene chains, the photo excitation probes immediately the whole backbone, since its length is far smaller than the determined effective conjugation length. Additionally, from quantum chemical semiempirical investigation (see paragraph 2.2.6) on model oligo(fluorene)s, containing a fluorenone moiety, it was predicted that the existence of the fluorenone unit within a heptamer, would induce a strong confinement effect of the created exciton. It was shown that the fluorenone defect eventually acts as a energetic trap that overlaps with the centre of mass of the exciton, while delocalisation of the latter could take place over the defect and its two neighbouring units. It was concluded that the created exciton is delocalised over the entire chain of the oligomer. Additionally, it was predicted that only after vibrational relaxation of the excited state the exciton was confined in the middle of the chain. But still, it was concluded that a considerable segment of the oligomeric chain could participate in the emission [95], [96]. Although the fluorene oligomers that were modelled were not substituted in the 9-position of the fluorene unit, no significant differences are expected to the photophysical properties in comparison with the oligomers studied in this work experimentally. Since exciton trapping was predicted to occur in an energetic level with non vanishing oscillator strength, it was concluded that keto-defects could be emissive with red-shifted emission, in respect with the inherent blue singlet emission of defect free pentamer. Therefore, the absence of the yellow emission of 530 nm in our studied system, that was in contrast observed in the case of dilute solutions of

oligo(fluorene)s and was attributed to the presence of on-chain chemical defects, reflects the high purity of the studied oligomers.

The chemical purity of our studied samples needs consideration of the actual synthetic route that was followed. Recently the effect of the synthetic routes followed for the preparation of poly(fluorene) derivatives on the chemical purity of the products has been addressed [79]. According to this report Suzuki synthetic route leads to more chemically pure polymers of far more larger molecular weight values than the Yamamoto route [79]. Comparison of the synthetic details should be done in order to identify the steps responsible for the introduction of the on-chain carbonyl functional group. Recently there was experimental evidence that the major origin of the fluorenone creation on to the polymeric backbone of π-conjugated polymers was the presence of mono-alkylated C-9 position of the monomer unit. This was a concsequence of the insufficient reaction time that did not allow the full alkylation of this highly sensitive to oxidation molecular position [3], [71]. Our experimental results demonstrate that the synthetic route, which was followed in order to obtain the presented oligomers, ensures the complete alkylation of the 9-position of the monomer unit and thus reduces the probability for detecting the carbonyl-based yellow emission in dilute solutions.

After optical excitation of the pentafluorene films, the different emission relaxation characteristics that were determined are the rate of singlet emission and the energy-transfer rate of the photo excitation to fluorescence quenching centres present in the films. The existence of these quenching centres is further supported from the time-resolved PL profiles (Figure 2.20b) where a broad featureless band is observed in the region of 480 – 500 nm. Since no indication of this spectral feature exists in the case of dilute solution (Figure 2.22b), we exclude the probability of singlet emission quenching via transfer to on-chain chemical defects. Therefore these quenching centres should be related to solid-state defects such as coming from interactions of the oligomer molecules. The fact that no new spectral features were identified in the absorption spectra of the oligomers as films, in comparison with the corresponding dilute solution, suggests that the intermolecular interactions should originate from molecules existing the excited electronic state. Excimer formation has been identified in the past as the responsible process for the observation of PL red shifting. According to our interpretation of the steady-state spectroscopic data for the studied oligomers, the derivatives that bear *n*-alkyl side chains are arranged in a more ordered manner in the solid-state giving rise to enhanced intermolecular interactions. Similarly, the observed broad featureless band in the region of 480 – 500 nm is strongly pronounced for the case case of BUT5FL, the derivative with the shortest *n*-alkyl side chain.

For confirming the hypothesis that the emission in the spectral region of 480 – 500 mn is related to an interchain interaction rather than being an inherent electronic characteristic of the oligomers, a comparison of the emission kinetics was presented for two different spectral regions of the PL emission in Figure 2.22. While for all the pentamers studied in dilute solution, both spectral regions were found to obey the same decay law, the situation was different in the solid state. As Figure 2.18c manifests, only the EH5FL film behaves as it is in solution. Due to the branched side chains, in this derivative inter-digitation of the side chains on neighbouring side chains is restricted, leading to efficient backbone shielding by the formation of isolated cylindrical objects. The case of the polymeric analogue is exhibiting the same behaviour (Figure 2.22d). While initially the decay of the two different spectral regions follows the same pattern, the low-energy region seems to decay slower. As the film of PF-EH was in its pristine state, we speculate that it existed in a glassy state that contained a combination of regions with different degree of order. We postulate that repetition of the same experiment of similar film that would have been glassified in its liquid crystalline state, would result in data similar to Figure 2.18c.

Our experimental results on thermal oxidation of the oligomers in the presence of air evidence the introduction of a new quenching centre that can act as an activator and traps the singlet excitation energy. This activator centre can then relax radiatively by emitting at 525 nm. The activation of the energy transfer process towards this defect is further suggested from the bi-exponential decay function that the singlet emission of all treated oligomers follows (Figure 2.24).

We propose that the nature of this thermally induced activator centre is the keto group. The formation of this centre has been detected experimentally via IR spectroscopy in films of PF after thermal treatment at ambient conditions. A conclusion can be drawn regarding the susceptibility of each of the OF5 in ambient conditions where $O_2$ is present. It seems that although OCT5FL and EH5FL as films, tend to have a monoexponential decay behaviour for measurements under vacuum, their film become much more susceptible to oxidation when their fluorescence is measured after annealing the film in air. This is obvious from the high amplitude of the extra relaxation channel that is detected after heating in air.

The steady-state photophysical studies of both the polymers and oligomers presented in this Chapter showed differences in room and low temperatures. Particularly for the emission profiles, comparison of the amplitude ratios for the two different temperatures reveals that the ratio has higher values at lower temperatures. This indirectly implies that, the excited state potential hypersurfaces adapt bond equilibrated geometries that are similar to those of the ground state and that no significant displacement of the potential energy minima exist after electronic excitation at

low temperatures. This has been shown for the low temperature (4.2 K) PL spectrum of PF-EH (Figure 2.12), in paragraph 2.4.1 and for the case of the oligomers in 2.4.3 (Figure 2.25). The data of Table 2.15 and Table 2.16 suggest that at the linear *n*-alkyl side chains induce bond alteration in the lowest excited electronic state in such a manner that the larger displacement of bond-length equilibrium is obtained for the shorter linear side-chain.

## 2.6  CONCLUSIONS

Poly(fluorene)s are thermotropic liquid crystalline materials that are considered excellent candidates for the development of polymer based light-emitting devices. However, their emissive performance still suffers from a low-energy green emission contribution. The origin of this unwanted emission has been debated for long time in the literature. Currently the dominant opinion supports that this emission is a result of on-chain chemical impurities that are created during synthesis or *in-situ* during device performance. Therefore ongoing rigorous optimisation is taking place in the synthetic route for the production of stable blue emitting poly(fluorene)s. The impact of inter-segment interactions in the solid state is also significant reason for the spectral contamination in the emission spectra of poly(fluorene)s. Interchain interactions are a result of aggregation that under certain conditions may lead to formation of low-energy emissive excimers. As interchain interactions are affected from the molecular packing of poly(fluorene)s in the solid state, manipulation of the molecular ordering via the control of liquid crystal mesophases, may improve the color stability of chemically pure poly(fluorene)s.

In this Chapter the effort of obtaining spectrally pure poly- and oligo-(fluorene)s derivatives was assessed. We used time-resolved photoluminescence spectroscopy in order to evaluate the quality of the photophysical properties of the materials studied.

It has been shown that the attachment of dendritic bulky side chains onto the polymeric backbone of poylfluorene could not improve the backbone shielding and could not prevent the interchain interactions in the solid state. Based on our steady-state spectroscopic results and in combination with the previously reported structural and thermal data, we conclude that the specific dendritic side chains that were used as bulky substituents, result in an amorphous material that contain separated polymer backbones at a close distance where edge to edge polymer backbone or terminal point interaction may take place (see *Appendix A*). In larger spatial scale within the material the degree of this intermolecular interactions varies thus giving rise to a broadening of the spectral characteristics of absorption and emission, as evidenced from the comparison with a conventional poly(fluorene) derivative.

Instead of the attachment of bulky side chains, it was shown that an increase in the colour stability of poly(fluorene) may take place by the control of the phase that this material exist. It was presented that for an ethylhexyl substituted poly(fluorene) (PF-EH) an increase in the blue emission was achieved after obtaining a glassy state of the material frozen in its liquid crystalline mesophase. The increased order of this liquid crystalline state was further evidence from the reduction of the low-energy band that the photoluminescence of a pristine PF-EH film has shown. The origin of this low-energy band was clarified from the time-resolved photoluminescence experiments that were performed in a series of pentafluorene oligomers.

Based on the time resolved spectra of the differently derivatised OF5s we concluded on the origin of observed delayed green spectral component. Time resolved studies of the pentamers in non-aromatic solvent in the regime of dilution where no interchain interactions are taking place, allowed us to support the high chemical purity of these compounds.

Subsequently in the case of OF5s films, the comparison of the kinetics of the singlet OF5 emission before and after exposing the studied films to $O_2$ with parallel heating, lead us to the conclusion that two distinct optical centres are contributing to the rise of the delayed greenish/yellow feature, namely an excimer defect and a chemical defect. We attribute the existence of the excimer defect on the extent at which the OF5 chains can interact efficiently and lead towards the crystalline phase.

The study of the pentafluorenes supports that the ability of the pentafluorene to form an excimer defect depends on the side chain attached on its backbone. The impact of side chain inter-digitation is found to be of great importance in the photophysical performance of the oligo(fluorene) derivatives. Oligo(fluorene) derivatives with branched pendant groups, that do not interdigitate with adjacent side chains in the solid state, are found spectrally clean while oligo(fluorene)s derivatised with short and linear alkyl chains are found to posses a significant contribution of unwanted spectral contamination in the region of 480 nm.

Additional thermal treatment of the oligo(fluorene) films at ambient conditions imposes a red-shift to the unwanted spectral feature. In accord with the theoretical models that have been suggested for the fluorenone-containing oligomers, we assign this spectral feature to the presence of fluorenone groups that were formed by thermal oxidation of the films.

Therefore the issue of spectral purity in poly- and oligo(fluorene) derivatives has a dual character. Once the chemical purity of the materials is established, appropriate side chains of the backbone must be chosen. The selection of this pendant groups should be based on the impact that the have on the molecular packing of the polymer/oligomer backbones in the solid state. Our present studies suggest that among the materials studied in this Chapter, the ethyl-hexyl fuorene

pentamer is the best candidate to be incorporated in polymer based light-emitting devices. Further studies should be performed for this material regarding its electrochemical stability and its device electruluminescence efficiency.

## 2.7  REFERENCES

1.      Leclerc M., *Polyfluorenes: Twenty Years of Progress.* J. Polym. Sci. Part A: Polym. Chem., 2001. **39**: p. 2867.
2.      Neher D., *Polyfluorene Homopolymers: Conjugated Liquid-Crystalline Polymers for Bright Blue Emission and Polarized Electroluminescence.* Macromol. Rapid Commun., 2001(22): p. 1365-1385.
3.      Scherf U., List E.J.W., *Semiconducting Polyfluorenes-Towards Reliable Structure-Property Relationships.* Adv.Mater., 2002. **14**(7): p. 477.
4.      Virgili T., Lidzey D.G.,Bradley D.D.C., *Efficient Energy Transfer from Blue To Red in Tetraphenylporphyrin-Doped Poly(9,9-dioctylfluorene) Light-Emitting Diodes.* Adv. Mater., 2000. **12**(1): p. 58.
5.      Laquai F., Im C., Kadashchuk A.,Bässler H., *Sensitized intrinsic phosphorescence from a poly(phenylene-vinylene) derivative.* Chem. Phys. Lett., 2003. **375**: p. 286.
6.      Li B., Li J.L., Fu Y.,Bo Z., *Porphyrins with Four Monodisperse Oligofluorene Arm as Efficient Red Light-Emitting Materials.* J. Am. Chem. Soc., 2004. **126**: p. 3430.
7.      Charas A., Morgado J., Martinho J.M.G., Alcácer L., Cacialli F., *Electrochemical and luminescent properties of poly(fluorene) derivatives for optoelectronic applications.* Chem. Commun., 2001: p. 1216.
8.      Charas A., Morgado J., Martinho J.M.G., Alcácer L., Cacialli F., *Tuning the optoelectronic properties of polyfluorenes by copolymerisation with thiophene moieties.* Synth. Met., 2002. **127**: p. 251.
9.      Ling Q.D., Kang E.T., Neoh K.G., Huang W., *Synthesis and Nearly Monochromatic Photoluminescence Properties of Conjugated Copolymers Containing Fluorene and Rare Earth Complexes.* Macromolecules, 2003. **36**: p. 6995.
10.     Geng Y., Chen A.C.A., Ou J.J., Chen S.H., *Monodisperse Glassy Nematic Conjugated Oligomers with Chemically Tunable Polarized Light Emission.* Chem. Matter., 2003. **15**: p. 4352.
11.     Wu F.-I., Reddy S., Shu C.-Fong, Liu M.S., Jen A.K.-Y., *Novel Oxadiazole-Containing Polyfluorene with Efficient Blue Electroluminescent.* Chem. Matter., 2003. **15**: p. 269.
12.     Chen X., Liao J.-L., Liang Y., Ahmed M.O., Tseng H.-E., Chen S.-A., *High-Efficiency Red-Light Emission from Polyfluorene Grafted with Cyclometalated Iridium Complexes and Charge Transport Moiety.* J. Am. Chem. Soc., 2003. **125**: p. 636.
13.     Hide F., Díaz-García M., Schwartz B.J., Anderson M.R., Pei Q., Heeger A.J., *Semiconducting Polymers:A New Class of Solid-State Laser Materials.* Science, 1996. **273**: p. 1833.
14.     Heliotis G., Bradley D.D.C., Turnbull G.A., Samuel I.D.W., *Light amplification and gain in polyfluorene waveguides.* Appl. Phys. Lett., 2002. **81**(3): p. 415.
15.     Schroeder R., Ullrich B., Graupner W.,Scherf U., *Excitation density and photoluminescence studies of polyfluorene excited by two-photon absorption.* J. Phys.: Condens. Matter, 2001. **13**: p. L313.
16.     Fytas G., Nothofer H.G., Scherf U., Vlassopoulos D., Meier G., *Structure and Dynamics of Nondilute Polyfluorene Solutions.* Macromolecules, 2002. **35**: p. 481.
17.     Wu L., Sato T., Tang H.-Z., Fujiki M., *Conformation of a Polyfluorene Derivative in Solution.* Macromolecules, 2004. **37**: p. 6183.
18.     Tang C.W., VanSlyke S.A., *Organic electroluminescence diodes.* Appl. Phys. Lett., 1987. **51**(12): p. 913.
19.     Burroughes J.H., Bradley D.D.C., Brown A.R., Marks R.N., Mackay K., Friend R.H., Burns P.L., Holmes A.B., *Light-emitting diodes based on conjugated polymers.* Nature, 1990. **347**: p. 539.

20.    Pei Q., Yang Y., *Efficient Photolumnescence and Electroluminescence from a soluble Polyfluorene.* J. Am. Chem. Soc., 1996. **118**: p. 7416.

21.    Tasch, S., Niko, A., Leising, G.,Scherf, U., *Highly efficient electroluminescence of new wide band gap ladder-type poly(para-phenylenes).* Applied Physics Letters, 1996. **68**(8): p. 1090-1092.

22.    Friend R.H., Gymer R.W., Holmes A.B., Burroughes J.H., Marks R.N., Taliani C., Bradley D.D.C., Dos Santos D.A., Brédas J.-L., Lögdlund M., Salaneck W.R., *Electroluminescence in conjugated polymers.* Nature, 1999. **397**: p. 121.

23.    Tessler N., Medvedev V., Kazes M., Kan S., Banin U., *Efficient Near-Infrared Polymer Nanocrystal Ligh-Emitting Diodes.* Science, 2002. **295**: p. 1506.

24.    Cleave V., Yahioglu G., Le Barny P., Friend R.H.,Tessler N., *Harvesting Singlet and Triplet Energy in Polymer LEDs.* Adv. Mater., 1999. **11**(4): p. 285.

25.    Leger J.M., Carter S.A., Ruhstaller B., H.-G. Nothofer, Scherf U., Tillman H., Hörhold H.-H., *Thickness-dependent changes in the optical properties of PPV- and PF-based polymer light-emitting diodes.* Phys. Rev. B, 2003. **68**: p. 054209.

26.    Redecker M., Bradley D.D.C., Inbasekaran M., Woo E.P., Appl. Phys. Lett., 1998. **73**: p. 1565.

27.    Redecker M., Bradley D.D.C., Inbasekaran M., Woo E.P., *Nondispersive hole transport in an electroluminescent polyfluorene.* Appl. Phys. Lett., 1998. **73**: p. 1565.

28.    Redecker M., Bradley D.D.C., Inbasekaran M., Wu W.W., Woo E.P., *High Mobility Hole Transport Fluorene-Triarylamine Copolymers.* Adv. Mater., 1999. **11**(3): p. 241.

29.    Sainova D., Miteva T., Nothofer H.-G., Scherf U., Glowacki I., Ulanski J., Fujikawa H., Neher D., *Control of colour and efficiency of light-emitting diodes based on polyfluorenes with hole-transporting molecules.* Appl. Phys. Lett., 2000. **76**: p. 1810.

30.    Miteva T., Meisel A., Knoll W., Nothofer H.-G., Scherf U., Müller D.C., Meerholz K., Yasouda A., Neher D., *Improving the performance of Polyfluorene-based Organic Light-Emitting Diodes via End-capping.* Adv. Mater., 2001. **13**(8): p. 565.

31.    Grozema F.C., Siebeles L.D.A., Warman J.M., Seki S., Tagawa S., Scherf U., *Hole conduction along molecular wires:  σ-Bond Silicon versus π-Bond-conjugated Carbon.* Adv. Mater., 2002. **14**: p. 228.

32.    Burrows H.D., Seixas de Melo J., Forster M., Güntner R., Scherf U., Monkman A.P., Navaratnam S., *Hole formation and transfer in poly[9,9-di(ethylhexyl)fluorene] and an amine end-capped derivative in solution.* Chem. Phys. Lett., 2004. **385**: p. 105.

33.    Redecker M., Bradley D.D.C., Inbasekaran M., Woo E.P., *Mobility enhancement through homogeneous nematic alignmnet of a liquid-crystalline polyfluorene.* Appl. Phys. Lett., 1999. **74**(10): p. 1400.

34.    Sirringhaus H., Wilson R.J., Friend R.H., Inbasekaran M., Wu W., Woo W.P., Grell M., Bradley D.D.C., *Mobility enhancement in conjugated polymer field-effect transistors through chain alignment in a liquid-crystalline phase.* Appl. Phys. Lett., 2000. **77**(3): p. 406.

35.    Collings P.J., Hird M., *Introduction to Liquid Crystals Chemistry and Physics.* The Liquid Crystals Book, ed. G.G.W.G.J.W.F. A. 1997, London, Bristol: Taylor & Francis Ltd.

36.    Sonin A.A., *The Surface Physics of Liquid Crystals.* 1995, Amsterdam: Gordon and Breach Publishers.

37.    Grell M., Bradley D.D.C., Inbasekaran M., Woo Ed.P., *A Glass-Forming Conjugated Main-Chain Liquid Crystal Polymer for Polarized Electroluminescence Applications.* Adv.Mater., 1997. **9**(10): p. 798.

38.    Grell M., Bradley D.D.C., Ungar G., Hill J., Whitehead K.S., *Interplay of Physical Structure and Photophysics for a Liquid Crystalline Polyfluorene.* Macromolecules, 1999. **32**: p. 5810.

39.    Sainova D., Zen A., Nothofer H.G., Asawapirom U., Scherf U., Hagen R., Bieringer T., Kostromine S., Neher D., *Photoaddressable Alignment Layers for Fluorescent Polymers in Polarized Electroluminescence Devices.* Adv. Funct. Mater. 2002, 2002. **12**(1): p. 49-57.

40.    Grell M., Bradley D.D.C, *Polarized Luminescence from Oriented Molecular Materials.* Adv. Mater., 1999. **11**(11): p. 895-905.

41.    Gulligan S.W., Geng Y., Chen S.H., Klubek K., Vaeth K.M., Tang C.W., *Strongly Polarized and Efficient Blue Organic Light-Emitting Diodes Using Monodisperse Glassy Nematic Oligo(fluorene)s.* Adv.Mater., 2003. **15**(14): p. 1176.

42.    Lieser G., Oda M., Miteva T., Meisel A., Nothofer H.G., Scherf U., Neher D., *Ordering, Graphoepitaxial Orientation, and Conformation of a Polyfluorene Derivative of the 'Hairy-Rod' Type on an Oriented Substrate of Polyimide.* Macromolecules, 2000. **33**: p. 4490.

43.    Kawana S., Durrell M., Lu J., MacDonald J.E., Grell M., Bradley D.D.C., Jukes P.C., Jones R.A.L., Bennett S.L., *X-ray diffraction study of the structure of thin polyfluorene films.* Polymer, 2002. **43**: p. 1907.

44.    Knaapila M., Lyons B.L., Kisko K., Foreman J.P., Vainio U., Mihaylova M., Seeck O.H., Lars-Olof P., Serimaa R., Torkkeli M., Monkman A.P., *X-ray Diffraction Studies of Multiple Orientation in Poly(9,9-bis(ethylhexyl)fluorene-2,7,-diyl) Thin Films.* J. Phys. Chem. B, 2003. **107**: p. 12425.

45.    Ariu M., Sims M., Rahn M.D., Hill J., Fox A.M., Lidzey D.G., Oda M., Cabanillas-Gonzalez J., Bradley D.D.C., *Exciton migration in β-phase poly(9,9-dioctylfluorene).* Phys. Rev. B, 2003. **67**: p. 195333.

46.    Winokur M.J., Slinker J., Huber. D.L., *Structure, photophysics, and the order-disorder transition to the β phase in poly(9,9-(di-n,n-octyl)fluorene).* Phys. Rev. B, 2003. **67**: p. 184106.

47.    Ariu M., Lidzey D.G., Lavrentiev M., Bradley D.D.C., Jandke M., Strohriegl P., *A study of the different structural phases of the polymer poly(9,9'-dioctyl fluorene) using Raman spectroscopy.* Synthetic Metals, 2001. **116**: p. 217.

48.    Chen S.H., Chou H.L., Su A.C., Chen S.A., *Molecular Packing in Crystalline Poly(9,9-di-n-octyl-2,7-fluorene).* Macromolecules, 2004. **37**: p. 6833.

49.    Ariu M., Lidzey D.G., Sims M., Cadby A.J., Lane P.A., Bradley D.D.C., *The effect of morphology on the temeprature-dependent photoluminescence quantum efficiency of the conjugated polymer poly(9,9-dioctylfluorene).* J. Phys.: Condens. Matter, 2002. **14**: p. 9975.

50.    Sainova D., Neher D., Dobruchowska E., Luszczynska B., Glowacki I., Ulanski J., Nothofer H.-G., Scherf U., *Thermoluminescence and electroluminecence of annealed polyfluorene layers.* Chem. Phys. Lett., 2003. **371**: p. 15.

51.    Rothe C., Hintschich S.I., L.-O. Palsson, Monkman A.P., Guentner R., Scherf U., *Pressure dependent radiative quantum yields of the prompt and delayed luminescence of polyfluorene films.* Chem. Phys. Lett., 2002. **360**: p. 111.

52.    Lemmer U., Mahrt R.F., Wada Y., Greiner A., Bässler H., Göbel E.O., *Picosecond hopping relaxation in conjugated polymers.* Chem. Phys. Lett., 1993. **209**(3): p. 243.

53.    Meskers S.C.J., Hübner J., Oestreich M., Bässler H., *Dispersive Relaxation Dynamics of Photoexcitations in a Polyfluorene Film Involving Energy Transfer: Experiment and Monte Carlo Simulations.* J. Phys. Chem. B, 2001. **105**: p. 9139.

54.    Meskers S.C.J., Hübner J., Oestreich M., Bässler H., *Time-resolved fluorescence studies and Monte Carlo simulations of relaxation dynamics of photoexcitations in a polyfluorene film.* Chem. Phys. Lett., 2001. **339**: p. 223.

55.    Bauer C., Ursbasch G., Giessen H., Meisel A., Nothofer H.-G., Neher D., Scherf U., Mahrt R.F., *Polarized Photoluminescence and Spectral Narrowing in an Oriented Polyfluorene Thin Film.* ChemPhysChem, 2000. **3**(142).

56.    Rauscher U., Bässler H., Bradley D.D.C., Hennecke M., *Exciton versus band description of the absorption and luminescence spectra in poly(p-phenylenevinylene).* Phys. Rev. B, 1990. **42**(16): p. 9830.

57.    Dias F.B., Macanita A.L., Seixas de Melo J., Burrows H.D., Güntner R., Scherf U., Monkman A., *Picosecond conformational relaxation of singlet excited polyfluorene in solution.* J. Chem. Phys., 2003. **118**(15): p. 7119.

58.    Papadopoulos P., Floudas G., Chi C., Wegner G., *Molecular dynamics of oligofluorenes: A dielectric spectroscopy investigation.* J. Chem. Phys., 2004. **120**(5).

59.    Buckley A.R., Rahn M.D., Hill J., Cabanillas-Gonzalez J., Fox A.M., Bradley D.D.C., *Energy transfer dynamics in polyfluorene-based polymer blends.* Chem. Phys. Lett., 2001. **339**: p. 331.

60.    Charas A., Morgado J., Martinho J.M.G., Fedorov A., Alcácer L., Cacialli F., *Excitation energy transfer and spatial exciton confinment in polyfluorene blends for application in light-emitting diodes.* J. Mater. Chem., 2002. **12**: p. 3523.

61.    Westerling M., Vijila C., Österbacka R., Stubb H., *Optical studies of excited-state relaxation in poly(9,9-dihexylfluorene-co-benzothiadiazole).* Phys. Rev. B, 2003. **67**: p. 195201.

62.    Gamerith S., Gaal M., Romaner L., Nothofer H.-G., Güntner R., Scandiuccy de Freitas P., Scherf U., List E.J.W., *Comparison of thermal and electrical degradation effects in polyfluorenes.* Synthetic Metals, 2003. **139**: p. 855.

63.    Tessler N., Harrison N.T., Thomas D.S., Friend R.H., *Current heating in polymer light-emitting diodes.* Appl. Phys. Lett., 1998. **73**(6): p. 732.

64.    Yan M., Rothberg L.J., Papadimitrakopoulos F., Galvin M.E., Miller T.M., *Defect Quenching of Conjugated Polymer Luminescence.* Phys. Rev. Lett., 1994. **73**(5): p. 744.

65.    Antoniadis H., L.J. Rothberg, Papadimitrakopoulos F., Yan M., Galvin M.E., Abkowitz M.A., *Enhanced carrier photogeneration by defects in conjugated polymers and its mechanism.* Phys. Rev. B, 1994. **50**(20): p. 14911.

66.    Rothberg L.J., Yan M., Papadimitrakopoulos F., Galvin M.E., Kwock E.W., Miller T.M., *Photophysics of phenylenevinylene polymers.* Synth. Met., 1996. **80**: p. 41.

67.    Sinha S., Rothe C., Güntner R., Scherf U.,Monkman A.P., *Electrophosphorescence and Delayed Electroluminecence from Pristine Polyfluorene Thin-Film Devices at Low Temperature.* Phys. Rev. Lett., 2003. **90**(12): p. 127402.

68.    Kreyenschmidt M., Klaerner G., Fuhrer T., Ashenhurst J., Karg S., Chen W.D., Lee V.Y., Scott J.C., Miller R.D., *Thermally Stable Blue-Light-Emitting Copolymers of Poly(alkyfluorene).* Macromolecules, 1998. **31**: p. 1099.

69.    Bliznyuk V.N., Carter S.A., Scott J.C., Klärner G., Miller R.D., Miller D.C., *Electrical and Photoinduced Degradation of Polyfluorene Based Films and Light-Emitting Devices.* Macromolecules, 1999. **32**(2): p. 361.

70.    List E.J.W., Guentner R., Scanducci de Freitas P., Scherf U., *The effect of Keto Defect Sites on the Emission Properties of Polyfluorene-Type Materials.* Adv.Mater., 2002. **14**(5): p. 374.

71.    Craig M.R., de Kok M.M., Hofstraat J.W., Schenning A.P.H.J., Meijer E.W., *Improving color purity and stability in a blue emitting polyfluorene by monomer purification.* J. Mater. Chem., 2003. **13**: p. 2861.

72.    Weinfurtner K.-H., Fujikawa H., Tokito S., Taga Y., *High efficient pure blue electroluminescence from polyfluorene: Influence of the molecular weight distribution on the aggregation tendency.* Appl. Phys. Lett., 2000. **76**: p. 2502.

73.    Romaner L., Piok T., Gadermaier C., Guentner R., Scandiucci de Freitas P., Scherf U., Gerullo G., Lanzani G., List E.J.W., *The influence of keto defects on photoexcitation dynamics in polyfluorenes.* Synthetic Metals, 2003. **139**: p. 851.

74.    Lupton J.M., Craig M.R., Meijer E.W., *On-chain defects emission in electroluminescent polyfluorenes.* Appl.Phys.Lett., 2002. **80**(24): p. 4489.

75.    Yang X.H., Neher D., Spitz C., Zojer E., Brédas J.-L., Güntner R., Scherf U., *On the polarisation of the green emission of polyfluorenes.* J. Chem. Phys., 2003. **119**(13): p. 6832.

76.    Hintschich S.I., Rothe C., Sinha S., Monkman A.P., Scandiuccy de Freitas P., Scherf U., *Population and decay of keto states in conjugated polymers.* J. Chem. Phys., 2003. **119**(22): p. 12017.

77.    Gong X., Moses D., Heeger A.J., Xiao S., *White light electrophosphorescence from polyfluorene-based light-emitting diodes:utilization of fluorenone defects.* J. Phys. Chem. B, 2004. **108**(25): p. 8601.

78.    Kulkarni A.P., Kong X., Jenekhe S.A., *Fluorenone-Containing Polyfluorenes and Oligofluorenes: Photophysics, Origin of the Green Emission and Efficient Green Electroluminescence.* J. Phys. Chem. B, 2004. **108**: p. 8689.

79.    Sims M., Bradley D.D.C., Ariu M., Koeberg M., Asimakis A., Grell M., Lidzey D.G., *Understanding the Origin of the 535 nm Emission Band in Oxidized Poly(9,9-dioctylfluorene): The Essential Role of Inter-Chain/Inter-Segment Interactions.* Adv. Funct. Mater., 2004. **14**(8): p. 765.

80.    Zhao W., Cao T., White J.M., *On the Origin of Green Emission in Polyfluorene Polymers:The Roles of Thermal Oxidation Degradation and Crosslinking.* Adv. Funct. Mater., 2004. **14**(8): p. 783.

81.    Pei J., Liu X.-L., Chen Z.-K., Zhang X.-H., Lai Y.-H., Huang W., *First Hydrogen-Bonding-Induced Self-Assembled Aggregates of a Polyfluorene Derivative.* Macromolecules, 2003. **36**: p. 323.

82.    Teetsov J., Fox M.A., *Photophysical characterization of dilute solutions and ordered thin films of alkyl-substituted polyfluorenes.* J. Mater. Chem., 1999. **9**: p. 2117.

83.    Marsitzky D., Klapper M., Müllen K., *End-functionalization of Poly(2,7-fluorene): A Key Step toward Novel Luminescent Rod-Coil Block Copolymers.* Macromolecules, 1999. **32**: p. 8685.

84.    Surin. M., Marsitzky D., Grimsdale A.C., Müllen K., Lazzaroni R., Leclére P., *Microscopic Morphology of Polyfluorene-Poly(ethylene oxide) Block Copolymers: Influence of the Block Ratio.* Adv. Funct. Mater., 2004. **14**(7): p. 708.

85.    Tsolakis T.K., Kallitsis J.K., *Synthesis and Characterisation of Luminescent Rod-Coil Block Copolymers by Atom Transfer Radical Polymerization: Utilization of Novel End-Functionalized Terfluorenes as Macroinitiators.* Chem. Eur. J., 2003. **9**(4): p. 936.

86.    Chochos C.L., Tsolakis T.K., Gregoriou V.G.,  Kallitsis J.K., *Influence of the Coil Block on the Properties of Rod-Coil Diblock Copolymers with Oligofluorene as the Rigid Segment.* Macromolecules, 2004. **37**(7): p. 2502.

87.    Gadermaier C., Lanzani G., *Photophysics of conjugated polymers: the contribution of ultrafast spectroscopy.* J. Phys.: Condens. Matter, 2002. **14**: p. 9785.

88.    Bjorklund T.G., Lim S.-H., Bardeen C.J., *Use if Picosecond Fluorescence Dynamics as an Indicator of Exciton Motion in Conjugated Polymers: Dependence on Chemical Structure and Temperature.* J. Chem. Phys. B, 2001. **2001**(105): p. 11970.

89.    Lemmer U., Heun S., Mahrt R.F., Scherf U., Hopmeier M., Siegner U., Göbel E.O., Müllen K., Bässler H., *Aggregate fluorescence in conjugated polymers.* Chem. Phys. Lett., 1995. **240**: p. 373.

90. Jenekhe S.A.,Osaheni J.A., *Excimers and Exciplexes of Conjugated Polymers*. Science, 1994. **265**: p. 765.

91. Guillet J., *Polymer Photophysics and Photochemistry , An Introduction to the Study of Photoprocesses in Macromolecules*. 1985, Cambridge, New York: Cambridge Univ. Press.

92. Cornil J., dos Santos D.A., Crispin X., Silbey R., Brédas J.-L., *Influence of Interchain Interactions on the Absorption and Luminescence of Conjugated Oligomers and Polymers: A Quantum-Chemical Characterization*. J. Am. Chem. Soc., 1998. **120**: p. 1289.

93. Lippert E., Walter H., *Darstellung und UV-Spektren einiger Fluorenon-Derivate*. Angew. Chem., 1959. **71**: p. 429.

94. Yoshihara K., Kearns D.R., *Spectroscopic Properties of the Lower-Lying Excited States of Fluorenone*. J. Chem. Phys., 1966. **45**(6): p. 1991.

95. Zojer E., Pogantsch A., Hennebicq E., Beljonne D., Brédas J.-L., Scandiucci de Freitas P., Scherf U., List E.J.W., *Green emission from poly(fluorene)s: The role of oxidation*. J. Chem. Phys., 2002. **117**(14): p. 6794.

96. Ignacio F., Tretiak S., *Electron-vibrational relaxation of photoexcited polyfluorenes in the prescence of chemical defects:A theoretical Study*. Chem. Phys. Lett., 2003. **372**: p. 403.

97. Cornil J., Gueli I., Dkhissi A., Sancho-Garcia J.C., Hennebicq E., Calbert J.P., Lemaur V., Beljonne D., Brédas J.-L., *Electronic and optical properties of polyfluorene and fluorene-based copolymers: A quantum-chemical characterization*. J. Chem. Phys., 2003. **118**: p. 6615.

98. Freeman A.W., Shannon C.K., Malenfant R.L., Thompson M.E., Fréchet J.M.J., *Dendrimer-Containing Light-Emitting Diodes: Toward Site-Isolation of Chromophores*. J. Am. Chem. Soc., 2000. **122**: p. 12385.

99. Setayesh S., Grimsdale A.C., Weil T., Enkelmann V., Müllen K., Meghdadi F., List E.J.W., Leising G., *Polyfluorenes with Polyphenylene Dendron Side Chains: Toward Non-Aggregating, Light-Emitting Polymers*. J. Am. Chem. Soc., 2001. **123**: p. 946.

100. Tang H.-Z., Fujiki M., Zhang Z.-B., Torimitsu K., Motonaga M., *Nearly pure blue photoluminescent poly{2,7-[9-{3,5-bis(benzyloxy)benzyloxy]benzyl}-9-(3,6-dioxaoctyl)fluorene} in film*. Chem. Commun., 2001: p. 2426.

101. Marsitzky D., Vestberg R., Blainey P., Tang B.T., Hawker C.J., Carter K.R., *Self-Encapsulation of Poly-2,7-fluorenes in a Dendrimer Matrix*. J. Am. Chem. Soc., 2001. **123**(29): p. 6965.

102. Lupton J.M., Schouwink P., Keivanidis E.P., Grimsdale A.C., Müllen K., *Influence of Dendronization on Spectral Diffusion and Aggregation in Conjugated Polymers*. Adv. Funct. Mater., 2003. **13**(2): p. 154.

103. List E.J.W., Pogantsch A., Wenzl F.P., Kim C.-H., Shinar J., Loi M.A., Bongiovanni G., Mura A., Setayesh S., Grimsdale A.C., Nothofer H.-G., Müllen K., Scherf U., Leising G. *A comparative Study of the Photophysics in Polyfluornes and Polyfluorenes with Polyphenylene Dendron SideChains*. in *Mat. Res. Soc. Symp. Proc.* 2001.

104. Schouwink P., Gadret G., Mahrt R.F., *Hampered excimer formation in a perylene derivative with bulky functional groups*. Chem. Phys. Lett., 2001. **341**: p. 213.

105. Pogantsch A., Wenzl F.P., Scherf U., Grimsdale A.C., Müllen K., List E.J.W., *Long lived photoexcitation dynamics in a dendronically substituted poly(fluorene)*. J. Chem. Phys., 2003. **119**(13): p. 6904.

106. Pogantsch A., Wenzl F.P., List E.J.W., Leising G., Grimsdale A.C., Müllen K., *Polyfluorenes with Dendron Side Chains as the Active Materials for Polymer Light-Emitting Devices*. Adv. Mater., 2002. **14**(15): p. 1061.

107.    Tirapattur S., Belletete, Leclerc M., Durocher G., *Study of excited state properties of oligofluorenes by the singles configuration interaction (CIS) theoretical approach.* J. Molec. Struct. (Theochem), 2003. **625**: p. 141.

108.    Belletete M., Ranger M., Beaupré S., Leclerc M., Durocher G., *Conformational, optical and photophysical properties of a substituted terfluorene isolated and incorporated in a polyester.* Chem. Phys. Lett., 2000. **316**: p. 101.

109.    Klaerner G., Miller R.D., *Polyfluorene Derivatives: Effective Conjugation Length from Well-Defined Oligomers.* Macromolecules, 1998. **31**: p. 2007.

110.    Tirapattur S., Belletete, Drolet N., Bouchard J., Ranger M., Leclerc M., Durocher G., *Spectroscopic Study of Intermolecular Interactions In Various Oligofluorenes: Precursors of Light-Emitting Polymers.* J. Phys.Chem. B, 2002. **106**: p. 8959.

111.    Jo J., Yoon D.Y., Wegner G., Hoeger S., *Synthesis and Characterization of well-defined monodisperse fluorene oligomers.* POLY.

112.    Jo J., Chi C., Höger S., Wegner G., Yoon D.Y., *Synthesis and Characterization of Monodisperse Oligofluorenes.* Chem. Eur. J., 2004. **10**: p. 2681.

113.    Geng Y., Gulligan S.W., Trajkovska A., Wallace J.U., Chen S.H., *Monodisperse Oligofluorenes Forming Glassy-Nematic Films for Polarized Blue Emission.* Chem. Matter., 2003. **15**(2): p. 542.

114.    Chen A.C.A., Gulligan S.W., Geng Y., Chen S.H., Klubek K.P., Vaeth K.M., Tang C.W., *Organic Polarized Light-Emitting Dioded via Förster Energy Transfer Using Monodisperse Conjugated Oligomers.* Adv.Mater., 2004. **16**(9-10): p. 783.

115.    Beldfield K.D., Bondar M.V., Morales A.R., Yavuz O., Przhonska O., *A new blue light-emitting oligofluorene glass: synthesis, characterization and photophysical properties.* J. Phys. Org. Chem., 2003. **16**: p. 194.

116.    Anémian R., Mulatier J.C., Andraud C., Stéphan O., Vial J.-C., *Monodisperse fluorene oligomers exhibiting strong dipolar coupling interactions.* Chem. Commun., 2002: p. 1608.

117.    Hertel D., Bässler H., Guentner R., Scherf U., *Triplet-triplet annihilation in a poly(fluorene)-derivative.* J. Chem. Phys., 2001. **115**(21): p. 10007.

118.    Grell M., Bradley D.D.C., Long X., Chamberlain T., Inbasekaran M., Woo E.P., Soliman M., *Chain geometry, solution aggregation and enhanced dichroism in the liquid-crystalline conjugated polymer poly(9,9-dioctylfluorene).* Acta. Polym., 1998. **49**: p. 439.

119.    Müllen K. & Wegner G., ed. *Electronic Materials: The Oligomer Approach.* 1998, Wiley-VCH: Weinheim, New York, Chichester, Brisbane, Singapore, Toronto.

120.    Chi C., in *Max Planck Institute for Polymer Research.* 2004, Johannes Gutenberg Universität: Mainz.

121.    Beljonne D., Pourtois G., Scholes G.D., Hennebicq E., Herz L.M., Friend R.H., Scholes G.D., Setayesh S., Müllen K., Brédas J.L., *Interchain vs. intrachain energy transfer in acceptor-capped conjugated polymers.* PNAS, 2002. **99**(17): p. 10982.

122.    Beljonne D., Pourtois G., Shuai Z., Hennebicq E., Scholes G.D., Brédas J.-L., *Energy transfer in π-conjugated polymers: Interchain vs. intrachain processes in polyindenofluorene.* Synthetic Metals, 2003. **137**: p. 1369.

# 3 POLY(INDENOFLUORENE)s: TOWARDS NEW BLUE LIGHT-EMITTING POLYMERS

 The optoelectronic properties of π-conjugated polymers can be tuned by chemical modification for applications in organic light-emitting diodes [1], [2], field-effect transistors [3] and solar cells [4]. Especially in the field of display-technology, the need for a combination of large-area manufacturing and low-cost processing has spurred research interest in the development of light-emitting polymers. In particular phenylene-based polymers have attracted considerable attention for their potential utilization as blue emitting materials with representative examples being poly(fluorene)s (PFs) [5], [6], [7] and ladder-type poly(*p*-phenylene)s (LPPPs) [8]. Poly(indenofluorene)s (PIFs, Scheme 3.1), are rigid-rod-shaped compounds intermediate in structure between PFs and LPPPs [9], [10], [11].
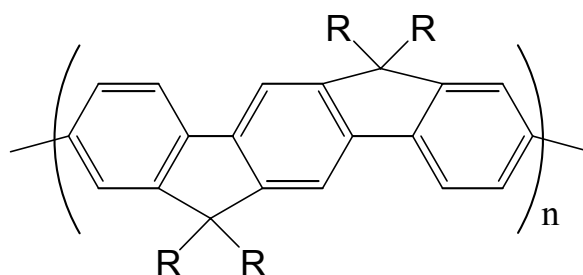


Scheme 3.1: The chemical structure of poly(indenofuorene) (PIF) unit.

 Based on photoluminescence results of oligo(indenofluorene)s with gradually increasing monomer units, the effective conjugation length of PIFs has been determined to be equal to 5-6 monomer units [9]. In contrast to PFs, the monomer unit of PIFs contains two ladder type bonds and therefore it exhibits and higher planarity than PF. This is evidenced from the emission maximum of 430 nm of PIFs in solution [9], in comparison with that of 420 nm for PFs [6]. This red shift of PL is a consequence of the extended electronic delocalisation of the π electrons that is assisted by the increased conjugation within the monomer unit. The blue emission of PIFs is making them suitable candidates for use in organic blue-light-emitting devices, due to the fact that the human eye has high sensitivity at this spectral range. The mentioned PIF derivatives are products of a polymerisation reaction that takes place in a linear fashion by exploiting the C-2 and C-8 carbons of the monomer unit. At this point it should be noted that initial studies on PIFs have been performed for derivatives that had a different way of polymerisation. Low-energy gap PIFs have been produced by polymerisation making use of the phenylene vinylene route where

the bridgehead carbon atoms of the monomer unit had been linked by an olefinic bond that resulted in thread like polymerisation along an axis perpendicular to the monomer long molecular axis [12]. The here presented PIFs are products of a polymerisation route that resulted in covalent linkage between aromatic carbon atoms of the monomer units, along the molecular axis of the monomers.

Like in the case of PFs, the ability for functionalisation of the bridgehead carbon atoms of the monomer unit with appropriate side chains, leads to higher solubility and consequently to better processing. The nature of the side chains that the bridgehead carbons may carry can be of aliphatic or aromatic nature. Tetraalkylindenofluorene derivatives, bearing branched or linear alkyl chains have been demonstrated [9]. More recently a new PIF derivative that bears aryl pendant groups has been reported [10]. The influence of the side chain substitution on the structural and morphological properties of the alkylated PIFs and their corresponding photoluminescence properties have been addressed [13], [14]. Moreover studies on the excited state absorption of the aliphatic substituted PIFs have resulted in information related to charge carrier photogeneration in these materials [15], [16], [17].

Interestingly, the arylated PIF material was found to exhibit relatively stable blue electroluminescence [10]. For the field of material science, this observation is a stimulus for further study of PIF-Aryl-Octyl as the need for stable and blue light-emitting materials is of great importance for the development of polymer-based light-emitting devices. In this Chapter the structural and optical properties of three PIF derivatives will be discussed. Chart 3.1 shows the chemical structures of the studied materials, two alkylated PIFs, bearing branched (PIF-EH) and linear alkyl chains (PIF-Octyl) and one arylated PIF derivative (PIF-Aryl-Octyl). Further more an monoindenofluorene-ketone (IF-K) will be presented.
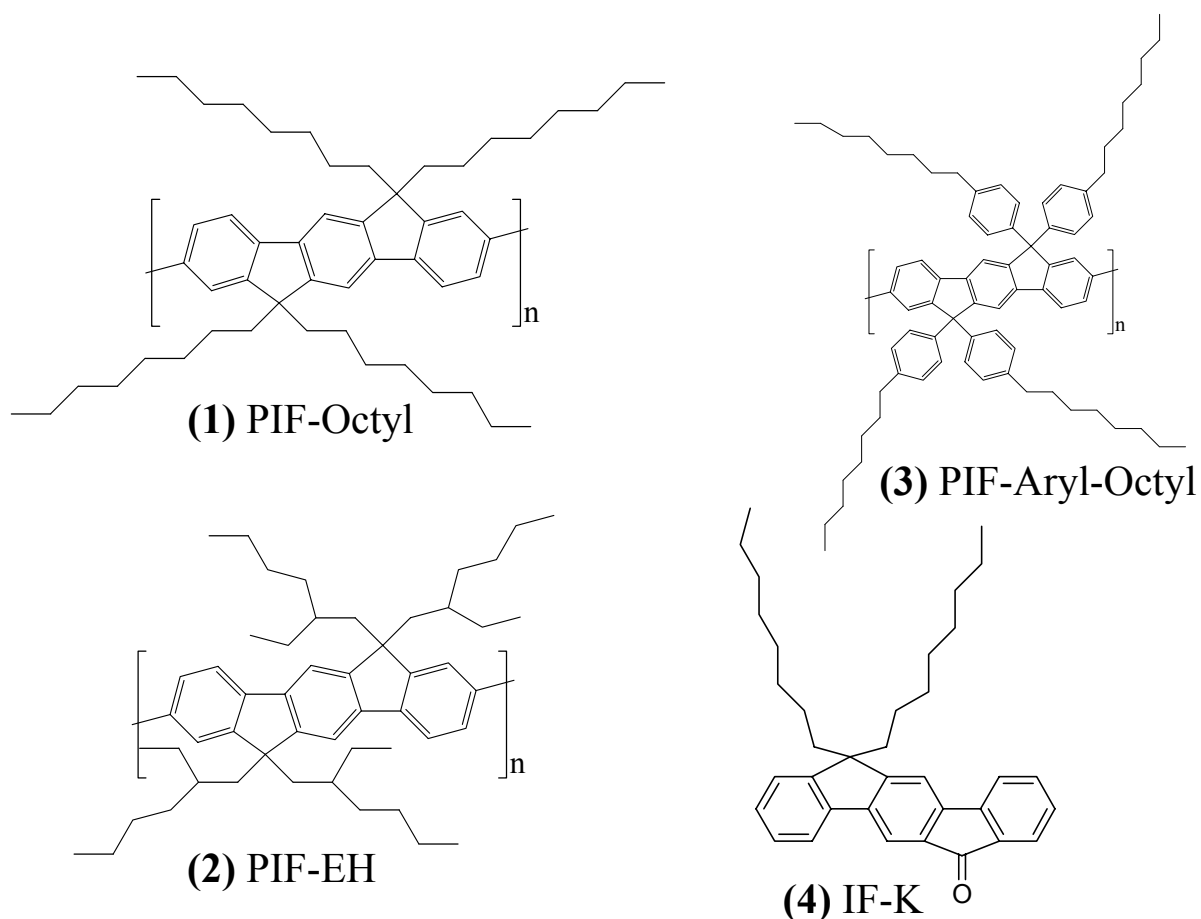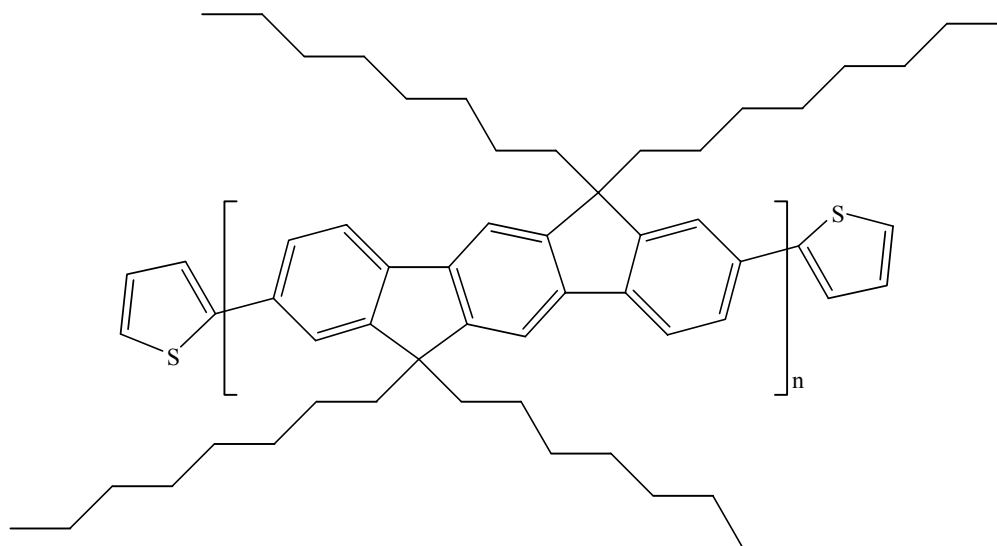
Chart 3.1: The chemical structures of the poly(indenofluorene) derivatives studied and the monoindenofluorene-ketone (IF-K) used for the doping experiments (see text).

Additional results from studies on a thiophene-endcapped PIF derivative ( PIF8S, Chart 3.2) will be presented. The endcapping of PIFs has been previously demonstrated when perylene had been chosen as the endcapper group. Especially for the case of this perylene endcapped-PIF derivative the intrachain excitation energy transfer process from the backbone to the endcapper has been addressed both from an experimental [18] and theoretical point of view [19]. The significance of interchain against intrachain energy transfer in poly(indenofluorene)s has been evaluated from correlated quantum-chemical calculations [20]. The same theoretical approach has been also used for the case of the perylene-endcapped PIF derivative [19].

**Chart 3.2:** The chemical structure of the thiophene-endcapped poly(indenofluorene) derivative (PIF8S).

# 3.1  STRUCTURAL STUDIES ON POLY(INDENOFLUORENE)s

## 3.1.1 PIFs in optical microscopy

 The thermal properties of the studied PIFs have been inestigated by means of the differential scanning calorimetry (DSC). Thermograms were recorded for the three different PIF derivatives during 1$^{st}$ cooling and 2$^{nd}$ heating cycles. The temperature range of the obtained DSCs was limited by a maximum temperature that was the decomposition temperature of each compound, as determined from thermogravimetric analyses.

 While for the case of PIF-Aryl-Octyl no phase-transition was observed in the whole range of the measured temperatures, the cases for the alkyl-derivatised PIFs are different. The thiophene-endcapped PIF (PIF8S) undergoes a unique endothermic process upon heating at about 328 K, associated with crystallization. Nearly similar phase behaviour is observed for the case of PIF-Octyl but at a temperature of 511 K.

 Particularly in the case of PIF8S, the phase behaviour was further investigated by means of a conventional polarised optical microscope (POM) by applying the same cooling and heating rates as for the DSC measurements. In agreement with the DSC analysis, no clearing point was observed for temperature below at which thermal degradation starts to occur. On the other hand, it was observed that the PIF8S melts and enters into an isotropic phase at temperatures that fit well to the DSC endothermic processes. Upon cooling from isotropic melt, birefringent domains were observed to appear in the temperature range corresponding to the crystallization peak that was by detected DSC.

As an example, the upper part of the Figure 3.1 illustrates the morphology obtained for a thin polymer film cooled from the isotropic state with a rate of 5 $^0$C*min$^{-1}$. Domains of PIF8S were formed which finally merge with each other to fill the whole field of view.

Morphology investigation was complemented by 2-Dimensional Small-Angle Light Scattering (2D-SALS) experiments under cross polarization H$_v$ [21]. The 2D SALS patterns obtained for PIF8S as obtained after POM observations exhibits a four-fold symmetry with the lobes oriented at 45° with respect to the axes of polarization.
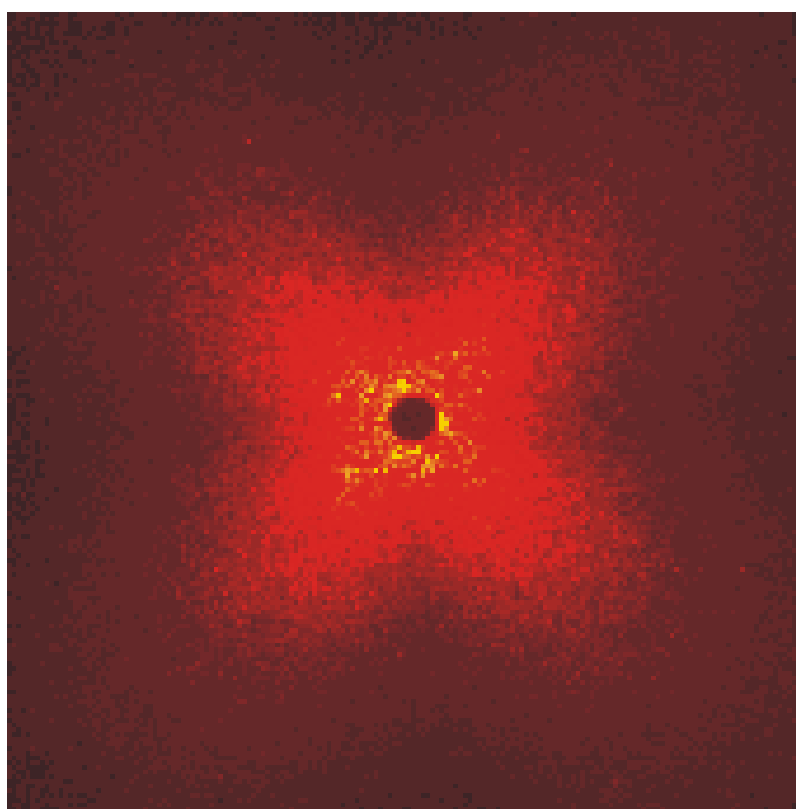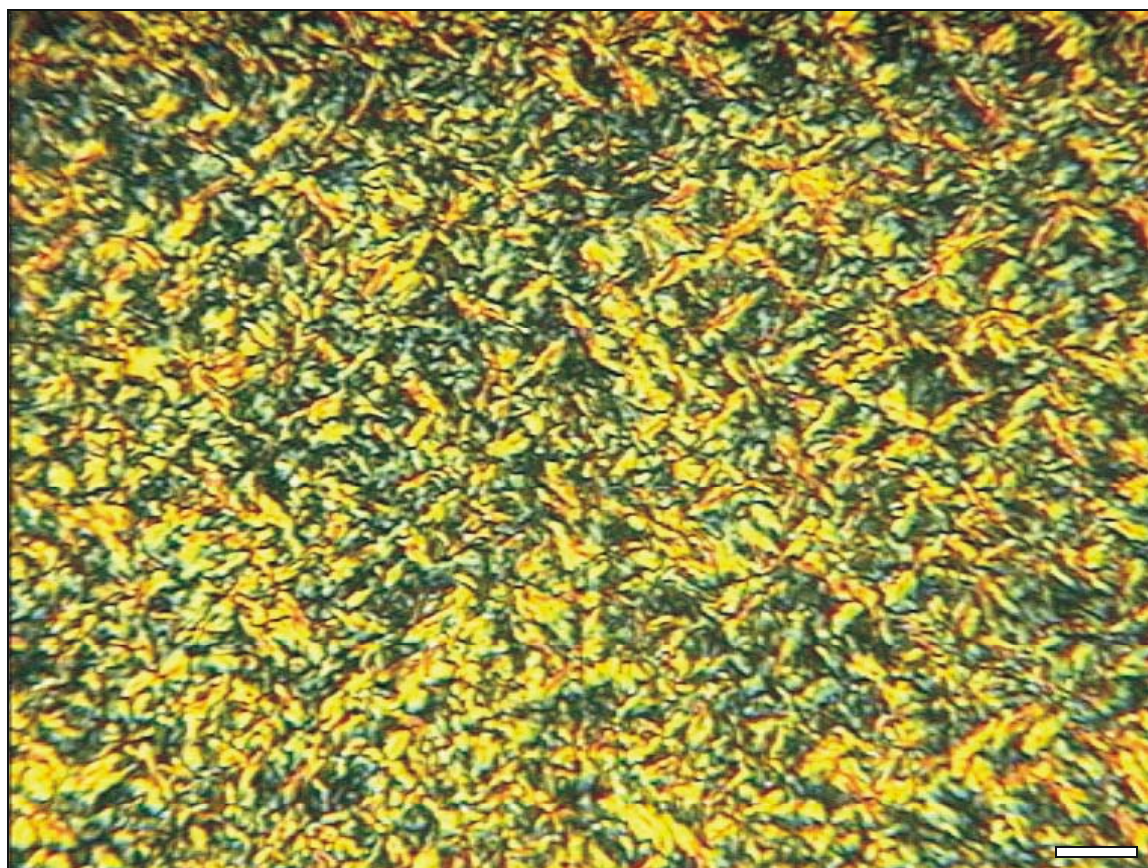
Figure 3.1: Top: Room temperature polarised optical microscope image of PIF8S powder that has been heated until the isotropic melt (513 K) and slowly cooled down at 5 $^0$C*min$^{-1}$. Note the observed birefringence. The scale bar is 10 μm. Bottom: 2-Dimensional Small-Angle Light Scattering frame, as obtained under $H_v$ geometry.

## 3.1.2 PIFs in Atomic Force Microscopy

As the AFM image in Figure 3.2 shows, PIF8S exhibits fibrilar morphology in the solid state.
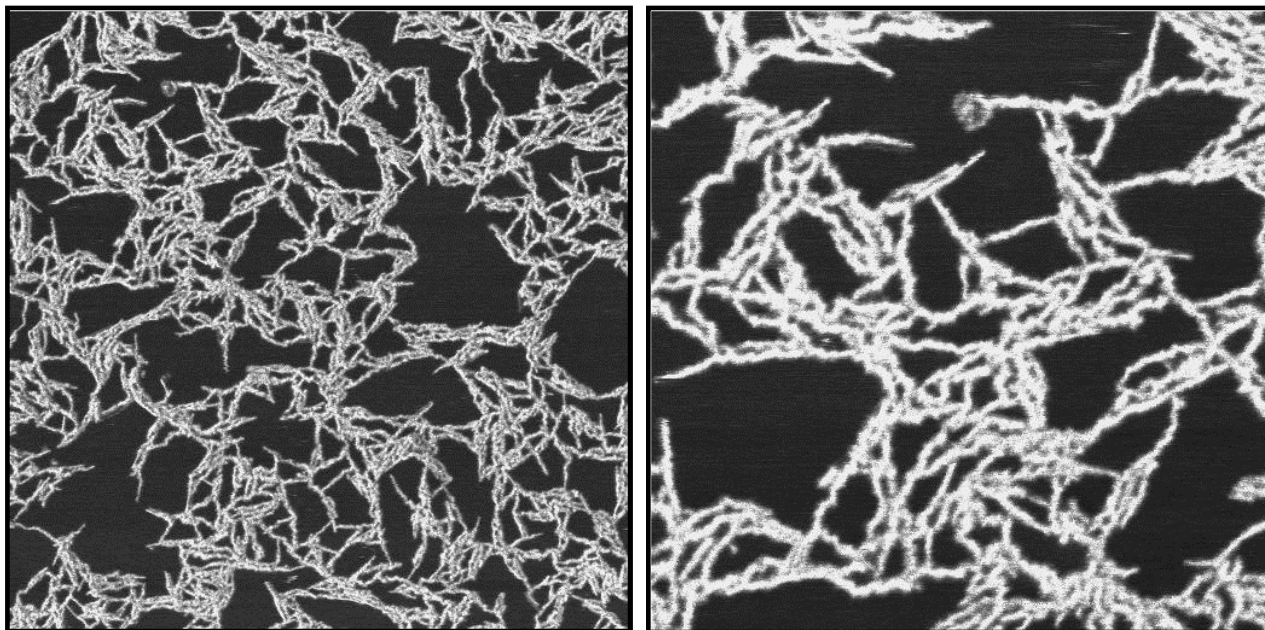


Figure 3.2: Tapping mode AFM phase images of thin deposit of PIF8S on mica. Left image: 2.5x2.5 μm²; Right image: 1.0x1.0 μm². From [22].

In Figure 3.3 AFM images of drop casted films of PIF-Aryl-Octyl from toluene solution, are shown. After drop casting, the films had been left under toluene-saturated atmosphere for 12 h. The same films did not give any evidence of optical dichroism when examined with the optical polarized microscope in transmission mode, indicating the absence of a preferential macroscopic alignment of the polymeric backbones in the solid state. The similar observation accounts for drop casted films of PIF-Aryl-Octyl that had undergone annealing up to 443 K, for 16 h.
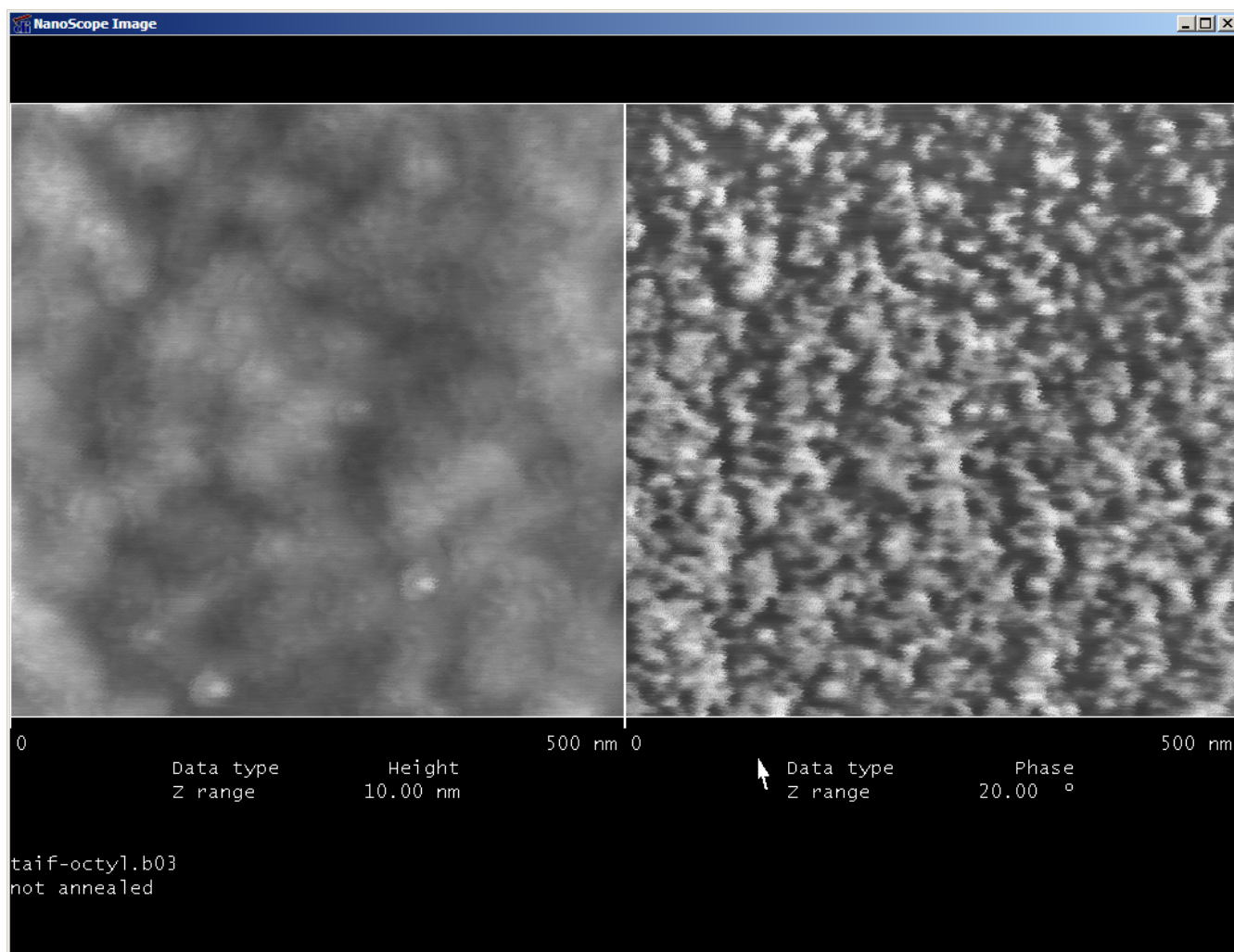
**Figure 3.3:** Tapping mode AFM image obtained showing topography (left) and phase (right) contrast of a drop casted PIF-Aryl-Octyl on a glass substrate, left to dry under toluene-saturated atmosphere.

## 3.1.3 PIFs in X-Rays

 Wide-Angle X-ray Scattering (WAXS) diffraction patterns were recorded using the X-ray beam with a pinhole collimation and a two-dimensional detector (Siemens) with $1024\times1024$ pixels. A double graphite monochromator for the CuK$\alpha$ radiation ($\lambda$=0.154 nm) was used. The beam diameter was about 0.5 mm and the sample to detector distance was 83.0 mm. Measurements were performed for powder samples and cylindrical filament [23] with a diameter of about 0.7 mm obtained by mechanical micro-extrusion. In the latter case, the pattern was recorded with vertical orientation of the filament axis and with the beam perpendicular to the filament. The recorded scattered intensity distributions were integrated over the azimuthal angle and are presented as functions of the scattering vector ($S$=2sin$\theta$/$\lambda$, where $2\theta$ is the scattering angle) [24].
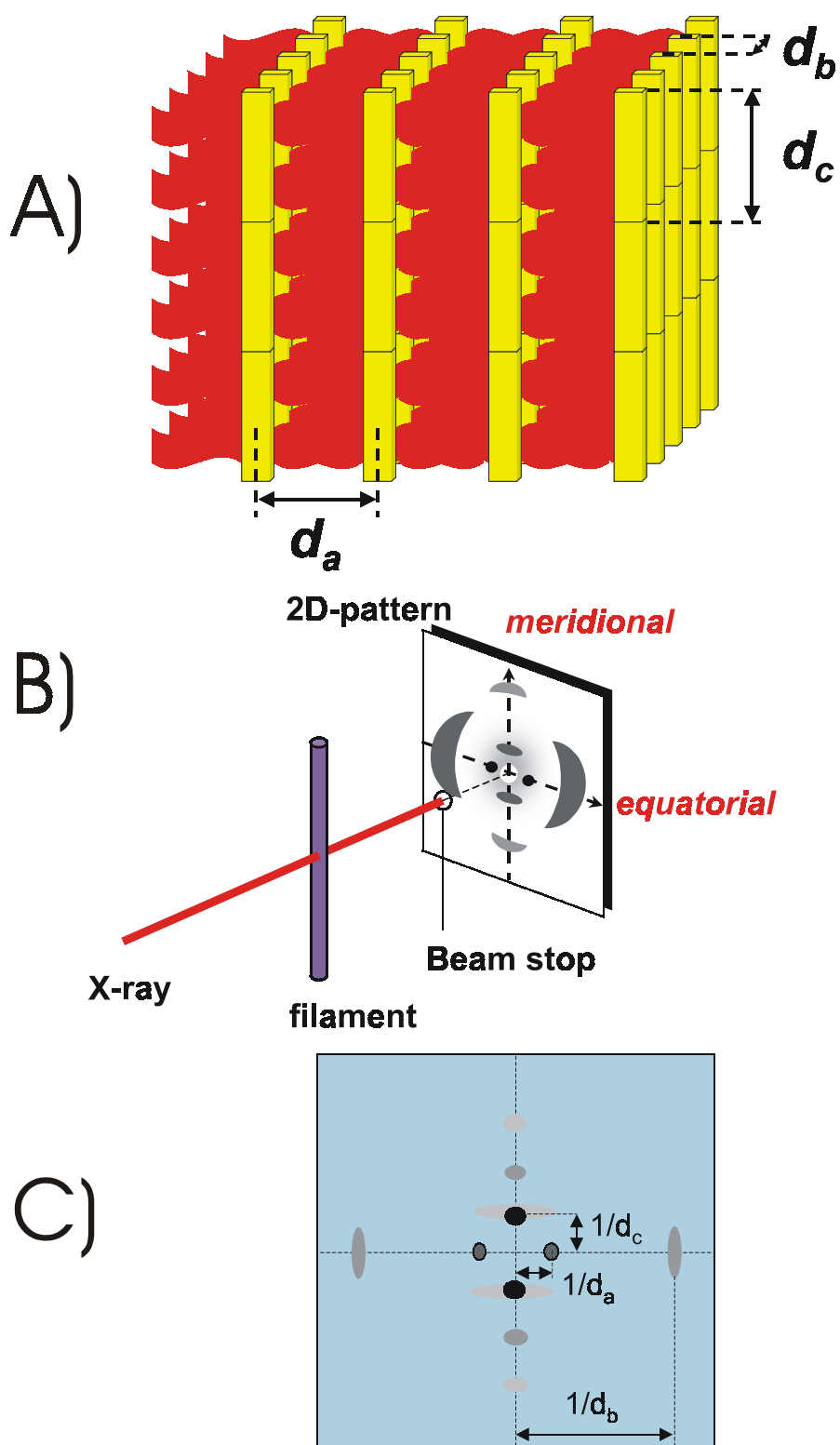
Scheme 3.2: A) A pictorial representation of a 3-D arrangement of a rigid-rod polymer in oriented state of the bulk. The structure is visualized as comprised of layers of polymer backbones that are separated from the side chains (from [23]). B) A schematic illustration of the 2D-WAXS set up and C) The detected characteristic distances as deduced from a 2D-WAXS pattern, that correspond to correlations between and within the layers of A).

### 3.1.3.1 Results of X-Ray Diffraction

WAXS experiments were performed for PIF-derivatives in both isotropic and oriented states to get an insight into the structural order on the molecular level. Figures 3.4-3.6 show the azimuthally averaged WAXS intensity distributions of powder samples of PIF-Octyl, PIF8S and PIF-Aryl-Octyl. In all cases, a diffraction peak is seen in the low-angle region. The correlation distances as extracted from the position of the maximum scattering X-ray intensity on the scattering vector axis increase from the alkyl substituted PIF ( for PIF-Octyl $d_1 \sim 1.2$ nm and for PIF8S $d_1 \sim 1.17$) to aryl substituted PIF-Aryl-Octyl ($d_1 \sim 1.9$ nm). The major difference is seen in the wide-angle region, where a diffuse halo is seen for PIF-Aryl-Octyl. In contrast to that, several more diffraction peaks are seen superimposed to the wide-angle halo for PIF-Octyl and PIF8S. The peaks at wider angle indicate a repeat distance of 0.42 nm.
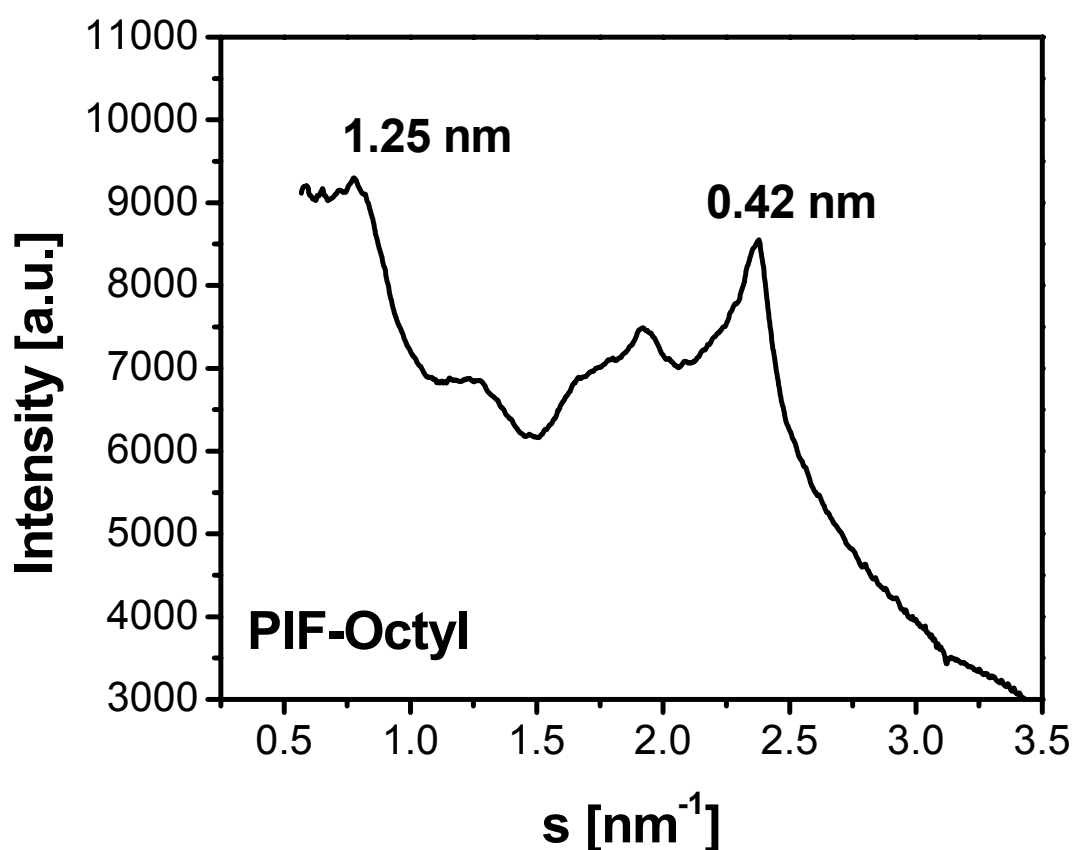


Figure 3.4: Azimuthally averaged WAXS intensity distributions for a powder sample of PIF-Octyl at room temperature.
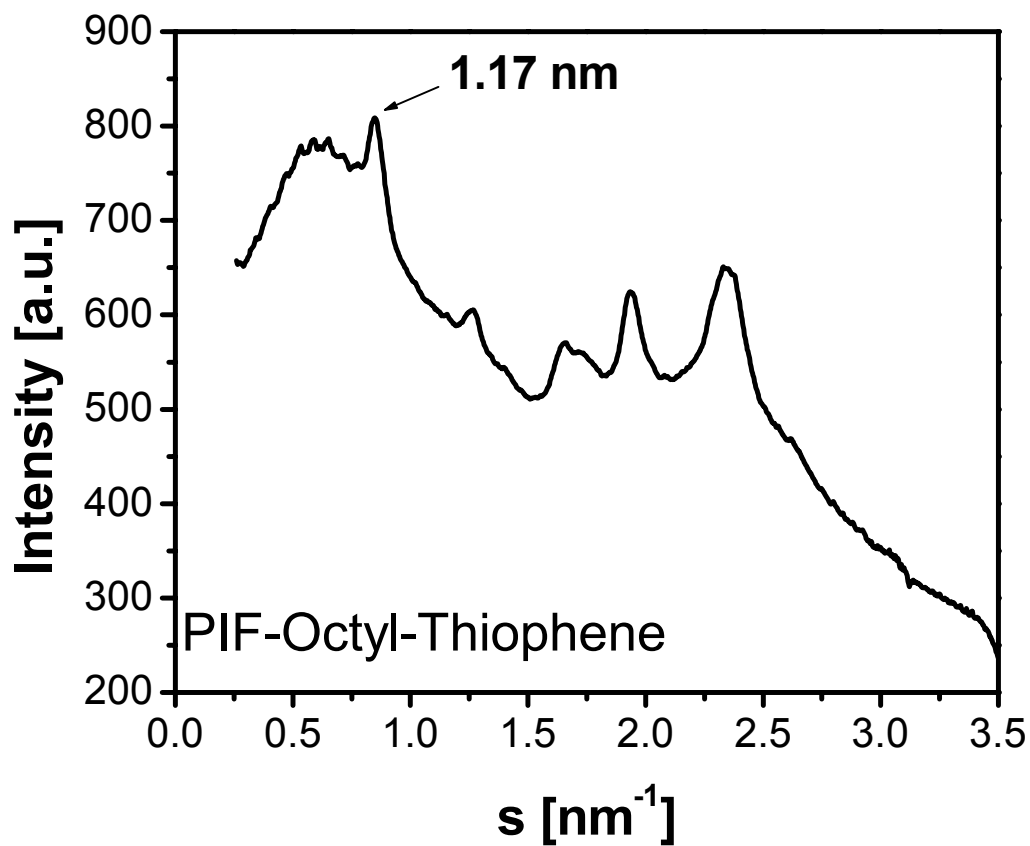
Figure 3.5: Azimuthally averaged WAXS intensity distributions for a powder sample of thiophene-endcapped PIF-Octyl (PIF8S), at room temperature.
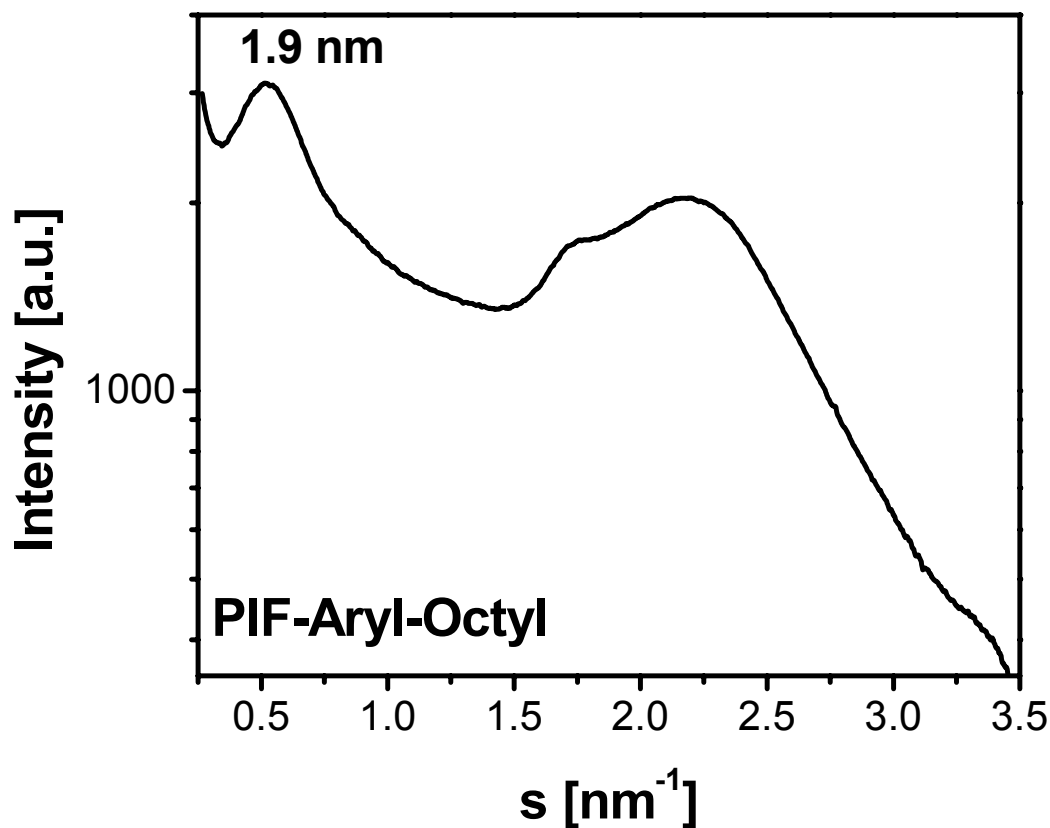
Figure 3.6: Azimuthally averaged WAXS intensity distributions for a powder sample of PIF-Aryl-Octyl, at room temperature.

Figure 3.7 shows a 2D X-Ray pattern obtained for PIF-Aryl-Octyl fiber that was drawn by mechanical micro-extrusion at 493 K (220°C). In spite of the weak degree of orientation observed, differentiation of the reflections over the azimuthal angle along the equatorial (horizontal) and meridional (vertical) directions was possible.
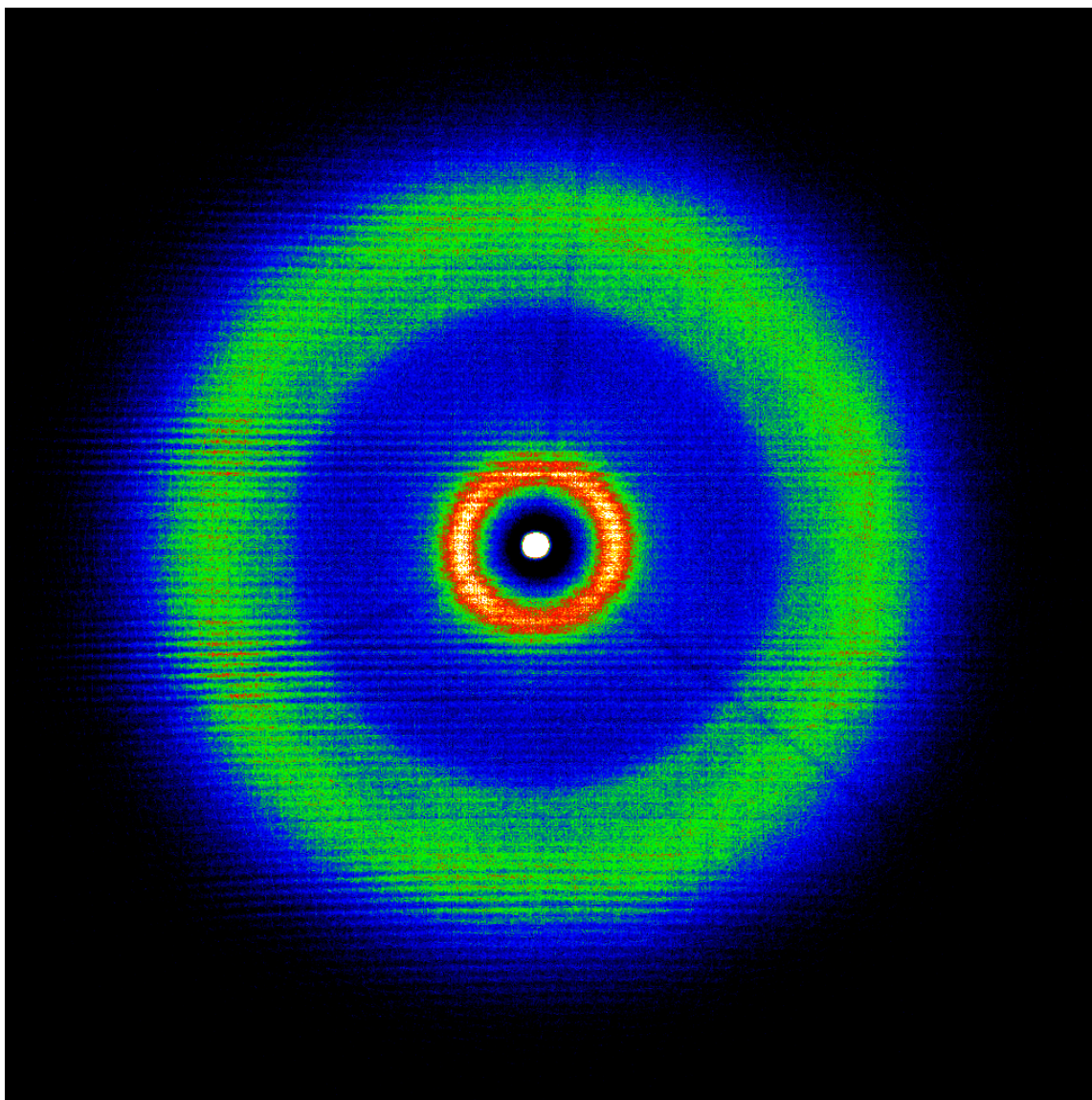
Figure 3.7: A 2D diffraction pattern of an extruded filament of PIF-Aryl-Octyl (see text).

In principle, the existence of thermotropic liquid crystalline phase creates a possibility to manipulate the molecular order by means of external forces such as extrusion from the mesophase. The 2D pattern obtained for a PIF8S fiber before and after annealing can be viewed in Figure 3.8.
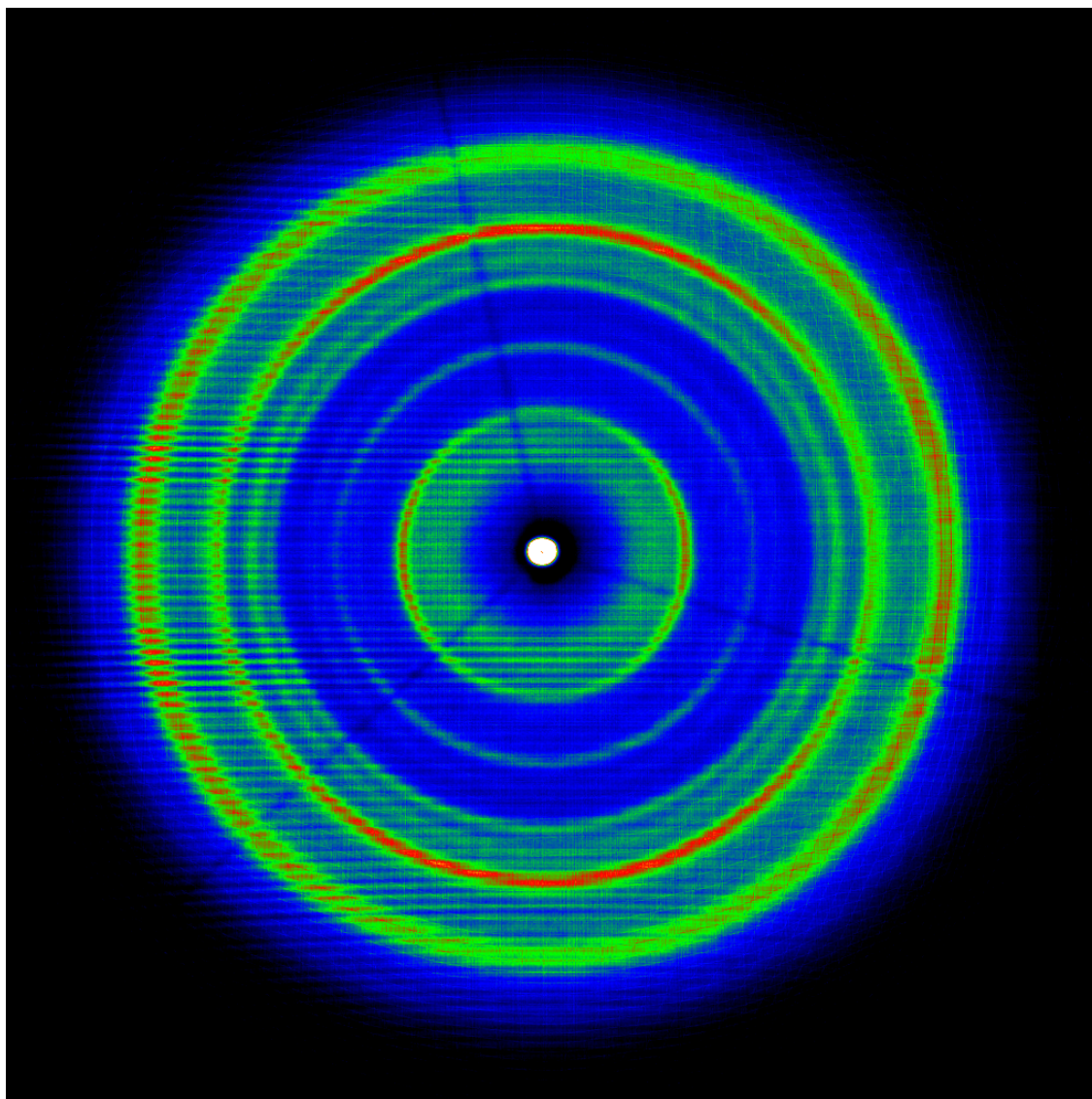
Figure 3.8: A 2D diffraction pattern of an extruded filament of thiophene-endcapped PIF-Octyl (see text).
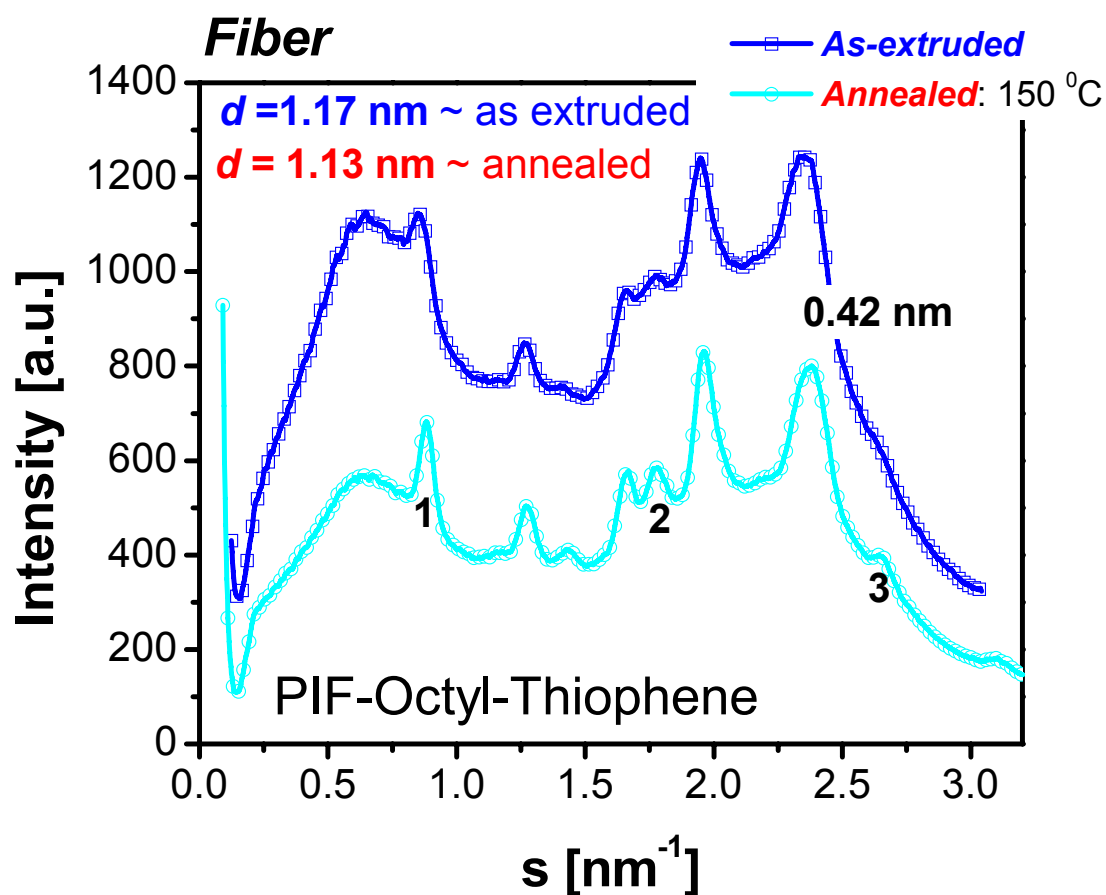
Figure 3.9: Azimuthally averaged WAXS intensity distributions for an extruded fiber sample of PIF8S, at room temperature (squares) and at 423 K (circles).

The effects of fiber annealing on the ordering of the chains of PIF8S within the fiber are shown in Figure 3.9. For the same annealed PIF8S fiber, Figure 3.10 shows the WAXS intensity distributions, for which the intensity distributions were recorded along the equatorial and meridional directions. The pattern indicates a clear ordering along the drawing direction, as well as in the perpendicular direction.
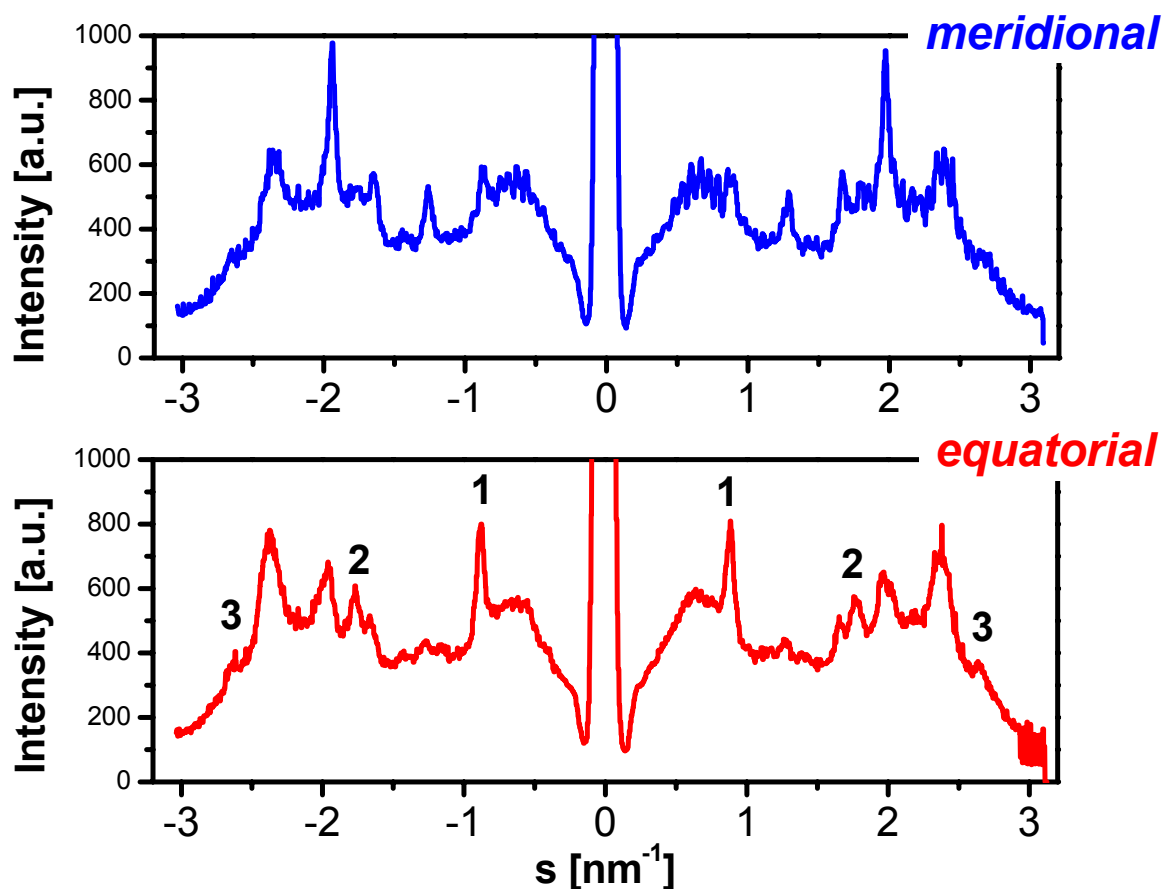
Figure 3.10: WAXS intensity distributions for an extruded fiber sample of PIF8S at 423 K. Integration along the meridional distance (top) and equatorial distance (bottom). For the equatorial recording, notice the high order peaks 2, 3 of the main peak 1.

## 3.1.4  Discussion

A previous report on the thermal properties of the PIF-Octyl derivative has determined the existence of two mesophases with transition temperatures $T_1=523$ K and $T_2=563$ K [9]. This derivative was of lower $M_w$ ($M_w=17.6*10^4$ gr*mole vs PS standard, D=5.2) than the one that is presented here. We attribute the lack of the previously observed mesophases to the higher $M_w$ of PIF-Octyl ($M_w=23.6*10^4$ gr*mole vs PPP standard, D=2.9).

Particularly for the case of PIF8S, the film morphology as obtained at room temperature was strongly influenced by cooling rates applied during the non-isothermal crystallization process [25]. The fact that a merging of the birefrigent domains was observed upon the gradual cooling of the PIF8S melt, might be an indication of liquid crystalline character that due to special disclinations give rise to the observed centrocymmetric objects. However the polarised optical microscope (POM) observations suggest that the structure formation in this polymer goes by the

simultaneous nucleation and growth of spherulitic objects. The results of 2D-SALS provide evidence for anisotropy of the refractive index in the film of PIF8S and they confirm the formation of spherulitic superstructures as presumed from the POM observations (see the bottom part of Figure 3.1).

Mesoscopic structures formed by indenofluorene homopolymers and co-polymers bearing linear or branched side chains, have been previously studied by AFM [14]. In the case of the linear side chain substituents, the mesoscopic order in these films was found to lead to the formation of long thin ribbons that appear as fibrilar bundles in the film. In contrast to this behaviour, poly(indenofluorene)s derivatized with branched ethyl-hexyl side chains were found to form small round-shaped objects of typically 10 nm size [14]. The different morphology observed for PIF-EH was attributed to the branched nature of the side chain that increases steric hindrance between adjacent chains in the solid state.

Likewise the observed nanoribons of PIF8S confirm the conclusions of [14] and come in agreement with the POM and 2D SALS observation that indicated spherulitic superstructures (paragraph 3.1.1.). For the case of PIF8S, the observed structures in Figure 3.2 have been interpreted as the result of  -stacked structures formed by PIF8S molecules that have their polymer backbones parallel to each other and perpendicular to the fibril axis [22].

In contrast to the PIF derivatives bearing alkyl chains and similarly to PIF-EH, the AFM images for the films of PIF-Aryl-Octyl indicate the existence of elongated rod-shaped aggregates with an averaged size of 150 x 0.75 nm.

In principle, the effect of dichroism is a result of the anisotropy in the transition dipole moment of the monitored sample, upon interaction with an electromagnetic field of specific polarisation. Since the transition dipole moment is strictly correlated with the molecular geometry, a potential anisotropy of the transition dipole must be a result of a preferential molecular orientation. The latter can be induced upon the effect of an external force, such as mechanical rubbing [6]. Annealing could also induce partially orientation within the film, in terms of formation of large- as even- monodomains, given that a temperature corresponding to a liquid crystalline mesophase could be applied. Locking the domains of this mesophase into a glassy state would then be possible by rapid cooling of the sample and the efficiency of orientation could be estimated from measurements of the dichroic and polarization ratios. Although no external force was applied to the films of PIF-Aryl-Octyl, the absence of dichroism in the films, agrees with the DSC measurement of this compound that did not give any indication for the existence of mesophase.

We consider that the long distance periodicities observed for all PIF powders studied by WAXS are controlled by the bulkiness of the side chains and are assigned to the average distance between polymeric backbones [26]. As for the observed diffuse halo seen for PIF-Aryl-Octyl, at this stage we attribute it to a local amorphous arrangement of the macromolecular fragments that may be an effect of the bulky alkyl substituted phenyl substitutents that prevent the close packing of the bulk material.

The peak that corresponds to 0.42 nm distance may reflect the spacing between adjacent side chains along the polymer backbone and therefore it is attributed to segregation of aliphatic side chains, which might be the driving force for existence of mesoscopic order in films of PIF-Octyl [14] and PIF8S (Figure 3.2). The assignment of this low-angle peaks to the periodicities between polymeric backbones was also supported by analysis of the 2D diffraction patterns recorded for macroscopically oriented filaments obtained by micro extrusion. Under shear in the course of the extrusion process, the polymer chains aligned in such a way that, the fiber axis lies nearly parallel to the extrusion direction. The diffractions at small-angles show increased intensity along the equatorial axis indicating periodicity perpendicular to the extrusion direction. The weak degree of orientation observed, may be explained by the fact that the PIF-Aryl-Octyl does not exhibit any mesophase up to 673 K, as evidenced from the recorded thermograms. By contrast to that, both alkylated PIF analogues were found to have signatures of liquid-crystalline character in the region of 523 – 563 K [14].

For the case of the WAXS intensity distributions of the annealed PIF8S fiber in Figure 3.10, a set of reflections is seen, along the equatorial direction, their positions fitting to the ratios 1 : 2 : 3. This indicates a layered structure in the direction transversal to the chains. In agreement with the above-presented results for the powder sample of PIF8S, the wide angle peak with nearly isotropic intensity distribution around the azimuthal angle is assigned to the close packing of the side chains.

For the same compound, the most intensive reflections in the 2D pattern (Figure 3.8) and in the WAXS intensity distributions (Figure 3.10) are seen along the meridional direction. They reflect a periodicity of 0.51 nm along the polymer chains that are oriented along the extrusion direction. Additional intramolecular reflections with a period of 0.784 nm are also seen in the medium angle region.

## 3.2  OPTICAL STUDIES ON POLY(INDENOFLUORENE)s

One of the most important issues to be resolved in the field of light-emitting polymers is the correlation of the materials' optical properties with the morphologies that the materials adopt in the solid state (thin films). This correlation becomes even more complicated when the studied polymer system contains chemical impurities that also affect the observed optical properties.

In this section, we report on detailed photophysical properties of three PIFs (see Chart 3.1), bearing different side chain substituents. A correlation is made between the emission dynamics of various PIFs and their film morphology as previously presented [14].

By comparing the observed optical properties of these derivatives, we evaluate the quality of the synthetic routes used for the preparation of the materials. We emphasize the fact that the greater spectral purity obtained by the new synthetic route chosen for the synthesis [10] of the novel PIF-Aryl-Octyl derivative is of relevance for the synthesis of the whole class of poly(*p*-phenylene) type blue emitting materials.

### 3.2.1 Experimental

The synthesis of the PIF derivatives has been reported elsewhere [9], [10]. The molecular mass and polydispersity of each PIF derivative are given in Table 3.1. Dilute solutions of the studied materials, were prepared in 2-methyltetrahydrofuran (MTHF) and toluene at a concentration of 20 μg/mL. MTHF was dried by reflux over sodium for several days and subsequently distilled under argon atmosphere. Prior to solution preparation, both of the solvents were further degassed by purging with He or Ar, under ultrasonication for 15 min.

Thin films of the materials were prepared via spin coating on glass substrates, at a rotational speed of 1200 rpm within 60 seconds. All solutions were filtered prior to spin coating. Appropriate micro-filters were used as the solubility of each derivative varied depending on its pendant side chain and its polydispersity. Film thickness was determined by a TENCOR P-10 Surface Profiler and varied between 30-90 nm. Absorption spectra were recorded by a UV-VIS Perkin-Elmer spectrometer (Lambda2). A Xe-lamp equipped spectrofluorometer (SPEX FluoroLog II (212)) was used to record continues-wave (cw) photoluminescence (PL) and photoluminescence excitation (PLE) spectra of films and dilute solutions. For the time-resolved PL measurements, excitation of the samples took place with a frequency-doubled mode locked Ti:Saph laser, producing approx. 200 *fs* pulses operating at a repetition rate of 80 MHz at 390 nm. The signal was dispersed by a 0.25 m monochromator with a 50 lines/mm grating and detected with a Hamamatsu C4742 streak camera. During the measurement, the samples were kept under vacuum in a continuous cold finger liquid nitrogen cryostat. All thin film

measurements were performed under a dynamic vacuum of $10^{-5}$ mbar. Time-resolved PL of dilute solutions was recorded using a home-built glass cell of 4 mm path length. For low-temperature measurements liquid $N_2$ was used for cooling down to 77 K. As the $T_g$ of MTHF is at 95  5K the optical properties of the measured systems correspond to a regime of high dilution in a vitrified matrix. For all time-resolved PL measurements care was taken to avoid *in situ* photo-oxidation of the samples during measurement time. The maximum average laser power was kept in the order of 500 μW while an aperture was used for reducing the laser spot diameter down to 1 mm. No focal lens was used for focusing the laser spot onto the surfaces of the films measured.

## 3.2.2 PIF-ARYL-OCTYL:Optimising the spectral purity of PIFs

A common problem of the poly(*p*-phenylene) materials is that this class has been suffering from a lack of spectral purity in the blue due to the presence of a low-level concentration of chemical defects in the polymeric backbone. Such chemical impurities may be introduced due to insufficiently rigorous synthetic procedures or as a result of an *in situ* photo-oxidation during the measurements (see Chapter 2, paragraph 2.25)

In the following we present extrinsic doping experiments. The material used is the impurity-free PIF-Aryl-Octyl derivative doped with known amounts of indenofluorene-monoketone (IF-K) molecules (see structure in Chart 3.1). The report for synthesis and characterisation of IF-K is under preparation [27]. The conclusions drawn from this experiment are based on the Stern-Volmer formalism (paragraph 3.3.2). The latter method enables the determination of the minimum level of ketone concentration in the PIF-Aryl-Octyl derivative that will affect the intrinsic optical properties of the material.

## 3.2.3 Room temperature cw-photoluminescence

Figure 3.11 presents the cw-PL spectra of all PIFs in solution and as thin films. For solutions, the fluorescence of all PIFs is located at 2.9 eVs (427 nm). At the concentration of 0.02 mg/mL used, the polymer chains can be considered to be isolated. In a previous study for PIF-EH with approximately half the $M_w$ of that which is presented here, the critical concentration $c^*$ was found to be $1.7*10^{-3}$ g/mL [28]. Critical solution concentration $c^*$ defines the limit at which free chains start to overlap with each other and form entanglements. Given the fact that all PIFs presented here are of comparable $M_w$ values, it is expected that in the above mentioned dilution regime, the chains are isolated and therefore the PL spectra are free of aggregate characteristics.
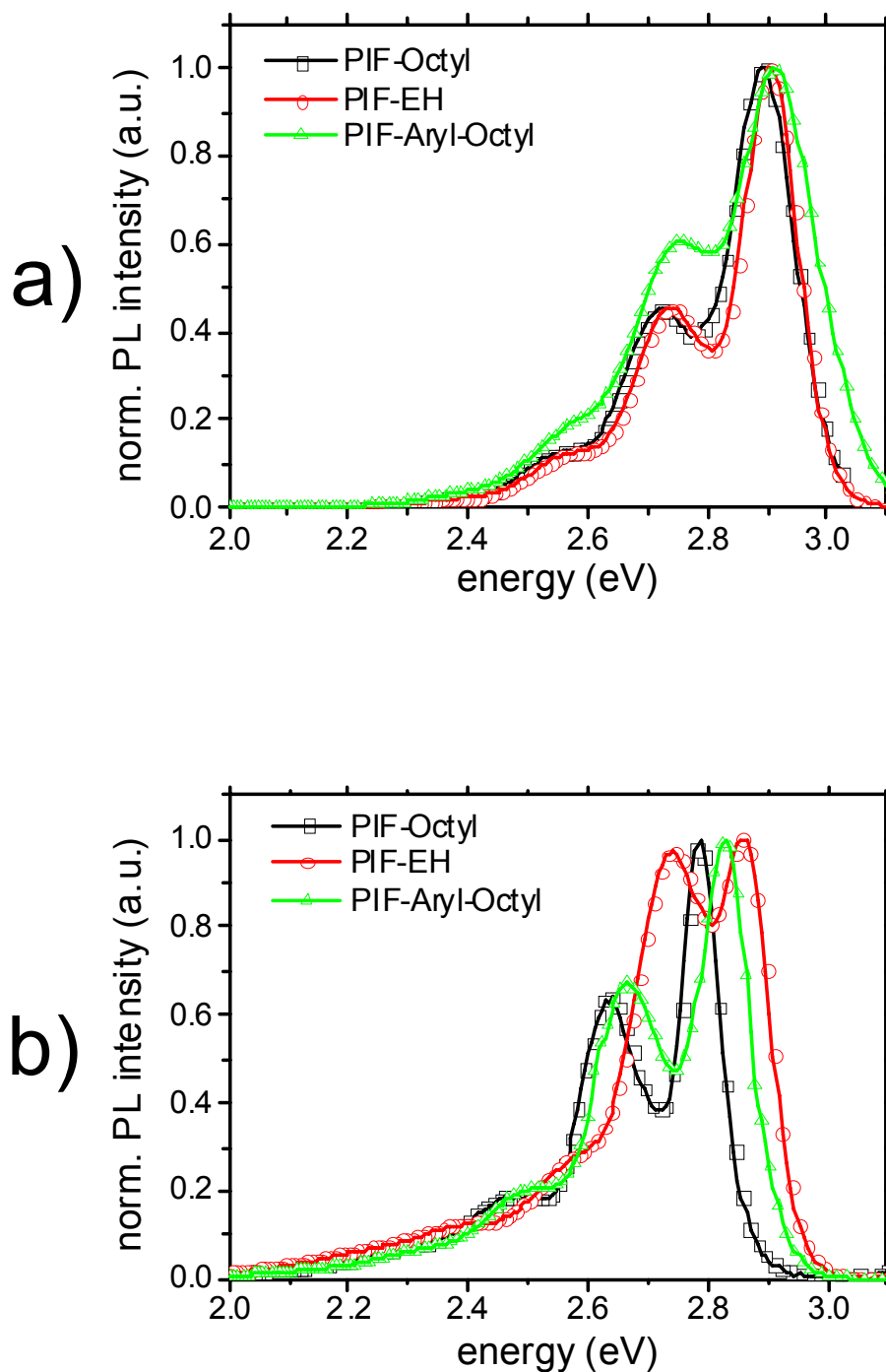
Figure 3.11: Room temperature normalized cw-PL spectra of PIF-Octyl (squares), PIF-EH (circles), PIF-Aryl-Octyl (triangles) a) as dilute solutions in toluene and b) as films on glass substrate. Excitation wavelength $\lambda_{exc}$ = 390 nm (3.18 eV).

Noticeable changes in the PL occur in the case of thin films, where the interaction between polymer chains is enhanced. The degree of the red shift observed in PL reflects the extent of interaction between adjacent PIF chains. The observed spectral shift varies from 40 meV for PIF-EH, through 70 meV for PIF-Aryl-Octyl up to 110 meV for the PIF-Octyl derivative. It should be emphasized that the cw-PL spectrum of PIF-Octyl is found to consist only of emission related to the singlet transition and its characteristic vibronic progression. No significant contributions are found in the region of 2.4 eV as previously observed [13] in films of PIF-Octyl.

## 3.2.4 Room temperature time-resolved photoluminescence

Figure 3.12 shows time-resolved PL spectra obtained for dilute solutions and thin films of PIFs.
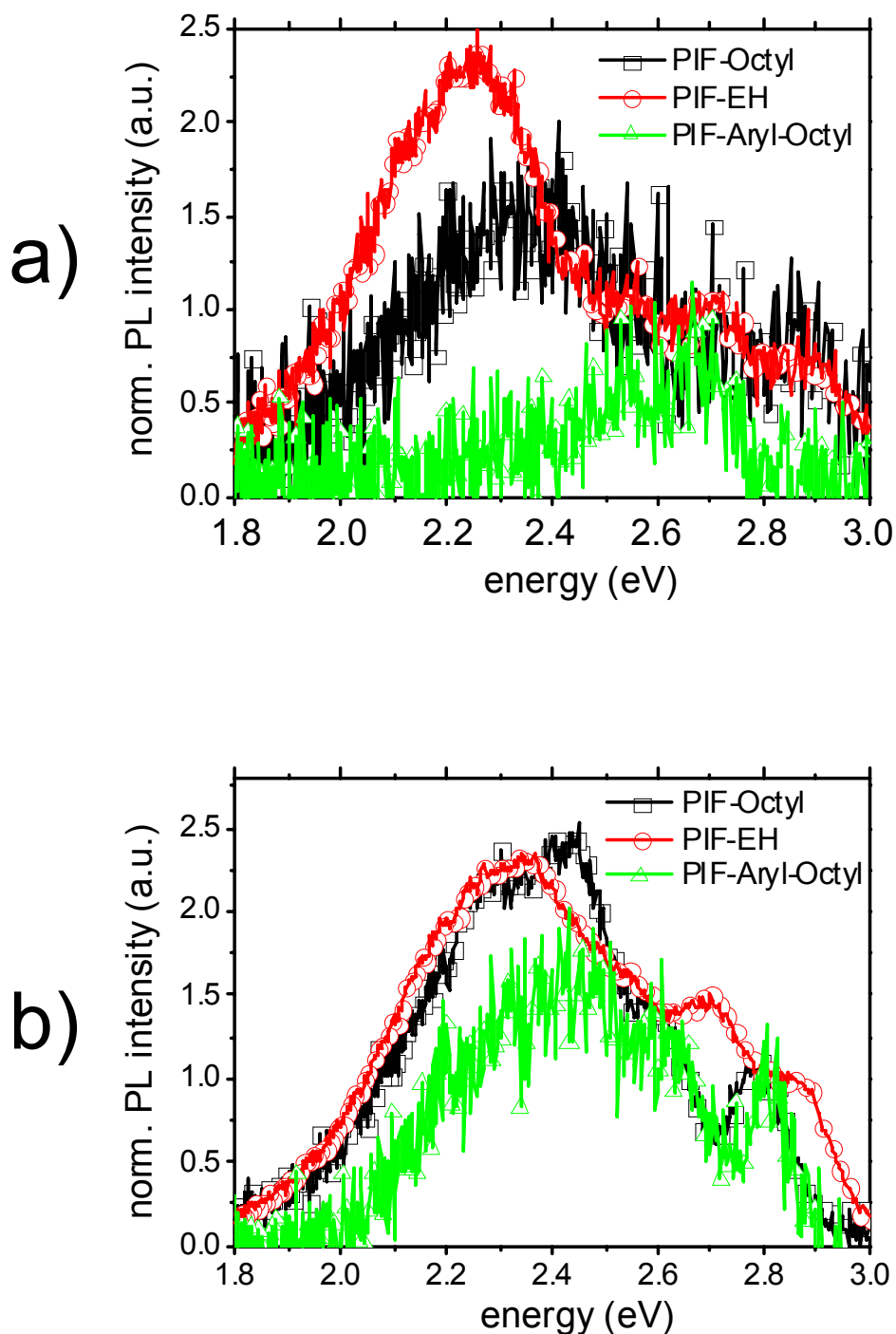
Figure 3.12: Room temperature normalized time-resolved PL spectra of PIF-Octyl (squares), PIF-EH (circles), PIF-Aryl-Octyl (triangles) a) as dilute solutions in toluene (0.02mgr/mL) and b) as films on glass substrate. Excitation wavelength $\lambda_{exc}$ = 390 nm (3.18 eV), p =$10^{-5}$ mbar. For solutions: detection app. 4 *ns* after excitation pulse, integration window of 1000 *ps*. For films: detection app. 2.5 *ns* after excitation pulse, integration window of 500 *ps*.

For comparison, all delayed spectra are normalized to the singlet emission spectral integral. In the case of dilute solutions, at sub-nanosecond delayed times after excitation (not shown here), emission of the PIFs resembles the characteristics of the cw-PL spectra. However, it is apparent that at long delayed times in order of *ns*, the PL signature of PIF-EH and PIF-Octyl is completely changed in comparison with the cw-PL spectrum in Figure 3.1a. Exceptionally, only the arylated PIF derivative preserves its initial prompt spectral structure at a delay of 3 *ns*. However this is not the case for thin films, where all three materials are found to show a new emissive feature located in the green part of the spectrum. This emission is centred at 2.3 eV for the alkylated PIFs and 2.4 eV for the arylated one. It has to be noted that those strong contributions in the PL of the PIF films have already started to emerge at 2 *ns* after the excitation pulse.

 As Figure 3.13 compares the normalized transient PL of the three PIF derivatives, it shows that the decay pattern of the PIF-Aryl-Octyl singlet emission also differs strongly from those of the corresponding alkylated PIF derivatives.

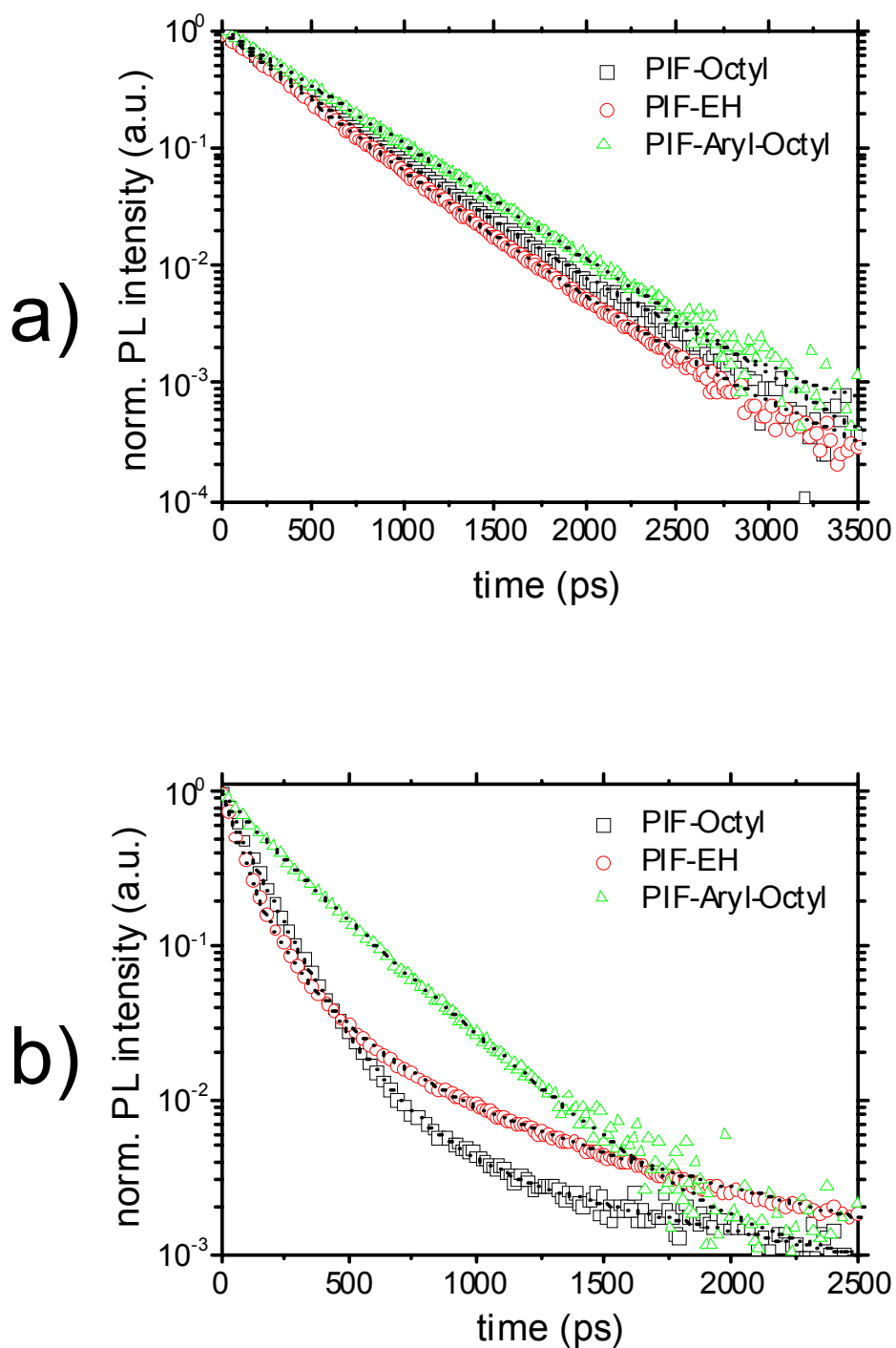Figure 3.13: Room temperature normalized transient decays of singlet emission monitored for PIF-Octyl (squares), PIF-EH (circles), PIF-Aryl-Octyl (triangles) a) in dilute solutions MTHF (0.02mgr/mL) and b) in films on glass substrate. Excitation wavelength $\lambda_{exc} = 390$ nm (3.18 eV), p $=10^{-5}$ mbar. Dotted lines in a) are fit to the data (see Table 3.1); Dotted lines in b) are guides to the eye.

This difference is remarkably pronounced in the case of thin films where PIF-Aryl-Octyl largely preserves the decay characteristics of the dilute solution regime. In contrast to this behaviour, the alkylated PIF derivatives change completely their photokinetic singlet decay transients in the solid state, compared with the corresponding emission dynamics in dilute solutions. Table 3.1 summarises the determined amplitudes and the corresponding emission lifetimes.

| SOLUTIONS | PIF-Octyl | PIF-EH | PIF-Aryl-Octyl |
|---|---|---|---|
| $M_w^{a}$ (gr/mole) | $1.7 * 10^5$ | $1.1 * 10^5$ | $2.57 * 10^5$ |
| D (polydispersity) | 5.2 | 2.75 | 3.87 |
| Concentration (mg/mL) | 0.020 | 0.020 | 0.020 |
| $A_1$ | $0.91 \pm 0.01$ | $0.87 \pm 0.02$ | $1 \pm 4.4 * 10^{-4}$ |
| $\tau_1$ (ps) | 360 | 330 | 445 |
| $A_2$ | $0.11 \pm 0.02$ | $0.15 \pm 0.02$ | - |
| $\tau_2$ (ps) | $620 \pm 20$ | $530 \pm 15$ | - |
| $\tau_{1/e}$ (ps) | 390 | 360 | 460 |

Table 3.1: Determined amplitudes and decay constants for dilute solutions of the PIF derivatives. Solution concentrations, $M_w$ and D values are also depicted.
a For alkylated derivatives GPC results were calibrated against polystyrene [9] while for the arylated derivative polyphenylene was used as a GPC standard [10].

For comparison, the $\tau_{1/e}$ lifetime values are also given. Table 3.2 summarises the values of $\tau_{1/e}$ lifetime values for the three derivatives in the solid state, as films.

| FILMS | PIF-Octyl | PIF-EH | PIF-Aryl-Octyl | |
|---|---|---|---|---|
| Thickness (nm) | 35 | 85 | 90 | 60 |
| $\tau_{1/e}$ (ps) | 120 | 86 | 250 | 258 |

**Table 3.2:** Determined $\tau_{1/e}$ lifetimes for the thin films of the PIF derivatives studied. Film thickness of each sample used is also given.

## 3.2.5 Time-resolved photoluminescence of the low-energy spectral regions

Figure 3.14 shows a comparison between the decay transient of the singlet emission and the low-energy spectral region emission, for each of the PIF derivatives studied as films. This comparison has been proven to be clarifying in the case of pentafluorene oligomers (see Figure 2.22, Chapter 2) in order to distinguish the contribution in the PL of the intrachain singlet excitons from that of other extrinsic emissive species. According to the upper and middle plots of Figure 3.14, the low-energy emission spectral area of the alkylated PIF derivatives is not following the decay pattern of the singlet emission.
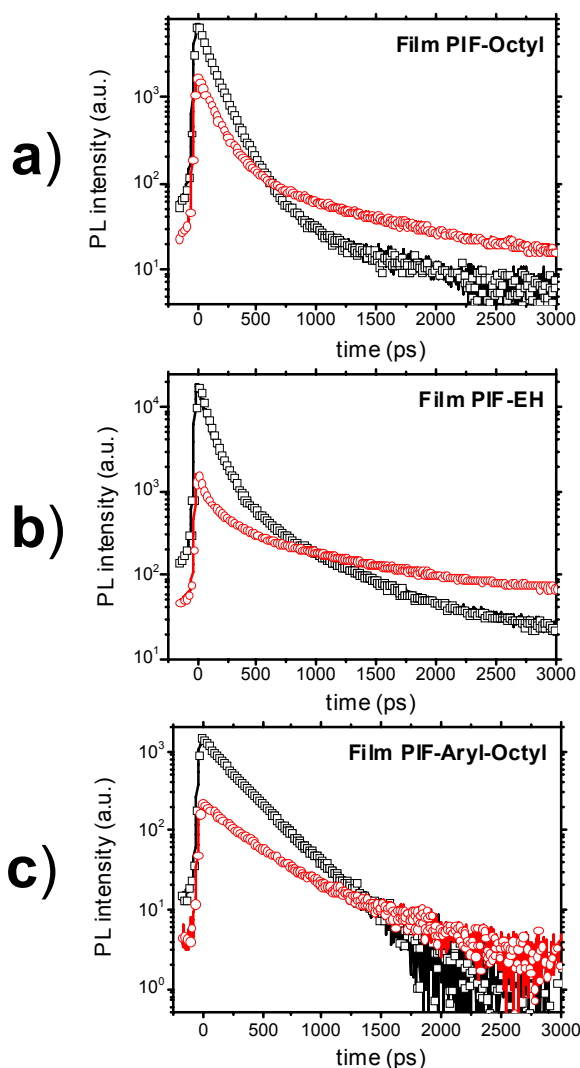
Figure 3.14: Room temperature transient decays of emission monitored for thin films on glass substrate of a) PIF-Octyl (35 nm thick), b) PIF-EH (85 nm thick) and c) PIF-Aryl-Octyl (88 nm thick). Excitation wavelength $\lambda_{exc}$ = 390 nm (3.18 eV), p =$10^{-5}$ mbar. Singlet emission decay transient is indicated in squares and the emission decay transient of the 2.00 – 2.58 eV (480 – 620 nm) spectral area is indicated in circles.

In contrast the green part of the PL emission is found to follow a slower decay law than that of the singlet emission. Also for the case of PIF-Aryl-Octyl, a difference in the decay pattern of both high and low-energy spectral region is observed. However it seems that only for the case of PIF-Aryl-Octyl, the low-energy emission has a comparable intensity to the one of the singlet emission, at 1.5 *ns* after excitation. In contrast, in the case of the alkylated PIFs the same spectral region seems to have a residue of intensity that is stronger than the corresponding singlet emission.

## 3.2.6 Discussion

As Figure 3.11 shows, all PIFs exhibit a noticeable spectral red shift of their singlet PL emission in the solid state as thin films. The particularly large spectral shift of 110 meV observed in the case of PIF-Octyl, reflects increased solid state interactions that force the polymer backbone to adapt an extended planarised conformation and thus to increase its effective conjugative length. Consequently this increase leads to the lowering of the electronically excited emissive state. The suggestion for enhanced interchain interactions in the solid state of PIF-Octyl is in agreement with the 0.42 nm spacing detected in the azimuthally averaged WAXS intensity distribution of PIF-Octyl powder (Figure 3.4). Evidence for periodicity in the solid-state was also reported previously for thin films of PIF-Octyl derivative [14] but it was attributed to face-to-face packing of π-conjugated backbones.

As it has been discussed in paragraph 3.1.4, the mesoscopic structures formed by indenofluorene homopolymers and co-polymers has been addressed by AFM investigations.

The relatively large red shift of the singlet PL observed for PIF-Aryl-Octyl films should reflect an enhancement of interchain interactions in the solid state. Based on the observed trend of PL red shift for these materials as films, in respect to their PL in dilute solutions, the postulated interchain interactions for PIF-Aryl-Octyl should be weaker than in the case of the PIF-Octyl but stronger than in PIF-EH. At this stage, the cw-spectroscopic and the X-ray data suggest that the structural ordering reaches a minimum starting from PIF-EH, going to PIF-Aryl-Octyl and ending with PIF-Octyl. This hypothesis is further supported from the AFM images obtained for drop casted films of PIF-Aryl-Octyl. Figure 3.13 shows the normalized decay transients of the singlet emission of the three PIF derivatives. For the dilute solutions studied, only in the case of PIF-Aryl-Octyl was a mono-exponential decay function appropriate for fitting the singlet transient. In the cases of PIF-Octyl and PIF-EH the sum of two exponential functions seemed to recover better the singlet emission decays. Previous time-resolved PL studies on PFs in solution addressed the issue of *ps* relaxation of singlet excited PF chains [29]. There the authors suggested that the two decays of the singlet emission could be correlated with conformational transitions of the chains in the dilute solution regime. However the recorded transients were obtained for a nearly monochromatic spectral window of the singlet emission. The herein presented decay transients of all PIF derivatives are obtained from time integration of a broad spectral window that covers the entire singlet zero-phonon emission band. Therefore the extracted amplitudes correspond to the average of the individual amplitudes that one could have obtained by selective integration of a narrower spectral window within the singlet emission.

The singlet decay dynamics are strongly affected upon shifting to the solid state. All three lifetimes are found to be decreased in comparison with the corresponding values obtained in dilute solutions (Figure 3.6). In the case of the alkylated PIFs, a strong reduction in the $\tau_{1/e}$ values is found in comparison to the $\tau_{1/e}$ value of the arylated PIF derivative. Figure 3.13b shows that PIF-Octyl has much faster singlet decay kinetics than the other PIFs. For this PIF derivative the observed fast decay rate of the singlet PL is attributed to an assisted excitation migration due to the enhanced interchain interactions in the solid state, as evidenced from the close chain packing of 0.42 nm distance (Figure 3.4).

As it has been discussed in paragraph of 2.2.6 of Chapter 2, the influence of interchain interactions on the luminescence properties of conjugated polymers has been addressed from a theoretical point of view. These studies concluded that there are two regimes of chain interaction that are defined by the interchain separation [30]. Even if an aggregate is formed from two adjacent conjugated chains, a primary photoexcitation on the aggregate will maintain the individual single chain characteristics, if the distance between the two chains comprising the aggregate remains larger than a critical value. For interchain distances larger than this critical value, the interchain coupling will not result in any mixing of the molecular orbitals of the two individual chains. Therefore in the case of the alkylated PIF derivatives, it is plausible that aggregation effects may take place without significant impact on the electronic properties of the PIF backbone. That is probably why the derivatives that have enhanced interchain interactions in the solid state and exhibit long-range order, still maintain the cw-PL characteristics of the isolated chains. However, a distinct influence of the packing effects on the luminescence dynamics should be expected. As the attachment of linear alkyl chains supports side chain segregation, which eventually is more favourable for the migration of the photoexcited states, PIF-Octyl decays faster than PIF-EH. While the initial decay rate of both materials is similar, after the transfer of the excitation energy to aggregate sites that still have singlet emission characteristics, the dynamics differ. Although, the long-range packing of PIF-Octyl further assists energy migration and makes the overall decay rate faster, the short-range order of PIF-EH results in a retardation of the decay rate indicated by an additional tail in the decay transient in Figure 3.13b. In contrast to these decay features of alkylated PIFs, the singlet PL of the arylated derivative decays with a time constant much higher than that of the alkylated PIF derivatives.

The observed differentiation of PL lifetime underlines further the different degree of order of each of the studied derivatives in the solid state. In principle, morphology conditions in the film greatly affect the migration of photoexcited states towards chemical defects. These defect sites can function as energy traps for the migrating photoexcitations. It was discussed in paragraph

2.2.5 of Chapter 2 that such defects in the case of PFs have been determined experimentally by means of FTIR and time-resolved laser spectroscopy, to be keto moieties, namely fluorenones, located on the bridgehead C-9 carbon of the fluorene unit . We attribute the differences observed in the decay dynamics of PIFs films to the presence of keto defects on the polymeric backbone for the alkylated PIF derivatives. The keto-free arylated PIF derivative preserves almost totally the singlet decay kinetics observed in the dilute solution regime. As the time-resolved PL spectral profile shows in Figure 3.11a, PIF-Aryl-Octyl is found to have long-delayed singlet PL characteristics identical to the cw-PL spectrum. On the contrary, both alkylated PIFs are found to have additional spectral features in their long-delayed PL that are characteristic of fluorenone-like moieties previously observed for dilute solutions of oligo(fluorene)s and corresponding polymers. The decay kinetics of the singlet emission in dilute solution also support this notion. While the transients of alkylated PIFs are better recovered with a double exponential decay fitting function, PIF-Aryl-Octyl singlet emission is found to decay monoexponentially. We attribute the absence of the second exponent in the singlet decay transient to the lack of keto defects onto the arylated PIF backbone that would provide additional relaxation channels for the relaxation of the excited singlet state.

In order to rationalise the probability for ketone detection onto the polymer backbone of the PIF derivatives the routes for the synthesis of the materials have to be discussed. Chart 3.2 summarises the two different routes for the synthesis of the alkylated and arylated PIF derivatives.
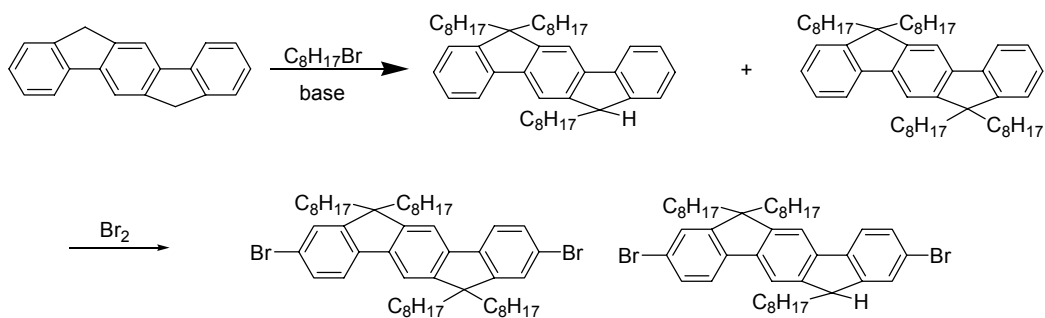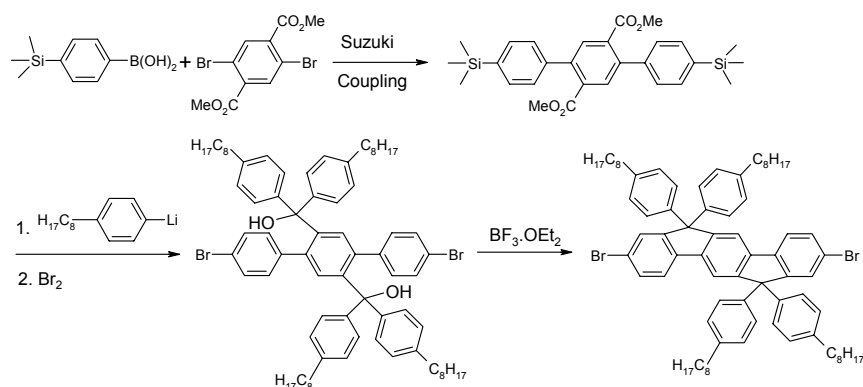
**Scheme 1**



**Scheme 2**

Chart 3.3: The two different synthetic routes followed for the preparation of alkylated (Scheme 1) and arylated (Scheme 2) indenofluorene monomers. Detailed description of the syntheses is reported in [9], [10].

It has been shown experimentally that the formation of keto defects in PF is related to partial alkylation of the C-9 position of the fluorene ring (For discussion on literature see paragraph 2.2.5, Chapter 2 ). The alkylation procedure for the alkylated PIF backbone is similar to that used to make alkylated PF and hence it is conceivable that here also partially alkylated sites exist which can be transformed to ketonic sites during sample preparation. Additionally, as the dynamic vacuum conditions of the experiment do not exclude the presence of $O_2$ in our cryostat chamber, keto defects may arise during measurement time as a result of photo-oxidation. The discrepancy observed in the here presented cw-PL spectrum of PIF-Octyl in comparison with the one previously published [13] can similarly be explained. The here presented PIF-Octyl was synthesised in such a way that full alkylation of the bridgehead carbons sites was achieved in greater degree than that used in the previous report. However, complete alkylation was not totally ensured as still in the dilute solution regime the ketonic emissive signature is present (Figure 3.12a). Yet the content of keto impurities was much lower as evident from the cw-PL spectrum (Figure 3.11b) and the film of PIF-Octyl emits in the blue spectral region. Contrary to

the case of the alkylated PIFs, arylated PIF derivative was synthesised in such a way that full arylation of the bridgehead carbon positions was achieved. It turns out that side-chain substitution of the C-6 and C-12 bridgehead carbons prior to ring formation on the polymeric backbone [10] increases the chemical purity of the product. It has to be noted that a similar synthetic process has been followed before for the preparation of a dendronised PF derivative [31], which also showed relatively stable blue emission [32]. Time-resolved PL studies on films of this material have revealed the presence of keto defects [33]. However it remains unclear whether those keto groups existed prior to measurement or they were a consequence of the experimental conditions. As the synthetic route followed for the dendronised PF derivative excluded the existence of a monosubstituted C-9 carbon atom on the fluorene unit, it is probable that the observed fluorenone sites were unintentionally created during measurement, as the average laser power used was in the order of 10 mW [33]. Our present results are obtained under excitation conditions in which the excitation intensity was kept at a much lower level and thus reflect the inherent spectral properties of the materials in their pristine state.

As shown in Figure 3.11b, thin films of all three PIF derivatives present a delay spectral feature in the region of 2.3 eV for the alkylated derivatives and 2.4 eV for the arylated one. It has been reported previously that PF films show aggregation effects that can lead to excimer formation [34]. Such interchain interactions were found to give rise to a red shifted emission relative to the singlet PL band, located approximately at 2.40 eV prior to photo-oxidation in air and 2.50 eV after photodegradation. This observed difference in the spectral shift was attributed to two subsequent processes taking place in the PF film, namely formation of excimers that afterwards resulted in photoinduced formation of keto defects. The delayed spectral feature of the arylated PIF derivative can be similarly attributed to packing effects arising from interactions of the side-chains in the solid state. Given the fact that excitations migrate towards lower lying energy sites within a density of states [35], [36], excimer formation would have had no significant impact in the solid state. As ketonic centres lie lower in energy than excimer sites, excitation energy would be transferred from excimers to ketone sites therefore making the existence of the excimer not so important [37]. However in the case of PIF-Aryl-Octyl that was found to be keto-free, the lowest energetic sites are those of the excimers. Hence the photoexcitations will be localised eventually on those sites and the emission will be blue shifted in respect to that arising from fluorenones. Indeed for the case of the arylated PIF derivatives, the long delayed PL is ~ 100 meV blue shifted compared to the delayed spectra of the alkylated derivatives. Complementary spectra obtained for low- temperature measurements of time-resolved PL at 77 K for PIF-Aryl-Octyl (not shown here) showed a structureless broad emission band located at 2.48 eV (500 nm) . As

indenofluorene-ketone is expected to have a structured emission profile at least at low temperatures, the observed band cannot be assigned to the existence of keto defects on the PIF-Aryl-Octyl backbone. From comparison of the relative emission ratios in Figure 3.12a it is shown that the excimer emission in PIF-Aryl-Octyl is comparable to the singlet intensity at *ns* delay. This reflects the small impact of the excimer in the singlet dynamics of the PIF-Aryl-Octyl and to its overall emissive performance. This is not the case for the alkylated derivatives where the red shifted delayed emission has an intensity value more than twice higher than the singlet delayed PL. The difference in the delayed intensity magnitude is further manifested from the decay transients of the 2.4 eV emission of PIF derivatives, in Figure 3.14. For the case of PIF-Aryl-Octyl, luminescence monitored in this spectral area is found to have a decay transient virtually similar to the singlet emission. In contrast to that, a different transient decay pattern with a slower decay rate is observed for the green spectral region of the alkylated PIF derivatives. This is in agreement with the recent PL time-resolved measurements in films of well defined fluorene-fluorenone copolymers [38]. While the intrachain singlet emission of these fluorene-containing molecules has been determined to have a lifetime in the order of *ps*, the characteristic fluorenone band of 2.32 eV (535 nm) was found to have a lifetime in the order of *ns*. In the same work, similar observations have been established also for the case of a model compound, a fluorene-fluorenone trimer. However, the latter has been studies only in dilute solution.

 The evidence of excimer instead of aggregate formation in films of PIF-Aryl-Octyl comes from the fact that absorption spectra of the films were not significantly different from these of dilute solutions. Therefore no ground state interactions should be responsible for the influence of the electronic properties in the films of PIF-Aryl-Octyl. However excimer formation could arise from an electronically excited chain that exists in close contact with close neighbouring chains. This could be the case, according to the diffuse wide-angle halo observed in X-ray data of PIF-Aryl-Octyl powder, that gives indication of a broad distribution of intermolecular distances corresponding to a locally amorphous-like arrangement (Figure 3.6).

## 3.3  DOPING EXPERIMENTS

 As mentioned above, due to the different synthetic approach that was followed for the synthesis of PIF-Aryl derivative, no keto sites were found to exist on its polymer backbone. Therefore the material is considered appropriate as a keto-free host model compound that simplifies the study of the energy transfer from host sites to keto centres embedded deliberately in a controlled manner. An indenofluorene-ketone (IF-K, see structure in Chart 3.1) molecule was chosen to act

a PL quencher in films of PIF-Aryl derivative. Blends of PIF-Aryl:IF-K were prepared with different IF-K content. All films prepared were of comparable thickness and their PL dynamics were monitored. Due to the compatible nature of the guest molecules of IF-K with the host matrix, no phase separation was expected to take place in the films and a homogeneous mixed system was anticipated. The following discussion of the results confirms the expected miscibility of the components.

## 3.3.1 Photoluminescence quenching

The absorption spectrum of IF-K (see structure in Chart 3.1) in a dilute (40 µM ) solution of toluene, is presented in Figure 3.15. The spectrum can be divided into two spectral regions, one of the high-energy and one of low-energy absorptions features [39].
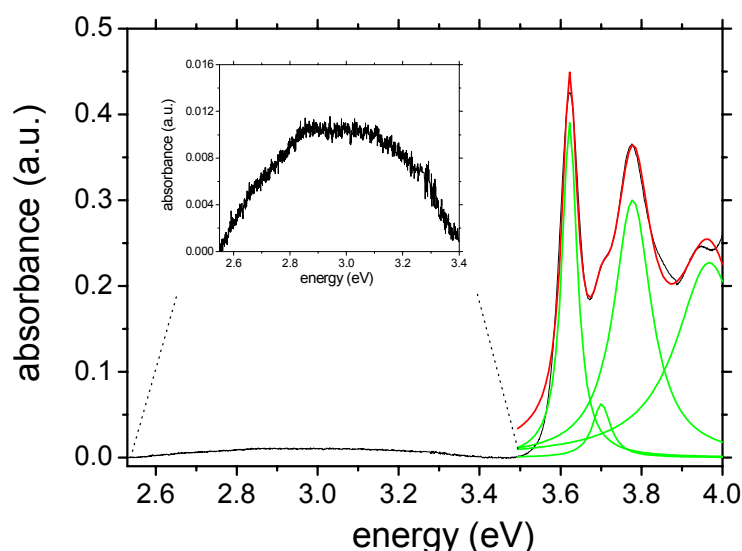


Figure 3.15: Room temperature absorption spectrum of IF-K dilute solution (40 µM) in toluene.

As it is seen, in the absence of inhomogeneous broadening, which is a common characteristic of the presence of an effective conjugation length in conjugated polymers, the vibronic bands of the absorption spectrum are clearly resolved. The spacing of these vibronic bands (~ 180 meV ) agrees with the spacing that is commonly observed in the PL spectra of the PPP-bridged derivatives, such as PF, PIF and MeLLLP. A broad featureless band of vanishing oscillator strengh is found centred around the region of 3 eV This low-energy absorption feature is attributed to the n$\rightarrow\pi^*$ of the carbonyl group [38], [39].

| | Indenofluorene | | | Ketone (carbonyl) | |
|---|---|---|---|---|---|
| Solution (40 µM) | $S_{0-0}\rightarrow S_{1-0}$ | $S_{0-0}\rightarrow S_{1-1}$ | $S_{0-0}\rightarrow S_{1-2}$ | 1 | 2 |
| **MTHF** | 3.62 | 3.78 | 3.97 | 3.70 | not resolved |
| **TOLUENE** | 3.62 | 3.78 | 3.96 | 3.70 | not resolved |

Table 3.3: Maxima of the room temperature absorption bands observed for IF-K in dilute solution of toluene and MTHF. All values were obtained after Lorentzian fitting of the data.

The absorption data for IF-K dilute solutions are summarised in Table 3.3. For the PIF-Octyl polymer that did not contain carbonyl groups, the absorption edge was found to be at ~2.9 eV and the absorption maximum at 3.02 eV, that is 0.6 eV lower in energy than the $S_{0-0} \rightarrow S_{1-0}$ transition of IF-K. This stabilisation energy of the first electronically excited level for the polymer case, is attributed to the delocalisation of the $\pi$ electrons of the molecule due to the effect of conjugation. The impact of the extended delocalisation length on the electronic properties of conjugated polymers has been discussed in Chapter 1.

 IF-K exhibits fluorescence when excited at 3.62 eV (342 nm). The observed PL is characterised by a low-energy broad emission band with a peak at 2.36 eV (526 nm) and a high-energy emission band positioned in the region 3.5–2.8 eV. Independent from the solvent used, the intensity of the low-energy PL band of 2.36 eV is dominant in respect to the PL intensity of the high-energy band. Dependence of the low-energy emission peak on the polarity of the solvents (toluene and MTHF) was not observed. Regarding the high-energy PL band, the change of the solvent polarity induced minor structural changes in its spectral distribution.

 The change of solvent polarity influences the PLE spectra of IF-K solutions. For both PL peaks of the IF-K monitored, the strongest contribution comes from the region of 3.7 eV. This indicates that the main emissive level corresponds to the second absorption feature of the $S_{0-0} \rightarrow S_{1-1}$ in Table 3.3. When the high-energy peak of IF-K is monitored, the PLE of the toluene solution is found better resolved exhibiting spectral features with PLE intensity maxima at 3.57 eV, 3.69 eV and 3.86 eV. For the case of the MTHF solution, the PLE spectrum of the 3.26 emission (380 nm) showed slightly broader spectral features located at 3.59 eV, 3.66 eV and 3.86 eV.
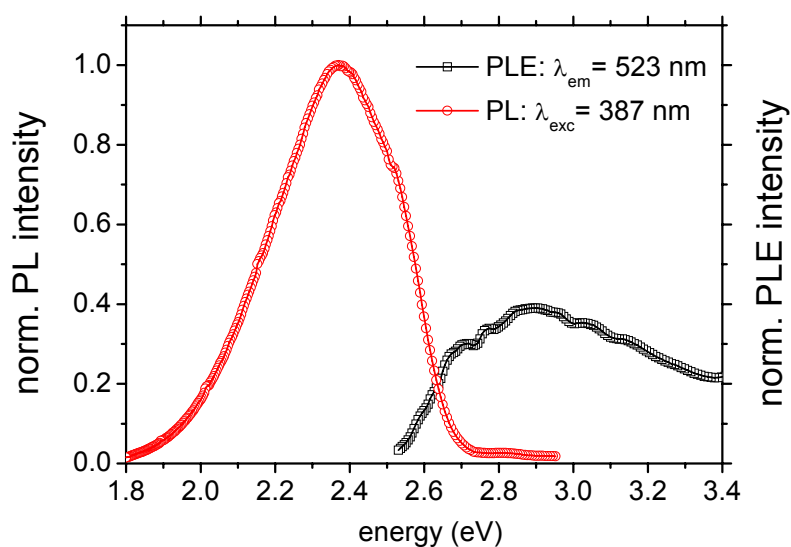
Figure 3.16: Room temperature PL (circles) and PLE (squares) spectra of a PS:IF-K 10% wt film drop casted on a glass substrate. Excitation was at 387 nm ( 3.20 eV) and the monitored emission was 2.37 eV (523 nm). Room prsessure.

Similar spectral characteristics were observed also for a drop-casted film of IF-K on glass. Poly(styrene) ($M_w$= 365100 gr/mole) was used as an intert matrix and IF-K was added at a 10 wt% fraction. A representative PL/PLE spectrum of the IF-K drop-casted film is presented in Figure 3.16. The PL of IF-K film also shows a small contribution in the high-energy region, a residue of the high-energy emission that is presumably quenched due to the presence of the carbonyl group.
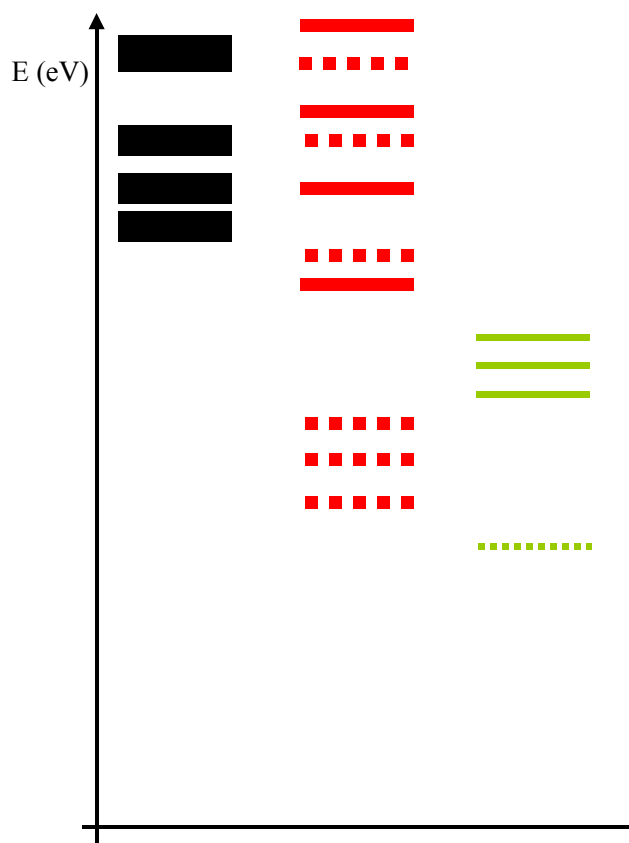
Figure 3.17: A qualitative energy level scheme of for IF-K in dilute solution, as deduced from the spectroscopy data of absorption, PLE and PL measurements. Left lines indicate the absorbing levels, middle lines indicate the levels responsible for the PL monitored, right lines indicate the fluorescent levels after optical excitation.

Upon doping films of PIF-Aryl-Octyl (see structure in Chart 3.1) with trace amounts of IF-K, a gradual PL quenching is observed for PIF-Aryl-Octyl, which is in parallel with an increase of PL in the region where the keto part of IF-K emits.
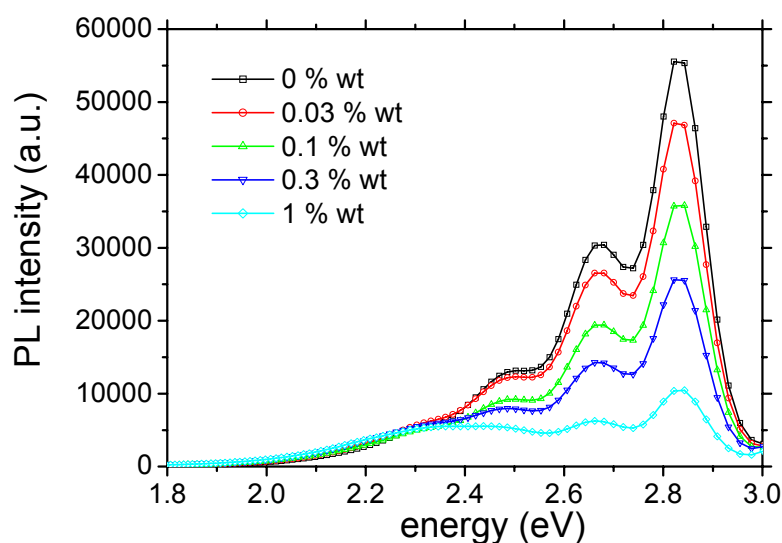
Figure 3.18: Room temperature PL spectra of PIF-Aryl-Octyl:IF-K thin films on glass substrate. Exitation at 3.18 eV (390 nm), at room pressure.

Figure 3.18 presents the room temperature cw-PL spectra of PIF-Aryl-Octyl blends as film on glass, when excited at 3.18 eV. At this excitation energy, the absorbance of IF-K is negligible. Therefore in the presence of PIF-Aryl-Octyl, the excitation energy is only absorbed from the matrix. The observed increase of the characteristic keto emission of IF-K, on the expense of the main singlet emission of PIF-Aryl-Octyl indicates that PL quenching is based on energy transfer from PIF-Aryl-Octyl to IF-K.

### 3.3.1.1  *Low-temperature time-resolved photoluminescence spectra*

Time resolved PL spectra recorded for the doped films of PIF-Aryl-Octyl showed that the increase of the IF-K emission is further enhanced within few *ns* after the excitation pulse. According to Figure 3.19, especially at low temperature of 77 K the low-energy emission observed at 2.37 eV is similar to the characteristic emission of IF-K in dilute solution.
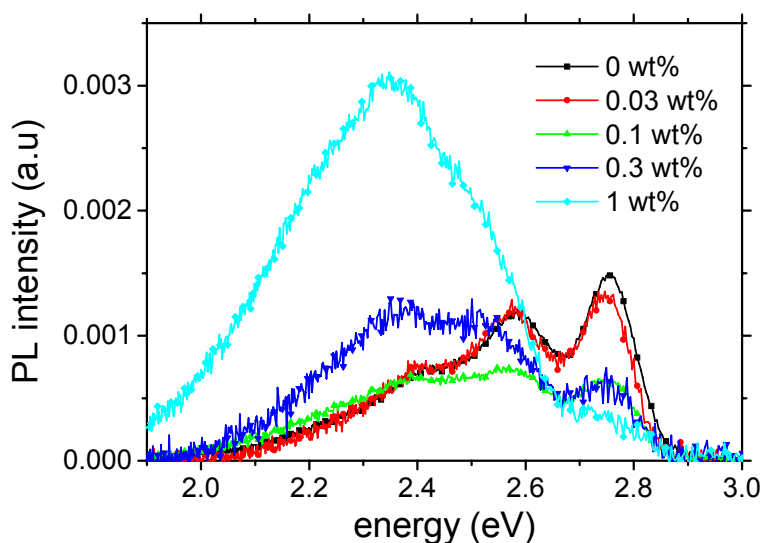
Figure 3.19: Low-temperature (77 K) time delayed PL spectra of PIF-Aryl-Octyl:IF-K thin films on glass substrate. Time delay of ~ 2.3 *ns* after the excitation pulse, 500 *ps* integration. 500 μW average laser power, excitation wavelength $\lambda_{exc}$ = 390 nm (3.18 eV), p =$10^{-5}$ mbar.

For the case of doping concentrations higher than 0.1 wt%, the low-energy feature bears evidence of spectral structure. In contrast to that, long-delayed PL of a neat PIF-Aryl-Octyl film at 77 K is consisted of a broad featureless broad band. Therefore the origin of this band is better assigned to the existence of excimer moieties in neat PIF-Aryl-Octyl films than to keto defects on the molecular backbone (see paragraph 3.2.6)

### 3.3.1.2  PIF-ARYL-OCTYL:IF-K Blends: Energy transfer mediated photoluminescence quenching

The cw-PL and the time-resolved PL of  PIF-Aryl-Octyl:IF-K blends demonstrate that after excitation of PIF-Aryl-Octyl an energy transfer mechanism from PIF-Aryl-Octyk to IF-K, is operative. This energy transfer process results in PL quenching of PIF-Aryl-Octyl singlet emission.

The concept of energy transfer and the mechanisms that have been proposed to explain it, have been presented in Chapter 1. Especially for the case of resonant energy transfer, which is based on a dipole-dipole interaction, the energy transfer rate has been expressed by Förster as:

$$k_T(r) = \frac{Q_D * \kappa^2 * 9000 * \ln 10}{\tau_D * r^6 * 128 * \pi^5 * N * n^4} * J(\lambda) \quad \text{(eq. 3.1)}$$

where J(λ) corresponds to the spectral overlap of the emission from donor and the absorption of the acceptor

$$J(\lambda) = \int_0^{\infty} F_D(\lambda) * \varepsilon_A(\lambda) * \lambda^4 * d\lambda \qquad \text{(eq. 3.2)}$$

Since there is a spectral overlap between the emission of PIF-Aryl-Octyl and the absorption of IF-Ketone (IF-K), it is expected that resonant energy transfer (RET) can be operative. According to the RET theory, there is a critical distance $R_0$ between donor and acceptor chromophores at which the rate of transfer is equal to the observed radiative rate of the donor, in the absence of the acceptor. This critical distance is termed as the Förster radius and it is expressed as:

$$R_0 = \left( \frac{9000 * Q_D * \ln 10}{128 * \pi^5 * N * n^4} * J(\lambda) \right)^{1/6} \qquad \text{(eq. 3.3)}$$

In the case of dilute solution of PIF-Aryl-Octyl and IF-K in toluene (n=1.496), the calculated Förster distance was found to be in the order of 2.2 nm. For deducing this value, the PL quantum yield of PIF-Aryl-Octyl was considered to be $Q_D=0.8$. However, since $R_0$ value is related to $Q_D$ of the donor in a sixth-route fashion (eq. 3.3) no significant deviations are expected for lower values. The spectral overlap J(λ) between PIF-Aryl-Octyl and IF-Ketone is presented in Figure 3.20.
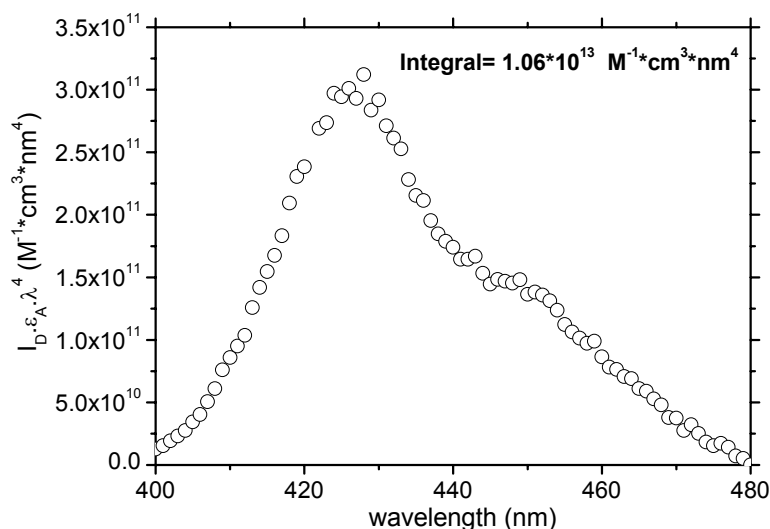
Figure 3.20: The spectral overalap between the emission of PIF-Aryl-Octyl and the absorption of IF-K as calculated from eq.3.2 for dilute solutions of the compounds, at room temperature.

## 3.3.2 Stern-Volmer formalism

Originally, collisional luminescence quenching was described by the Stern-Volmer formalism (eq. 3.4), which was applied to cases where an excited state of a system in solution was rapidly relaxed back to the ground state due to collisions with quencher molecules in the neigbourhood [40].

$$\frac{F_0}{F} = \frac{\tau^0_{obs}}{\tau_{obs}} = 1 + k_q * \tau_{obs} * [Q] \quad \text{(eq. 3.4)}$$

These bimolecular collisions are considered as an additional relaxation channel that provides an extra decay path towards the ground state and therefore as eq. 3.4 describes, a concomitant decrease has to be observed in the luminescence intensity and lifetime values. Due to the dynamic nature of the quenching encounters, collisional quenching has been alternatively described as dynamic quenching [40]. This term was initially applied for distinguishing collisional quenching from static quenching phenomena. Static quenching reflects a process where a fraction of the donor molecules forms a non-fluorescent ground state complex with the quenchers and therefore it becomes 'invisible' in measurements of photoluminescence lifetime. This is why static and dynamic quenching can be easily distinguished in a time-resolved photoluminescence experiment. While in a dynamic process the ratio $\frac{\tau^0_{obs}}{\tau_{obs}}$ will be dependent on

167

[Q] as (eq.3.4) describes, in a static quenching process the $\frac{\tau^0_{obs}}{\tau_{obs}}$ will be independent of [Q] and always equal to unity. This will arise as a result of the fact that the fraction of the host molecules that are not complexed with the quenchers, will undergo relaxation to the ground state without the existence of additional decay channels due to bimolecular collisions. As in static quenching conditions the collisional process is not operative, the quenchers interact with the host only in the ground state hence only the fraction of the non-complexed host will be able to reach the excited state. Subsequently these excited states will undergo relaxation to the ground state following the intrinsic relaxation rate of the system without the contribution of a new relaxation channels for the dissipation of the excitation energy.

### 3.3.2.1 *Photoluminescence-decay transients*

Figure 3.21 presents the normalised singlet decay transients obtained for the differently doped PIF-Aryl films at room temperature. For reasons of comparison, the transient of PIF-Aryl singlet emission in dilute solution is also presented.
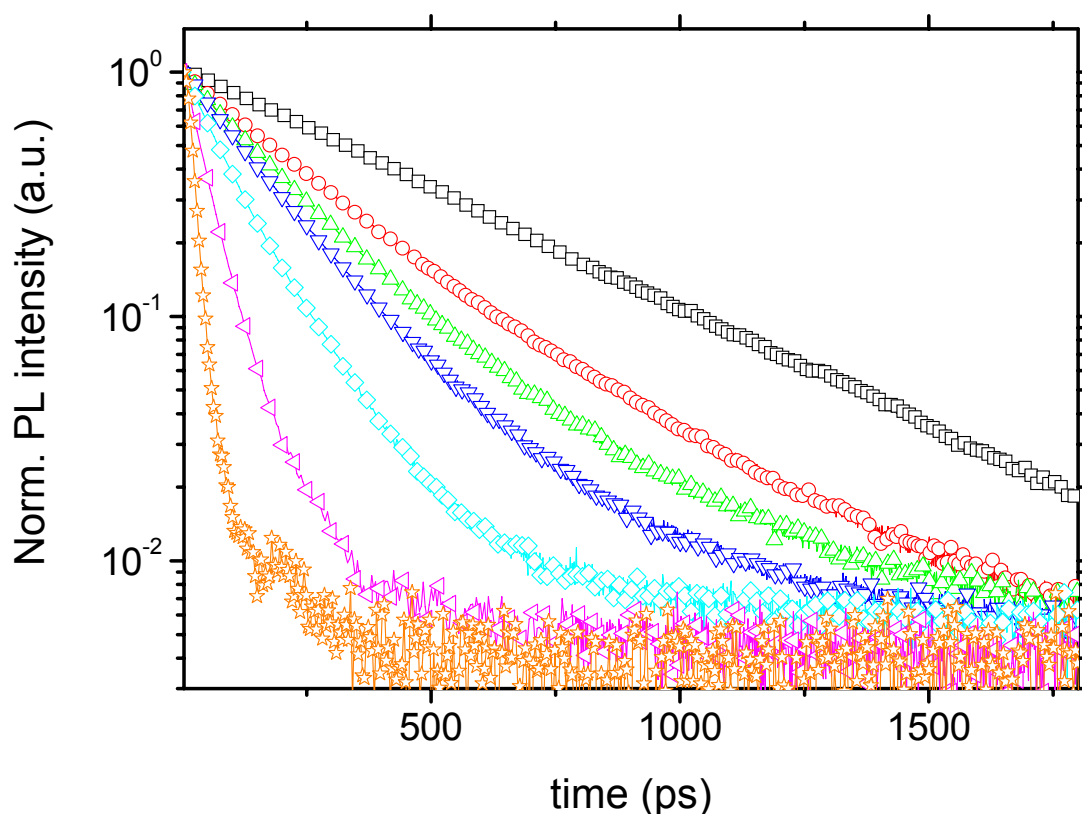
Figure 3.21: Room temperature normalised transient decays of singlet emission monitored for thin films on glass substrate, of blends consisting of PIF-Aryl-Octyl with increased IF-K content (see chart 1): 0 wt% IF-K solution (squares), 0 wt% IF-K film (circles), 0.03 wt% IF-K film (up-triangles), 0.1 wt% IF-K film (down-triangles), 0.3 wt% IF-K film (diamonds), 1 wt% IF-K film (tilted triangles), 4.5 wt% IF-K film (stars). 500 µW average laser power, excitation wavelength $\lambda_{exc}$ = 390 nm (3.18 eV), p =$10^{-5}$ mbar.

Based on these decays, the $\tau_{1/e}$ time constants were extracted and a Stern-Volmer plot was constructed. Figure 3.22 presents the Stern-Volmer plot for two different temperatures together with the linear fits obtained in the given range of doping concentration. As the inset of Figure 3.22 shows, a concomitant decrease of the cw-PL singlet intensity and corresponding singlet lifetime can be observed. The parallel reduction of fluorescence intensity and fluorescence lifetime in combination with the observed Stern-Volmer linearity excludes the formation of a non-fluorescent excited complex between IF-K and PIF-Aryl-Octyl [23].
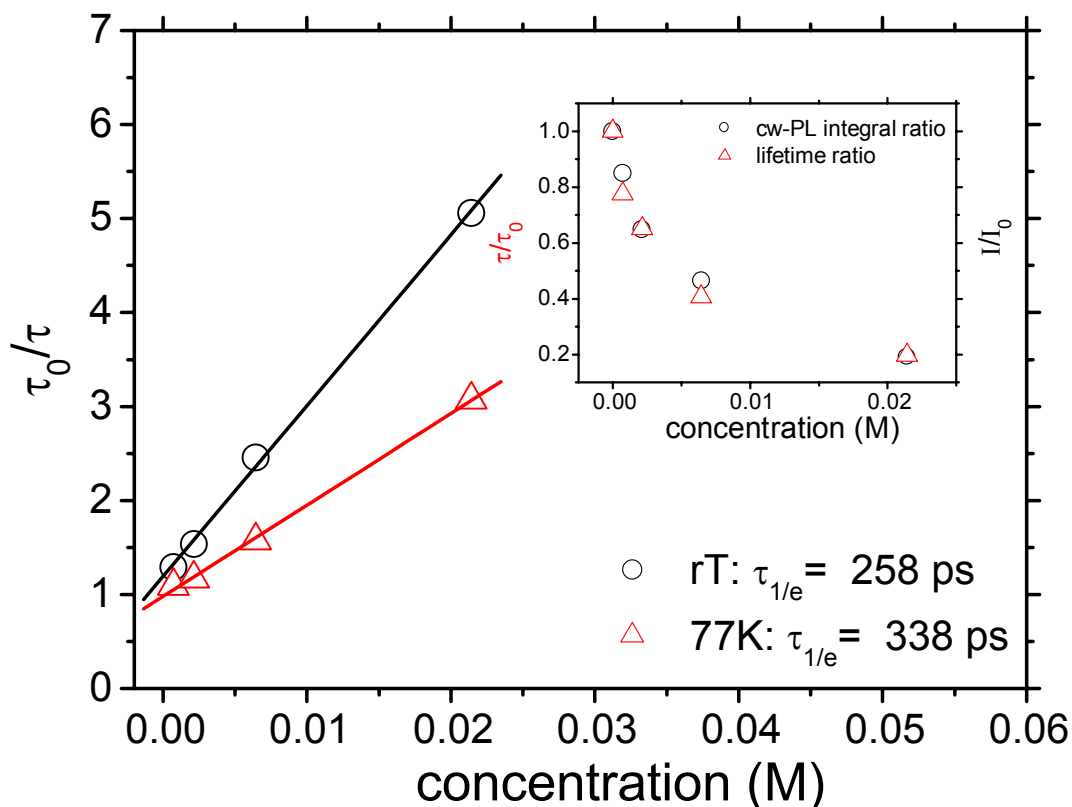
Figure 3.22: Stern-Volmer plot of PIF-Aryl-Octyl singlet emission for films of blends consisting of PIF-Aryl-Octyl with increased IF-K content (see chart 1) at room temperature (circles) and 77 K (triangles). Solid lines are linear fits to the data (see text) $\lambda_{exc}$ = 390 nm (3.18 eV), p =$10^{-5}$ mbar. Inset: comparison of the relative decrease in lifetime (triangles) and cw-PL singlet intensity of PIF-Aryl-Octyl as film with increased IF-K content. Intensity ratios correspond to PL integral ratios determined from spectral integration of obtained cw-PL spectra.

## 3.3.3 Efficiency of energy transfer

The efficiency of the RET process is described from the fraction of the photons absorbed by the donor that are transferred to the acceptor:

$$E = \frac{k_{ET}}{k_{obs} + k_{ET}} = \frac{R_0^6}{R_0^6 + r^6} \quad \text{(eq. 3.5)}$$

where $R_0$ is the Förster distance and r is the distance between donor-acceptor chromophores. For very small distances of r in respect to $R_0$, the efficiency of RET reaches the maximum value of unity.

Alternatively, the efficiency can be expressed in terms of lifetime values of the donor, that are parameterised in respect to acceptor concentration:

$$E = 1 - \frac{F_{DA}}{F_D} = 1 - \frac{\tau_{DA}}{\tau_D} \quad \text{(eq. 3.6)}$$

where DA and D represent the physical quantity measured for the donor in the presence and in the abscence of the acceptor respectively. This physical quantity can be either the cw-PL intensity F or the lifetime value $\tau$. For the case of Figure 3.21, where the transient decays of PIF-Aryl-Octyl are deviating from the monoexponential decay, it is more appropriate to make use of the average decay times that eq. 3.7 describe. Therefore eq. 3.6 becomes:

$$E = 1 - \frac{F_{DA}}{F_D} = 1 - \frac{\int_0^\infty I_{DA}(t)dt}{\int_0^\infty I_D(t)dt} \quad \text{(eq. 3.7)}$$

because the integrals of eq. 3.7 are directly proportional to the cw-PL intensity F. It has to be noted that the eq. 3.7 has been alternatively considered as the expression of PL-quenching efficiency [41], once the energy transfer meachanism assists the PL quenching of a donor that is embedded in an environment of energy scavengers that act as acceptors. In the following the term energy transfer efficiency will be used, unless indicated otherwise.

 From Figure 3.23, it seems that energy transfer efficiency is reduced at 77 K. This is in agreement with the notion that exciton diffusion is slower at low temperatures (Figure 3.22). Moreover it is observed that a room temperature, the 50% of energy transfer efficiency is approximately reached at a doping concentration of ~0.3 wt%.
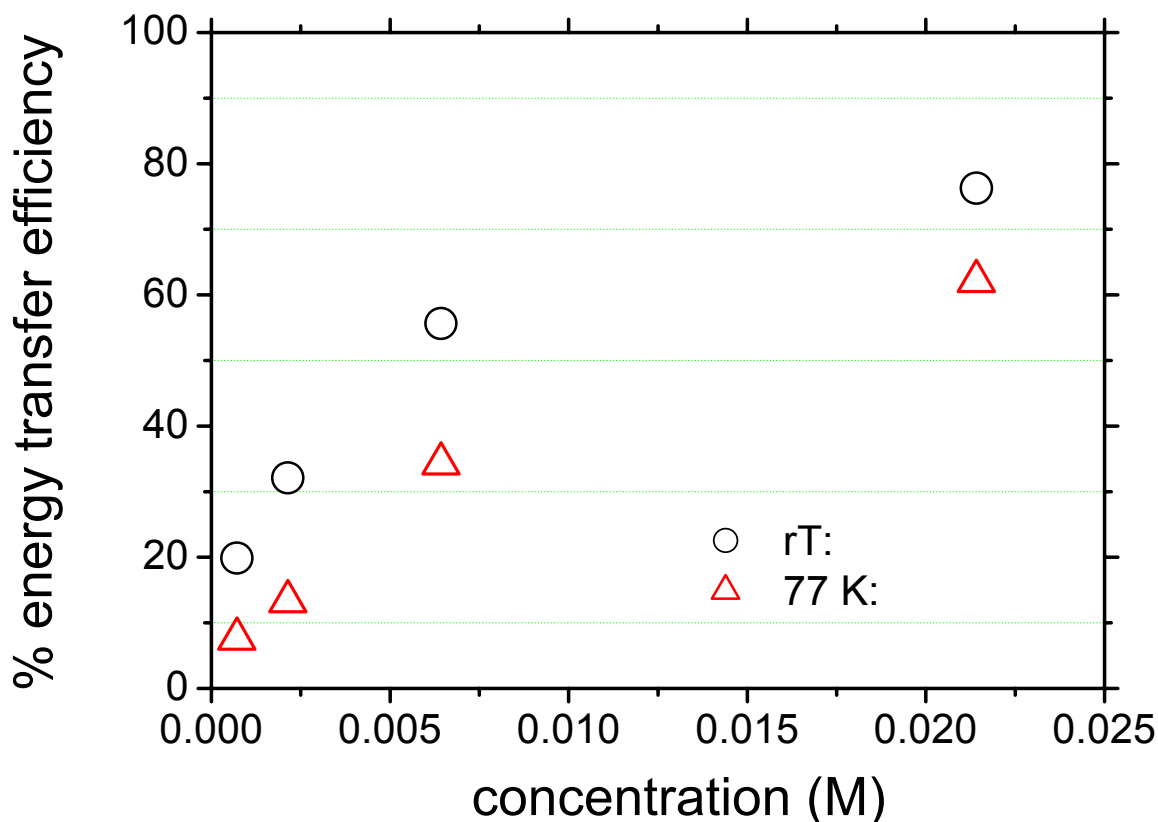
Figure 3.23: Room temperature (circles) and 77 K (triangles) energy transfer efficiency, for the studied films of PIF-Aryl-Octyl:IF-K blends. The determination of the values was based on the time resolved PL data of Figure 3.21.

A simple polynomial fit to the data of Figure 3.23 informs that the maximum efficiency of PL quenching via energy transfer, takes place at a doping concentration of 0.017 M at room temperature and at 0.021 M at 77 K.

## 3.3.4 Discussion

In paragraph 3.3.1 we have presented results of absorption and PL spectra for IF-K molecule in dilute solutions (toluene and MTHF) and as film. We should note here that in a very recent report [39] dealing with the photophysical solution properties of a molecule similar to IF-K, namely molecular fluorenone, the authors claimed the existence of fluorenone excimer formation even in a high degree of dilution, similar to the one we have used for the IF-K studied solutions. However, unlikely to this work, in the case of PIF-Aryl-Octyl films doped with IF-K (Figure

172

3.18), we observe the characteristic IF-K contribution in the low-energy part of the PL spectra even for the 0.03 wt% doping level.

Moreover, in contrast to the observed solvatochromism effect of molecular fluorenone [39] or a fluorene-fluorenone trimer [38], we don't observe any spectral change in the low-energy PL band of IF-K upon going from toluene to MTHF. We presume that the change in the polarity of is not so drastic in order to make obvious the solvent effects in the IF-K excited states.

We start the discussion by taken as granted that the Förster formalism for energy transfer is valid in our studied systems. Our confidence regarding this issue arises from the results presented in paragraph 3.3.1.2, where the required spectral overlap of IF-K and PIF-Aryl-Octyl has been presented. It has to be mentioned though, that the obtained Förster $R_0$ value has been extracted from the classical dipole-dipole approximation of eq. 3.1. Since in the case of long polymeric chains one of the interacting dipoles can not be considered as a point, it is very probable that the Förster theory fails to describe fully the energy transfer process between a small organic chromophore acting as a acceptor and a long polymeric chain acting as a donor. The main problem is that the local concentration of segments of the polymer is not identical to the total volume concentration. Another important reason that has to be invoked for the failure of Förster theory is the existence of exciton migration within the polymeric chain prior to the energy transfer step. The Förster distance is underestimated in the case of a conjugated polymer where the polymer host is considered as an array of monomer-donors in which exciton migration can take place, prior to energy transfer. More precisely, the units that constitute the array are polymeric segments comprised of monomers that are effectively conjugated without any disruption in the delocalisation of their π-electrons along the polymer segments. This process of exciton migration within the donor matrix occurs within a density of excited states that reflect a distribution of the polymeric segments of different conjugation lengths (see Chapter 1). That is why larger Förster radii should be expected for polymers that may exhibit different average conjugation length in the solid state.Under conditions of exciton migration the real value of the $R_0$ Förster radius can be higher than the one that eq. 3.3 predicts. Particularly for electronic energy transfer systems within doped polymeric systems, there are several experimental works that have pointed out the weakness of the Förster theory [42], [43], [44]. However, very recent reports have given the most comprehensive theoretical approach in energy and charge transfer processes within doped of polymeric systems that characterized by energetic disorder [41], [45].

The linearity observed in the Stern-Volmer plot, reflects the homogeneous mixing of guest to host in the blended films, at least for the doping concentrations used. We attribute the observed reduction of PIF-Aryl-Octyl PL to a dynamic quenching process that arises from the excitation

energy transfer from host to guest. Based on the Stern-Volmer formalism the quenching rates of energy transfer can be deduced to be in the order of *ps*. The energy transfer times for each doping level are presented in Table 3.4. From linear fitting of the obtained Stern-Volmer plots, $k_q$ was found to be in the order of $7.05*10^{11}$ $M^{-1}*sec^{-1}$ and $2.88*10^{11}$ $M^{-1}*sec^{-1}$ at room temperature and at 77 K, respectively. Alternatively, these rate values imply that at room temperature, even in the presence of 0.3 wt% ketone concentration, quenching of an initially singlet exciton will take place within ~220 *ps*, which is comparable to the observable radiative lifetime of the neat PIF-Aryl-Octyl film. Since the energy transfer time is reciprocally related with the concentration of the quenching molecules [46] it seems clear that the ketone concentration should be much lower than 0.3 wt% in order to achieve more favourable conditions for singlet emission than for energy transfer to the existing quenching sites.

| Doping Level (%wt) | [Q] (mmole/Lt) | Singlet Lifetime $\tau_{1/e}$ (*ps*) | Energy Transfer time $\tau_{ET}$ (*ps*)[b] | % Energy Transfer Efficiency |
|---|---|---|---|---|
| 0 | 0 | 258 | - | - |
| 0.03 | 0.70 | 200 | 2029 | 20 |
| 0.1 | 2.14 | 168 | 663 | 32 |
| 0.3 | 6.43 | 105 | 221 | 56 |
| 1 | 21.41 | 51 | 66 | 76 |

Table 3.4: Doping concentration of IF-K in PIF-Aryl-Octyl films (see Chart 3.1) studied. Film thickness was 60 nm for all samples. Singlet lifetime of PIF-Aryl-Octyl was determined from data presented in Figure 3.21. The calculated times from energy transfer from PIF-Aryl-Octyl to IF-K are also quoted.
[b] For a room temperature quenching rate constant $k_q= 7.04*10^{11}$ $M^{-1}*sec^{-1}$, $\tau_{ET}=([Q]*k_q)^{-1}$ (see [46]).

The observed decrease of the quenching rate at lower temperatures comes also in agreement with previous reports on the existence of a thermally activated component in the energy transfer rate from polymeric hosts to guest molecules [44], [47]. Energy transfer from polymeric host to guest was described as a two-step process where diffusion of the photoexcitations within the polymer matrix was followed by energy transfer to the dopant. Therefore as at lower temperatures the excitation diffusion process into the polymer host is retarded, a reduction in the observed energy transfer rate is found. Eventually it comes out that the doping experiment can only provide information regarding an observed quenching rate $k_q$, which presumably consists of a product between the intrinsic rate of Förster type energy transfer and the rate of exciton migration within the polymeric host prior to energy transfer to IF-K guest.

In paragraph 3.3.3 the issue of energy transfer efficiency has been addressed. A 50% reduction has been determined for the PL of PIF-Aryl-Octyl films when doped with 0.3% IF-K. Since from the Förster theory the 50% PL quenching is expected to occur when the donor-acceptor distance

becomes equal to the Förster radius $R_0$, it is concluded that in films of PIF-Aryl-Octyl:IF-K blends, the value of $R_0$ between PIF-Aryl-Octyl:IF-K is reached at 0.3 wt % (6.43mM, see Table 3.4) doping. This concentration corresponds to a distance of $d$~8 nm between two neighbouring IF-K molecules, by the rough approximation of a sphere-like molecular shape in the solid state, that occupies a volume of $(4/3)*\pi*d^3$ and is homogeneously dispersed within the PIF-Aryl-Octyl matrix. This determined distance should be the lower limit in the value of the intermolecular distance between two neighbouring IF-K molecules due to the intervention of the matrix molecules that in reality enlarge the IF-K spatial separation.

 The data of Figure 3.23 suggest that the maximum quenching efficiency value of 100% is never reached in the films of PIF-Aryl-Octyl:IFK blends, within the investigated doping concentration range. Phenomena of aggregation between the dopants that eventually would lead to a reduced energy transfer efficiency, have been excluded from the observed Stern Vomer linear plots. At this stage we consider that our study systems can tolerate loadings of IF-K higher than the maximum doping level that has been used.

## 3.4  DELAYED FLUORESCENCE

 One of the most important questions in respect with the nature of the excited states in conjugated polymers is the magnitude of electron-electron interaction [48]. In small organic molecules electron-electron interactions exist, and therefore the degree of exchange energy between a pair of electrons becomes significant. Experimentally the strength of electron-electron interactions is determined from the energy difference between the emission maxima of fluorescence and phosphorescence. According to the enumerative system of electronic state hierarchy of Jablonski [49], [50], fluorescence originates from the first electronically excited singlet state $S_{1-0}$ whereas phosphorescence originates from the first electronically excited triplet state $T_{1-0}$. This energy difference corresponds to the exchange energy of electrons and reflects the stability of the first triplet state $T_1$ (spin parallel) in respect to the first singlet state $S_1$ (spin antiparallel). Singlet and triplet states not only differ in their spectral positioning but also in their probability for emission. As singlet states are strongly coupled to the ground state their luminescence lifetime lies in the order of *ps-ns*. By contrast, triplet states posses small values of oscillator strength, therefore their photoluminescence lies in the order of *μs-sec*.

 As it has been described in Chapter 1, there are cases where after optical excitation of a material, long-lived luminescence is observed that possesses a lifetime comparable to phosphorescence but yet is positioned in a spectral region where fluorescence is observed. This phenomenon of delayed fluorescence (DF) was widely observed in organic molecular crystals

[48]. More specifically, the occurrence of DF was assigned to the interaction of two long-lived triplet states that after fusion resulted in the population of a high electronically excited singlet state and the ground state. Subsequently after the electronic relaxation of the high electronically excited state to the lowest lying electronically excited state, emission takes place with the characteristic energy of a singlet state. Since in this process the triplet state acts as a precursor of the emitting singlet state, the observed fluorescence emission is following the dynamics of the triplet state. Due to the fact that the participant photo-excited species are two triplet states that take part in a collisional process, DF has been alternatively termed as triplet-triplet annihilation (TTA).

## 3.4.1 Delayed fluorecence in $\pi$-conjugated polymers

 Triplet-triplet annihilation has been firmly established for the case of conjugated polymers [51], [52], [53], [54], [55]. The observation of DF in films and vitrified glasses of a series of conjugated polymers has further contributed to the belief that electron-electron interactions in these systems are of appreciable importance. Hence the molecular exciton model seems to be more appropriate for the description of low-level electronic properties in these systems. Primary excited states in conjugated polymers are believed to posses a charge-transfer (CT) character [48]. Except the experiments performed for the investigation of delayed fluorescence by optical excitation [52], [54], [55], [56], the existence of triplet states in conjugated polymers has been addressed by the experimental techniques of triplet-triplet absorption and optically detected magnetic resonance experiments [51], [57]. Moreover via the method of pulse radiolysis [53], the energy values of the triplet states for a large group of conjugated polymers, have been systematically investigated [58].

 Beside the fundamental scientific interest for the nature of the triplet state, studies on phosphorescence of conjugated polymeric systems are of great technological interest [59]. Conjugated polymers are considered as one of the most promising class of functional materials for the development of display-devices that can be driven by electrical bias. As it was discussed in Chapter 2, electroluminescence, the emission of light after electrical excitation, is now a well-known process in conjugated polymers. Very recently the electrophosphorescence of a poly(fluorene) derivative has been reported [60].

### *3.4.1.1  The importance of triplet states in π-conjugated polymers*

Among the many important parameters that influence the electroluminescence efficiency of an light-emitting diode, is the fraction of the singlet excitons that are formed after charge carrier recombination [61], [62], [63], [64] .

Linear optical resonance excitation of a material eventually leads to the population of a singlet electronically excited state. After one-photon-excitation the states that are strongly optically coupled to the ground state are of singlet character. In contrast to that, the primary excited state of a conjugated polymer which is excited electrically can be of a singlet or a triplet as there are no restrictions regarding the way that injected charge carriers will recombine in order to form neutral excitons. Hence a mixture of singlet and triplet excitons is formed after charge injection. Simple spin statistics can estimate roughly that one in the four possible reached excited states will be of singlet character. As it was discussed in Chapter 1,  for conjugated polymers the primary excited states formed after charge injection are considered to be of charge-transfer (CT) nature. These CT states can be either of singlet or triplet multiplicities and the strength of their coupling to the neutral singlet and triplet states depends on the corresponding difference of CT-$S_1$/$T_1$ energy gaps. Alternatively, these CT states have been termed as geminate pair states [65], [66].

Triplet states are metastable states that are not able to contribute to the electroluminescence due to their weak radiative coupling to the ground state [67]. Therefore, the aforementioned assumption regarding to spin statistics introduces an inherent upper boundary of 25% in the electroluminescence efficiency. This percentage value has been extracted by the rough approximation that the formation cross-section of singlet excitons has a value close to that of any one of the three equivalent non-radiative triplet exciton states. However experimental work employing combinatory measurements of cw-photoinduced absorption and photoinduced absorption detected magnetic resonance have shown that for a large group of conjugated polymers, the ratio of singlet/triplet cross-section formation may be greater than unity [57]. Furthermore the value of this ratio has been found to depend on the exact nature of the electroluminescent polymer studied. Computational calculations have complemented the experimental results regarding the value of the singlet/triplet excited states fraction [63], [68]. In extended conjugated chains the energy difference between CT and $S_1$ excited states becomes of the order of a few tenths of an electronvolt. This fact assists further the intersystem-crossing rate between CT and $S_1$ states, thus exhibiting a singlet/triplet fraction, which exceeds the statistical limit of 25% [68].

### *3.4.1.2 Kinetics of the triplet state and delayed fluorescence*

The rate equation which describes the temporal dependence of the concentration of a triplet excited state $[T_1]$ should take into account the radiative rate $k_r$ and the non-radiative rate $k_{nr}$ of phosphorescence emission. Usually the sum of these two rates represents the observed decay rate $k_{obs}$ of the emission. Additionally, the bimolecular constant $\gamma_{TTA}$ that accounts for the triplet-triplet collisions should not be ignored. The value of $\gamma_{TTA}$ ($cm^3*sec^{-1}$) is directly related to the diffusion coefficient D ($cm^2*sec^{-1}$) of the excitations according to:

$$\gamma_{TTA} = 8 * \pi * \langle R \rangle * D \quad (eq.\ 3.8)$$

where $\langle R \rangle = \left( \dfrac{3 * \gamma_{TTA}}{4 * \pi * \beta} \right)^{1/3}$ represents the critical radius at which triplet-triplet annihilation between two excitations becomes probable. Under these conditions the temporal dependence of $[T_1]$ can in principle be written as:

$$\frac{d[T_1]}{dt} = G_T(t) - k_r * [T_1] - k_{nr} * [T_1] - \gamma_{TTA} * [T_1]^2 \Rightarrow$$

$$\frac{d[T_1]}{dt} = G_T(t) - \frac{1}{\beta_0} * [T_1] - \gamma_{TTA} * [T_1]^2 \quad (eq.\ 3.10)$$

where $\beta_0 = \dfrac{1}{k_{obs}} = \dfrac{1}{k_r + k_{nr}}$. The solution of eq. 3.10 gives

$$[T]_t = [T]_0 * \exp(-t/\beta_0); \text{ for } \frac{1}{\beta_0} * [T_1] \geq \gamma_{TTA} * [T_1]^2 \quad (eq.\ 3.11) \text{ and}$$

$$[T]_t = \frac{[T]_0}{(1 + \gamma_{TOT} * [T]_0 * t)}; \text{ for } \frac{1}{\beta_0} * [T_1] \leq \gamma_{TTA} * [T_1]^2 \quad (eq.\ 3.12)$$

The kinetic schemes of the phosphorescence intensity decay transients will be:

$$I_{Ph}(t) = k_r * [T]_t = k_r * \left[ [T]_0 * \exp(-t/\beta_0) \right] \Rightarrow I_{Ph}(t) \propto \exp(-t/\beta_0); \quad (eq.\ 3.13)$$

for $\dfrac{1}{\beta_0} * [T_1] \geq \gamma_{TTA} * [T_1]^2$

$$I_{Ph}(t) = k_r * [T]_t = k_r * \left[ \frac{[T]_0}{(1 + \gamma_{TTA} * [T]_0 * t)} \right] \Rightarrow I_{Ph}(t) \propto \frac{1}{(1 + \gamma_{TTA} * [T]_0 * t)}; \quad (eq.\ 3.14)$$

for $\dfrac{1}{\beta_0} * [T_1] \leq \gamma_{TTA} * [T_1]^2$

As delayed fluorescence originates from the biphotonic process that results in the encounter of two excited triplet states, the intensity of the delayed fluorescence is expressed as:

$$I_{DF} = \frac{1}{2} * f * \gamma_{TTA} * [T_1]^2 \quad \text{(eq. 3.13)}$$

where $0 \leq f \leq 1$ describes the fraction of the effective triplet-triplet collisions that result in population of the first excited singlet state.

The decay law that governs the intensity of the delayed fluorescence is described as:

$$I_{DF} = \frac{1}{2} * f * \gamma_{TTA} * [T]_0^2 * \exp(-\frac{2*t}{\beta_0}) \text{ if } \frac{1}{\beta_0} * [T_1] \geq \gamma_{TTA} * [T_1]^2 \quad \text{(eq. 3.15)}$$

or

$$I_{DF} = \frac{1}{2} * f * \gamma_{TTA} * \frac{[T]_0^2}{(1 + \gamma_{TTA} * [T]_0 * t)^2} \text{ if } \frac{1}{\beta_0} * [T_1] \leq \gamma_{TTA} * [T_1]^2 \quad \text{(eq. 3.16)}$$

It has to be emphasized that the presented solution of the temporal dependence of the concentration of a triplet excited state $[T_1]$ only reflects the extreme cases where TTA either completely dominates over or is totally diminished by the other kinetic processes that deplete the triplet reservoir. In reality, it can not be excluded that TTA occurs simultaneously with other monomolecular events, at high excitation laser intensities. For that case, the solution for the temporal dependence of $[T_1]$ has been described as:

$$[T_1]_t = [T_1]_0 * \exp(-\frac{t}{\beta}) * \left[1 + \gamma_{TTA} * [T_1]_0 * \beta * \left(1 - \exp(-\frac{t}{\beta})\right)\right]^{-1} \quad \text{(eq. 3.17)}$$

Finally it has to be underlined that the presence of energetic disorder in materials such as conjugated polymers, impart to the $\gamma_{TTA}$ coefficient a time-dependent character that increases the level of difficulty in the numerical analysis for the temporal dependence of $[T_1]$. Monte-Carlo simulations have addressed the inherent time dependence of $\gamma_{TTA}$ of an energetically random system of point sites of which the one percent was occupied by triplet excitations. Experimental evidence for the existence of a time-depended $\gamma_{TTA}$ in a poly(fluorene) derivative has also been reported [52].

## 3.4.2 Delayed fluorescence in PIF-Aryl-Octyl derivative

The observation of DF has been reported numerous times for different types of conjugated such as derivatives of poly(*p*-phenylene ethynylene) [51], poly(fluorene) [52], poly(phenylene vinylene) [51], [54] and poly(phenylquinoxaline) [55]. For the case of ladder-type polymers such as MeLLLP [69] and alkyl-derivatised PIFs [70] DF investigations have also been performed.

DF is not an exclusive result of triplet-triplet annihilation. It has been argued that the observation of DF in films of MeLLLP is a result of geminate pair recombination [65]. On the other hand, in the case of PFO, DF was attributed fully to triplet-triplet annihilation, although no

electric-field dependence of the DF was demonstrated to exclude the impact of charge-transfer state recombination to the generation of DF [52]. The branching ratio of triplet-triplet annihilation in respect to that of geminate pair recombination for the generation of DF has been evaluated for the case of a PPV derivative [54].

In materials such as phenylene-based conjugated polymers, the triplet state has been determined to have a radiative lifetime close to one *sec*. It is common that phosphorescence is hardly observed in the solid state, even at lower temperatures where the triplet state is much longer lived due to the deactivation of thermal non-radiative relaxation. There are yet some exceptions where phosphorescence has been observed after optical [52], [70], and electrical [60] excitation, in films of conjugated polymers, at low temperatures.

In the following we present spectroscopic studies of delayed fluorescence and phosphorescence for PIF-Aryl-Octyl, the arylated PIF derivative that has been introduced in paragraph 3.2.2. The chemical structure of this compound is given in Chart 3.1.

### 3.4.2.1 Experimental

Thin films and dilute solutions of PIF-Aryl-Octyl were prepared. For the thin films, quartz substrates were used in order to avoid the long-lived luminescence that the normal glass substrates exhibit after optical UV-Vis excitation. Dilute solutions were prepared in MTHF solvent. The process of sample preparation was like section 3.2.1 describes.

For phosphoroscopic detection, excitation of the samples took place with the third harmonic of a Nd-YAG laser at 3.02 eV (410 nm) producing approx. 10 *ns* pulses operating at a repetition rate of 10 Hz. The signal was dispersed by a monochromator with a 300 lines/mm grating blazed at 500 nm and detected with a gated optical multichannel analyser (OMA). The resolution of this set up was of 2 nm.

Synchronisation of the OMA detector was in respect to the laser pulse and it was achieved by using the electrical trigger of the laser output. The width of the OMA detection window was kept at 10 *ms* duration whereas the gate triggering was delayed in respect to the laser pulse with a variable delay. A home-built shutter was used in order to reduce the repetition rate of the laser down to 0.5 Hz. The laser pulse triggered both the OMA and the shutter and a software routine for the OMA system was used in order to establish synchronisation with the shutter. Averaging of 100 accumulations was preferred for increasing the signal-to-noise ratio of the registered luminescence. During the measurement, the samples were kept under vacuum in a continuous cold finger liquid nitrogen cryostat. All thin film measurements were performed under a dynamic vacuum of $10^{-5}$ mbar. Time-resolved PL of dilute solutions was recorded using a home-built

glass cell of 4 mm path length. Both for the case of thin films and dilute solutions, an aperture was used for reducing the laser spot diameter down to 2 mm. No focal lens was used for focusing the laser spot onto the surfaces of the samples measured.

### 3.4.2.2  Results

In the discussion presented in 3.2.6, it was argued that PIF-Aryl-Octyl is a blue light-emitter that by virtue of the synthetic route used for its preparation, does not contain chemical impurities that can quench its photoluminescence. In the following an additional photophysical characterisation of PIF-Aryl-Octyl is presented regarding its capability to exhibit phosphorescence. In the absence of chemical impurities the quantum yield of the intersystem crossing rate should be increased thus making phosphorescence observation highly probable.

Figure 3.24 presents the emission spectrum of PIF-Ary-Octyl in a vitrified dilute solution of MTHF. The presented spectra were obtained for a time delay of 500 µs after the excitation pulse. The time gate of the detector was of 10 ms and accumulation of 100 pulses took place for increasing the signal-to-noise ratio. The excitation intensity used was in the order of 30µJ/pulse. According to Figure 3.24, emission is observed in the same spectral position where fluorescence was observed (Figure 3.11). Since the observed emission possesses identical spectral positions and vibronic splittings to that of fluorescence emission, it is attributed to delayed fluorescence (DF) of PIF-Aryl-Octyl. Additionally to DF, new emissive features are observed in the lower lying region 2.1–1.8 eV. The main emission band is red-shifted by ~0.7 eV from the DF and the vibronic splitting is like that of DF. The observed emission is attributed to phosphorescence that originates from the lower lying triplet state $T_1$ of PIF-Aryl-Octyl. Table 3.5, summarises the values of the spectral features of Figure 3.24, after implementation of a Lorentzian fit to the data.
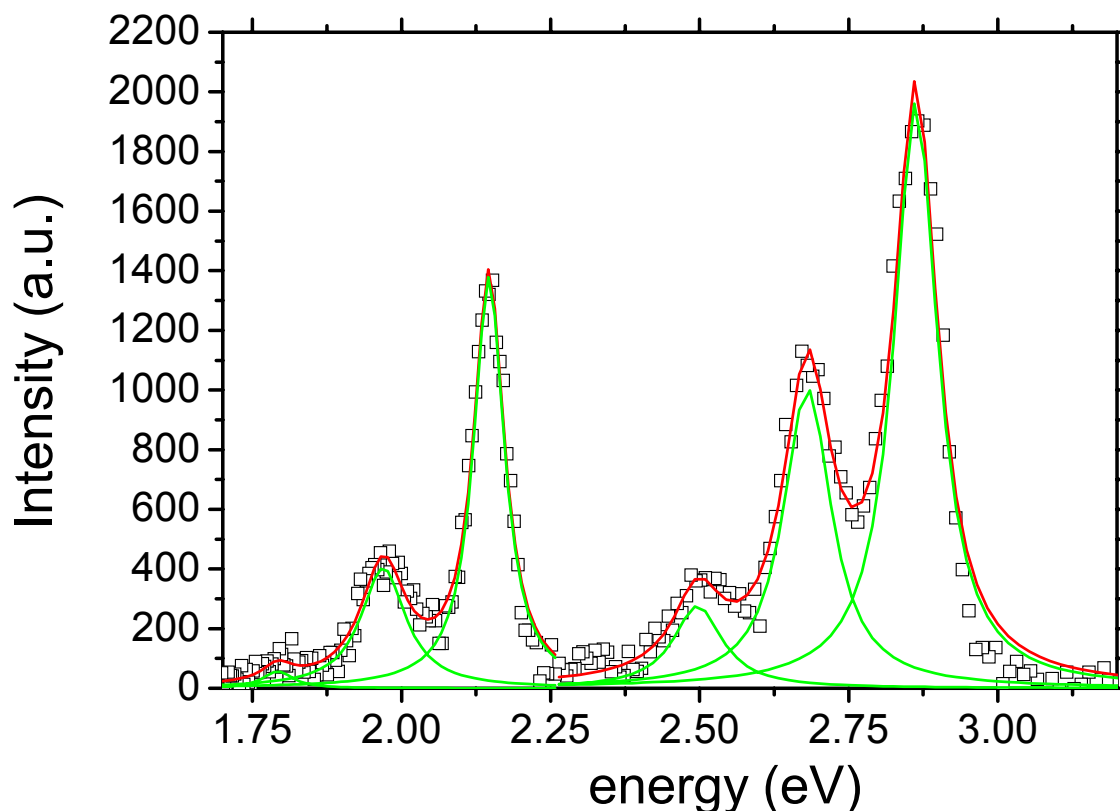
Figure 3.24: Low-temperature delayed luminescence (squares) of PIF-Aryl-Octyl in a vitrified and degassed dilute solution in MTHF. Excitation was at 3.02 eV (410 nm) of 30μJ/pulse intensity. The spectrum was recorded at 500 *μs* delay after the excitation pulse and in a time window of 10 *ms*. Averaging was performed over 100 excitation pulses. The solid lines are Lorentzian fit on the data.

The energy gap of $S_{1-0}$-$T_{1-0}$ levels is typical of that observed in a series of PPP derivatives, and apparently reflects a low degree of inhomogeneous broadening for PIF-Aryl-Octyl.

Figure 3.25 presents the decay transients of DF and Ph emissions of PIF-Aryl-Octyl. It is found that the Ph decay is nicely recovered by a monoexponential decay function, which exhibits $\tau_{Ph}$=0.96±0.02 sec.
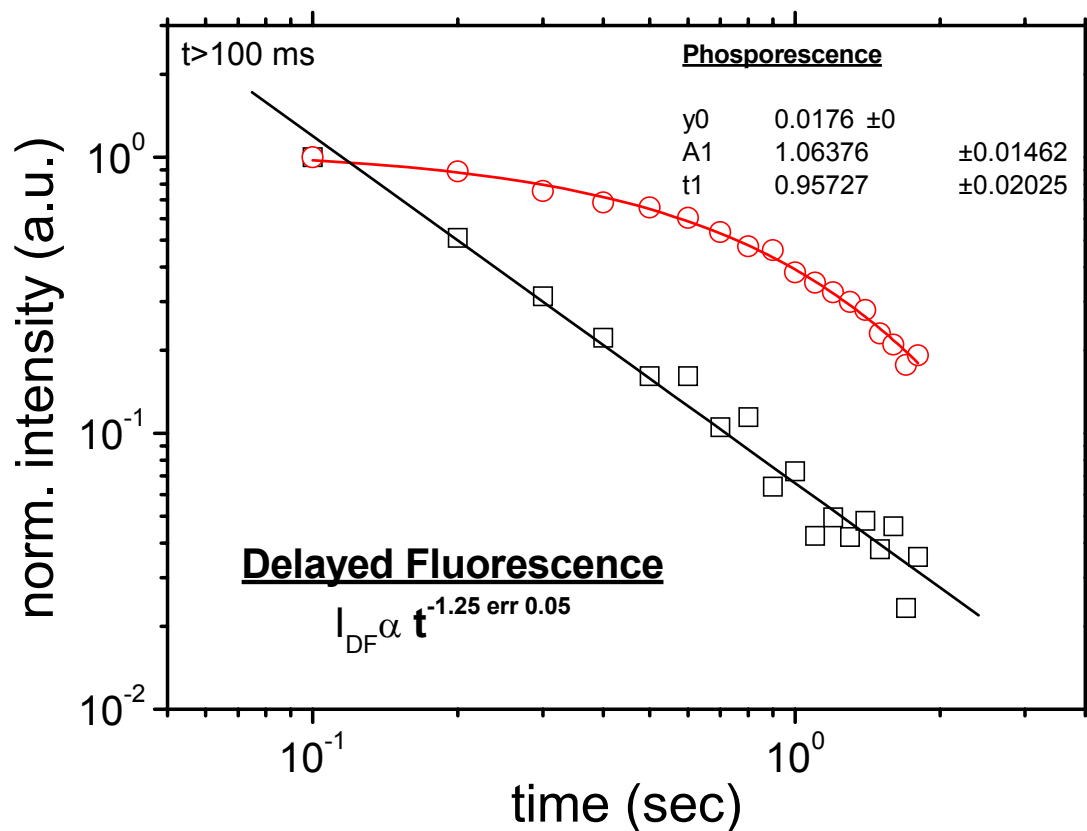
Figure 3.25: Normalised decay transients of low temperature (77 K) delayed fluorescence (DF, squares) and phosphorescence (Ph, circles) for PIF-Aryl-Octyl in a vitrified and degassed dilute solution in MTHF. Excitation was at 3.02 eV (410 nm) of 30μJ/pulse intensity. Recording of the signal started after the first 100 *ms* after the excitation pulse. The solid lines are fit on the data.

As Figure 3.25 depicts, DF intensity is found to follow a power decay law. No indication of a reduction in the slope of phosphorescence power dependence exists that could indicate the initiation of a bimolecular process between the $T_1$ state of PIF-Aryl-Octyl, beyond a critical excitation intensity. Moreover DF intensity also varies linearly with the excitation intensity without any evidence of a quadratic character that could indicate a square dependence on the $T_1$ state.
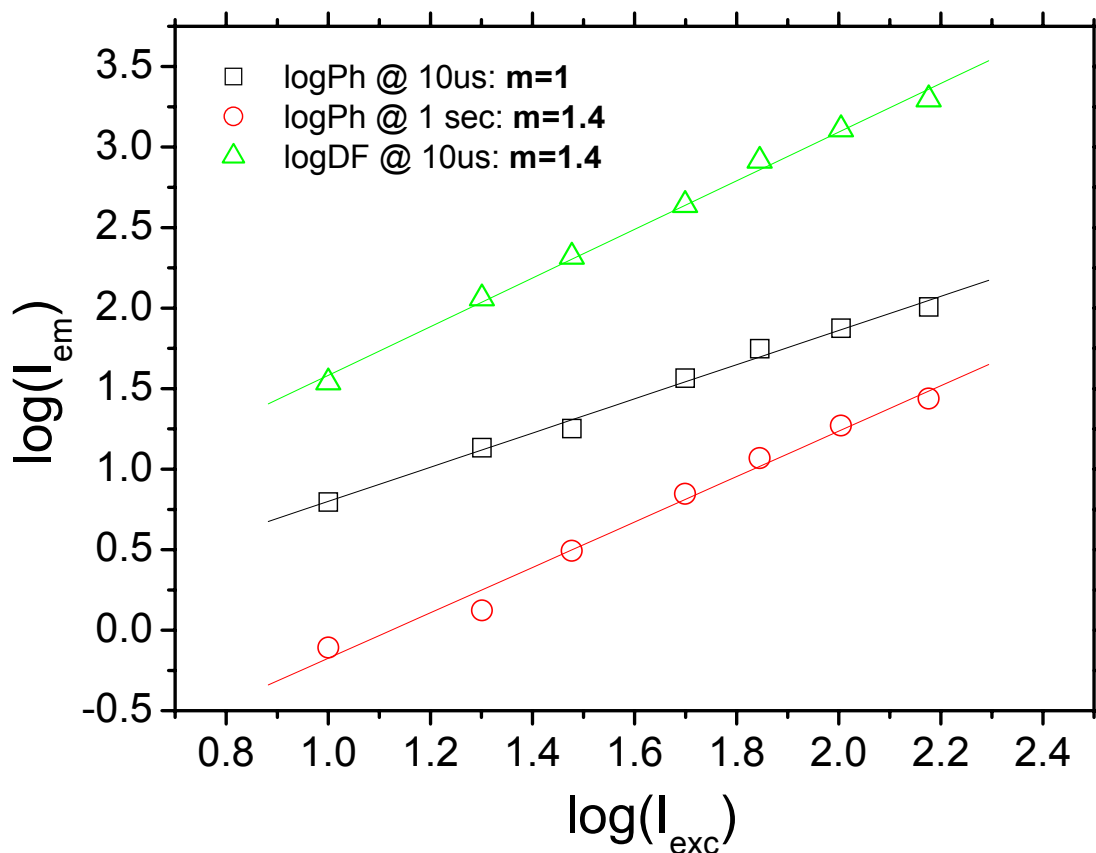
Figure 3.26: Excitation intensity dependence of luminescence in vitrified and degassed dilute solution of PIF-Aryl-Octyl in MTHF. Phospshorescence intensity is shown as recorded for 10 $\mu s$ delay (squares) and 1 *sec* (circles) after the excitation pulse. Delayed fluorescence intensity is shown as recorded for 10 $\mu s$ delay (triangles) after the excitation pulse. In all cases the monitored emission was recorded within a time window of 10 *ms*.

As Figure 3.27 shows, DF of PIF-Aryl-Octyl is observed also for the case of thin films at 77 K. The presented spectrum represents the registered DF intensity for a time delay of 1ms after the excitation pulse. The gate time of the detector was of 10 ms and accumulation of 100 pulses took place for increasing the signal-to-noise ratio.

Figure 3.27: Low-temperature delayed luminescence (squares) of a PIF-Aryl-Octyl film on quartz substrate. Excitation was at 3.02 eV (410 nm) of 30µJ/pulse intensity. The spectrum was recorded at 1 *ms* delay after the excitation pulse and in a time window of 10 *ms*. Averaging was performed over 100 excitation pulses. The solid lines are Lorentzian fit on the data.

Taking into account the observed red-shift of DF spectral positions, the investigated films should similarly exhibit phosphorescence at ~1.9 eV. Indeed there is some measurable intensity in this spectral region of Figure 3.27. It is considered likely that phosphorescence of PIF-Aryl-Octyl is masked from the strong contribution DF. However this argument can not be strongly supported at this time delay where DF intensity posses a significant emission intensity.
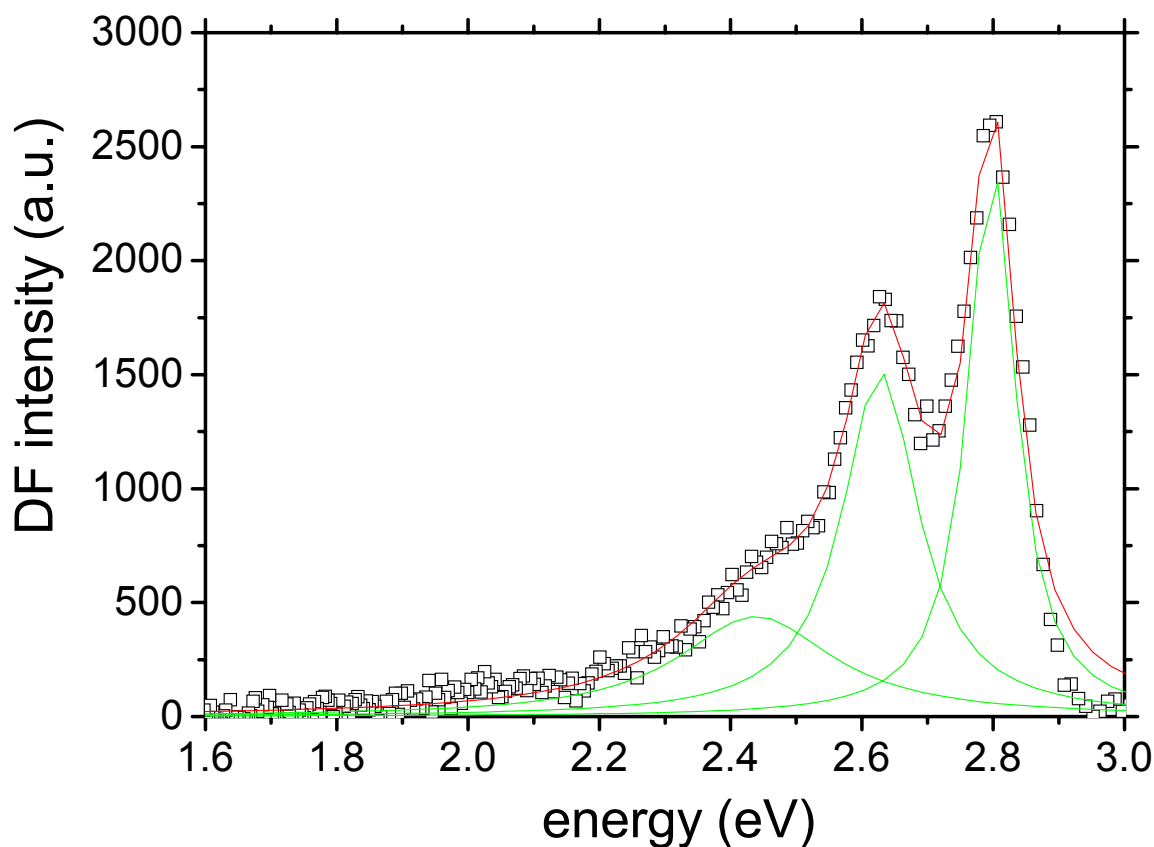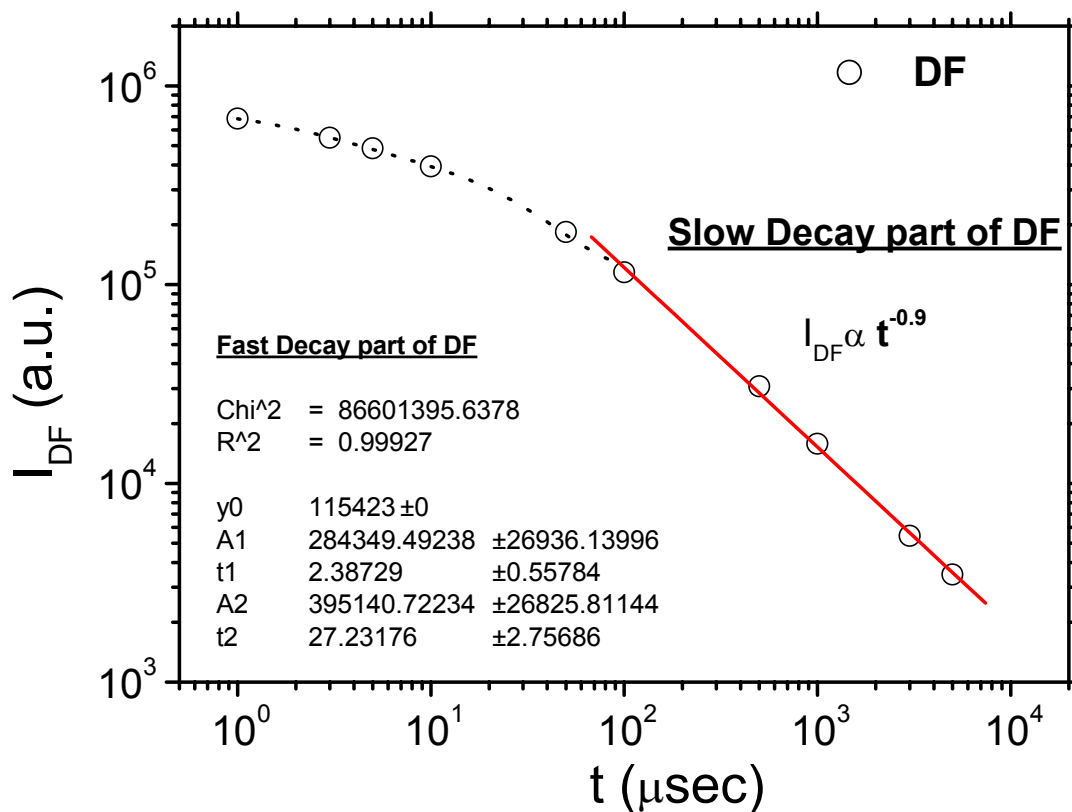
Figure 3.28: Normalised decay transient of low temperature (77 K) delayed fluorescence (circles) of a PIF-Aryl-Octyl film on quartz substrate. Excitation was at 3.02 eV (410 nm) of 30µJ/pulse intensity. The lines are fit on the data. Note the two time domains at which the signal has been separated by a bi-exponential decay (fast part, dotted line) and a power law decay (slow part, solid line).

The decay pattern of DF emission intensity is presented in Figure 3.28. Although the relatively early part of DF intensity decay is better recovered by a biexponential function, the late part of the decay seems to follow a power-law decay with an exponent of α=-0.9.
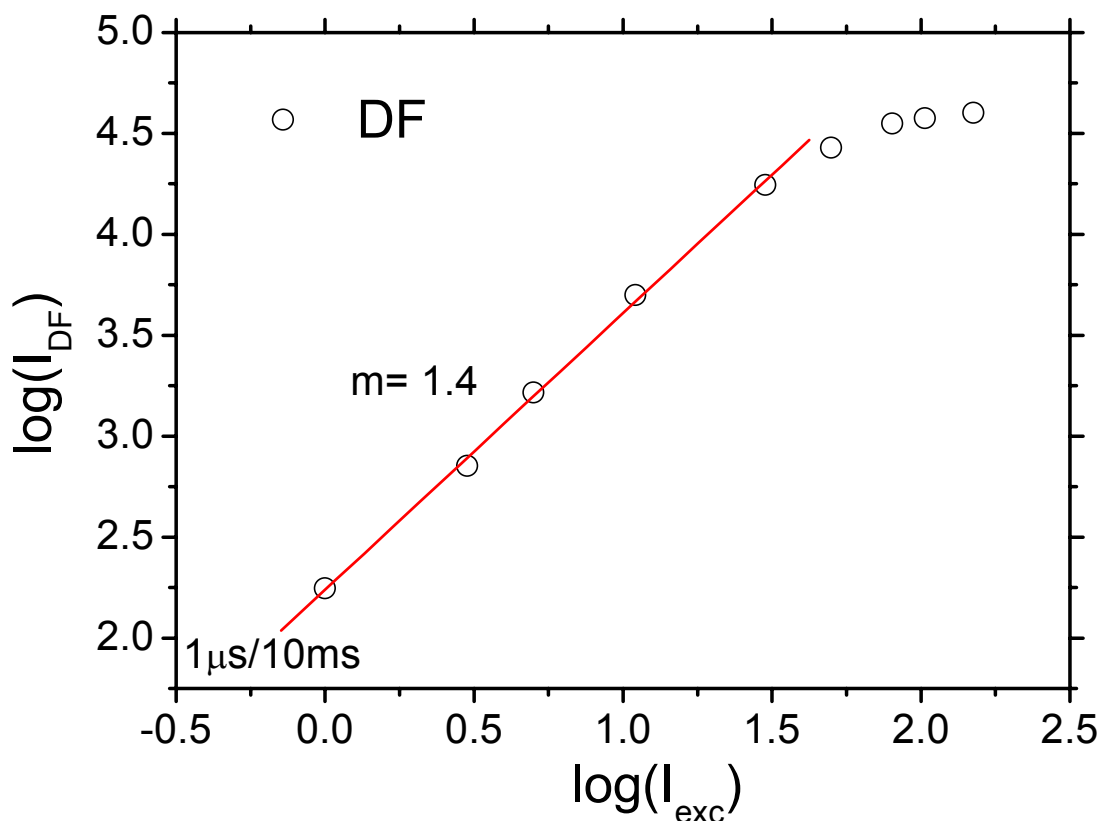
Figure 3.29: Excitation intensity dependence of delayed fluorescence (circles) of a PIF-Aryl-Octyl film on a quartz substrate. The delayed fluorescence intensity is shown as recorded for 1 *μs* delay after the excitation pulse, in a time window of 10 *ms*.

The observed power dependence of DF emission intensity at 1 μs after the excitation pulse is presented in Figure 3.29. The power dependence of DF intensity is found to follow the same trend as the one found in the case of vitrified dilute solutions of PIF-Aryl-Octyl, shown in Figure 3.26.

| | **Delayed Fluorescence** | | | **Phosphorescence** | | |
|---|---|---|---|---|---|---|
| | $S_{0-0} \leftarrow S_{1-0}$ | $S_{0-1} \leftarrow S_{1-0}$ | $S_{0-0} \leftarrow S_{1-0}$ | $S_{0-0} \leftarrow T_{1-0}$ | $S_{0-1} \leftarrow T_{1-0}$ | $S_{0-0} \leftarrow T_{1-0}$ |
| **Solution 77K** | 2.86 | 2.68 | 2.49 | 2.14 | 1.97 | 1.80 |
| **Film 77K** | 2.81 | 2.63 | 2.43 | not resolved | not resolved | not resolved |

Table 3. 5: Maxima of the low-temperature delayed luminescence emission bands observed for PIF-Aryl-Octyl in dilute and vitrified degassed solution of MTHF and as film. All values are in eVs, as obtained after Lorentzian fit on the data.

### 3.4.2.3 Discussion

As Figure 3.24 shows, dilute and vitrified solutions of PIF-Aryl-Octyl exhibit well-resolved phosphorescence. The determined phosphorescence lifetime $\tau_{Ph}=0.96$ in Figure 3.25 is a realistic value no matter if the initial part of the observed phosphorescence before 100 ms was not taken into account. Contrary to what has been observed for other PPP derivatives [70], PIF-Aryl-Octyl exhibits slightly shorter phosphorescence lifetime.

The observation of DF in PIF-Aryl-Octyl should be attributed to one of the aforementioned mechanism: the fusion of two long-lived triplet states $T_1$ that lead to re-population of the first excited singlet state $S_1$ (TTA) or to the recombination of a geminate pairs that are created after the formation of a singlet exciton in PIF-Aryl-Octyl. The alternative scenario of direct re-population of the $S_1$ via a thermalised backtransfer from the $T_1$ (E-type fluorescence, see Chapter 1) can not be supported. According to Table 3.5, the extracted energy gap of $S_{1-0}$-$T_{1-0}$ (700 meV) in this PIF-Aryl-Octyl, excludes any possibility for the existence this backtransfer mechanism, especially due to the fact that DF has been observed at 77 K, a temperature where thermal feedback to the singlet state from hot vibronic levels if the triplet state is rather improbable.

According to eq. 3.15, in the case where DF of PIF-Aryl-Octyl was an origin of TTA, it should decay monoexponentialy with $\tau_{DF}= \frac{1}{2} \tau_{Ph}$. However in Figure 3.25 it is shown that DF is not following an exponential decay function. It better described by a power decay law with an exponent of $\alpha =-1.26\pm0.06$, similarly to what has been observed for the case of MeLLLP [65]. This fact implies that DF in the vitrified solutions of PIF-Aryl-Octyl originates from the recombination of geminate pairs that are formed after photoexcitation. This hypothesis is additionally supported from the power dependence of DF and phosphorescence in Figure 3.26. Both of the monitored emission are found to have the same dependence on the excitation average laser power.

This is the first time that geminate pair recombination is found to be responsible for the observation of DF of vitrified dilute solutions. So far, charge carrier recombination was considered only for the cases of condensed systems of conjugated polymers, eg films, in order to justify the observed DF. In the case of thin films, the confirmation regarding the charged character of the precursor excited states that lead to the observation of DF, is achieved with the application of an electric field on the irradiated film area. However this experiment can not be performed in the case of vitrified solutions of PIF-Aryl-Octyl. Alternatively, the charge nature of these precursor states might be possible to be confirmed by usage of electrolytes added to the PIF-Aryl-Octyl solution, prior vitrification.

The interacting charged states in PIF-Aryl-Octyl that lead to DF after photoexcitation should be localised onto the same polymeric backbone. In that way on-chain diffusion could lead to the encounter that would result in DF. Alternatively, if geminate pairs are formed on different chains, their interaction would have to be assisted from the supramolecular order in the vitrified solution, that would allow two different polymeric chains to be in close proximity. X-ray scattering experiments should be performed in vitrified dilute solutions of PIF-Aryl-Octyl in order to shed more light on the question of interchain order.

Finally, the contribution of the solvent to the assistance of exciton diffusion has to be taken into account. Other good glass-forming solvents of different polarity should be used in order to elucidate whether solvent molecules contribute to the exciton migration among the different polymeric chains.

The hypothesis for the existence of a geminate pair recombination mechanism that lead to the observation of DF in the vitrified solutions of PIF-Aryl-Octyl is further supported from the case of PIF-Aryl-Octyl thin films. Although no clear evidence for the existence of phosphorescence has been given, DF has been recorded at the temperature of 77 K (Figure 3.27). In comparison with the DF spectrum of dilute solutions at 77 K, DF emission peaks for films are found red-shifted by 50 meV (see Table 3.5) and slightly broader. This is attributed to the enhanced interchain interactions in the solid state that result in an increase of the dispersive forces of interaction.

According to Figure 3.28, the case of PIF-Aryl-Octyl films exhibits a power law decay transient behaviour with an exponent of $\alpha=-0.9$ As it is already mentioned, a power-law decay has been previously observed for the DF intensity in films of MeLLLP at 77 K [65]. The in here determined value for PIF-Aryl-Octyl is in good agreement with the one reported for the reported one for MeLLLP ($\alpha=-0.8$).

# 3.5 THIOPHENE-ENDCAPPED POLY(INDENOFLUORENE) DERIVATIVE

In material design strategies, amid the several methods that aim to control the optical properties of a chromophore is the attachment of a functional unit targeted to the modify the chromophore's electronic properties. Such a functional group can induce a change in the optical properties of the chromophore either by a change in the extend of conjugation of the or by excitation energy transfer processes in which the chromophore will participate as donor and the added functionality as acceptor.

Such energy transfer processes are considered to be similar to intrinsic doping effects where the dopant (acceptor) is covalently attached to the host (donor).

Scheme 2 presents the chemical structure of a thiophene-endcapped poly(indenofluorene)-octyl (PIF8SF) derivative. Thiophenes are well known systems that are studied both by computational and experimental approaches. It is known that α-substitution of thiophenes results in better π-π stacking effects in the solid state.

$$S \quad H \quad -\alpha \text{ position}$$
$$H \quad -\beta \text{ position}$$
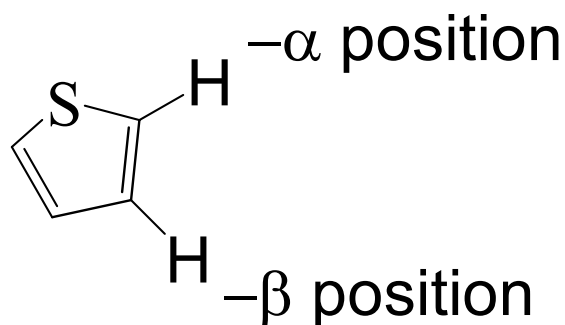
Scheme 3.3: The chemical structures of thiophene and the characteristic -α and -β positions on the heteroatomic ring.

## 3.5.1 Results

Figure 3.30 presents representative steady-state photoluminescence spectra of a series of oligothiophenes ($TH_n$) in dilute solutions. A gradual red shift is observed in the PL maximum as the number of the thiophene monomer units is increased. Such spectral trends are common in the class of conjugated polymers [71], [72]. As the number of units comprising the polymer is increased the ability for extended π-conjugation is assisted. Therefore additional delocalisation phenomena take place for the electron positioned in the π-orbitals of the molecule. The observed red shift reflects the excited state stabilisation that is induced by the electronic delocalisation.
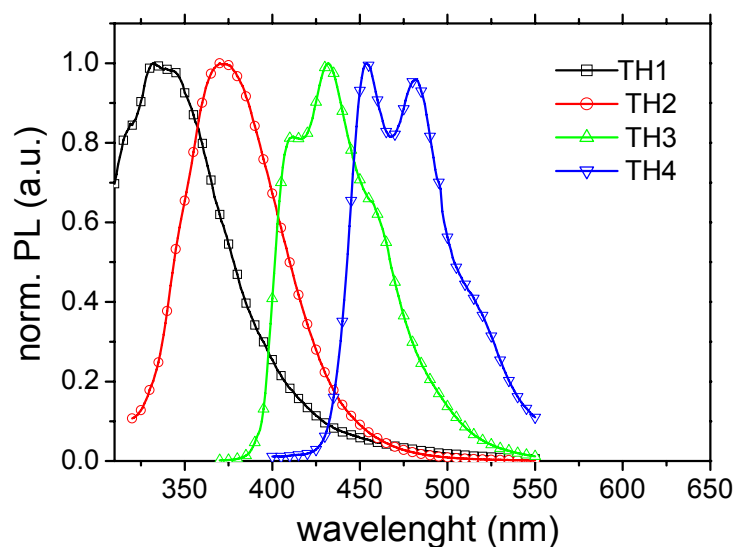
Figure 3.30: Room temperature steady-state PL spectra of oligothiophenes (TH$_n$) in dilute solutions of toluene. For n=1: $\lambda_{exc}$=290 nm (squares), n=2: $\lambda_{exc}$=304 nm (circles), n=3: $\lambda_{exc}$= 350 nm (triangles up), n=4: $\lambda_{exc}$= 385 nm (triangles down). Optical excitation was performed at the corresponding absorption maximum of each compound.

The following discussion is focused on the optical properties of PIF8S. As a reference compound the previously presented PIF-Octyl (PIF8) that has been presented in Chart 3.1 is used. The photoluminescence dynamics of both of the systems are informative for the excitation migration processes that take place in these materials. It turns out that the presence of the octyl side-chains on the PIF backbone of both of the derivatives strongly influences the exciton migration process.. Since PIF8S is mainly a candidate-compound for integration in polymer-based field effect transistors [22], the information obtained regarding mobility processes is of relevant importance. Charge carrier mobility and exciton migration are two processes that resemble one another therefore the information following is indirectly related to the evaluation of PIF8S as a functional polymeric material.

### 3.5.1.1 CW-photoluminescence spectroscopy of PIF-Octyl-Thiophene-endcapped derivative

Absorption spectra recorded for dilute solutions of PIF8 and PIF8S in toluene and in MTHF show no significant differences in the spectral positions of the observed transitions. No substantial differences were observed for the two solvents chosen. Photoluminescence (PL) and photoluminescence excitation (PLE) spectra were also recorded for comparing the emissive

properties of the two materials. Figures 3.31 and 3.32 present the steady state optical characteristic of PIF8 and PIF8S solutions at room temperature.



Figure 3.31: Room temperature normalised absorption (squares) and cw-PL spectra (circles) of PIF8, in dilute solutions of toluene. Excitation was at 3.18 eV (390 nm).



Figure 3.32: Room temperature normalised absorption (squares), cw-PL spectra (circles) and PLE spectra (triangles) of PIF8, in dilute solutions of toluene. Excitation was at 3.18 eV (390 nm). PLE spectrum monitored the 510 nm emission wavelength of PIF8S.

Although both of the materials seem to absorb similarly in the same region of the spectrum, the case of PIF8S differs in the region of 430 – 480 nm. A weak broad absorption peak can be observed which is reproducible also by the PLE spectra (not shown here) of the solution, when

the $\lambda_{emi}$= 510 nm emission is monitored. The compared solutions were of the same concentration. However for PIF8S, the absorption edge starts to level off after 480 nm. In contrast to that, PIF8 shows a rise in the absorption edge after 445 nm. Both of the solutions though have the same absorbance in the region of 430 nm. Comparing the PL spectra, no significant differences can be observed between the emissions of the two materials. Both of the PIF derivatives emit in the blue with the emission of PIF8 centred at 430 nm.

The optical properties of PIF8S are strongly modified in the solid state. Figures 3.33 and 3.34 present the room temperature steady-state optical spectra of PIF8 and PIF8S as thin films on glass substrates. The absorption spectra of both of the materials still are similar and they consist of a broad unstructured band that peaks at 410 nm for PIF8 and 390 nm for PIF8S. The absorption spectrum of PIF8S seems to consist of an overlap of two absorption peaks with maxima at 390 nm and 410 nm. Like to the case of dilute solutions, PLE spectra monitoring emission of wavelengths in the region of 500 nm revealed that in the solid state, PIF8S also possesses an additional weak absorption feature located in the region of 450 – 480 nm. Figure 3.35 presents a comparison of the PLE spectra of the two PIF derivatives.

Different PL spectra are observed for the two PIF derivatives. PIF8 shows an emission that has its maximum in the region of 445 nm, followed by its vibronic progression with peaks at 470 nm and 505 nm. In contrast to that, the main emission peak of PIF8S is centred at 475 nm and a broad vibronic band at 500 nm follows it. A residue of the 445 nm emission can also be seen in the PL spectrum of PIF8S. By selectively exciting at 460 nm, the PL spectrum of PIF8S exhibits relatively weak fluorescence at 500 nm (spectra not shown).
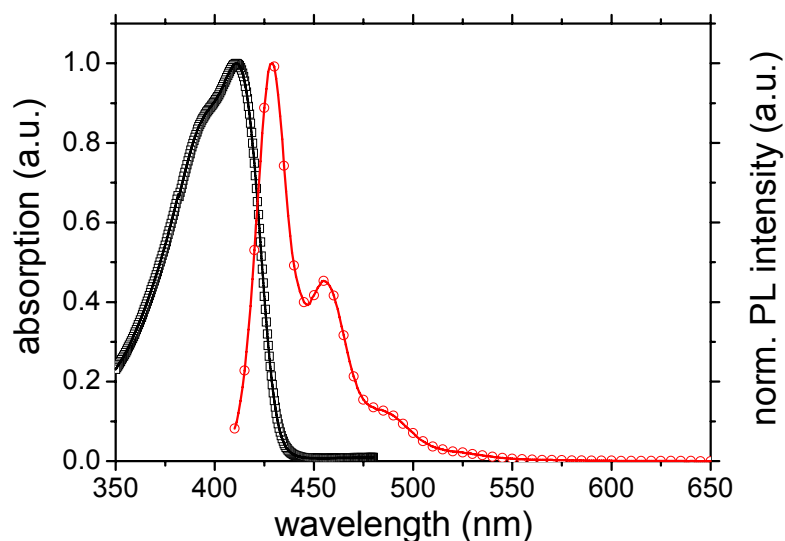
Figure 3.33: Room temperature normalised absorption (squares) and cw-PL spectra (circles) of PIF8, as film on glass substrate. Excitation was at 3.18 eV (390 nm).
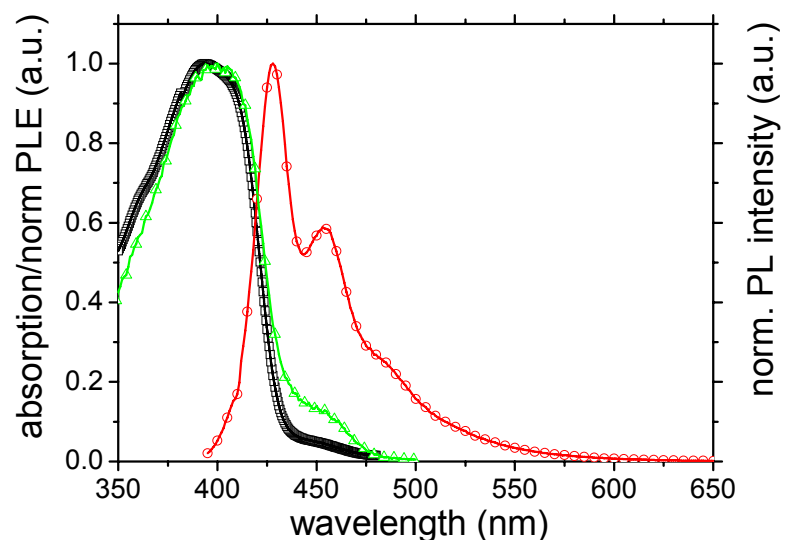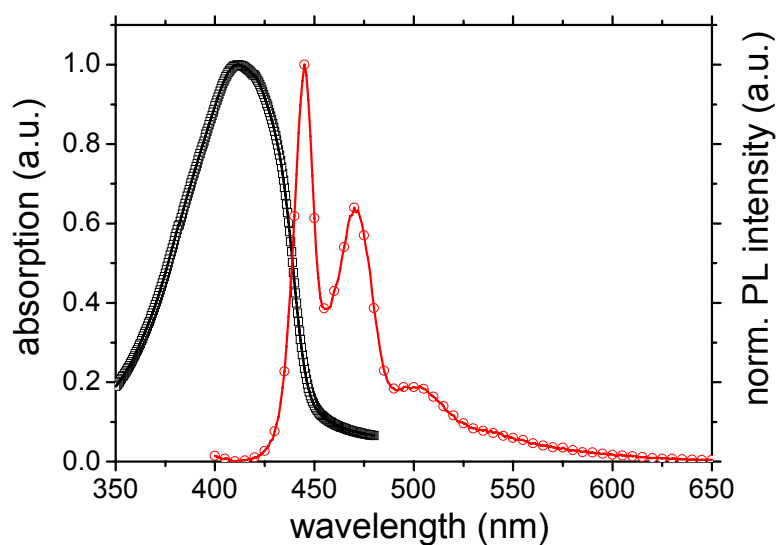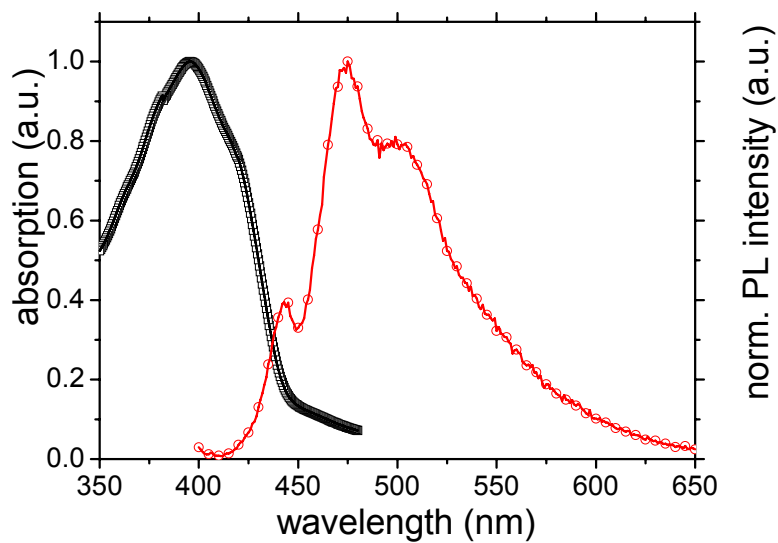


Figure 3.34: Room temperature normalised absorption (squares) and cw-PL spectra (circles) of PIF8S, as film on glass substrate. Excitation was at 3.18 eV (390 nm).
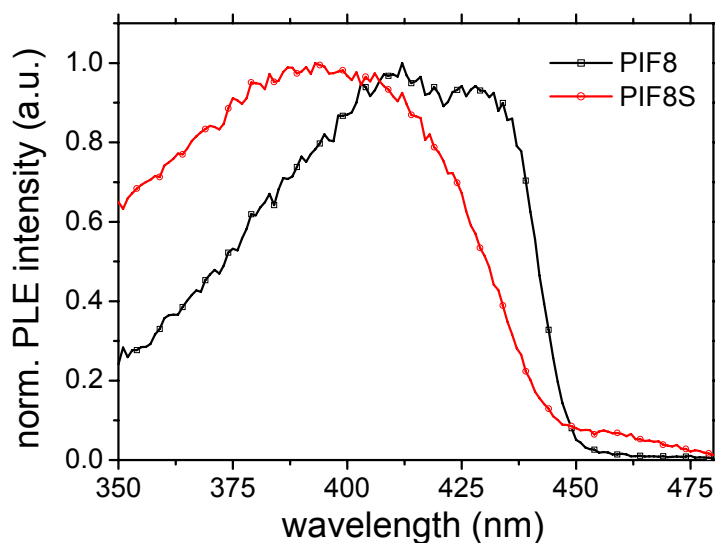
Figure 3.35: Room temperature normalised PLE spectra of PIF8 (squares) and PIF8S (circles), as films on glass substrates. Excitation was at 3.18 eV (390 nm). In both cases the 500 nm emission wavelength was monitored.

## 3.5.1.2 Time-resolved photoluminescence spectroscopy of PIF-Octyl-Thiophene-endcapped derivative

### 3.5.1.2.1 SPECTRAL PROFILES

Figure 3.36 depicts time-resolved PL spectra of PIF8S. A comparison is presented between the prompt and delayed PL for dilute solutions at room temperatures and at 77 K. Room temperature time resolved spectra of a PIF8S thin film are also presented. Figure 3.36a shows that at the temperature of 77 K, the optical properties of PIF8S solution are very similar to PIF8S as in solid state.

Figure 3.36b presents delayed PL spectra recorded several *ns* after excitation pulse. As it is shown for the case of thin films, the spectral distribution has completely changed, no matter the state of the PIF8S (solution, vitrified matrix or film). Especially for the film case the spectral changes arise shortly as 2 ns after the excitation pulse. A broad featureless band centred at 2.3 eV is observed. The same spectral features, albeit at longer delayed observation window is found for the case of the frozen PIF8S solution. A high-energy spectral residue can also be seen, located at ~2.9 eV. Furthermore the low-energy broad band possesses slightly structured features, most probably due to the low-temperature conditions.

The case of room temperature long delayed spectrum for dilute solution of PIF8S is quite different. Even at the very long delay regime after the excitation pulse, the spectrum seems to have more spectral similarities to the prompt PL. Although a broad band located at 2.6eV dominates the spectrum, its intensity scales up with the residue of the singlet emission band.
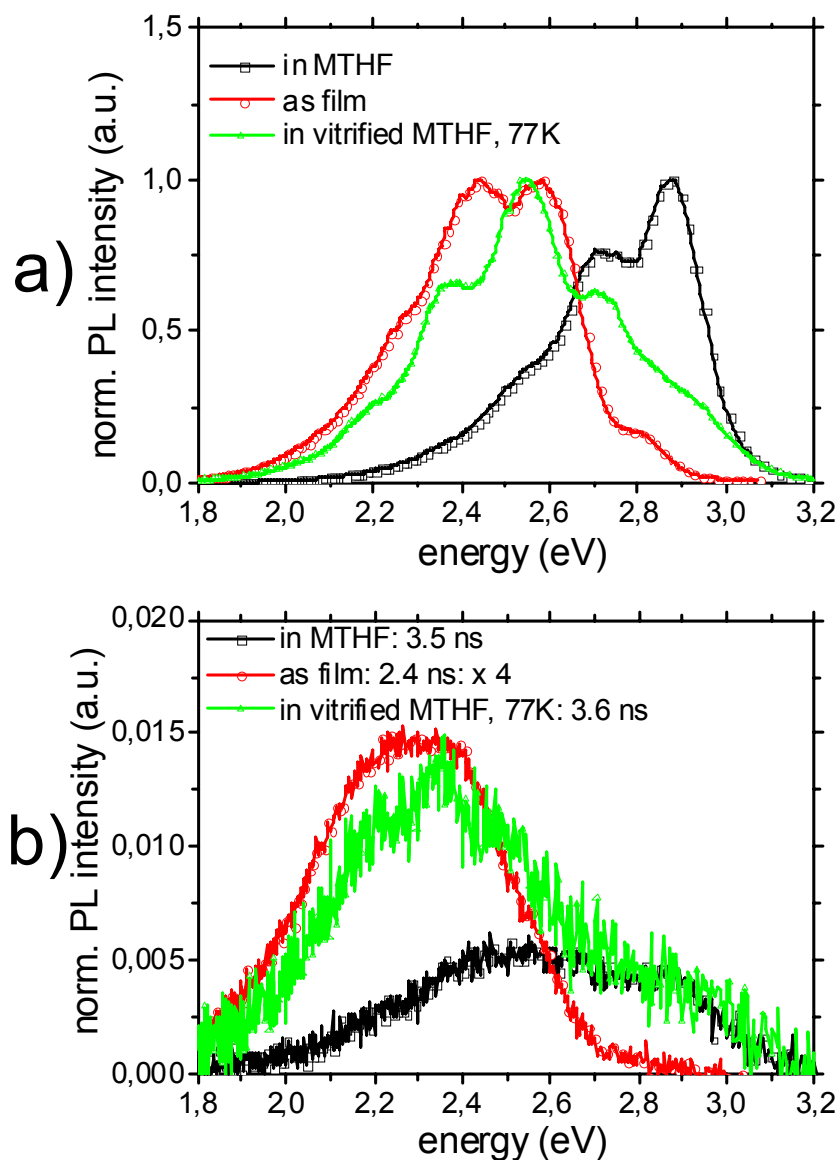


Figure 3.36: Time resolved PL spectra of PIF8S in dilute solution of MTHF at room temperature (squares), as film on glass substrate (circles) and as vitrified dilute solution in MTHF at 77 K (triangles). Excitation was at 3.18 eV (390 nm) of 500 μW average laser power. For film and vitrified solution, p~$10^{-5}$. The spectra were recorded in a time window of 500 *ps* a) promptly and b) at a time delay of several *ns* after the excitation pulse (see legend). In the case of the delayed spectra for PIF8S as film, the data were multiplied by a factor of 0.25.

### 3.5.1.2.2  **DECAY TRANSIENTS**

Figure 3.37 presents a comparison of the singlet decay transients for dilute solutions of PIF8 at room temperature and 77 K. It is seen that the singlet decay transient at 77 K is more close to the room temperature decay transient observed for thin films of PIF8 (see Figure 3.13).

The inset of Figure 3.37 presents the prompt spectra of the PIF8 solutions at room temperature and at 77 K. A large red shift is observed for the spectra at 77 K that supports the notion of enhanced solid-state interaction in PIF8 at low temperatures.
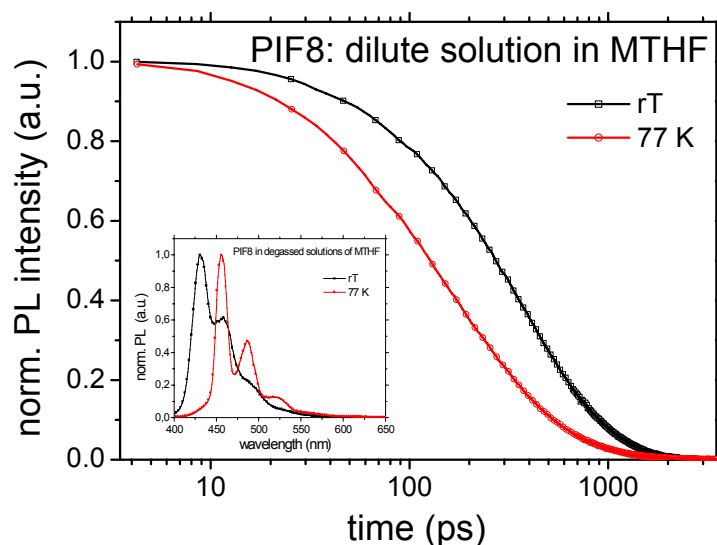


Figure 3.37: Normalised decay transients of the singlet emission of PIF8 in dilute solutions of MTHF at room temperature (squares) and at 77 K (circles). Excitation was at 3.18 eV (390 nm) of 500 µW average laser power. The inset shows the prompt PL spectra of PIF8 before and after lowering the temperature. Notice the acceleration of the decay rate for the case of the vitrified solution that is parallel to a red shift of the PL maximum.

In order to assess the impact that thiophene moieties have on the transient decay patterns when used as endcappers in PIF8, the decay kinetics of thin films of both PIF8 and PIF8S should be compared. Figure 3.38 presents the emission decay transients of PIF8 and PIF8S thin films at room temperature. For PIF8 the decay transient monitors the high-energy emission band (singlet emission). For the case of PIF8S, two spectral areas have been monitored, the singlet residue of weak intensity in the region of 410-445 nm and the more intense emission of the low-energy region at 450-480 nm (see Figure 3.34).
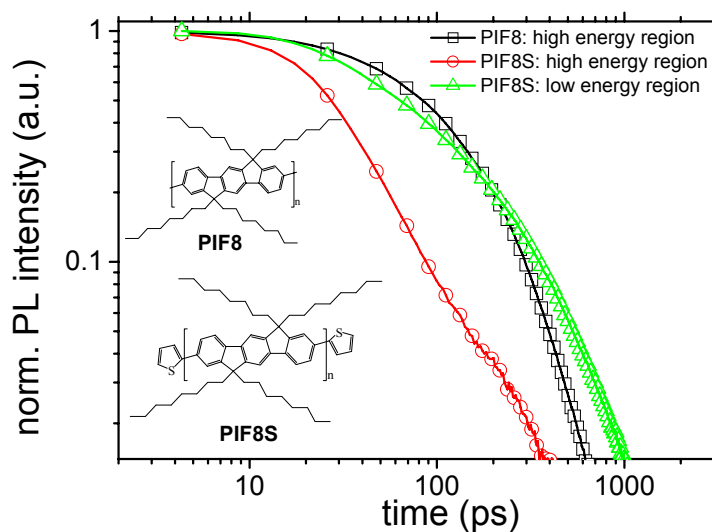
Figure 3.38: Normalised decay transients of the singlet emission of PIF8 and PIF8S thin films on glass substrate. Excitation was at 3.18 eV (390 nm) of 500 µW average laser power. For PIF8 the high-energy spectral area is monitored (squares) while for PIF8S the high (circles) and the low (triangles) energy spectral areas are shown (see text). The inset shows the chemical structures of PIF8 and PIF8S.

 As it is shown In Figure 3.38, the singlet emission of PIF8 and the low-energy peak of PIF8S decay in exponential manner whereas the singlet emission of PIF8S seems to follow a power-law decay rate. This difference in the decay law of the two monitored spectral areas of PIF8s emission is evaluated in the next paragraph. However, for the case of vitrified solutions of PIF8S in MTHF, the dependence of emission intensity of these two spectral areas, on the average laser power was found to be the same.
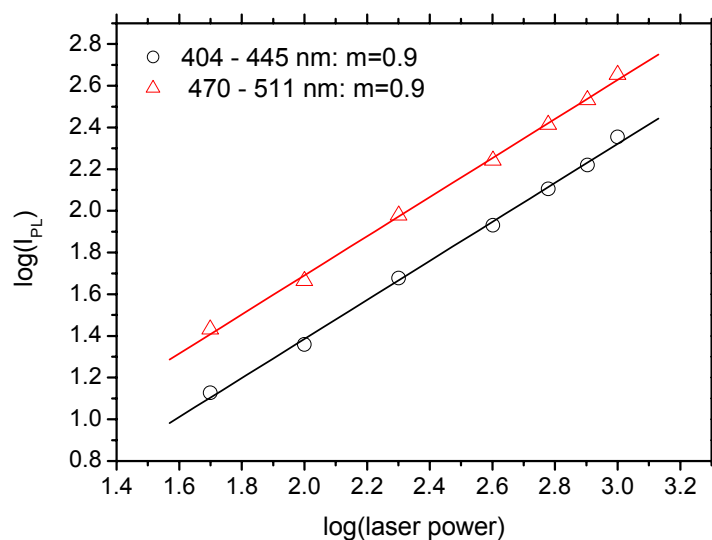
Figure 3.39:  Excitation power dependence of fluorescence for PIF8S vitrified dilute solution in MTHF, of the high (circles) and the low (triangles) energy spectral area. Power units are in mW. Excitation was at 3.18 eV (390 nm).

 Figure 3.40 shows the decay transient patterns of PIF8S singlet emission at three different states, namely as dilute solutions at room temperature, as vitrified solutions at 77 K and as thin film at room temperature. The decay transients are depicted for three different spectral areas of the spectrum. The horizontal comparison of the decay transient in each of the plots that consist Figure 3.40 evidence that the luminescence decay rate rapidly increases when the material is measured as thin film.
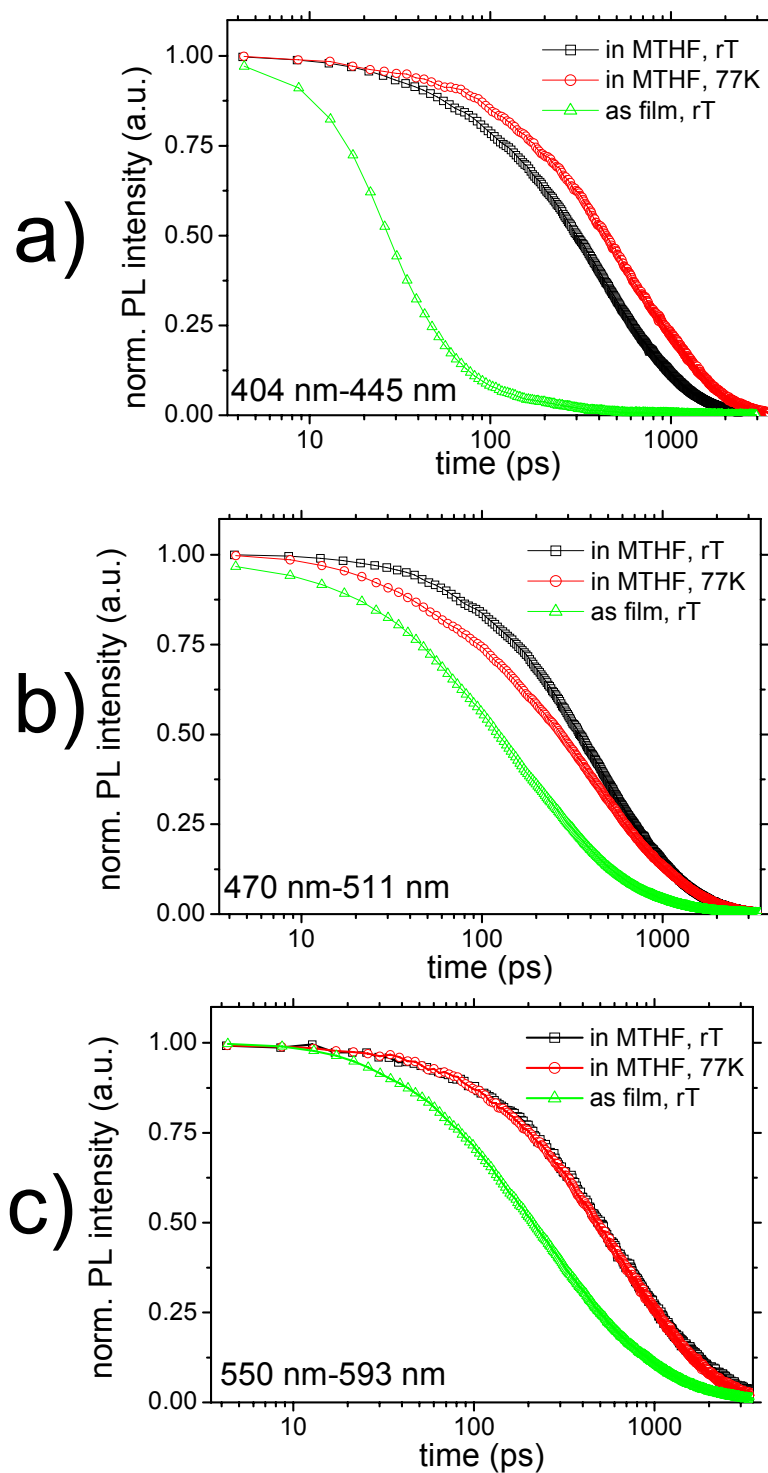
Figure 3. 40: Normalised decay transients of PIF8S monitoring the emission at a) 404-445 nm, b) 470-511 nm and c) 550-593 nm. PIF8S was studied as dilute solution in MTHF at room temperature (squares), as vitrified solution in MTHF at 77 K (circles) and as thin film on glass substrate at room temperature (triangles). Excitation was at 3.18 eV (390 nm) of 500 µW average laser power. For film and vitrified solution, p~10⁻⁵.

## 3.5.2 Discussion

The spectral red shift of PIF8 that is observed between the emission of dilute solution and thin film has been already attributed to the enhanced chain interactions that arise in the solid state due to packing effects. It seems that PIF8 can adapt a well-defined positional order even in dilute solution that has been vitrified. Additional evidence for this assumption results from the decay kinetic patterns of the singlet emission of PIF8 in solution, at room temperature and 77 K. These data are presented in paragraph 3.5.1.2. In order to rationalise the solid state packing effects we recall that in Section 3.1 results obtained from polarised optical microscopy and AFM imaging have supported the hypothesis for the existence of superstructures in films of PIF8S. These superstructures eventually were found to result in fibrilar film morphology. For the case of a poly(fluorene) derivative bearing linear octyl chains, it was found that aggregation effects were induced by moderately or poor solvents quality [73]. As a result of the low solubility in these poor solvents, microcrystallization effects took place that forced neighbouring chain to aggregate and form clusters. The latter act as physical cross-linking points that lead to the macroscopic observation of gelation. Later on, studies on the structural investigation of these systems concluded that this forced proximity of adjacent chains resulted in highly planar conformations of the polymer backbone due to crystallization effects of the linear alkyl chains [26]. In the aspect of photophysical properties, aggregation of this type induces a red shift of the photoluminescence maximum. We consider the same processes to be responsible for the red shift of PIF8S in the solid state. At room temperature and in respect with the case of dilute solutions, PIF8S films show a similar red shift of the high-energy emission band (Figure 3.34).

The main backbone of this PIF derivative is identical to the thiophene-free PIF8, therefore the solid-state packing should resemble to that of PIF8 in a thin film. However the intensity of the 443 nm emission band in comparison with that of 475 nm is much more reduced. The same situation accounts also for the low temperature spectra of a PIF8S film recorded at 77 K. The emissions peaks of the low temperature PL were found to be slightly narrower but no important changes were observed in the obtained spectral distribution. The presence of the thiophene moieties may further increase the packing efficiency. However the intensity of the 443 nm emission band in comparison with that of 475 nm is much more reduced. Phenomena of re-asborption operating in PIF8S may safely be excluded as the optical density of PIF8 at the observed weak absorption band in PIF8S is located in the region of 450–480 nm and therefore no re-asborption process in this spectral area can explain the observed reduction of the 444 nm intensity in PIF8S. The strong increase in the intensity of the 475 nm PIF8S emission in the solid state at the expense of the 444 nm emission indicates the existence of an electronic interaction in

the PIF8S thin film that operates as an additional energy loss channel of the photoexcitations initially existing on PIF8S. This additional relaxation channel is further implied from the luminescence decay dynamics of the singlet emission band, monitored in thin films of PIF8S. We assign the enhanced spectral feature of the 475 nm band to the endcapping thiophene molecules, that act as acceptors in an electronic energy transfer process between backbone and endcappers. Our assignment is also supported from the fact that the 500 nm emission of PIF8S film is observed after direct excitation at 460 nm. A similar process has been studied for the case of a PIF derivative that was endcapped with perylene molecules [18], [19].

It is concluded that in a vitrified matrix, the interchain interactions of PIF8S are so strongly enhanced so that the electronic properties of the system receive a character similar to the solid-state regime. As PIF8S is embedded in the vitrified matrix the PL spectral position of the emissions bands almost overlap with these obtained from a PIF8S at room temperature. In the studied solutions it expected that the polymer chains are isolated due to the high dilution that was used. Therefore at low temperatures the freezing of polymer segments should take place under conditions of minimised steric hindrance effects induced from the surroundings. Therefore the planarisations of the units consisting the polymer chains should take place more effectively thus giving rise to the observed spectral red shift of 100 meV.

For elucidating clearly whether the presence of the thiophene endcappers contributes significantly to the enhanced interchain coupling of PIF8S in the vitrified matrix, a thiophene-free PIF8 derivative was used. The data of Figure 3.37 suggest that tight interchain coupling is an intrinsic trend for PIF8 derivatives independent of the existence of thiophene endcappers. A red shift of PL is also observed for the thiophene-free PIF derivative (inset Figure 3.37).

The only stark difference between PIF8 and PIF8S derivatives is presented in the decay transients of Figure 3.38. The existence of a power-law decaying emission component in the emission of PIF8S has not been seen in the case of PIF8 compound. This observation suggests that the monitored high-energy emission of PIF8S is a result of geminate pair recombination in the ultrafast regime of PL detection. It further implied that the involved charged species should have been created in the sub-*ps* regime after excitation and subsequently give rise to the emission of the monitored spectral region. Ultra-fast charge photogeneration must have arose from the presence of thiophene endcappers. This is presumed from the fact that thiophene-free PIF derivative did not show any power-law decay pattern in the whole spectral region that emits light. The combination of tight interchain packing that occurs in PIF8 derivative and the presence of thiophene units assists the harvesting of charged species after their formation due to optical excitation. Previous studies in PIF derivatives have concluded on the formation of charged states

after optical excitation [15], [16], [17]. However no discussion had been presented regarding the radiative recombination dynamics of these charged states. This was only recently presented for the case of poly(fluorene) derivatives [74], where luminescence of isolated chains has been observed after the recombination of charged separated pairs. The question that still remains to be answered is the mechanism of these geminate pairs in PIF8S. In the case of poly(fluorene) derivatives, the charged states were found to be a result of dissociation of a higher excitonic state that was created by sequential photon absorption during the pumping pulse. In the present case, a linear power dependence pattern was found both the high and low-energy spectral areas of PIF8S vitrified solutions (Figure 3.39). This fact indicates that the charged states are formed upon the absorption of one photon therefore no sequential mechanism operates in the PIF8S vitrified solutions, at least for the excitation intensities used. The formation of charged species should therefore be attributed to the ionisation potential of the thiophene endcappers. This could be confirmed easily from a photocurrent measurment. Alternatively, pump-probe experiments should detect the presence of the transient states in which the charged excited states will exist.

 Figure 3.40 shows an acceleration of the decay transients of PIF8S takes place, for interchain interactions in the solid state. This acceleration of the decay is independent of the spectral range that is monitored. For once more, the observed enhanced decay rate has to be correlated with the high degree of order that exists in molecular level of PIF8S in the solid state. As it is already mentioned, such order effects are known to support diffusion of the excited states to chemical or physical defects that are present in the matrix that the material consist of. In the particular case of PIF8S, the role of the chemical defect plays the thiophene chropmophore. As Figure 3.34 has indicated thiophene endcapper acts a acceptor group of the initially created photoexcited states. In combination with the notion that charged states are formed after photoexcitation, we speculated that the thiophene acceptor act as a dissociation centre of the neutral exciton of the polymer backbone. This implies that the step involved in the PL quenching of the high-energy peak of 443 nm, observed in Figure 3.34, reflects a charge transfer rather than an electronic energy transfer process. Especially in the solid state, the interaction of closely packed thiophene units can give rise to a new thiophene based superstructure that can act as a scavenger of the excitation energy originally localized on PIF8S.

 In a film of PIF8S an ensemble of distances exist between the polymer backbone and the thiophene chromophore. As exciton diffusion is supported towards a three-dimensional direction in the solid state, energy transfer of the mobile excitations can take place both via inter- and intra- interactions. Therefore the charge transfer rate can be substantially increased. Previous studies on poly(indenofluorene)s endcapped with perylene dyes have shown that the rate of

intrachain energy transfer is much slower than the case of interchain energy transfer process that occurs in three dimensional direction in films [18], [19].

Most particularly in Figure 3.40a, in the case of dilute solutions, the fact that the singlet decay transient is slightly retarded at 77 K confirms the hypothesis for charge mediated singlet fluorescene in PIF8S. It was shown that in vitrified matrices of thiophene-free PIF8 solutions the decay rate of the singlet emission was accelerated due to enhanced interchain coupling (Figure 3.37). Additionally, it was shown that in films of thiophene-containing PIF8S, the singlet emission band was following a power-law decay that mostly reflects the recombination of geminate pairs (Figure 3.38). It is conceivable that even in a vitrified matrix where environmental conditions strongly resembles to these of a solid-state thin film, charge carrier formation also takes place after photoexcitation. A fraction of the photoinduced electron-hole pairs may subsequently recombine to neutral singlet excitations and give rise to the population of the singlet manifold. This populating feedback path is macroscopically observed as a retardation of the singlet emission decay, at 77 K. The exponential character of the singlet emission decay of PIF8S dilute solution, at room temperature excludes the possibility for dissociation processes on a single chain. Therefore charge carrier generation requires close proximity of polymer backbones and it takes place between adjacent polymer chains.

Figure 3.40b compared the decay transients of a lower energy region that centres at 500 nm (see Figure 3.34). The decay rate of this spectral region is increased for the case of vitrified dilute solutions of PIF8S. Apparently this spectral region is not subject to any feedback processes and is mostly related to emission occurring from the thiophene moieties. Under supportive conditions for enhanced interchain coupling at 77 K the transient decays faster. This is however not the case in Figure 3.40c, for the lower energy part of the spectrum where the spectral area that is monitored centres at 570 nm. A slight increase of the decay rate takes place for the case of vitrified dilute solutions that make the overall decay to be similar to that of the dilute solutions at room temperature. Most probably this retardation of the decay rate is related to the electronic coupling of this spectral range with the PIF8S singlet reservoir. As this low-energy region contains the vibronic features of the singlet manifold, it has to follow similar kinetic trends like the spectral region of the main singlet band, shown in Figure 3.40a.

# 3.6  CONCLUSIONS

Poly(indenofluorene)s belong to the class of rigid-rod polymers and they are intermediate in structure between poly(fluorene)s (PFs) and ladder-type poly(*p*-phenylene)s (LPPPs). Like PFs, PIFs are considered promising candidates to be used as blue light-emitting components in

optoelectronic devices. The performance of a material as a functional component strongly depends from the inteplay between the structure and the optical properties of the material in the solid state [75]. Therefore our approach to PIFs had a two-fold character in order to consider this interdependence.

In this Chapter structural investigations have been presented for the case of the three different PIF derivatives. Subsequently, in the light of the information that was obtained from the structural studies, the optical properties of these derivatives have been evaluated. Ultra-fast laser spectroscopy has been employed for the monitoring of the photoluminescence dynamics in these derivatives. Especially for the case of solid state, the obtained results for each PIF derivative correlate well with the corresponding structural property that has   been addressed.

The issue of chemical purity has been found for once more to be one of the important aspects that related to the performance of the studied materials. Especially for PIFs, the here in presented results demonstrate an alternative synthetic route that can optimise the level of chemical defects in the resulting products, in such a way that the optical properties of a film virtually remain the same with those of solutions. Additionally, the use of a model-defect monomer that was deliberately incorporated into the matrix of a PIF derivative gave quantified information regarding the minimum number of chemical defects that can reduce the spectral purity of the matrix.

In the particular case for one of the studied PIF derivatives, delayed fluorescence was studied. In accord to the observation of phosphorescence from related polymers, phosphorescence was observed for PIF-Aryl-Octyl. This finding further supports the molecular excitonic character of this π-conjugated polymer rather than the band model.  Delayed fluorescence was also observed for PIF-Aryl-Octyl at 77 K both for vitrified solutions and films. The main interesting result for this experiment was the attribution of delayed fluorescence of a vitrified dilute solution on the recombination of geminate pairs. The assumption that charged species are the precursor states for the delayed fluorescence was based on the excitation intensity dependence and on lifetime determination, both of delayed fluorescence and phosphorescence.

Further evidence for the participation of charged species in the creation of emissive states came from the results of a thiophene-endcapped PIF derivative. In contrast to the so far common observation, the charged species in this derivative are postulated to contribute in the emission of the compound in sub-*ps* time scale. Especially for this compound, further studies should go on, aiming for the efficiency of charge carrier photogeneration.

## 3.7  REFERENCES

1.    Kraft A., Grimsdale A.C., Holmes A.B., *Electroluminescent conjugated polymers - Seeing polymers in a new light.* Angew. Chemie Int. Ed., 1998. **37**(4): p. 402.
2.    Mitschke U., Bauerle P., *The electroluminescence of organic materials.* J. Mater. Chem., 2002. **10**(7): p. 1471.
3.    Dimitrakopoulos C.D., Malefant P.R.L., *Organic Thin Film Transistors For Large Area Electronics.* Adv. Mater., 1999. **14**(2): p. 99.
4.    Brabec C.J., Sariciftci N.S., Hummelen J.C., *Plastic solar cells.* Adv. Funct. Mater., 2001. **11**(1): p. 15.
5.    Leclerc M., *Polyfluorenes: Twenty Years of Progress.* J. Polym. Sci. Part A: Polym. Chem., 2001. **39**: p. 2867.
6.    Neher D., *Polyfluorene Homopolymers: Conjugated Liquid-Crystalline Polymers for Bright Blue Emission and Polarized Electroluminescence.* Macromol. Rapid Commun., 2001(22): p. 1365-1385.
7.    Scherf U., List E.J.W., *Semiconducting Polyfluorenes-Towards Reliable Structure-Property Relationships.* Adv.Mater., 2002. **14**(7): p. 477.
8.    Scherf U., *Ladder-type materials.* J. Mater. Chem., 1999. **9**: p. 1853.
9.    Setayesh S., Marsitzky D., Müllen K., *Bridging the Gap between Polyfluorene and Ladder-Poly-p-phenylene: Synthesis and Characterization of Poly-2,8-indenofluorene.* Macromolecules, 2000. **33**: p. 2016.
10.   Jacob J., Zhang J., Grimsdale A.C., Müllen K., Gaal M., List E.J.W., *Poly(tetraarylindenofluorene)s: New stable Blue-Emitting Polymers.* Macromolecules, 2003. **36**: p. 8240.
11.   Jacob J., Oldridge L., Zhang J., Gaal M., List E.J.W., Grimsdale A.C., Müllen K., *Progress towards stable blue light-emitting polymers.* Current Applied Physics, 2004. **4**(2-4): p. 339.
12.   Reisch H., Wiesler U., Scherf U., Tuytuylkov N., *Poly(indenofluorene) (PIF), a novel low band gap polyhydrocarbon.* Macromolecules, 1996. **29**(25): p. 8204.
13.   Herz L.M., Silva C., Phillips R.T., Setayesh S., Müllen K., *Exciton migration to chain aggregates in conjugated polymers: influence of side-chain substitution.* Chem. Phys. Lett., 2001. **347**: p. 318.
14.   Grimsdale A.C., Leclére P., Lazzaroni R., Mackenzie J.D., Murphy C., Setayesh S., Silva C., Friend R.H., Müllen K., *Correlation Between Molecular Structure, Microscopic Morphology, and Optical Properties of Poly(tetraalkylindenofluorene)s.* Adv. Funct. Mater., 2002. **12**(10): p. 729.
15.   Silva C., Russell D.M, Stevens M.A., Mackenzie J.D., Setayesh S., Müllen K., Friend R.H., *Excited-state absoprtion in luminescent conjugated polymer thin films: ultrafast studies of a processable polyindenofluorene derivative.* Chem. Phys. Lett., 2000. **319**: p. 494.
16.   Silva C., Stevens M.A., Russell D.M., Setayesh S., Müllen K., Friend R.H., *Ultrafast charge photogeneration in conjugated polymer thin films.* Synthetic Metals, 2001. **116**: p. 9.
17.   Silva C., Russell D.M, Dhoot A.S, Herz L.M., Daniel C., Greenham N., Arias A.C., Setayesh S., Müllen K., Friend R.H., *Exciton and polaron dynamics in a step-ladder polymeric semiconductor: the influence of interchain order.* J. Phys.:Condens. Matter, 2002. **14**: p. 9803.
18.   Herz L.M., Silva C., Friend R.H., Phillips R.T., Setayesh S., Becker S., Marsitsky D, Müllen K., *Effects of aggregation on the excitation transfer in perylene-end-capped polyindenofluorene studied by time-resolved photoluminescence spectroscopy.* Phys. Rev. B, 2001. **64**: p. 195203.

19.   Beljonne D., Pourtois G., Scholes G.D., Hennebicq E., Herz L.M., Friend R.H., Scholes G.D., Setayesh S., Müllen K., Brédas J.-L., *Interchain vs. intrachain energy transfer in acceptor-capped conjugated polymers.* PNAS, 2002. **99**(17): p. 10982.

20.   Beljonne D., Pourtois G., Shuai Z., Hennebicq E., Scholes G.D., Brédas J.-L., *Energy transfer in π-conjugated polymers: Interchain vs. intrachain processes in polyindenofluorene.* Synthetic Metals, 2003. **137**: p. 1369.

21.   Stein R.S., *Photographic Light Scattering by Polyethylene Films.* J. Appl. Physics, 1960. **31**(11).

22.   P. Sonar, in *Max Planck Institute for Polymer Research.* 2004, Johannes Gutenberg Universität: Mainz.

23.   Carbonnier B., Pakula T., Egbe D. A. M., *Self-Organization of comb-like macromolecules comprised of four-fold alkoxy substituted (PPV-PPE) rigid backbone repeat units: role of length variation of side chains attached on phenylene ring surrounded by vinylene moieties.* J. Mater. Chem., 2005: p. DOI: 10.1039/b412937g.

24.   Guinier A., *X-Ray Diffraction in Crystals, Imperfect Crystals and Amorphous Bodies.* 1963, San Fransisco: W. H. Freeman & Co.

25.   Strobl G., *The Physics of Polymers: Concept for Understanding Their Structure and Behaviour.* 2nd ed. 1997, Berlin, Heidelberg: Springer-Verlag.

26.   Grell M., Bradley D.D.C., Ungar G., Hill J., Whitehead K.S., *Interplay of Physical Structure and Photophysics for a Liquid Crystalline Polyfluorene.* Macromolecules, 1999. **32**: p. 5810.

27.   Oldridge L., Grimsdale A.C., Müllen K., *Unpublished results.* 2004: Max-Planck Institute for Polymer Research, Mainz.

28.   Somma E., Loppinet B., Fytas G., Setayesh S., Jacob J., Grimsdale A.C., Müllen K., *Collective orientation dynamics in semi-rigid polymers.* Colloid. Polym. Sci., 2004. **282**: p. 867.

29.   Dias F.B., Macanita A.L., Seixas de Melo J., Burrows H.D., Güntner R., Scherf U., Monkman A., *Picosecond conformational relaxation of singlet excited polyfluorene in solution.* J. Chem. Phys., 2003. **118**(15): p. 7119.

30.   Cornil J., dos Santos D.A., Crispin X., Silbey R., Brédas J.-L., *Influence of Interchain Interactions on the Absorption and Luminescence of Conjugated Oligomers and Polymers: A Quantum-Chemical Characterization.* J. Am. Chem. Soc., 1998. **120**: p. 1289.

31.   Setayesh S., Grimsdale A.C., Weil T., Enkelmann V., Müllen K., Meghdadi F., List E.J.W., Leising G., *Polyfluorenes with Polyphenylene Dendron Side Chains: Toward Non-Aggregating, Light-Emitting Polymers.* J. Am. Chem. Soc., 2001. **123**: p. 946.

32.   Pogantsch A., Wenzl F.P., List E.J.W., Leising G., Grimsdale A.C., Müllen K.,, *Polyfluorenes with Dendron Side Chains as the Active Materials for Polymer Light-Emitting Devices.* Adv. Mater., 2002. **14**(15): p. 1061.

33.   Lupton J.M., Schouwink P., Keivanidis E.P., Grimsdale A.C., Müllen K., *Influence of Dendronization on Spectral Diffusion and Aggregation in Conjugated Polymers.* Adv. Funct. Mater., 2003. **13**(2): p. 1.

34.   Bliznyuk V.N., Carter S.A., Scott J.C., Klärner G., Miller R.D., Miller D.C., *Electrical and Photoinduced Degradation of Polyfluorene Based Films and Light-Emitting Devices.* Macromolecules, 1999. **32**(2): p. 361.

35.   Rauscher U., Bässler H., Bradley D.D.C., Hennecke M., *Exciton versus band description of the absorption and luminescence spectra in poly(p-phenylenevinylene).* Phys. Rev. B, 1990. **42**(16): p. 9830.

36.   Meskers S.C.J., Hübner J., Oestreich M., Bässler H., *Dispersive Relaxation Dynamics of Photoexcitations in a Polyfluorene Film Involving Energy Transfer: Experiment and Monte Carlo Simulations.* J. Phys. Chem. B, 2001. **105**: p. 9139.

37.     Lupton J.M., Craig M.R., Meijer E.W., *On-chain defects emission in electroluminescent polyfluorenes.* Appl.Phys.Lett., 2002. **80**(24): p. 4489.

38.     Kulkarni A.P., Kong X., Jenekhe S.A., *Fluorenone-Containing Polyfluorenes and Oligofluorenes: Photophysics, Origin of the Green Emission and Efficient Green Electroluminescence.* J. Phys. Chem. B, 2004. **108**: p. 8689.

39.     Sims M., Bradley D.D.C., Ariu M., Koeberg M., Asimakis A., Grell M., Lidzey D.G., *Understanding the Origin of the 535 nm Emission Band in Oxidized Poly(9,9-dioctylfluorene): The Essential Role of Inter-Chain/Inter-Segment Interactions.* Adv. Funct. Mater., 2004. **14**(8): p. 765.

40.     Lakowicz J.R., *Principles of Fluorescence Spectroscopy.* 2nd ed. 1999, New York, Boston, Dordrecht, London, Moscow: Kluwer Academic/Plenum Publishers.

41.     Arkhipov V.I., Emelianova E.V., Bässler H., *Quenching of excitons in doped disordered organic semiconductors.* Phys. Rev. B, 2004. **70**: p. 205205.

42.     Lemmer U., Ochse A., Deussen M., Mahrt R.F., Göbel E.O., Bässler H., Bolivar H.P., Wegmann G., Kurz H., *Energy Transfer in molecularly doped conjugated polymers.* Synthetic Metals, 1996. **78**: p. 289.

43.     Dicker G., Hohenau A., Graupner W., Tasch S., Graupner M., Hermetter A., Schlicke B., Schulte N., Schlüter A.D., Scherf U., Müllen K., Leising G., *Emission Properties of a Molecularly Doped Higly Fluorescent Polymer.* Synthetic Metals, 1999. **102**: p. 873.

44.     List E.J.W., Creely C., Leising G., Schulte N., Schlüter A.D., Scherf U., Müllen K., Graupner W., *Excitation energy migration in highly emissive semiconductive polymers.* Chem. Phys. Lett., 2000. **325**: p. 132.

45.     Wong K.F., Bagchi B., Rossky P.J.,, *Distance and Orientation Dependence of Excitation Transfer Rates in Conjugated Systems: Beyond the Förster Theory.* J. Phys. Chem. A, 2004. **108**: p. 5752.

46.     Haugeneder A., Neges M., Kallinger C., Spirkl W., Lemmer U., Feldmann J., Scherf U., Harth E., Gügel A., Müllen K., *Exciton diffusion and dissociation in conjugated polymer/fullerene blends and heterostructures.* Phys. Rev. B, 1999. **59**(23): p. 15346.

47.     Buckley A.R., Rahn M.D., Hill J., Cabanillas-Gonzalez J., Fox A.M., Bradley D.D.C., *Energy transfer dynamics in polyfluorene-based polymer blends.* Chem. Phys. Lett., 2001. **339**: p. 331.

48.     Pope M. & Swenberg C.E., *Electronic Processes In Organic Crystals and Polymers.* Second ed. 1999, New York, Oxford: Oxford University Press.

49.     McGlynn S.P.& Azumi T. & Kinoshita M., *Molecular Spectroscopy of THE TRIPLET STATE.* 1969, Englewood Cliffs, New Jersey: Prentice-Hall, Inc.

50.     Klessinger M. & Michl J., *Excited States and Photochemistry of Organic Molecules.* 1995, New York, Weinheim, Cambridge: VCH Publishers, Inc.

51.     Partee J., Frankevich E.L., Uhlhorn B., Shinar J., Ding Y.,Barton T.J., *Delayed Fluorescence and Triplet-Triplet Annihilation in π-Conjugated Polymers.* Phys. Rev. Lett., 1999. **82**(18): p. 3673.

52.     Hertel D., Bässler H., Guentner R.,Scherf U., *Triplet-triplet annihilation in a poly(fluorene)-derivative.* J. Chem. Phys., 2001. **115**(21): p. 10007.

53.     Monkman A.P., Burrows H.D., Hamblett I.,Navaratnam S., *Intra-chain triplet-triplet annihilation and delayed fluorescence in soluble conjugated polymers.* Chem. Phys. Lett., 2001. **340**: p. 467.

54.     Gerhard A.,Bässler H., *Delayed fluorescence of a poly (p-phenylenevinylene) derivative: Triplet-triplet annihilation versus geminate pair recombination.* J. Chem. Phys., 2002. **117**(15): p. 7350.

55.    Hayer A., Bässler H., Falk B.,Schrader S., *Delayed Fluorescence and Phosphorescence from Polyphenylquinoxalines.* J. Phys. Chem. A., 2002. **106**: p. 11045.

56.    Hertel D., Romanovskii Y.V., Schweitzer B., Scherf U.,Bässler H., *Spectroscopy of Conjugated Polymers:Phosphorescence and Delayed Fluorescence.* Macrom. Symp., 2001. **175**: p. 141.

57.    Wohlgenannt M., Tandon K., Mazumdar S., Ramasesha S.,Vardeny Z.V., *Formation cross-sections of singlet and triplet excitons in π-conjugated polymers.* Nature, 2001. **409**: p. 494.

58.    Monkman A.P., Burrows H.D., Hartwell L.J., Horsburgh L.E., Hamblett I.,Navaratnam S., *Triplet Energies of π-Conjugated Polymers.* Phys. Rev. Lett., 2001. **86**(7): p. 1358.

59.    Dhoot A.S.,Greenham N.C., *Triplet Formation in Polyfluorene Devices.* Adv. Mater., 2002. **14**(24): p. 1834.

60.    Sinha S., Rothe C., Güntner R., Scherf U.,Monkman A.P., *Electrophosphorescence and Delayed Electroluminecence from Pristine Polyfluorene Thin-Film Devices at Low Temperature.* Phys. Rev. Lett., 2003. **90**(12): p. 127402.

61.    Friend R.H., Gymer R.W., Holmes A.B., Burroughes J.H., Marks R.N., Taliani C., Bradley D.D.C., Dos Santos D.A., Brédas J.-L., Lögdlund M., Salaneck W.R., *Electroluminescence in conjugated polymers.* Nature, 1999. **397**: p. 121.

62.    Cleave V., Yahioglu G., Le Barny P., Friend R.H.,Tessler N., *Harvesting Singlet and Triplet Energy in Polymer LEDs.* Adv. Mater., 1999. **11**(4): p. 285.

63.    Shuai Z., Beljonne D., Silbey R.J.,Brédas J.-L., *Singlet and Triplet Exciton Formation Rates in Conjugated Polymer Light-Emitting Diodes.* Phys. Rev. Lett., 2000. **84**(1): p. 131.

64.    Köhler A.,Wilson J., *Phosphorescence and spin-dependent exciton formation in conjugated polymers.* Organic Electronics, 2003. **4**: p. 179.

65.    Schweitzer B., Arkhipov V.I., Scherf U.,Bässler H., *Geminate pair recombination in a conjugated polymer.* Chem. Phys. Lett., 1999. **313**: p. 57.

66.    Burrows H.D., da G.Miguel M., Monkman A.P., Horsburgh L.E., Hamblett,Navaratnam S., *Pulse radiolysis studies on charge carriers in conjugated polymers.* J. Chem. Phys., 2000. **112**(6): p. 3082.

67.    Stein G.,Würzberg E., *Energy gap law in the solvent isotope effect on radiationless transitions of rare earth ions.* J. Chem. Phys., 1975. **62**(1): p. 208.

68.    Beljonne D., Ye A., Shuai Z.,Brédas J.-L., *Chain-Length Dependence of Singlet and Triplet Exciton Formation Rates in Organic Light-Emitting Diodes.* Adv. Funct. Mater., 2004. **14**(7): p. 684.

69.    Romanovskii Y.V., Gerhard A., Schweitzer B., Scherf U., Personov R.I.,Bässler H., *Phosphorescence of π-Conjugated Oligomers and Polymers.* Phys. Rev. Lett., 2000. **84**(5): p. 1027.

70.    Hertel D., Setayesh S., Nothofer H.-G., Scherf U., Müllen K.,Bässler H., *Phosphorescence in Conjugated Poly(para-phenylene)-Derivatives.* Adv. Mater., 2001. **13**(1): p. 65.

71.    de Melo J. S., Silva L.M., Arnaut L.G., *Singlet and triplet energies of α-oligothiophenes: A spectroscopic, theoretical, and photoacoustic study: Extrapolation to polythiophene.* J. Chem. Phys., 1999. **111**(12): p. 5427.

72.    Sariciftci N.S., ed. *Primary Photoexcitations in Conjugated Polymers: Molecular Excitation versus Semiconductor Band Model.* 1997, World Scientific, Singapore.

73.    Grell M., Bradley D.D.C., Long X., Chamberlain T., Inbasekaran M., Woo E.P., Soliman M., *Chain geometry, solution aggregation and enhanced dichroism in the liquid-crystalline conjugated polymer poly(9,9-dioctylfluorene).* Acta. Polym., 1998. **49**: p. 439.

74.    Xu Q.H., Moses D., Heeger A.J., *Delayed emission from recombination of charge-separated pairs on polyfluorene chains in dilute solution.* Phys. Rev. B, 2004. **69**(11): p. 113314.

75.    Wegner G., *Functional Polymers.* Acta mater., 2000. **48**: p. 253.

# 4 PHOTON ENERGY UP-CONVERSION IN π-CONJUGATED POLYMERS

## 4.1 PORPHYRIN DERIVATIVES IN LIGHT-EMITTING DEVICES OF π-CONJUGATED POLYMERS

In the previous chapters it has been discussed that π-conjugated polymers can exhibit electroluminescence when their thin films are used as the electronically active medium in which recombination of injected charge carriers can take place. For tuning the electroluminescence colour of a polymer-based light-emitting device the utilisation of energy transfer processes between donor-acceptor systems has been exploited (paragraph 2.1). Additionally, for stabilising the performance of a polymer-based light-emitting device hole transporting materials have been used (paragraph 2.2.1). More importantly, the efficiency of electroluminescence needs to be optimised, as the losses due to the formation of non-radiative excited triplet states after charge injection (paragraph 3.4.1.1) are considered to be of a large extent.

### 4.1.1 Triplet harvesting

In order to overcome the limitation where only a fraction of the excitations is emissive while the greater part is lost due to non-radiative decay and/or weak radiative coupling, efforts are made for an efficient harvesting of the created triplet excitons (paragraph 3.4.1.1). Hence, the understanding of all aspects of the triplet state in conjugated polymers is urgently sought. Clarifying the nature of the triplet state will provide further tools for manipulating it via triplet harvesting based on energy transfer mechanisms [1], [2], [3].

Several approaches aiming for triplet state harvesting in conjugated polymers have been demonstrated. The common approach in the issue of triplet harvesting is the doping of the electroluminescent polymer with a heavy-atom-containing porphyrins [4], [5], [6], [7], [8], [9], [10], [11], [12]. The presence of the heavy atom within these dyes increases the probability for radiative relaxation of the triplet state in the polymer. As the porphyrin dyes are phosphorescent, sensitised phosphorescence could take place via triplet-triplet energy transfer from the polymer matrix to the dye, presumably based on the Dexter transfer mechanism (see Chapter 1). The origin of triplet activation lies on the external spin-orbit coupling effect.

## 4.1.2 Spin-orbit coupling

Any electronic transition, radiative or non-radiative which occurs between states of different spin-multiplicity is highly forbidden by virtue of the selection rules discussed in Chapter 1. Lifting of the spin selection rules originates from the spin purity of the levels that are involved in the transition. The term pure spin state describes an electronic state where the spin angular momentum is time-independent [13].

Upon the interaction of an electromagnetic field with a one-electron-system that consists of two pure spin states of different multiplicity, the electron is promoted from the lower pure state to the higher spin state. These electronic transition results in a change in the spin momentum. Hence, according to the momentum conservation this change must be counter balanced by corresponding changes elsewhere. Since the perturbation induced from the electromagnetic field is not a function of electric or magnetic moment operators, the imposed momentum change cannot be due the radiation field. Therefore the magnitude of these electronic transitions is restricted and practically these transitions are considered forbidden. This restriction is relaxed when coupling takes place between the magnetic dipole that is generated by the spin motion of the electron and the magnetic dipole that is generated by the orbital motion of the electron. To describe explicitly this particular interaction, the term spin-orbit coupling is used.

In the simple case of one-electron atom system, spin-orbit coupling could be envisaged by the transformation of the spatial coordinates from a nucleus-fixed system to an electron-fixed system. In such a representation of the one-electron atom, the atomic nucleus is orbiting the electron and thus it produces a magnetic field that surrounds the electron. The vector that describes the orientation of this magnetic field is directed perpendicularly to the plane of the orbit. In parallel to the revolutional motion of the nucleus around the fixed electron, the latter performs spin motion along its spin-axis. Due to some asymmetry of charge distribution on the electron, spinning results in the production of a second magnetic field along the electron spin axis. The interaction of the vectors of these two magnetic fields reflects the origin of the aforementioned spin-orbit coupling.

The rate of intersystem crossing induced from spin-orbit coupling has been expressed as [14]:

$$k_{ISC} = B * (c_C^* * c_X * \xi)^2 \qquad \text{(eq. 4.1)}$$

where B refers to the rate constant of the intersystem crossing (ISC) process in the absence of the heavy atom substituent, whereas $c_C^*$ and $c_X$ are the atomic orbital coefficients for the substituted C atom in the appropriate excited state and the heavy atom, respectively. Given a specific

substitution site, the atomic orbital coefficients are assumed to be constant and variations in the observed $k_{ISC}$ values can be attributed to the atomic spin-orbit coupling constant $\xi$ .

## 4.1.3 Porphyrins

 A well known phosphorescent dye containing a heavy atom centre is Pt(II)OEP [12] (see structure in Scheme 4.1), a porphyrin ring decorated with aliphatic chains onto each of the four pyrole rings that comprise the macrocycle of the porphyrin. Due to the basicity of the pyrole nitrogens, coordination of the Pt metallic center takes place in the cavity of the porphyrin ring, giving rise to a metallated porphyrin complex of $D_{4h}$ symmetry.
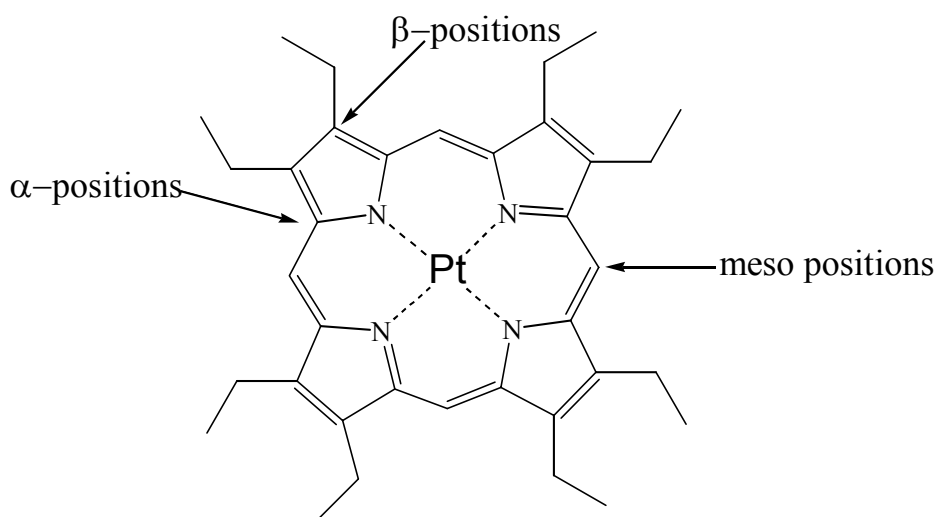


Scheme 4.1: The chemical structure of (2,7,8,12,13,17,18-octaethyl-porphyrinato)Pt(II), alternatively PtOEP. The arrows indicate the characteristic α-, β- and meso-positions of the porphine ring.

 In general, introduction of metallic centres is considered as a perturbation of the electronic and optical properties of the free base porphine and as such it imposes distinct differences in the absorption spectra [15]. An obvious distinction can be observed. In the free base a four-banded absorption spectrum is observed and the metal type has a two-banded visible spectrum. Coordination of metal cations within the ring cavity can also alter the electronic properties of the porphyrins by causing electronic perturbations [16]. Halogen substitution has been found also to affect the photophysical properties of porphyrins. The major impact of halogen substitution is the effect of spin orbit coupling due to the heavy atom of halogens [14]. Other ways of controlling the electronic properties of porphyrins include chemical modification of the porhyrin ring by the attachment of functional groups that can enhance conjugation.

213

This plethora of electronic properties of porphyrins is difficult to be handled without a consisting approach. There were efforts for a systematic categorisation of the known metalloporphyrin derivatives with the most recent one to be that of Gouterman. The electronic taxonomy of all the central substituted porphyrins has been achieved and the so-called 'Periodic Table of the porphyrins' is nearly completed [15].

It should be noted that coordination can take place by almost all atoms of metalic and semimetalic nature that can coordinate to the porphyrin ring cavity. The terms of *regular* and *irregular* porphyrins have been used in order to describe effects that arise from the electronic nature of the central atom it itself. According to this classification, all central metal cations of a closed shell form *regular* metal porphyrin derivatives and they are diamagnetic. In contrast, *irregular* metalloporhyrins are formed from paramagnetic metal cations with electronic configurations of partly filled shells.

In principle, optical spectra of the porphyrins are reflecting electronic transitions within their π-orbitals [15], [16], [17], [18]. Particularly the optical spectra of irregular porphyrins are expected to possess new low-energy features as a consequence of effects of metal orbitals on the orbitals of the macro ring. Also mixing of the metal and ring orbitals is probable and transitions that were considered forbidden in free base porphyrins can now take place. This perturabation is weak in the case of closed metal shells; therefore regular porphyrins are not expected to exhibit the aforementioned additional spectral characteristics. In porphyrins, the presence of paramagnetic or diamagnetic species is known that influences the ISC rate. It was found that paramagnetic metal centres are increasing $k_{ISC}$ more than the diamagnetic metal centres do. This $k_{ISC}$ enhancement was attributed to the exchange coupling between the triplet state of the porhyrin ring and the unpaired electrons of the metallic centre incorporated in the ring [19].

The energy level scheme of the molecular orbital that results from coordination of a porphin ring on metallic inorganic centres is depicted in Figure 4.1. However this is only a general visualisation of the relative positions of the energy levels. The exact relative positions of the energy levels are actually determined from the specific interactions between the *d* orbitals of the metals and the orbitals of the free porphin. More over the presence of axial ligands impose further interelectronic interactions dependent on their electron donating or withdrawing character [17], [18].
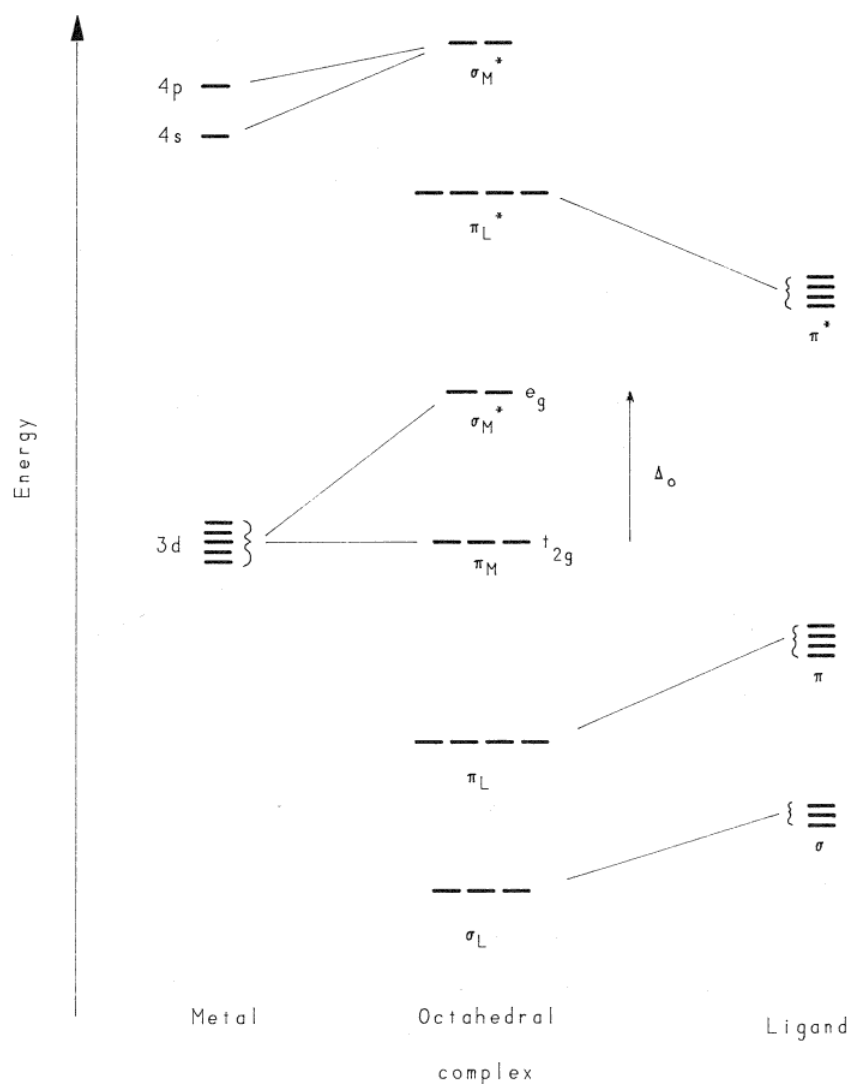
Figure 4.1: The molecular orbital energetic hierarchy of an octahedral inorganic complex after the coordination of the ligands on the metal cation. The atomic *d* and molecular orbitals of the metal and the ligands, respectively, are also shown. From [20].

Within this context of metalloporhyrin classification, two representative metalloporhyrin derivatives are presented: PtOEP is an irregular porphyrin due to the presence of the open shell $Pt^{2+}$: $d^8$ metal cation and PdOEP is an regular porphyrin due to the presence of the closed shell $Pd^{2+}$: $d^8$ metal cation. Although both metal cations have the same number of electrons in the *d* orbitals, the electronic configuration, which describes the ground state of each complex differs. $Pt^{2+}$ has lone *d* electrons and is paramagnetic whereas $Pd^{2+}$ has no unpaired *d* electrons and is diamagnetic. These emission spectra of the two derivatives in solution and in the solid state are shown in Figure 4.2, normalised to the lowest energy electronic transition that corresponds to their lower electronically excited triplet level.
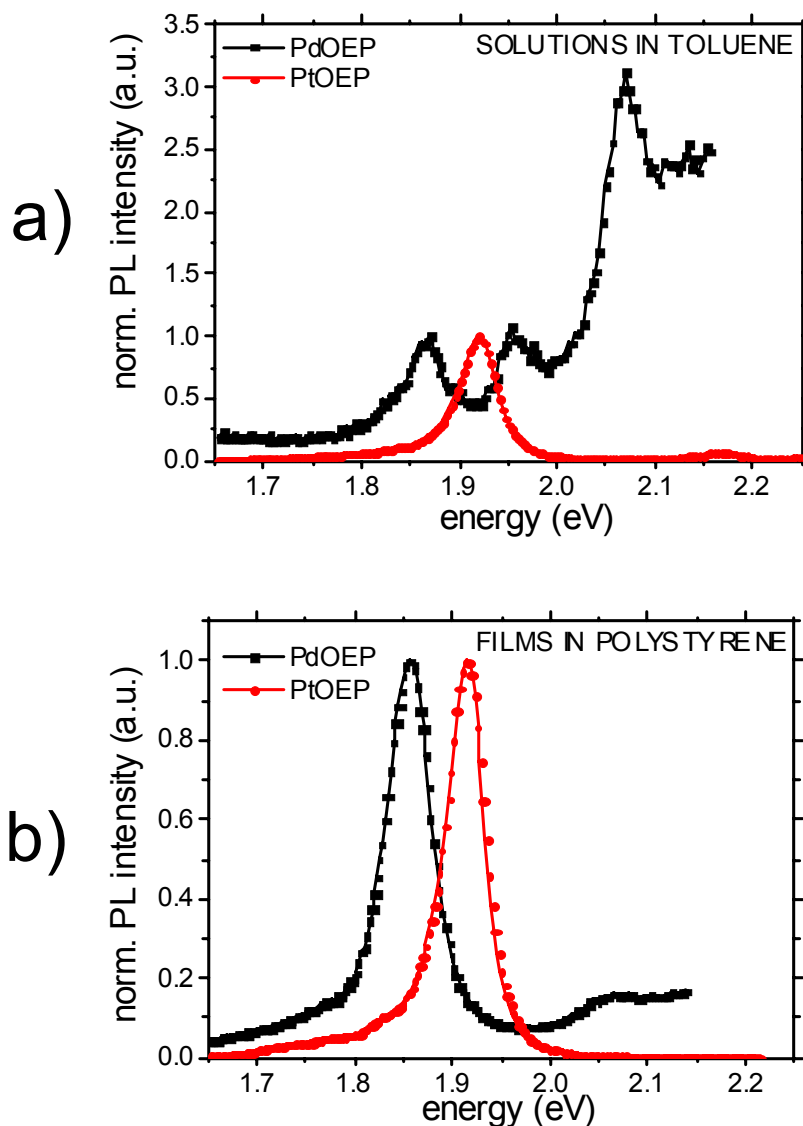
Figure 4.2: Room temperature photoluminescence spectra of PdOEP (square) and PtOEP (circles) in a) solution and b) as film, doped at 10 wt% in poly(styrene). Excitation wavelength at 532 nm (2.33 eV).

## 4.1.4 Contemporary applications of porphyrin derivatives and related compounds

Porphyrins are considered important elements for the construction of porphyrin-based materials and devices [21], [22]. The general class of porphyrinoids is an attractive field for investigation on photoinduced electron transfer processes in systems of donor-acceptor. Particularly fullerene-porphyrin archtectures have been studies systematically [23], [24], [25]. Together with

phthalocyanines, porphyrins have emerged as a promising area for study of non-optical processes such as optical limiting [26], [27], [28], [29].

The process of optical limiting refers to the phenomenon where the transmittance of a sample under high intensity of light is decreased. The observed decrease takes place because the cross section of the excited state in the molecules of the sample is larger than that of its ground state [30]. Therefore, molecules exhibiting optical limiting are defined as reverse-saturable-absorbers (RSA). According to Scheme 4.2 optical limiting in RSA molecules occurs after their excitation on the first electronically excited singlet manifold. After a rapid internal conversion step and an intersystem-crossing step, the first electronically excited triplet manifold is populated. Provided that the intersystem-crossing step is efficient and faster than the duration of the excitation pulse, a continuous increase of the triplet level population during the excitation pulse occurs. Heavy atoms have been used for the enhancement of the intersystem crossing step due to spin orbit coupling. For the case where the reached excited triplet state has a lifetime longer than the duration of the excitation pulse, excited state absorption occurs that results in the observation of nonlinear absorption.
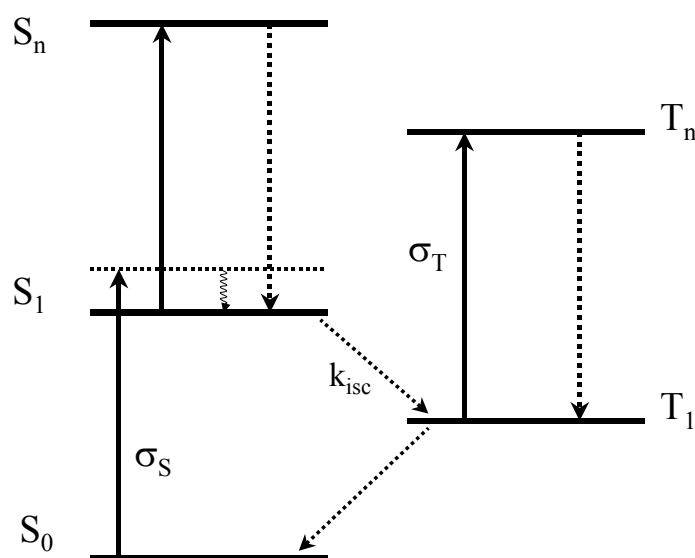


Scheme 4.2: A general five-level scheme that explains the optical limiting process. For a pulse of $\tau$ duration, the $S_0 \rightarrow S_1$ excitation in the vibronic level of $S_1$, is followed by rapid internal conversion. In the presence of a relative fast intersystem crossing $k_{isc}$ and for an excited state cross-section $\sigma_S$ higher than the ground state cross section $\sigma_T$, an optical transition occurs from the lowest lying triplet $T_1$ to a higher excited triplet state $T_2$, during the pulse. The competition of excited state absorption between singlet excited states $S_1 \rightarrow S_n$ and triplet excited states $T_1 \rightarrow T_n$ will be influenced from the $\tau_{isc}/\tau$ ratio.

The application of the optical limiting that heavy-atom substituted porphyrins and phthalocyanines exhibit, targets to the development of light attenuators to be used for the protection of sensors and the human eye.

An other active area of research in porphyrins is the one related with porphyrin-based sensors that aim in the detection of oxygen [31], [32] or the determination of temperature [33]. Due to their efficiently reached long-lived triplet states, octaethyporphyrins (OEPs) have been used as photosensitizers of singlet oxygen. This process has been applied in photodynamic therapy of tumors [34], [35].

## 4.2  PHOTON ENERGY DOWN-CONVERSION IN POLY(9,9-ETHYL-HEXYL-FLUORENE):2,3,7,8,12,13,17,18 OCTAETHYL-21H, 23H, PORPHIRINATO PLATINUM(II) BLENDS

### 4.2.1 Introduction

For the reasons discussed in paragraph 4.4.1, there is a considerable effort for studying the energy transfer process from blue light-emitting polymers to heavy-atom containing porphyrins. Recent studies in poly(fluorene) derivatives blended with a metal-free tetraphenyl porphyrin have addressed the issue of energy transfer from the polymer to the dye, after optical exciation [36], [37], [38]. This process is assumed to take place within the framework of dipole-dipole electronic energy transfer (paragraphs 1.4 and 3.3.1.2) that the Förster formalism describes. The extracted Förster radii (eq. 3.3) for these systems have been deduced from the doping concentration dependence of poly(fluorene) photoluminescence quantum yield [36] or decay lifetime [37]. These Förster radii values at which these independent studies have arrived differ in some extend, partially due to the fact that the experimental results used were based on different measuring techniques. However, the main reason for the deviation in the obtained Förster radii values should be attributed on the inefficiency of the classical Förster formalism to describe the electronic energy transfer processes that take place in conjugated polymers (see paragraph 3.3.4). In the aforementioned studies, two different poly(fluorene) derivatives have been used; an *n*-octyl derivatised poly(fluorene) (PFO) [36] and a branched ethyl-hexyl derivatised poly(fluorene) (PF 2/6) [37]. As it has been discussed in paragraph 2.2.3, these two derivatives exhibit a different structural pattern as films in the solid state. As film, PFO has been found to

adapt more planar geometries than PF2/6. Presumably, this fact results in longer average conjugational length values for PFO than for PF2/6. Therefore this may explain why for the case of PFO the Förster radius has been reported to be $R_{PFO}= 5.4$ nm [36] while for PF2/6 has been reported to be $R_{PF2/6}= 3.7$ nm [37]. For a similar system comprised of blends of PFO and PtOEP photoluminescence quantum yield investigation resulted in a Förster radius equal to $R_0= 1.9$ nm [8]. In comparison with the previously reported values, a decrease of $R_0$ was found presumably due to the weaker spectral overlap of PtOEP absorption with PFO emission. It was only recently that the Förster theory of electronic transfer has been theoretically refined, particularly for the case of a poly(fluorene) derivative, doped with a metal-free tetraphenyl porphyrin [39].

The determination of energy transfer rate from the polymeric host to the porphyrin dye, can be treated as being equivalent to a quenching rate determination. The dopants are energy scavengers that operate in the framework of dynamic quenching of the PF emission (paragraph 3.3.3). Photoluminescence quenching is a known process that has been observed in many donor-acceptor systems [40], like e.g. anthracene-bromobenzene solutions [41]. By exploiting the Stern-Volmer formalism that has been introduced in paragraph 3.3.2, the quenching rate determination is proven to be accurate for the case where dopant and matrix are well miscible.

In the experiments described below data obtained from steady-state and time-resolved photoluminescence are used for the application of the Stern-Volmer formalism in PF2/6:PtOEP system.

## 4.2.2 Experimental

Degassed toluene was used as a solvent for the preparation of mother solutions of PF2/6 endcapped with tri-arylamine groups (see structure in Chart 4.1) and PtOEP. Prior to the addition of the materials, the solvent had been ultrasonicated for 15 min concomitant purging of He. The solution concentration of PF2/6 was in the order of 10 mg/mL whereas the one of PtOEP (Scheme 4.1) was of 0.3 mg/mL. Mixing of appropriate amounts of these solutions resulted in the final solutions, ranging from 0.1 wt% to 10 wt% doping of PtOEP in PF2/6. Table 4.1 summarises the obtained quantities of the mother solutions.

| wt % | $m_{host}$ (mg) | $V_{host}$ (mL) | $m_{PtOEP}$ (mg) | $V_{PtOEP}$ (mL) | $m_{total}/V$ (mg/mL) |
|------|-----------------|-----------------|------------------|------------------|-----------------------|
| 0.1 | 3 | 0.300 | 0.0032 | 0.100 | 7.508 |
| 0.2 | 2.997 | 0.300 | 0.0063 | 0.100 | 7.508 |
| 1 | 2.994 | 0.299 | 0.0320 | 0.100 | 7.583 |
| 2 | 2.970 | 0.297 | 0.0630 | 0.100 | 7.640 |
| 10 | 2.680 | 0.268 | 0.3200 | 0.100 | 8.152 |

Table 4.1: The concentration of the mother solutions of PF2/6 and PtOEP that were prepared.

Quartz substrates that had been cleaned repeatedly in acetone, aqueous surfactant 2 wt% and isopropanol, were used as substrates for the preparation of thin films of the obtained solutions via spin coating. Spin velocity was chosen to be 1500 rpm within 60 sec. As a reference, a sample of 10 wt% PS:PtOEP was used. Table 4.2 gives the $M_n$ and polydispersity values of the compounds used.
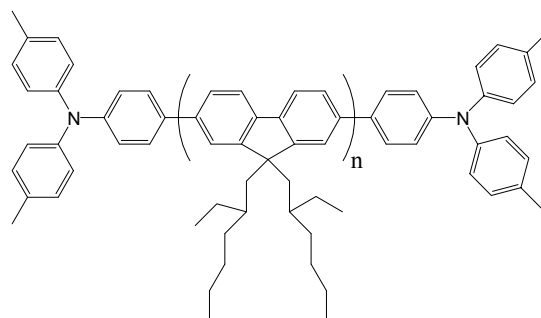


Chart 4.1: The chemical structure of the endcapped PF2/6 derivative that was studied.

| Material | $M_w$ (gr/mole) | Polydispersity D |
|----------|-----------------|------------------|
| PtOEP | 727.87 | - |
| PF2/6 endcapped | 63765 | 1.417 |
| PS | 355100 | 1.067 |

Table 4.2: The $M_n$ values of the components that are used. For the case of polymer the polydispersity (D) value is also given.

Table 4.3 describes the quantities that were used for the polymer host and guest, in order to obtain thin films of blends that were corresponding to doping concentration of 0.1% wt, 0.2% wt, 1% wt, 2% wt, 10% wt.

| wt % | $m_{host}$ (mg) | $V_{host}$ (mL) | $m_{PtOEP}$ (mg) | $V_{PtOEP}$ (mL) | $m_{total}/V$ (mg/mL) |
|------|------|------|------|------|------|
| 0.1 | 3 | 0.300 | 0.0032 | 0.100 | 7.508 |
| 0.2 | 2.997 | 0.300 | 0.0063 | 0.100 | 7.508 |
| 1 | 2.994 | 0.299 | 0.0320 | 0.100 | 7.583 |
| 2 | 2.970 | 0.297 | 0.0630 | 0.100 | 7.640 |
| 10 | 2.680 | 0.268 | 0.3200 | 0.100 | 8.152 |

Table 4.3: The wt% values of PtOEP used for the doping the studied PF2/6 films. The appropriate mixed volumes of the PtOEP and PF2/6 solutions, together with the corresponding masses of the components are given.

## 4.2.3 Results

As it was previously mentioned in paragraph 4.1.1, doping of a light-emitting polymer with small amounts of PtOEP could enhance the triplet radiative rate of a triplet state of PF by means of external heavy atom effect due to the presence of the heavy $Pt^{2+}$ cation. In the case of appropriate spectral overlap (eq. 3.2), optical excitation of PF can also lead to resonant energy transfer towards PtOEP. As Figure 4.3 shows, a spectral overlap exists between the emission of PF and the absorption spectra of PtOEP.
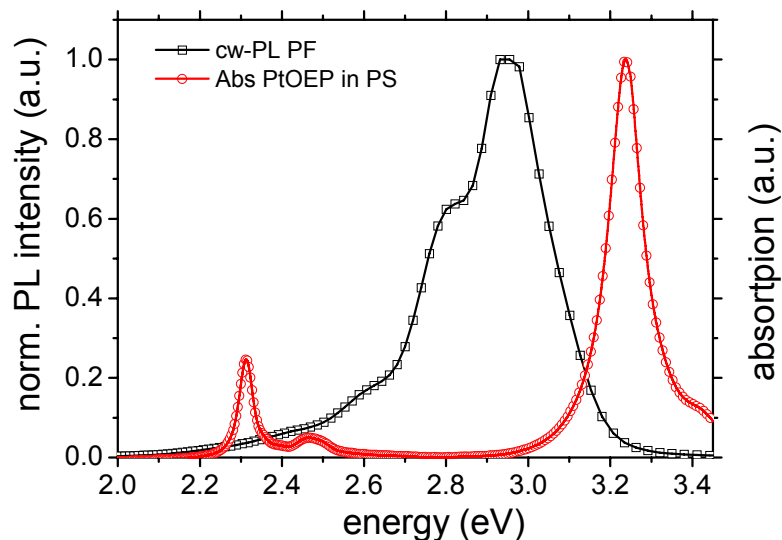


Figure 4.3: Room temperature cw-PL spectrum of a PF2/6 film (squares) and absorption spectrum of a PS:PtOEP 10 wt % film (circles).

Therefore, according to the Förster energy transfer formalism (paragraph 3.3.1.2 ) the probability for energy transfer form PF to PtOEP instead of PF emission is satisfied. Figure 4.4, shows the cw-PL spectra of a film that consisted of PF2/6:PtOEP 3%wt and was excited with different average laser power at 405 nm.
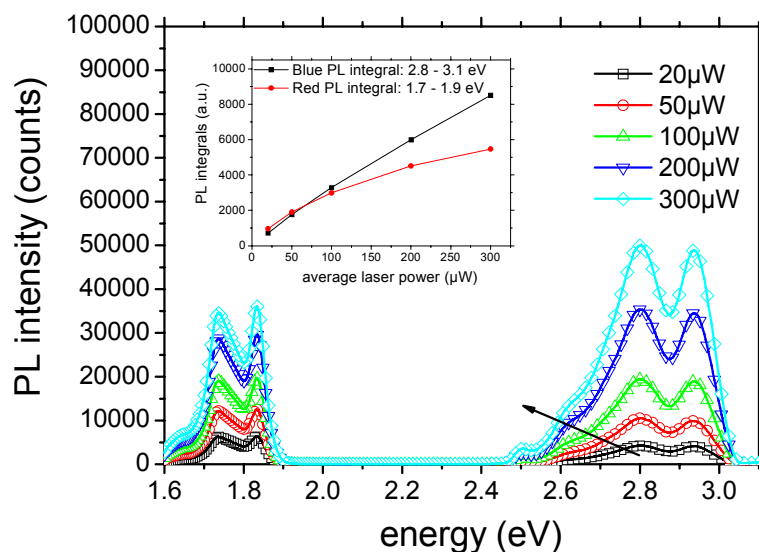
Figure 4. 4: Room temperature cw-PL spectra of a PF2/6:PtOEP 3 wt% film. Excitation was at 405 nm (3.06 eV) for different average laser powers. The inset shows the dependence of the PF2/6 (squares) and PtOEP (circles) spectral integrals on the excitation power. The spectral areas of emission that are monitored are given in the inset.

Under this excitation condition, non-linear signals are not expected to occur due to the relatively low excited state population that the excitation density is creating. However comparison of the cw-spectral integrals of PF and PtOEP emission show that a non-linear process must be involved in the emission. PtOEP emission is found to have a power law rise that follows an exponent of 0.6 while PF is following an exponent of 0.9. This indicates that PF emission is growing faster than PtOEP emission as excitation the density is increased.

Figure 4.5 presents the decay transients of the singlet emission manifold of PF2/6 as a function of concentration of PtOEP content.
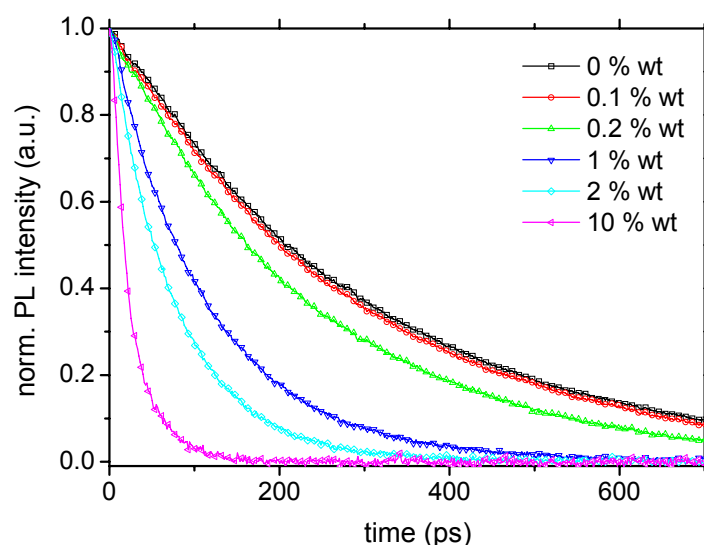
**Figure 4.5:** Normalised decay transients monitoring the PF2/6 singlet emission of the PtOEP doped PF2/6 films. Excitation was at 405 nm (3.06 eV), at room temperature. Pressure was kept at ~$10^{-5}$ mbar.

The determined $\tau_{1/e}$ lifetime values of the decay transients that Figure 4.5 presents are given in Table 4.4. Based on the these lifetime values, the PL quenching efficiency of PF2/6 host emission due to energy transfer to the PtOEP guest is determined, for each of the doping concentration.

| PF2/6:PtOEPwt % | PtOEP Molarity (mole/Lt) | PF2/6 $\tau_{1/e}$ (*ps*) |
|---|---|---|
| 0 | - | 302 |
| 0.1 | 0.00147 | 291 |
| 0.2 | 0.00288 | 217 |
| 1 | 0.01464 | 122 |
| 2 | 0.02882 | 80 |
| 10 | 0.14655 | 34 |

Table 4.4: The molar concentration of PtOEP in the films of PF2/6:PtOEP studied. A film density of 1gr/cm$^3$ was assumed. The $\tau_{1/e}$ values of PF2/6 emission as determined from Figure 4.5 are also given.

Figure 4.6 presents the determined energy transfer efficiency as a function of PtOEP doping concentration in PF2/6. For reasons of comparison, the energy transfer efficiency, as determined from the cw-PL intensity of the doped PF2/6 films, is shown.
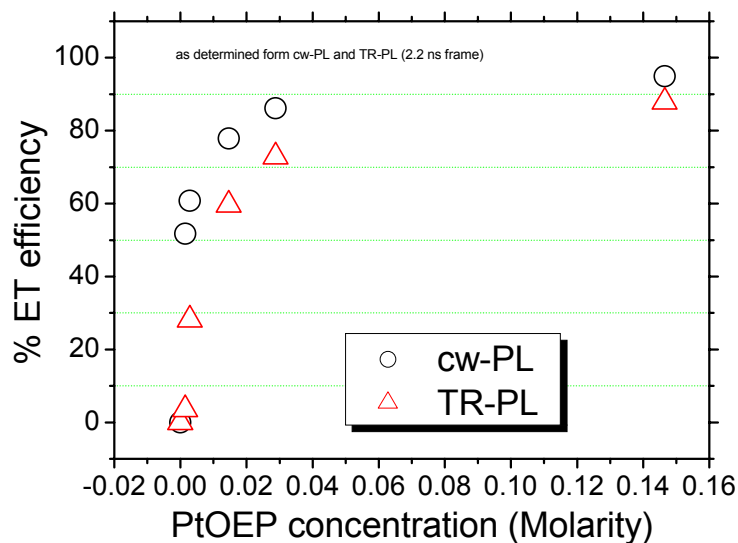
Figure 4.6: The electronic energy transfer efficiency from PF2/6 to PtOEP, after excitation at 405 nm (3.06 eV), as a function of the PtOEP concentration in PF2/6.

As it has been described in paragraph 3.3.3, eq. 3.6 can be used for the energy transfer efficiency determination.
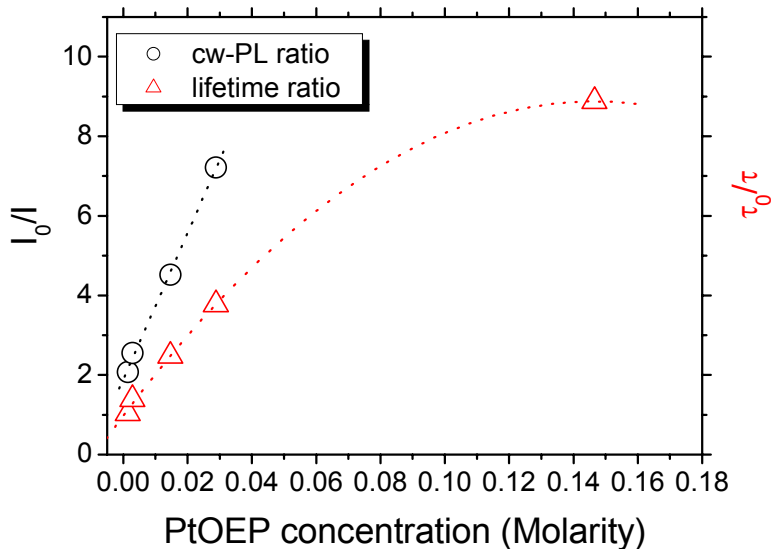


Figure 4.7: A Stern-Volmer plot for the films of PF2/6:PtOEP studied, after excitation at 405 nm (3.06 eV), as a function of the PtOEP concentration in PF2/6.

A Stern-Volmer plot is presented in Figure 4.7, based on the determined lifetime values of PF2/6 for each of the doping concentration of PtOEP. A downwards curvature behaviour can be observed in the case of the data based on observable decay lifetimes of PF2/6.

224

We employed transmission electron miscroscope (TEM) in order to interrogate the degree of host/guest miscibility. TEM results are considered representative for the bulk of the sample in case of thin films and they are not restricted to surface information. Hence TEM was chosen instead of the atomic force miscroscopy (AFM) technique, as the latter provides information that accounts for the composition of the surface. Two different thin spin coated films were studied that consisted of PF2/6:PtOEP 2 wt % and PF2/6:PtOEP 10 wt %, respectively. As Pt(II) cation is heavy enough, detection of potential Pt clusters formed due to PtOEP aggregation would be detectable with TEM. As a result we did not find any indication of PtOEP aggregation for doping levels up to 2 wt%. In contrast, TEM studies on a PF2/6:PtOEP at 10 wt% gave evidence of PtOEP aggregation. Therefore, molecular homogeneous dispersion of PtOEP is assumed within the PF matrix for doping concentration up to 2 wt%.
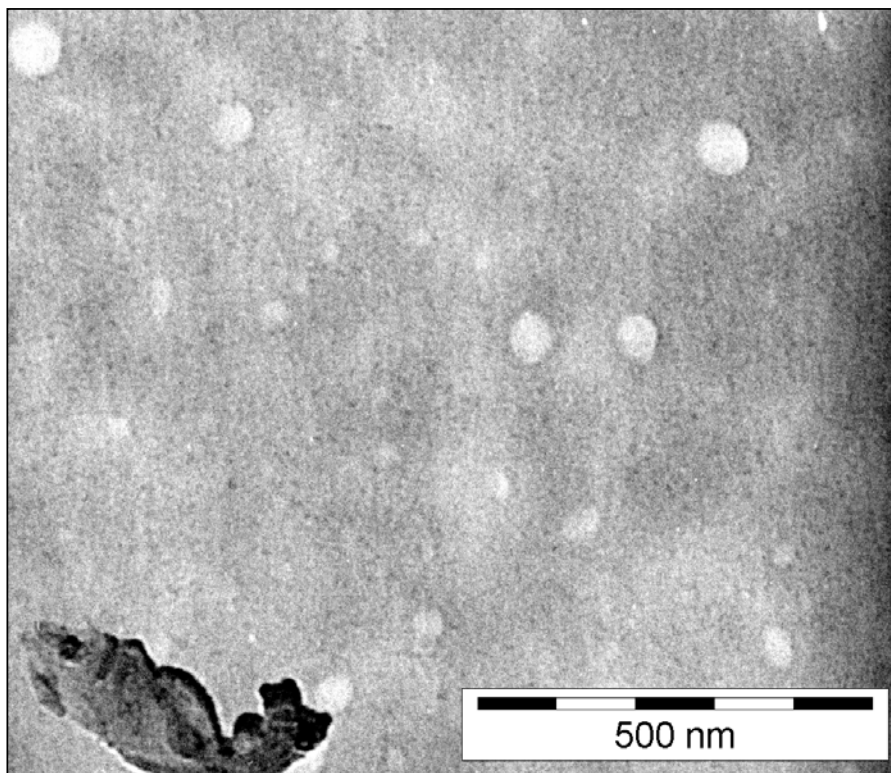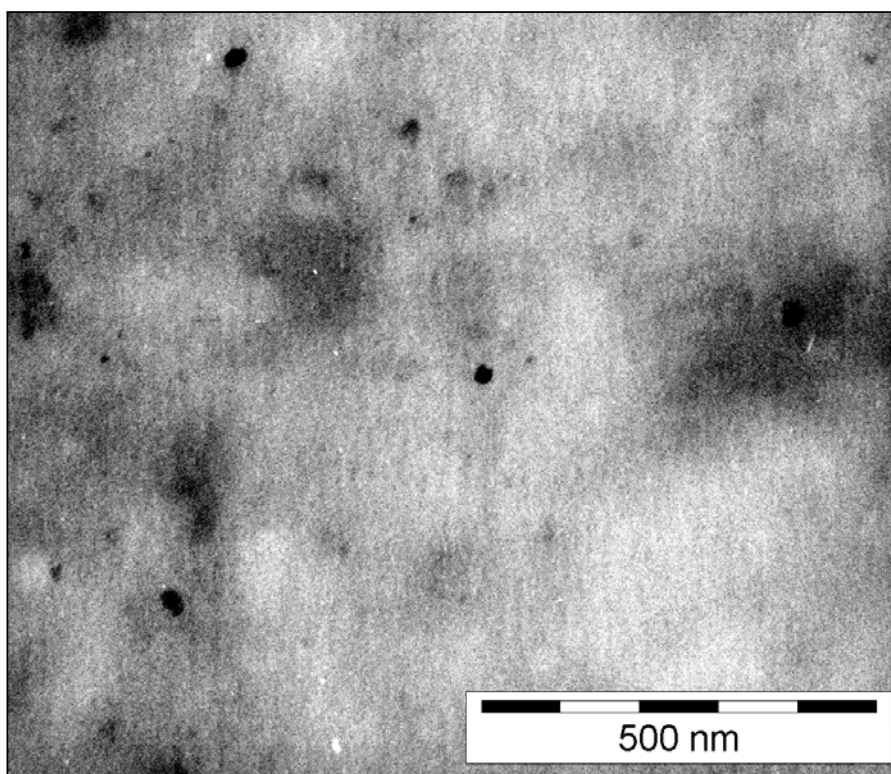
Figure 4.8: Bright field transmission electron microscope images for two PF2/6 films doped with a) 2 wt% PtOEP and b) 10 wt% PtOEP. Films were prepared by spin-coating of solutions on glass substrates. Images were obtained by Dr. G. Lieser (MPI-P).

## 4.2.4 Discussion

We have addressed the quenching efficiency of PF2/6 photoluminescence in thin films of PF2/6 doped with PtOEP quenchers (Figure 4.6). By using the Stern-Volmer formalism we observed an inefficient quenching of PF2/6 from the quenching influence of PtOEP, which is reflected in a Stern-Volmer non-linearity. A downward curvature such as the one of Figure 4.7 practically implies that at a given concentration of the dopant, the value of $\tau_0/\tau$ is lower than expected or in other words the observed $\tau$ of the given doping is higher than in the ideal case of a linear behaviour.

Downward curvature of the Stern-Volmer plot has been observed in solutions of anthracene quenched by bromobenzene [41]. In this particular case, the quadratic dependence of the $I_0/I$ ratio on bromobenzene concentration had been then attributed to the dependence of the activity coefficients of the quencher on concentration in the transition state. In the present case, our results are obtained from thin film conditions where the influence of ionic effects is not relevant. Thus our observations could potentially be explained by the influence of miscibility effects between host and dye (paragraph 3.3.2).
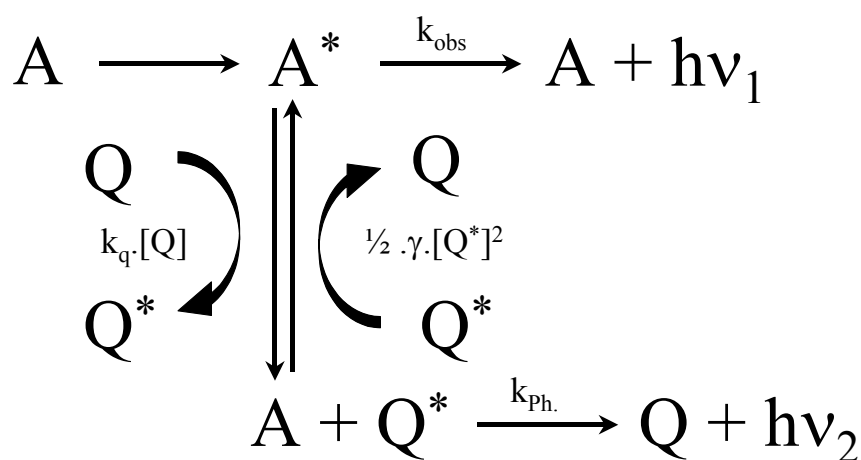
As it was discussed in paragraph 3.3.2, linear Stern-Volmer kinetics are obtained for the cases where donor molecules are fully accessible to all acceptor molecules. Deviations from the expected Stern-Volmer linearity should be expected when a combination of static and dynamic quenching occurs or when only a fraction of the excited donors are accessible to the quenchers. Immiscible components may cause problems with phase separation. Consequently, film inhomogeneities can exist due to local aggregation effects in the solid state. In this case non-linear Stern-Volmer plots which are curved towards the x-axis have been observed [40].

According to TEM investigation, the molecules of PtOEP are molecularly dispersed in the PF2/6 matrix in a doping regime up to 2 wt% (Figure 4.8). Since the spectral conditions of excitation energy transfer from PF2/6 to PtOEP are fulfilled (Figure 4.3), the phenomenologically observed insufficient PL quenching should implies the existence of an energy feedback channel from PtOEP to PF2/6. The existence of energy backtransfer channels from excited states of octaethyl metalloporphyrins to fullerenes is known from photo induced absorption experiments [23].

Our approach towards interpreting our presented experimental results goes like follows. After the excitation energy transfer from PF2/6 to PtOEP, a feedback channel is created under conditions of cw-excitation that supports energy backtransfer from PtOEP to PF2/6. The sub-linear slope observed in the excitation intensity dependent emission of PtOEP in the inset of Figure 4.4, is explained as a result of a bimolecular process occurring between two long lived excited PtOEP triplets (see paragraph 3.4.1.2). We emphasize the fact that under the described

circumstances such a non-linear interaction of PtOEP molecules can be anticipated even at this low excitation regime because of a small portion of PtOEP molecules that is directly excited from our laser (Figure 4.3). Due to the existence of the high-energy Soret band in the absorption spectrum of PtOEP at 400 nm, the excitation wavelength of 405 nm can be directly absorbed. However due to the low concentrations of PtOEP, in comparison with the host, this fraction of direct PtOEP optical excitation may be neglected. Yet, in combination with the excitation energy transfer from PF2/6 to PtOEP, the conditions of bimolecular PtOEP annihilation can be met.

 Given the fact that the sum of two PtOEP triplet quanta exceeds the energy of the PF2/6 singlet level, energy back transfer from PtOEP to PF2/6 can take place via triplet-triplet collision of two excited PtOEP molecules subsequently followed by energy transfer to PF2/6. The kinetic scheme that could potentially describe the suggested mechanism is depicted in Scheme 4.3. Based on the kinetic equation of each photoexcited specie (eq. 4.2-4.4), we derive (see *Appendix B*) a modified Stern-Volmer equation (eq. 4.5)

$$A \longrightarrow A^* \xrightarrow{k_{obs}} A + h\nu_1$$

$$Q \quad \big)_{k_q.[Q]} \quad \big(_{\frac{1}{2}.\gamma.[Q^*]^2} \quad Q$$

$$Q^* \qquad\qquad Q^*$$

$$A + Q^* \xrightarrow{k_{Ph.}} Q + h\nu_2$$

Scheme 4.3: A simple kinetic scheme of the photophysical process that is discussed in paragraph 4.2.4. PF2/6 is indicated from term A, while PtOEP is indicated from term Q.

$$\frac{d[A^*]_0}{dt} = I - k_1 * [A^*]_0 \qquad \text{(eq. 4.2)}$$

$$\frac{d[A^*]}{dt} = I - k_1 * [A^*] - k_q * [Q] * [A^*] + \frac{1}{2} * \gamma * [Q^*] \qquad \text{(eq. 4.3)}$$

$$\frac{d[Q^*]}{dt} = -k_2 * [Q^*] + k_q * [Q] * [A^*] - \frac{1}{2} * \gamma * [Q^*]^2 \qquad \text{(eq. 4.4)}$$

$$\frac{I_0}{I} = 1 + k_q * \tau_0 * [Q] - \frac{1}{2} * \gamma * k_q^2 * \tau_0 * \tau_{Ph} * I * [Q]^2 \qquad \text{(eq. 4.5)}$$

Our scheme also may possibly explain the departures of the Stern-Volmer plot from linearity, observed earlier in solutions of anthracene containing bromobenzene [41]. Due to the heavy atom effect of bromine atom [34], the singlet state of anthracene may be converted to its triplet analogue. Anthracene is a known system that follows the kinetic route of triplet-triplet fusion [42]. Thus, upon increasing the concentrations of bromobenzene, a large fraction of anthracene triplets can be generated that will undergo triplet-triplet annihilation and subsequently result in delayed fluorescence. The contribution of this process will result in a deviation of Stern-Volmer plot from linearity.

Another option for the presence of a backtransfer channel in the presented system could be described from triplet-triplet annihilation events within the host matrix after triplet energy backtransfer from PtOEP to PF. Studies performed in similar systems have shown that upon doping a PFO film with 8 wt% PtOEP, an increase of the PFO triplet lifetime is observed by a factor of 1.6 [7]. Even more interestingly, upon going from 1% to 8% wt PtOEP doping of PFO a 40% decrease of PtOEP PL quantum efficiency has been observed [7]. The authors of [7] have attributed the decrease in the PtOEP PL quantum efficiency in concentration quenching of PtOEP upon higher loadings. They based their arguments on triplet lifetime measurements of PtOEP doping of poly(styrene). Regarding the observed increase of PFO triplet lifetime after doping, they claimed that it occurs by virtue of the external heavy atom effect that PtOEP induces in the PFO matrix. Therefore they assigned the observed PFO increased triplet yield on spin orbit coupling effects. However, it is known that spin orbit coupling can increase the radiative phosophorescent rate by two orders of magnitude, thus a decrease of phosphorescence lifetime has to be expected in the presence of a heavy atom [43]. Therefore the increased triplet lifetime of PtOEP-doped PFO should reflect a triplet energy backtransfer from PtOEP to PFO.

For the case of the here presented PF2/6, the triplet level lies 0.4 eV higher than PtOEP triplet, therefore the alternative thermalised backtransfer description should exhibit temperature dependence characteristics and be possible for room and higher temperatures. The topic of temperature dependence of this specific activation channel will be discussed in paragraph 4.3.5.

We further comment on the fact that an inefficient PL quenching has also been found for the case of PtOEP doped films of a ladder-type poly(*p*-phenylene) derivative [9]. This makes us to believe that our hypothesis regarding the energy feed back channel from PtOEP to PF2/6 may be extended to other blue light-emitting hosts. This issue is discussed in Section 4.4.

## 4.3 LOW-ENERGY PHOTON UP-CONVERSION IN FILMS OF POLY(9,9-BIS(2-ETHYL-HEXYL) FLUORENE) DOPED WITH 2,3,7,8,12,13,17,18-OCTAETHYL- 21H, 23H, PORPHYRINATO PALADIUM(II)

In the following paragraphs we present experimental evidence for the existence of a energy back transfer feedback channel, in films comprised of PF2/6:MeOEP blends. We utilise quasi-CW laser photoluminescence spectroscopy in for exciting directly the phosphorescent MeOEP component of the blends by avoiding direct excitation of the polymer host. Our excitation intensities are in the order of kW/cm$^2$. Under this excitation conditions and in steady-state mode detection we detect the characteristic PL emission of the host, a spectral feature that from now onwards will be described as up converted PL or up-conversion.

### 4.3.1 Experimental

A homebuilt vacuum chamber was used for the up-conversion experiments. Dynamic vacuum higher than $10^{-4}$ mbar was reached by using a turbo pump. An electronically controlled one-stage Peltier-element was used to define the temperature of the sample. As pumping sources an intracavity frequency doubled (532 nm) diode pumped cw-Nd:YAG laser (Verdi V10), a green line (543 nm) HeNe laser and a violet (405 nm) laser diode (Nichia Corp.) were used. A combination of specially designed mirrors with high transmittance for the regions below 490 nm and above 655 nm, and reflectivity higher than 99% for the region between 490 nm and 655 nm and low absorption colour filters were used in order to eliminate scattered light from the pump laser beams. Achromatic lenses for focus and collection of the emitted PL were used. The excitation and emission inherently coincided on the same focal spot of the samples. The spot sizes of the pump lasers were as follows: ca. 80 μm diameter at 532 nm and 543 nm; ca. 4 μm at 405 nm. An arbitrary wavefunction generator (TTi 40 MHz Arbitrary Waveform Generator, TGA1242) was used to synchronise the laser shutter and the registration system. The irradiation time used was kept at 200 ms. The collected emission signal was dispersed in a 0.3 m

monochromator equipped with a 150 lines/mm grating and registered by a CCD (Hamamatsu Photonics, PMA50). A schematic representation of the optical set-up is provided in Scheme 4.4.
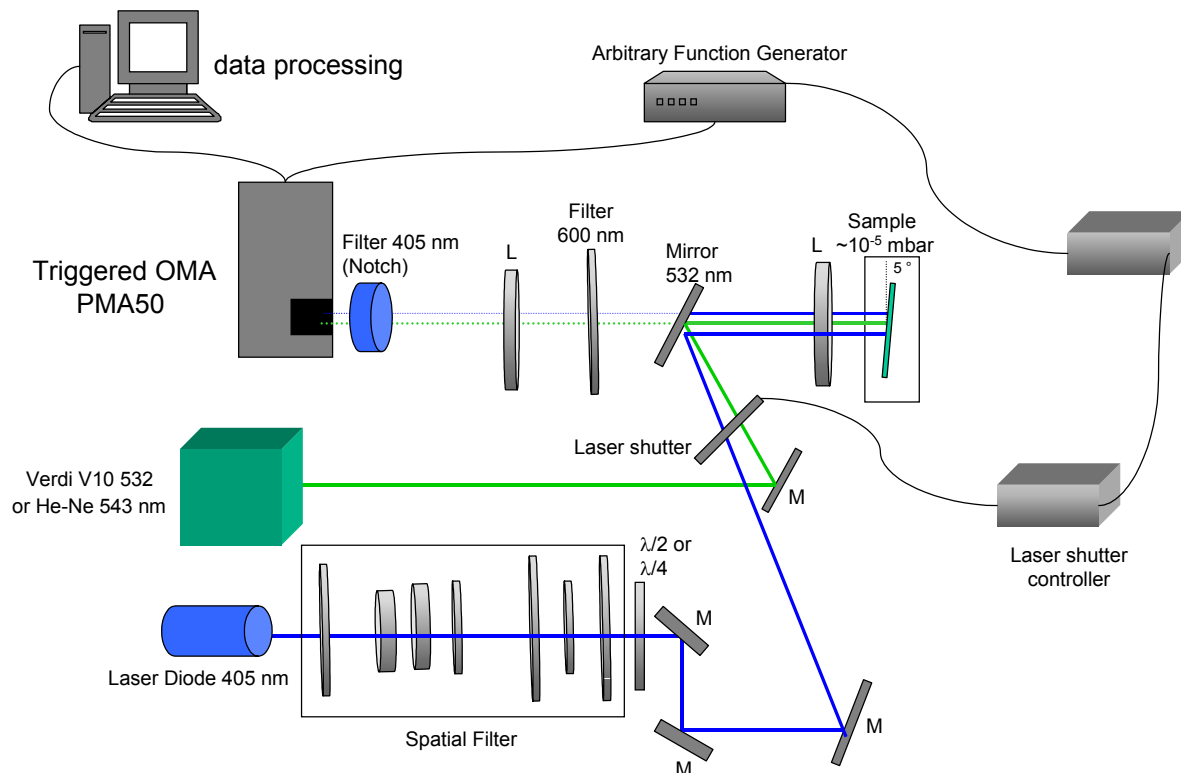


Scheme 4.4: A schematic representation of the set-up that was used for the performance of the up-conversion experiments (see text).

Table 4.5 gives the molecular weight values of all the MeOEPs used together with the $M_w$ and polydispersity values of the polymers that were used.

| Material | $M_w$ (gr/mole) | Polydispersity D |
|----------|-----------------|------------------|
| CoOEP    | 592             | -                |
| CuOEP    | 596             | -                |
| NiOEP    | 591             | -                |
| PtOEP    | 728             | -                |
| PdOEP    | 639             | -                |
| PF2/6    | 190000          | 2.076            |
| PS       | 355100          | 1.067            |
| PMMA     | 1535            | 1.170            |

Table 4.5: The M(II)OEP derivatives and the host polymer matrices that were used for the preparation of Host:Me(II)OEP films. The molecular weights and polydispersity (D) values are given.

## 4.3.2 Observing the up-conversion process

The steady state spectral characteristics of poly(fluorene) and PdOEP as thin films are presented in Figure 4.9. Due to crystallisation effects, PdOEP has bad film forming properties ; therefore inert matrices such as poly(styrene) (PS) or poly(methacrylic) acid (PMMA) were used. The presented spectra are normalised and for reasons of clarity PF spectra are shown offset by a factor of two. The most important spectral characteristics to be noticed in Figure 4.9 are the strong spectral overlap of PF emission and PdOEP absorption in the blue region of 390–430 nm, the negligible values of PF optical density in the region of 532 nm and the strong absorbance of PdOEP in the region of 525–530 nm. Comparing the optical density of PdOEP in 532 nm to 543 nm one obtains a factor of app. 5 times more efficient light absorption at 543 nm than at 532 nm (see also the following paragraph 4.3.4)
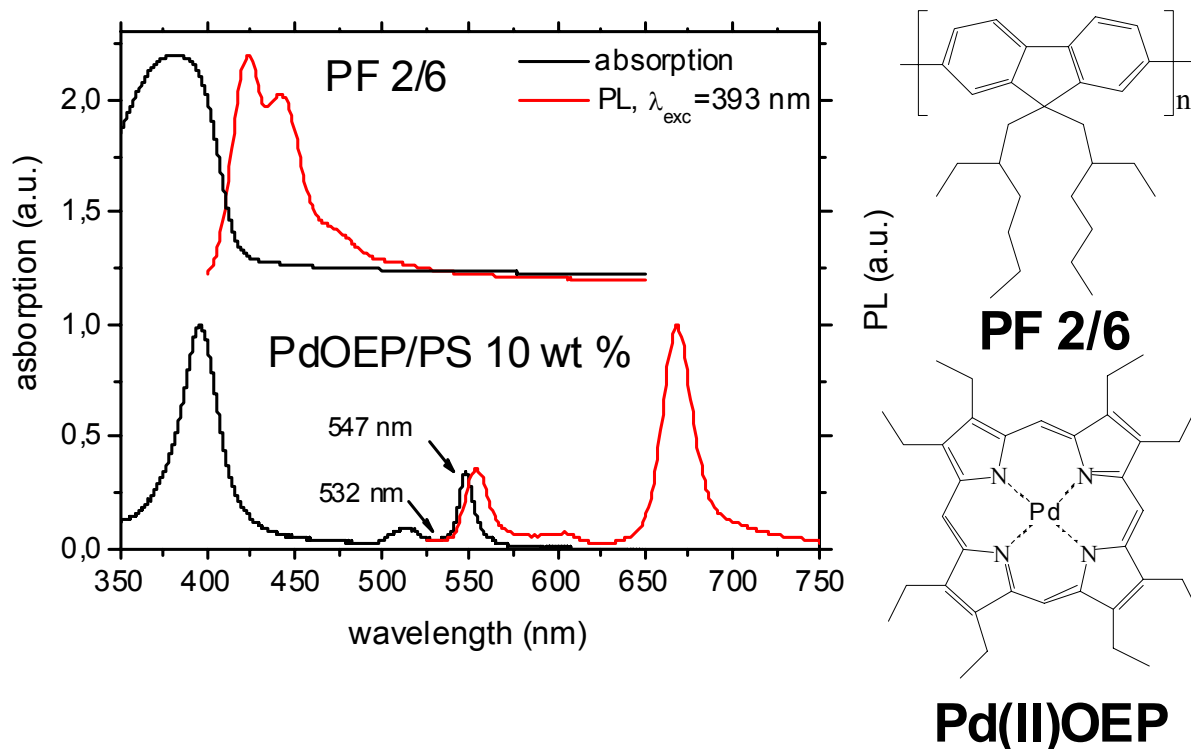
Figure 4.9: The room temperature normalised absorption and PL spectra of a PF2/6 film (top) and a PS:PdOEP 10 wt% film (bottom). The chemical structures the PF2/6 derivative and PdOEP are also shown.

In order to confirm the hypothesis of energy back transfer from PtOEP to PF that was suggested in 4.2.4 direct excitation of PtOEP is performed at 532 nm under steady-state laser excitation of 13.5 kW/cm$^2$ intensity. In these quasi-cw excitation conditions, the characteristic emission of PF is observed. The spectrum of figure 4.10a was obtained by using the described optical set up in 4.3.1 where the major intensity part of the spectral region between 490 nm -655 nm has been eliminated. Under this conditions the emission of PF is more pronounced and the detection of PF PL signal can be optimised efficiently.
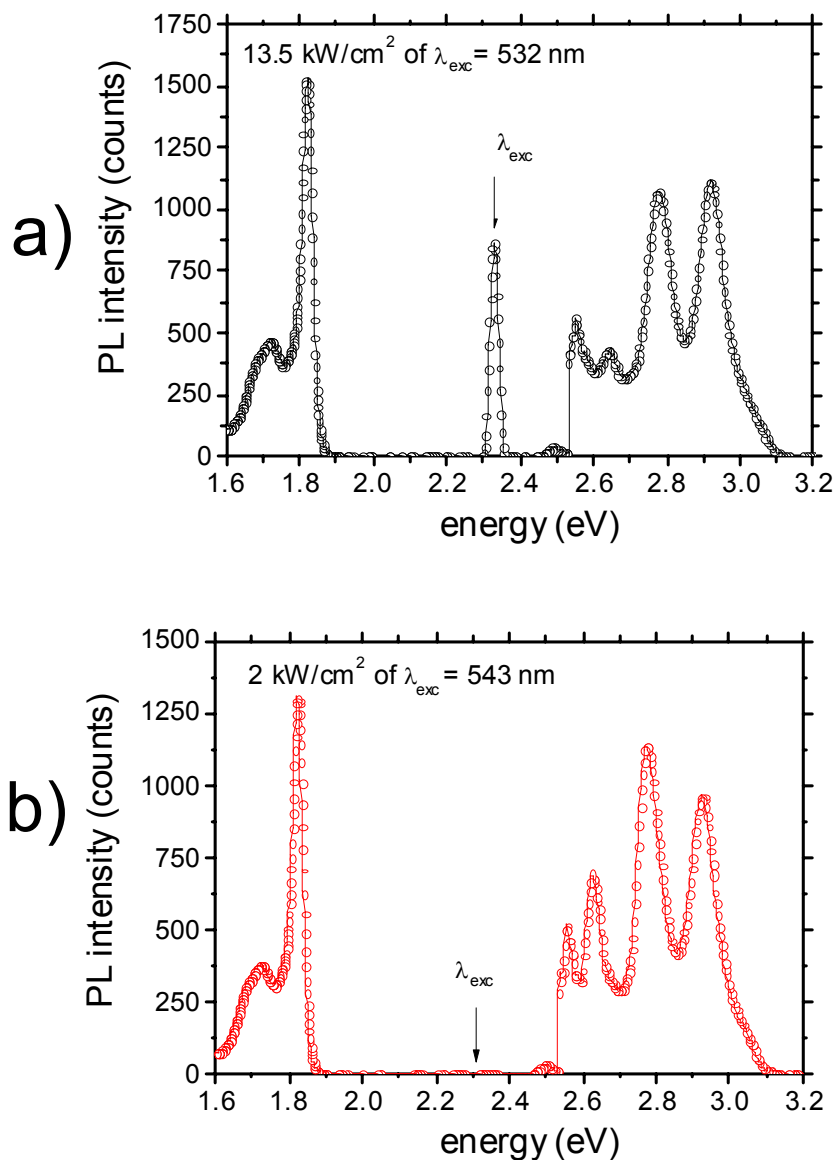
Figure 4.10: Room temperature PL intensities of film of PF2/6 doped with 3 wt. % PdOEP. Laser excitation at: a) 532 nm (2.33 eV) and b) 543 nm (2.28 eV). The excitation intensities are given in the top left corner of each plot. In order to present the spectra on comparable intensity scale, multiplication factors for the spectral regions were applied as follows: 1.89 – 2.53 eV a), b) – factor $10^{-6}$ ; 1.55 eV – 1.89 eV a) – factor 0.025, b) – factor 0.0125. Pressure was kept ~$10^{-5}$.

In figure 4.10b the PL spectrum of the same sample is presented when is excited at 543 nm under steady-state laser power of 2 kW/cm$^2$ intensity. Once more the characteristic PL emission spectrum of PF is observed. Interestingly, it appears with approximately the same PL intensity like when excitated at 532 nm of 13.5 kW/cm$^2$ intensity. Therefore the same PL integral can be obtained for PF by exciting in the region of 543 nm where PdOEP has an optical density 5 times higher than 532 nm, when the excitation intensity was lowered by a factor of ~7. This implies

that under excitation in the region of maximised PdOEP absorbance, the same PL integral could be obtained by even lower excitation intensities.

### 4.3.3 Efficiency of the up-conversion process

In order to estimate the efficiency of the up-conversion process in PF2/6:PdOEP, by using the same optical set-up and registration scheme, we performed direct excitation of the active host polymer by pumping at 405 nm by a quasi-cw violet laser diode, close to the absorption peak of PF2/6. Figure 4.11 shows PL spectrum obtained by direct excitation of PF at 405 nm. By comparing the data of Figures 4.10a and 4.11 and by taking into account, that about 10% of the incident laser light is absorbed by the PdOEP component in the sample, we recalculated the experimentally measured laser intensity. A ratio of about 1/5000 between the integral intensities of the PL emission of PF when pumped at 532 nm and at 405 nm was derived.
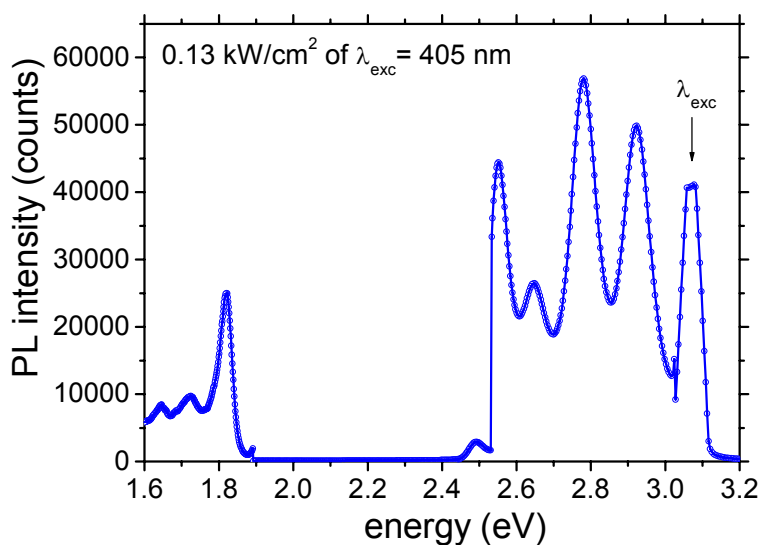


Figure 4.11: Room temperature PL intensities of film of PF2/6 doped with 3 wt. % PdOEP. Laser excitation at: 405 nm (3.06 eV). The excitation intensity is given in the top left corner of the plot. A multiplication factor of $10^{-6}$ was used for the spectral region corresponding to energies between 1.89 – 2.53 eV. Pressure was kept $\sim 10^{-5}$.

## 4.3.4 Optimising the up-conversion process by using different MeOEPs

From the group of metallated octaethyl porphyrins that we have studied, it is found that PtOEP (Figure 4.12) has a dual differentiation from the absorption spectra of the rest porphyrin rings. It posses a maximised exctinction coefficient $\varepsilon_{532nm}$ by shifting the absorption Q-bands towards the 532 nm region and due to the presence of Pt(II) cation it promotes the intersystem crossing (ISC) rate, by virtue of the heavy atom effect.
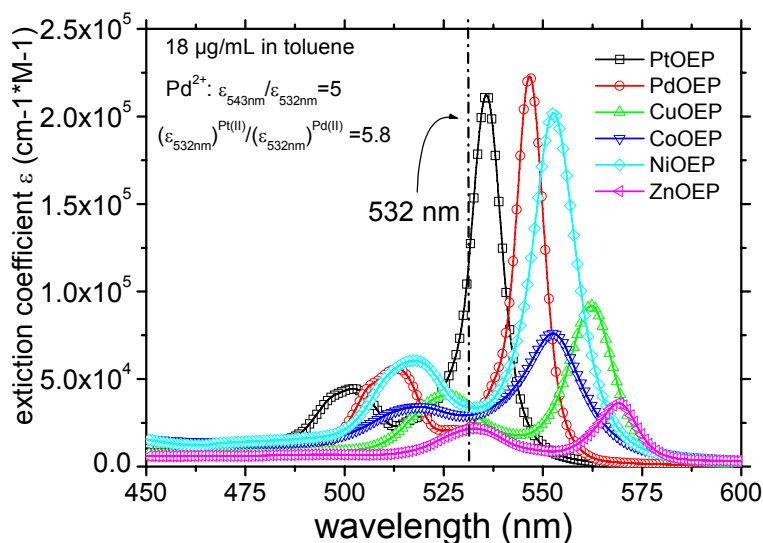


Figure 4.12: Room temperature absorption spectra for a series of Me(II)OEP solutions studied with concentration of ~ 20µg/mL in toluene. Note the difference of the 532 nm absorbance between each of the Me(II)OEP derivatives.

In Figure 4.13 a comparison is presented for the obtained excitation intensity dependences of up-conversion emission intensities of PF2/6 when blended with different metallated porphyrins. From all the porphyrin derivatives studied, PtOEP is found to have the more efficient impact on PF2/6 up-conversion for all the excitation intensities used.
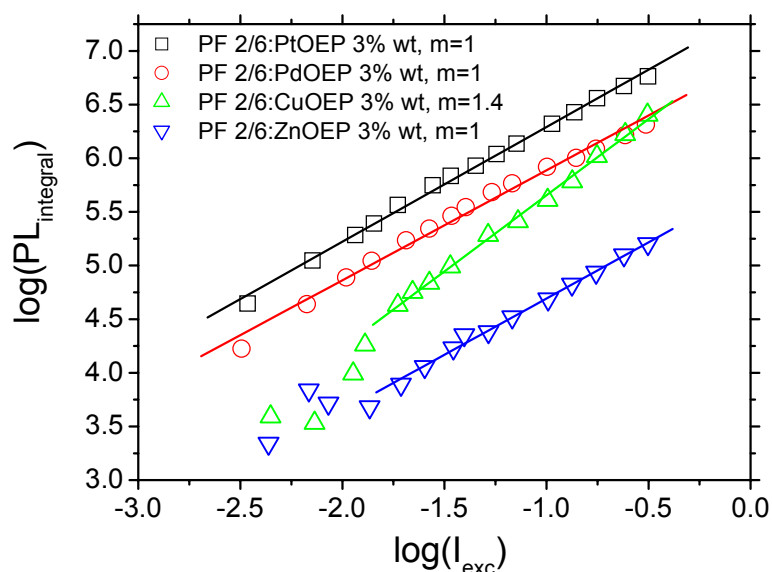
Figure 4.13: The excitation intensity dependence of the up-conversion spectral integrals obtained from each of the films of PF2/6:Me(II)OEP studied. The doping concentration was at 3 wt%. Excitation intensity units are in MW/cm$^{-2}$. The lines are fit to the data. The slopes *m* are given in the top left corner of the plot. For the case of PtOEP, PL intensity values are reduced by a factor of 0.33.

## 4.3.5 Temperature dependence

As the up-converted process is initially proceeding from the first triplet level of PtOEP, it should be dependent from the macroscopic temperature of the system. It is known that phosphorescence is sensitive to temperature because at higher temperatures the excited triplets have a higher probability to decay non-radiatively. Figure 4.14 presents the temperature dependence of up-conversion process in a PF2/6:PtOEP 10 wt% film on quartz substrate. A three-fold increase is seen for a decrease in temperature range of 348 K . It is known that the quantum yield of PF luminescence is increased at lower temperatures [44]. However, the percentage increase of up-converted PF2/6 emission observed within this studied temperature region exceeds the value of 200% and cannot solely be assigned to the increase in the quantum yield value of PF.

Since the triplets have an increased lifetime at lower temperatures [45], [10], triplet-triplet annihilation may occur with higher efficiency due to an increased probability for efficient collisions and thus up-conversion can be enhanced.
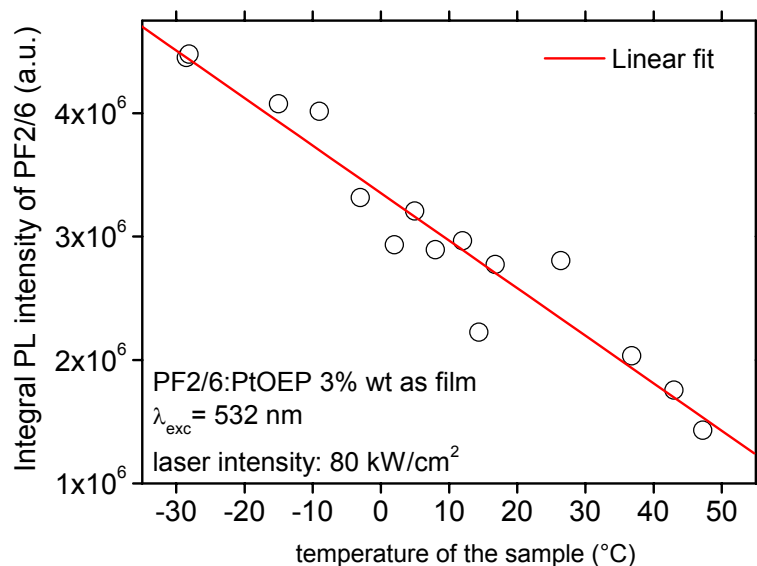
Figure 4.14: Temperature dependence of the integral PL intensity of the film of PF2/6 doped with 3 wt% PdOEP. Excitation wavelength is 532 nm, laser intensity was kept at 80 kW/cm². The solid line is a linear fit to the data points.

## 4.3.6 Discussion

We attribute the observation of the high-energy host emission in Figure 4.10, to a non-linear optical process that initiates by the quasi-cw laser excitation in the low-energy region of the spectrum, where the host possesses negligible absorbance.

Two-photon absorption of PF emission has been previously demonstrated by the exploitation of high excitation intensities in the region of GW/cm² [46]. In this work, the two-photon excitation experiment of PF2/6 has been performed by a pulsed laser, which had been delivering steep excitation pulses approximated by a δ-function temporal pulse profile with pulse duration in the order of 250 *fs* and excitation energy of 1.54 eV (805 nm). In this spectral region the one-photon absorption of PF is vanishing. Therefore the experiment described in [46] is an example of a simultaneous two-photon absorption process that is based on a virtual level located at energy equal to the half of the PF optical gap. Alternatively, two-photon absorption of high-energy pulses of short duration can lead similar effects, if the excitation is in resonance with an existing electronic level. This case of two-photon absorption reflects a sequential absorption mechanism that Figure 4.2 describes as the mechanism of optical limiting process.

On the other hand, two-photon excitation can be a result of a bimolecular process such a fusion of the reached excited states. For the case of conjugated polymers both singlet and triplet exciton-exciton annihilation effects are a common observation [47] (see also paragraph 3.4.1). The fact that presently, we observe up-conversion of the host emission by using excitation

intensities in the order of $kW/cm^2$ in quasi-cw excitation regime (200 *ms*), makes the existence of the virtual level mediated-excitation mechanism highly improbable. Similarly to our results, up-conversion of a relatively low intensity (10 $W/cm^2$) red (1.96 eV) laser light in films of poly(N-vinylpyrrolidone ) doped with xanthene dyes has yielded the generation of higher energy yellow fluorescence [48].

 The fluorescence quantum yield of PtOEP has been determined to be less than $2*10^{-5}$ [49]. Based on excited state absorption experiments performed by *ps* laser spectroscopy on PtOEP solutions in THF, the $S_1 \rightarrow T_1$ intersystem crossing time of PtOEP has been determined to have an upper limit of 15 *ps* [17]. In this work it was found that the lowest lying electronically excited triplet level of PtOEP has an observable lifetime that is greater than 50 *ns*. Moreover the triplet level lifetime of the similar porphyrin, Pt(etio) has been determined to be 63 *μs* [49]. More recently the electrophosphorescence lifetime of PtOEP embedded in PFO have been determined to be 51-56 *μs*, dependent on the variation of PtOEP loading in PFO (0.2% wt-8 wt% ) [8]. We have performed independent phosphorescent lifetime determination for PtOEP embedded in PF2/6. the results of which are presented in paragraph 4.5.2. Our data are in close agreement with the previously reported ones. Therefore we are convinced that after the optical excitation of our studied systems, the larger fraction of the photoexcitation has been converted to population of the first excited triplet state of PtOEP.

 Given the fact that the precursor state of the observed up-conversion is the PtOEP triplet state, there are four alternative excitation pathways that may lead to up-conversion of our low-energy excitation light. Namely, a) excited state triplet absorption within PtOEP. As it has been described in 4.1.4 porphyrins and porphyrinoids in general can exhibit the process of optical limiting, b) triplet-triplet annihilation within PtOEP, c) triplet energy transfer from PtOEP to PF2/6, followed by triplet-triplet annihilation within PF2/6 and d) thermalised backtransfer from PtOEP triplet state to PF2/6 singlet state (E-type fluorescence, see Chapter 1). All four alternative excitation pathways are depicted schematically in Scheme 4.5.
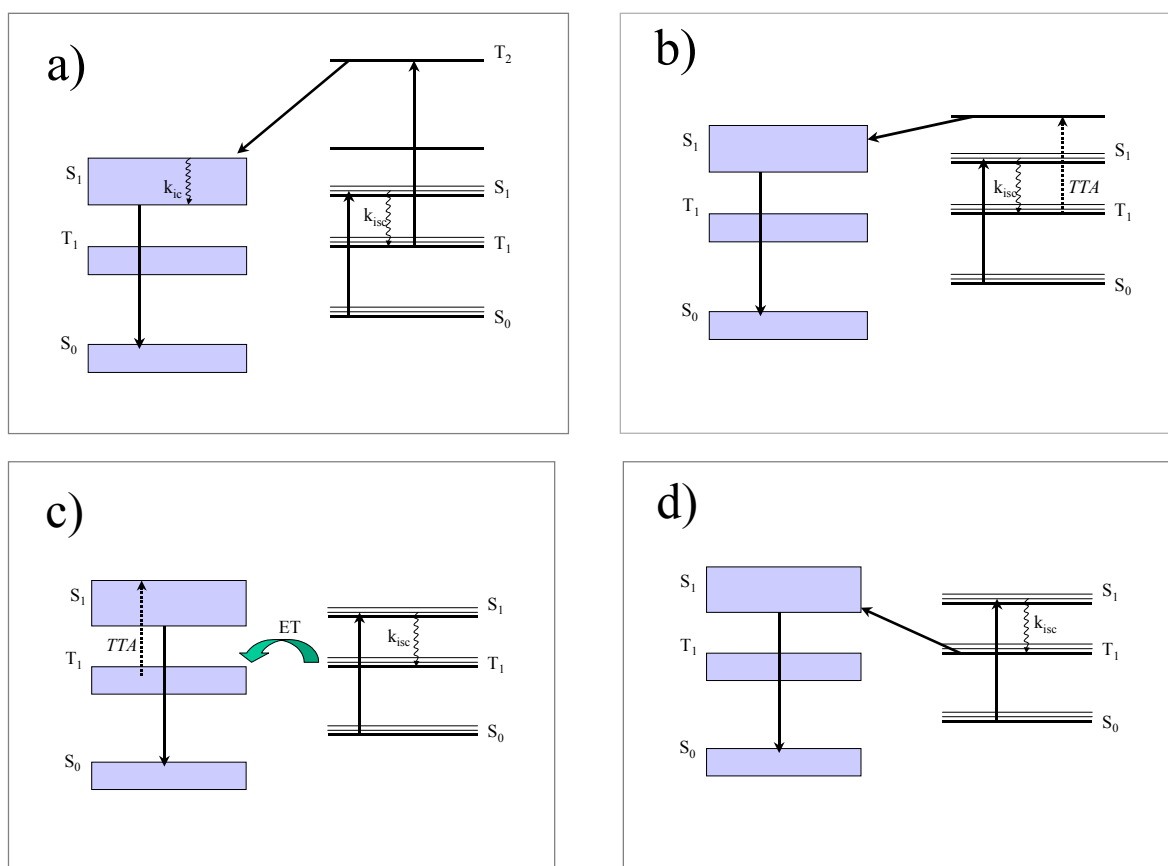
Scheme 4.5: The alternative energetic pathways that may lead to the observed up-conversion in the films of PF2/6:Me(II)OEP studied. Thin lines represent PtOEP levels, thicker lines represent PF2/6 levels. After excitation of PtOEP at 532 nm a) optical limiting takes place that is followed from energy transfer from PtEOP to PF2/6, b) fast ISC takes place that is followed by TTA within PtOEP molecules. Subsequently singlet-singlet energy transfer occurs from PtOEP to PF2/6, c) after ISC in PtOEP triplet-triplet energy transfer takes place from PtOEP to PF2/6. Subsequently TTA within PF2/6 molecules occurs, d) thermalised transfer occurs from the triplet manifold of PtOEP to the singlet manifold of PF2/6. See text for discussion.

The assumption that up-conversion process initiates from the lowest triplet excited level of the porphyrin molecules is further supported from the fact that the efficiency of the process is increased when the population of the porphyrin triplet level becomes more efficient. Effective triplet level population can occur when the singlet-triplet $k_{ISC}$ intersystem crossing rate will be enhanced and thus an increased spin-flipping rate can be obtained. The increase of this rate is assisted by spin-orbit coupling interactions in the presence of heavy atoms. Since a laser wavelength of 532 nm was employed for the excitation of the system, a shift of the porphyrin Q-absorption bands towards the 532 nm region would also enhance the up-converted emission. This is why larger up-conversion PL integrals of poly(fluorene) are obtained for the case that the heavy PtOEP was used as dopant. Therefore the intensity of the obtained up-conversion efficiency can be, in principle, expressed as:

$$I_{up-conv} = \phi * \varepsilon_{532nm} * k_{ISC} \qquad \text{(eq. 4.6)}$$

where $\varepsilon_{532nm}$ represents the extinction coefficient of the employed metalloporphyrin for the 532 nm excitation, $k_{ISC}$ the ISC rate of this metaloporphyrin derivative and $\phi$ the fraction of the created triplet excited states that participate in the triplet-triplet fusion process, which leads to up-conversion of the host emission. The efficiency $n$ of ISC process is directly related to the $k_{ISC}$ through $n = \dfrac{k_{ISC}}{\sum_i k_i}$, where $\sum_i k_i$ includes all the possible deactivation channels of the first electronically excited singlet state $S_1$ of the metaloporphyrin derivative, after the absorption of the 532 nm photon.

According to Scheme 4.5a an alternative excitation pathway leading to up-conversion is the excited state triplet absorption. This alternative is plausible as the duration of our excitation pulse is much more longer than the intersystem crossing rate of PtOEP (~15 ps [17] ). However, it has been argued that in case that this excitation channel would be the origin of up-conversion it should exhibit a quadratic dependence on the excitation intensity [48]. Figure 4.13 shows that the up-conversion emission integral depends virtually linearly from the excitation intensity. Therefore the excited state triplet absorption should not be the channel for the energy back transfer to PF. Moreover, previous photoinduced absorption spectroscopy performed for blends of PFO:PtOEP have revealed that PtOEP exhibits excited triplet absorption at an energy range between 1.5–1.7 eV [8]. No indication of excitation absorption features at 2.33 eV, the region where our excitation laser operates, have been reported. Further discussion on the linear dependence of the up-conversion process on the excitation intensity, is presented in paragraph 4.4.3. We also present excited state absorption spectra of PtOEP solutions in toluene in paragraph 4.6.5.

Based on the observed temperature dependence of up-conversion we can also exclude the alternative excitation channel of the E-type activation (see in Scheme 4.5d). If indeed thermal activation of the singlet level of PF would occur by the triplet state of PtOEP, we should observe a decrease in the determined up-conversion integral at lower temperatures. Instead, Figure 4.14 shows that up-conversion is favoured at lower temperatures, indicating the importance of the PtOEP triplet level lifetime for the process. The lifetime of PtOEP has been found to increase by a factor of two on going from 295 K to 77 K [49]. For the moment we can not attribute the observed increase of the up-conversion efficiency only to the increased lifetime of PtOEP. Low temperature absorption spectra of PtOEP should be recorded in order to study the impact of $\varepsilon_{532nm}$ extiction coefficient in PtOEP. Previous temperature dependent optical density

measurements for Pb-containing *meso*-tetra-alkynyl porphyrin have shown the existence of a temperature dependence component in the optical density of the material studied [50]. At this stage of our knowledge we consider a combination of presses like the increase of PF quantum yield, the prolonged PtOEP triplet level lifetime and morphological changes in the film to be responsible for the observed increase of the up-conversion process. We should emphasize the fact that the temperature range that we investigated is too short for extracting conclusion regarding the activation $E_a$ of the up-conversion efficiency. A larger temperature range needs to be explored in order to conclude on the exact temperature dependent character of the up-conversion. It is expected that at lower temperatures much more up-conversion integrals can be obtained. The observable triplet lifetime of PtOEP has been determined to be 700 $\mu s$ at 5 K[10] therefore higher probability for efficient triplet-triplet annihilation leading to up-conversion, may exist at this temperature.

## 4.4 EXTENDING THE UP-CONVERSION PROCESS TO OTHER BLUE EMITTING HOSTS

So far it has been demonstrated that a photon-energy up-conversion process is operative in films of PF2/6 blended with small amounts of metallated porphyrin derivatives. The participation of PtOEP triplet states as the precursor levels of a bimolecular process that leads to triplet-triplet annihilation events has been identified.

In the following we demonstrate that the up-conversion process is operative in films based on a broad range of polymeric blue light emitters.

### 4.4.1 Experimental

A series of blue emitters was used as hosts to be doped with trace amounts of PtOEP in such a way that the resulting HOST:PtOEP series had dopant concentration of the order 0.1% wt, 0.3 wt%, 1 wt%, 3 wt%, 10 wt%. Chart 4.2 presents the chemical structures of the host polymers. The $M_n$ and D values of all the materials tested are given in Table 4.6.

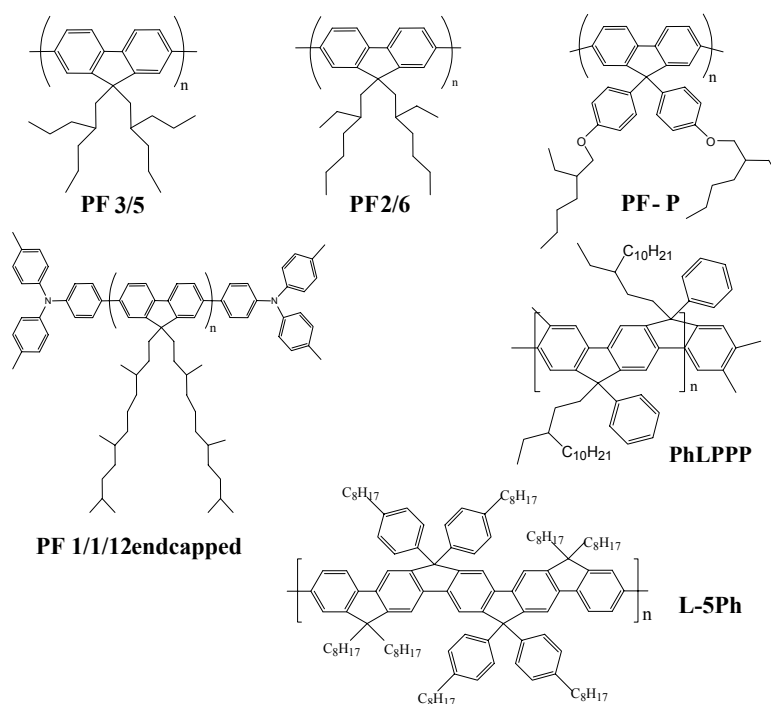| HOSTS | $M_n$ (gr/mole) | D |
|---|---|---|
| PF2/6 | $9.1*10^4$ | 2.08 |
| L-5Ph | $2.64*10^5$ | 2.79 |
| PhLLLP | 11460 | 1.54 |
| PF-P | $2.1*10^5$ | 2.19 |
| PF 3/5 | $3.2*10^4$ | 2.04 |
| PF 1/1/1/12am5 | $2.24*10^4$ | 2.37 |

Table 4.6: The polymer used as hosts and the $M_n$, D values.



Chart 4.2: The chemical structures of the polymer used as hosts.

For preparing the studied samples, five differently concentrated solutions of PtOEP were prepared by subsequent dilution of an initial PtOEP solution with concentration of 2.5 mg/mL. The mother solution had been stirred for 20 min and filtered with a 0.45 μm pore diameter hydrophobic filter. Toluene was used as solvent, after degassing in Ar with concomitant ultrasonication for 15 min. In order to obtain the PtOEP mass needed for the preparation of the mother solution, PtOEP material of 98 % purity was used. In order to obtain the targeted concentration that the second column of Table 4.7 shows, subsequent dilutions of the mother solution were perfored, as eq. 4.7 describes. From the mother solution a fraction of volume was obtained ($V_i$=0.5 mL) and diluted with a volume of toluene $V_i$ up to a final volume $V_f$. This process was iteratively repeated for each new solution that was prepared.

$$C_i * V_i = C_f * V_f \text{, where } V_f = V_i + V_x \text{ and } V_i = 0.5 ml \qquad \text{(eq. 4.7)}$$

The five different PtOEP concentrated solutions are shown in Table 4.7.

| wt % | $C_{PtOEP}$ (mg/mL) | $m_{PtOEP}$ (mg) | $V_f$ (mL) | $V_i$ (mL) | $V_x$ (Toluene mL) |
|------|------|------|------|------|------|
| 10 | 2.550 | 4.000 | 1.567 | 1.567 | - |
| 3 | 0.850 | - | 1.500 | 0.5 | 1.000 |
| 1 | 0.260 | - | 1.635 | 0.5 | 1.135 |
| 0.3 | 0.080 | - | 1.625 | 0.5 | 1.125 |
| 0.1 | 0.020 | - | 2.000 | 0.5 | 1.500 |

Table 4.7: The wt% values of PtOEP used for the doping the studied host films, together with the concentration of each PtOEP solution prepared. The appropriate volumes $V_i$ and $V_x$ as indicated from eq. 4.7 are given.

The solutions of the different hosts were similarly prepared by diluting an initial mass of each host in freshly degassed and ultrasonicated toluene in order to obtain a soution of 10 mg/mL. A hydrophobic micro filter of 5 μm pore diameter was used for filtering each of the polymer solutions that were prepared. The amounts of polymer and PtOEP solution that were mixed for obtaining the final solutions of Host:PtOEP mixtures are given in Table 4.8.

| wt % | $m_{host}$ (mg) | $V_{host}$ (mL) | $m_{PtOEP}$ (mg) | $V_{PtOEP}$ (mL) | $m_{total}/V$ (mg/mL) |
|------|------|------|------|------|------|
| 10 | 2.250 | 0.225 | 0.255 | 0.100 | 7.7 |
| 3 | 2.680 | 0.268 | 0.085 | 0.100 | 7.5 |
| 1 | 2.475 | 0.248 | 0.026 | 0.100 | 7.2 |
| 0.3 | 2.758 | 0.276 | 0.008 | 0.100 | 7.4 |
| 0.1 | 2.498 | 0.250 | 0.002 | 0.100 | 7.1 |

Table 4.8: The appropriate mixed volumes of the PtOEP and PF2/6 solutions, together with the corresponding masses of the components are given.

The final solutions were shaken for 20 min. Then, the solutions were spin coated onto appropriately cleaned quartz substrates. Spin coating took place at a rotational speed of 1200 rpm within 60 sec.

## 4.4.2 Testing for up-conversion in different polymeric hosts

Figure 4.15 shows a representative comparison of up-conversion for all the hosts that were tested as active matrices for doping with PtOEP. The characteristic blue emission of each of the hosts was observed upon excitation at 532 nm, the main $S_0 \rightarrow S_1$ transition of PtOEP. Once more it has to be stated that absorption spectra of all the polymeric hosts did not show any absorption feature at the energies lower than 500 nm. Hence no direct electronic excitation of the host matrices is taking place upon excitation at 532 nm. From Figure 4.15 it becomes evident that that L-5Ph [51] host exhibits significantly stronger up-conversion emission intensity in comparison with all of the other hosts tested.
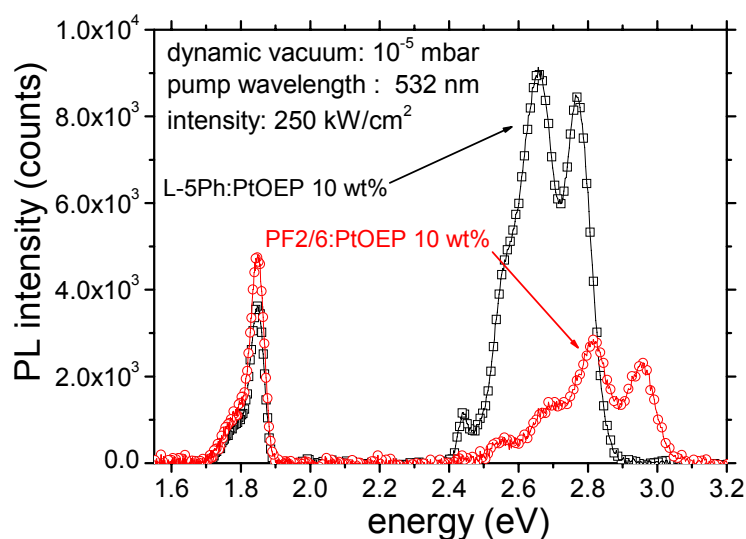
Figure 4.15: Up-conversion emission observed for L-5Ph (squares) and PF2/6 (circles) doped with 10 wt% PtOEP. The measurement performed at room temperature and pressure ~ $10^{-5}$ mbar. Excitation at 2.33 eV (532 nm).

## 4.4.3 Excitation intensity dependence in the different hosts

We performed excitation intensity dependence measurements in a series of doping concentrations of PtOEP in three of the most representative classes of bridged poly(*p*-phenylene) derivative presented in Scheme 4.2. The analysis of the obtained experimental results provides further evidence for the existence of a bimolecular electronic process such as triplet-triplet fusion, that may be involved in the generation of the up-conversion. Additionally, the optimum doping concentration is deduced in regard to the maximum ratio of blue/red emission integrals.

Since emission of light has been detected in a spectral region of higher energy than the excitation energy used, an uphill photon process must be involved that is related to a bimolecular interaction of two excited porphyrin molecules. In principle multi-photon processes are recognised from the characteristic power dependence patterns of the emission intensities that correspond to the level that participate in the studied processes. Figure 4.16 shows the intensity dependence of both PdOEP and PF2/6 emissions of a PF2/6:PdOEP 10 wt% film on quartz. It is obvious that PdOEP emission follows a sub-linear dependence on the excitation laser intensity, similar to the one presented in the inset of Figure 4.4. In contrast to this behaviour, the excitation intensity dependence of the up-conversion host emission is found to have a virtually linear character.
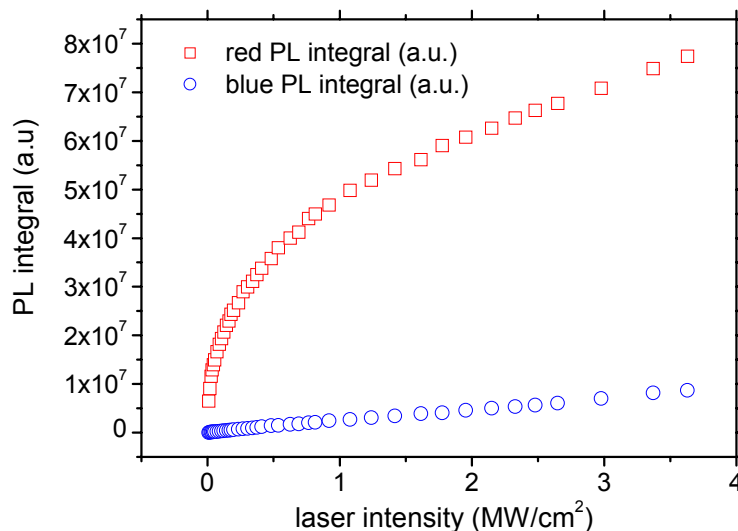
Figure 4.16: The excitation intensity dependence of PdOEP phosphorescence spectral integral (circles) and the up-conversion spectral integrals of PF2/6 (circles) obtained for a film of PF2/6:PdOEP 10 wt% for excitation at 2.33 eV (532 nm). The measurement performed at room temperature and pressure ~ $10^{-5}$ mbar. Excitation intensity units are in MW/cm$^{-2}$.

We performed a systematic investigation of excitation dependence on a series of hosts, similar in structure to PF2/6, doped with PtOEP. This metalloporhyrin derivative is found to be more efficient in exhibiting up-converted emission of the host. The emission intensity behaviour of both of the components could be recovered with a function of the type:

$$I_{PL} = 10^a * (I_{exc.})^b \Leftrightarrow \log(I_{PL}) = a + b * \log(I_{exc.}) \qquad \text{(eq. 4.8)}$$

Particularly for L-5Ph and PhLLLP, a range of PtOEP doping concentrations were investigated. Figures 4.17 qand 4.18, illustrate the power dependence of PtOEP and host up-converted emission for thin films on quartz that correspond to 3 wt% PtOEP doping. From the fitting process performed on the presented data, it established that a quasi-quadratic relationship exist between the PtOEP and the host emission.
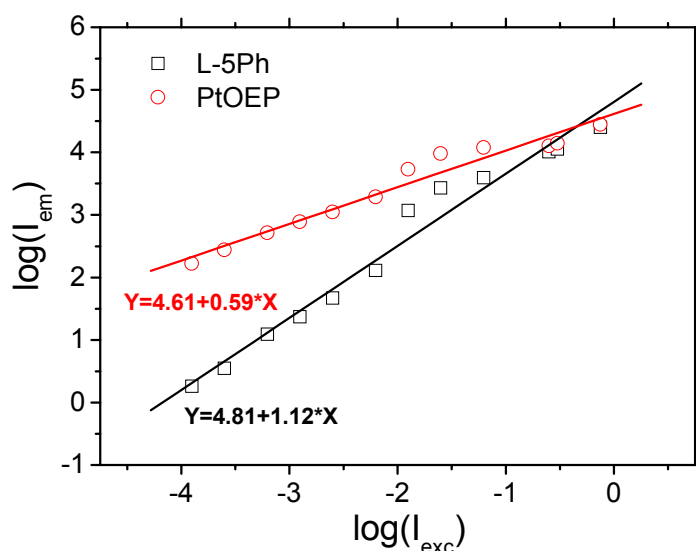
Figure 4.17: The excitation intensity dependence of PtOEP phosphorescence spectral integral (circles) and the up-conversion spectral integral of L-5Ph (squares) obtained from a film of L-5Ph:PtOEP 3 wt% studied. The measurement performed at room temperature and pressure ~ $10^{-5}$ mbar. Excitation intensity units are in MW/cm$^{-2}$, for excitation at 2.33 eV (532 nm). The lines are fits to the data.
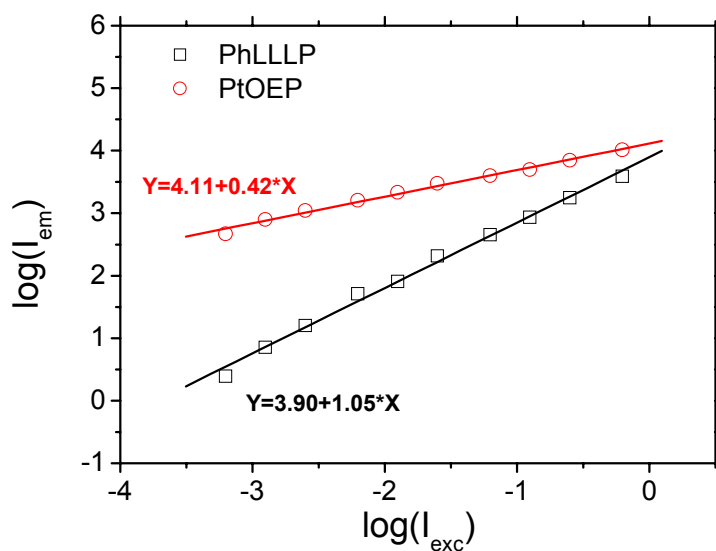


Figure 4.18: The excitation intensity dependence of PtOEP phosphorescence spectral integral (circles) and the up-conversion spectral integral of L-5Ph (squares) obtained from a film of PhLLLP:PtOEP 3 wt% studied. The measurement performed at room temperature and pressure ~ $10^{-5}$ mbar. Excitation intensity units are in MW/cm$^{-2}$, for excitation at 2.33 eV (532 nm). The lines are fits to the data.

$$\log(I_{exc}) = A + B * \log(I_{em}) \Leftrightarrow$$

$$\log(I_{exc}) - A = \log(I_{em})^B \Leftrightarrow$$

$$\log(I_{exc}) - \log A^{'} = \log(I_{em})^B \Leftrightarrow$$

$$\log\left(\frac{I_{exc}}{A^{'}}\right) = \log(I_{em})^B \Leftrightarrow$$

$$\frac{I_{exc}}{A^{'}} = (I_{em})^B \Leftrightarrow$$

$$I_{exc} = A^{'} * (I_{em})^B \Leftrightarrow$$

$$I_{exc} = 10^A * (I_{em})^B$$

$$\text{since } A = \log A^{'} \Leftrightarrow A^{'} = 10^A$$

In the above presented expression, coefficient $A^{'}$, represents the up-conversion PL emission integral of the host that is obtained for excitation intensity $I_{exc}$ corresponding to 1 MW/cm$^2$. Therefore the value A which results from the fitting procedures of Figures 4.17 and 4.18 can be used as reference value for the rough estimation the relative up-conversion efficiency in different hosts.

| Host:PtOEP 3 wt% | A | $I_{up\text{-}conv}$ integral (a.u) |
|---|---|---|
| PF2/6 | 4.20 | 15849 |
| 5-LPh | 4.81 | 64565 |
| PhLLLP | 3.90 | 7943 |
| PF-P | 4.27 | 18621 |
| PF 3/5 | 4.05 | 11220 |
| PF 1/1/1/12am5 | 3.65 | 4467 |

Table 4.9: The values of term A as extracted from the fitting of the data by using eq.4.8 and the corresponding up-conversion integrals (see text).

## 4.4.4 Doping concentration dependence in the different hosts

Up-conversion has been observed in the whole series of doping concentrations for all hosts used for the preparation of the blends with PtOEP. Figure 4.19 illustrates a representative example of a family of curves, for the excitation intensity dependence of the PL integral ratio between the up-conversion emission and the emission of PtOEP. It is once more underlined that the range of

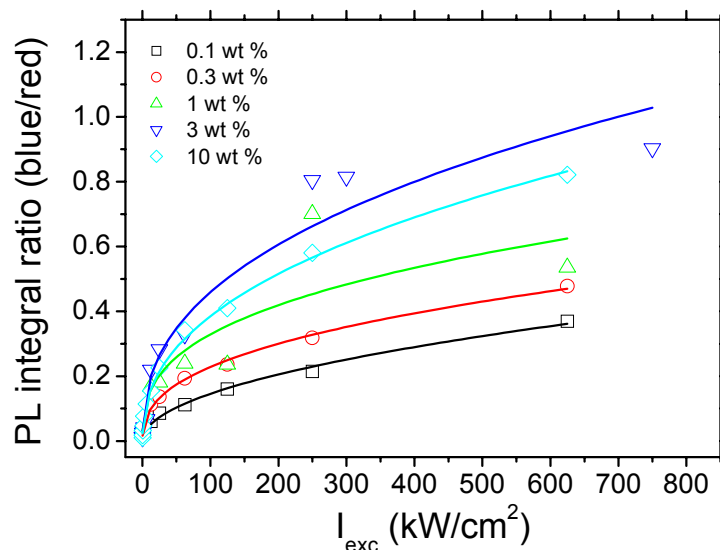excitation intensities used for the observed trend of PL integral ratio was within the order of kW/cm$^2$.



Figure 4.19: A family of excitation intensity dependence curves, obtained for films of L-5Ph:PtOEP. The curves are parameterised on the doping concentration of PtOEP in the films. The measurement performed at room temperature and pressure of ~10$^{-5}$ mbar. Excitation intensity units are in kW/cm$^{-2}$, for excitation at 2.33 eV (532 nm). The lines are fits to the data.

By parameterising the excitation dependence of the PL integral ratio on the doping concentration, the optimum doping concentration of PtOEP in the host can be extracted, that corresponds to the maximum PL integral ratio obtained. Figures 4.20 and 4.21 illustrate the dependence of the PL integral ratio for the cases of L-5Ph and PhLLLP host matrices.
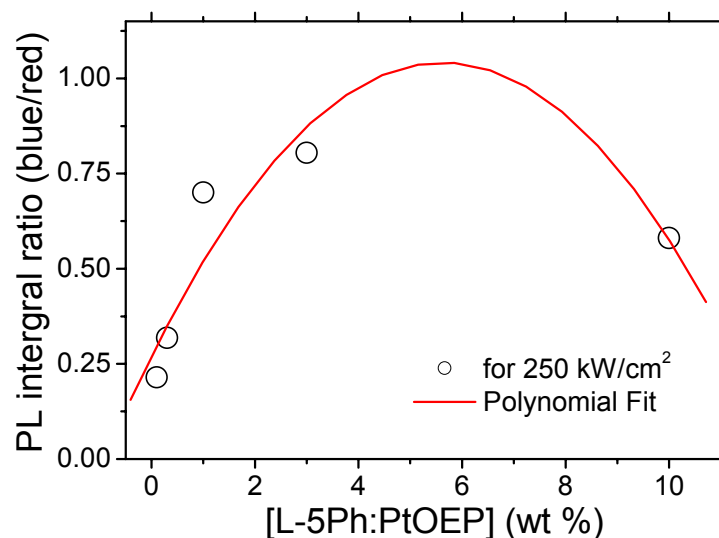
Figure 4.20: The dependence of the determined up-conversion spectral integral on the doping concentration of PtOEP, in films of L-5Ph:PtOEP on quartz substrate (circles). Excitation was at 532 nm (2.33 eV), excitation intensity was 250 kW/cm$^2$. The measurement performed at room temperature and pressure of ~10$^{-5}$ mbar. The line is a polynomial fit to the data.

Comparison of the maximum PL integral ratios for the case of L-5Ph and PhLLLP, shows that L-5Ph is much more efficient in exhibiting up-converted blue emission. This observation that the up-converted PL integral of L-5Ph corresponded to stronger PL intensity than that of PF2/6 further manifests that L-5Ph host exhibits unusually large up-conversion efficiency (see also Figure 4.15).
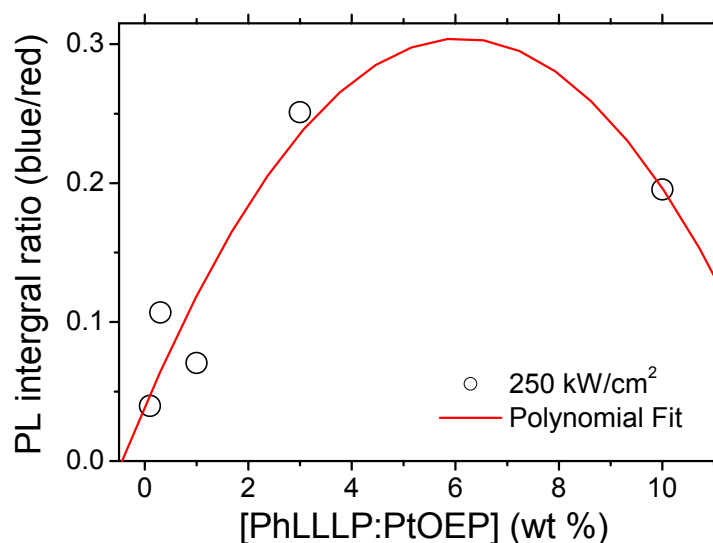
Figure 4.21: The dependence of the determined up-conversion spectral integral on the doping concentration of PtOEP, in films of PhLLLP:PtOEP on quartz substrate (circles). Excitation was at 532 nm (2.33 eV), excitation intensity was 250 kW/cm$^2$. The measurement performed at room temperature and pressure of ~10$^{-5}$ mbar. The line is a polynomial fit to the data.

## 4.4.5 Discussion

The experimental results of this section have unambiguously proven that the up-conversion process that has been described in Section 4.3 for blends of PF2/6:MeOEP can be further extended in a broad range of blue light-emitting polymer hosts. Up-conversion is kinetically related to the metaloporphyrin derivative by using the excited triplets of MeOEP as the precursor states. Therefore it is not surprising at all that this non-linear optical process is found to follow a quasi-linear excitation dependence character instead of possessing the typical quadratic excitation dependence character. The excitation intensity dependence measurements that have been presented in this section support the notion that excited state triplet absorption within the PtOEP molecules can not be the excitation pathway that leads to the electronic activation of the hosts [48].

From the fitting of the excitation intensity dependence data, the parameters of Table 4.9 have been determined that allow a rough estimation for the relative up-conversion efficiency of the host in which PtOEP is embedded. It has to be mentioned though that comparison of the values of Table 4.9, requires the condition that the trend of the excitation dependence remains the same in the whole range of the tested pumping intensities. Moreover, by doing this comparison, we have assumed that all the investigated hosts exhibit the same stability in their emission profile during the illumination time of the laser spot onto the films surface. However this is not practically true, as we had to reduce the illumination time dependent on the measured doped

host, in order to obtain the same intensity of the up-conversion emission. This may be related mostly with the thermal stability of the host that is used as the active electronic matrix and consequently must be related with its $T_g$ value. Local temperatures on the film, in the region of area which illuminated by the laser, may result in phase separation effects that eventually can lead to PtOEP aggregation. This process will reduce the up-conversion efficiency. Our up-conversion concentration dependence results in Figures 4.20 and 4.21 agree with the results we obtained from TEM, regarding the existence of a critical doping concentration beyond which aggregation effects in PtOEP molecules start to occur. Similar indication for PtOEP concentration quenching have been observed before [7]. Presumably due to this concentration quenching, up-conversion is negatively affected.

We emphasize that the presented data are coming from measurements obtained for films of unequal thickness values. Thickness of the measured film is a crucial parameter that defines the impact of the oxygen in the measured up-converted process. PtOEP has been reported as an efficient oxygen sensor [31]. As the precursor levels for the up-conversion process are those of the triplet excited state in the metaloporphyrin derivatives, we attribute partially the differences of the up-conversion emission efficiency, for different hosts, to the different permeability of oxygen molecules into the measured films that is determined from the film thickness.

Finally the chemical purity of the host materials measured is another parameter that has to be considered regarding the efficiency of the up-conversion process. As it has been discussed in Chapter 2, the chemical purity of bridged-PPP derivatives is dramatically influenced from the presence of chemical defects on the polymeric backbone that tend to reduce the PL efficiency of the host material. Therefore, even if all the parameters that influence up-conversion efficiency would be the same, a host containing chemical defects would be less efficient than another one that would be prepared by more rigorous synthetic routes. The issue of stability of the up-converted process in each of the host studied, is related to parameters that are both intrinsic and extrinsic to the active host in which the dopant has been embedded into.

Based on the experimental results of this Section we continue the discussion of paragraph 4.3.6 on the nature of the up-conversion mechanism. It is very likely that two PtOEP molecules that are in the lowest lying excited triplet level interact via a triplet-triplet annihilation process in order a higher excited singlet PtOEP level to be reached. This higher singlet level must presumably be the second excited singlet $S_2$ of PtOEP, which is responsible for the PtOEP Soret absorption band in the blue region of the absorption spectra. Eventually, this level is isoenergetic to, if not higher than the first excited singlet level of the host and therefore energy transfer is possible from electronically excited PtOEP[*] to matrix molecules. The nature of this energy

transfer process can involve a dipole-dipole interaction similar to the Förster type or the formation of a highly excited exciplex between PtOEP and the host. Charged intermolecular species between PtOEP or related porphyrin derivatives and fullerenes have been detected by laser flash photolysis [23], [24].

So far our experimental results can not distinguish whether the occurrence of triplet-triplet annihilation process is taking place in PtOEP molecules or in the host molecules after the electronic excitation as Scheme 4.5b and 4.5c, respectively. For the elucidation of this matter the dynamics of the up-conversion process need to be determined and to be compared with the inherent phosphorescence kinetics both of a neat polymer host and a neat PtOEP. This subject is discussed in the following section.

## 4.5  DYNAMICS OF THE UP-CONVERSION PROCESS

So far the presented experimental evidence of the previous paragraphs, support the occurrence of a bimolecular photophysical process that leads to up-conversion of the low-energy excitation, in films of bridged-PPP derivatives that are blended with trace amounts of metaloporphyrin complexes.

The precursor states that participate in this bimolecular process are triplet excited states of the dopant molecules. The observation of the characteristic high-energy emission of the host after excitation at the low-energy absorption band of the phosphorescent guest, suggested the participation of the lowest electronically excited triplet manifold of the guest as source of the activation of the host emission. This suggestion was supported by demonstrating the temperature depended character of the process of up-conversion (Section 4.3.5). Finally, the experimental results of the excitation intensity dependence of the observed up-conversion emission gave evidence for the biphotonic character that the mechanism of up-conversion process posses (Section 4.4.3).

If in these studied systems, the up-converted photons are a result of triplet-triplet annihilation that occurs between the dopant molecules, the decay transient of the up-converted emission should decay twice faster as the phosphorescence of the metalloporhyrin derivative that is incorporated in the matrix of the host (see paragraph 3.4.1.2) . Similarly, in the case that up-conversion takes place in the host matrix, its kinetics should be related with the phosphorescence kinetics of the host.

In an early study, the room temperature observable phosphorescence lifetime of PtOEP has been determined to be greater than 50 *ns* [17]. Due to the limited dynamical range of their equipment, the authors speculated that PtOEP should resemble the lifetime of Pt(etio) porphyrin and thus

they reported a triplet lifetime of 63 *μs* for PtOEP, in THF solutions. Later on for the case of PtOEP embedded in inert poly(styrene), a triplet lifetime of 21 *μs* has been reported [31] together with a phosphorescent yield value of 0.5. The measurement was performed in air and probably this is the reason of the short value of the reported PtOEP lifetime. Another determination of PtOEP triplet lifetime has been reported for measurements of photoinduced absorption spectroscopy [7]. Again poly(styrene) was used as an inert matrix in which PtOEP was embedded at different doping levels. For 1% wt and 4% wt a room temperature triplet lifetime of 204 *μs* and 170 *μs* has been determined, respectively, for a pump pulse of 3.42 eV (363 nm). Although the authors did inform whether these experiments have been performed in vacuum or not, their reported values are unexpectedly high. With the same experimental conditions a PFO was used as a matrix for 1% wt PtOEP loading and the determined triplet lifetime has been found to be 56 *μs* [8]. This value agreed with triplet PtOEP lifetime values as determined by monitoring the PtOEP phosphorescence that was pumped optically or electrically [8]. The large deviation between triplet lifetime of PtOEP embedded in an electronically active matrix as PFO and an inactive one like PS indicate the existence of an energy transfer channel from PtOEP to PFO.

 The triplet lifetime of PF derivatives has also been reported. Initially the phosphorescence lifetime of PFO as determined from pulse radiolysis experiments in benzene solutions, has been reported to be 108 *μs* [52]. Studies of optical excitation (3.05 eV ~ 407 nm) of vitrified PF2/6 solutions at 80 K have reported a phosphorescence lifetime of 1 *sec* [53], [54], whereas at the same temperature, PF2/6 films have been found to have phosphorescence and delayed fluorescence lifetimes equal to 0.8 *sec* and 0.4 *sec*, respectively, after excitation at 3.49 eV (355 nm) [54]. The same studies have found that the delayed fluorescence of PF2/6 films at room temperature decays quadratically in time [54]. In a very recent study [55], the electrophosphorescence and delayed electroluminescence of a light-emitting device based on endcapped PF2/6 derivatives have been reported to be as long as 217 *μs* and 97 *μs*, respectively at 28 K. However, the registration of these emissions was set to begin after a time interval longer than 60 *ms* post the electrical pulse. Therefore the electrophosphorescence was long lived with a lifetime of the order of *ms*, as previously seen for the low temperature optical excitation results [54]. In the case where photo induced absorption has been employed for the triplet lifetime determination of PFO, large deviations from the previously mentioned data exist. For a neat PFO film the low temperature (80 K) and for excitation at 3.42 eV (363 nm), the PFO triplet lifetime has been reported to be 2.5 ms whereas in the case of doping PFO with 8 wt% PtOEP the triplet lifetime has been found to increase to 4 ms, with a concomitant increase of PFO triplet yield [7].

In both cases of doped and pristine PFO a second component of 15 % weighting has been found with a lifetime of 0.1 ms. For room temperature photo induced absorption experiments and for excitation at 3.42 eV (363 nm), the triplet emission of neat PFO has been reported to decay biexponential with a 72% weight component of 3.2 ms and a 28% component of 0.3 ms [8]. More importantly, in [8] it was shown that these values did not change when doping PFO with 8wt % PtOEP. The authors have not yet given a reason why the phosphorescence lifetime of neat PFO has been found to decrease at lower temperatures.

In order to parameterise the phosphorescence lifetime of PtOEP on the doping concentration, in the system of our interest, we performed phosphorescence lifetime concentration depended measurements on blends of PF2/6:PtOEP. The samples measured were the same as the ones used for the time resolved PL experiment presented in paragraph 4.2.3 (Figure 4.5). Additionally the up-conversion dynamics of two different polymer host doped with PtOEP at 3 wt% are determined.

## 4.5.1 Experimental

The phosphorescence dynamics of PtOEP and the up-conversion emission dynamics of PF2/6 are relatively long-lived radiative processes that occur in the kHz frequency range. Slow repetition rate of excitation source and registration system are sought that can operate in a period much more longer than at least five times the period of the probed emissive process. Since PtOEP and the related metaloporphyrins have phosphorescence lifetimes in the order of ~ 1 *ms*, an excitation source with repetition rate close to 200 Hz or slower would be appropriate for following the dynamics of these emissions.

The set up used for the investigation of long-lived luminescence processes is depicted in Scheme 4.6. The measured samples were kept in the chamber that section 4.3.1 has described. Excitation of the samples was performed with the first order deflection of the 532 nm laser line of a Verdi V10 solid state laser (see 4.3.1. section). An acousto-optic modulator was employed for modulating the excitation wavelength by the contribution of the acoustical field. The chosen wavelength-modulation resulted in a periodic deflection of the excitation wavelength, with a deflection period close to 500 *μs*. By using the deflection period as the excitation pulse width and by delivering pulses with a repetition rate of 200 Hz, a 10% duty cycle of the modulation was established, resulting in periodic excitation of the samples that allowed phosphorescence lifetime measurements. An arbitrary waveform generator (TTi 40 MHz Arbitrary Waveform Generator, TGA1242) was used for gating the modulation of the acousto-optic modulator. The wavefunction signal produced by the arbitrary waveform generator was sent as modulation

function to a high frequency generator (150 MHz). The synthesised function was amplified from a high frequency amplifier and applied on the acousto-optic modulator.

Like in the experimental set-up described 4.3.1, the excitation and emission was inherently coinciding on the same focal spot of the measured samples. After collecting the emission signal, appropriate mirrors of low transmittance in the region of 532 nm were used for extinguishing the 532 nm excitation intensity residue. Additionally, a 532 nm Notch filter ( 3 nm stop band spectral width) was used in order to ensure that the excitation intensity residues were vanished before detection.

Dielectric beam splitters (DMB) were used for the separation of emission signal to the spectral regions of interest, before the detection system. The latter was composed from three different photo multipliers (PM), each of them aiming for the collection of a different spectral region of the collected emission. Broadband interference filters (IF) were positioned in front of each of the PMs to ensure filtering of the wavelengths that were not of interest. The width of IFs was in the range of ~50 nm. Especially for the case where the detected area was in the region of 532 nm, a second Notch filter for 532 nm was employed. The temporal resolution of the employed PMs was 2 *μs*, while the dynamical range was in the order of 1:2500.

All three signal of the PMs were read out and digitally stored by using cables (C) of 2kΩ loading resistance for connecting the PMs with an oscilloscope ( 100 MHz, AGILENT, 54622A). Subsequently, the signals were sent to a personal computer for further processing.
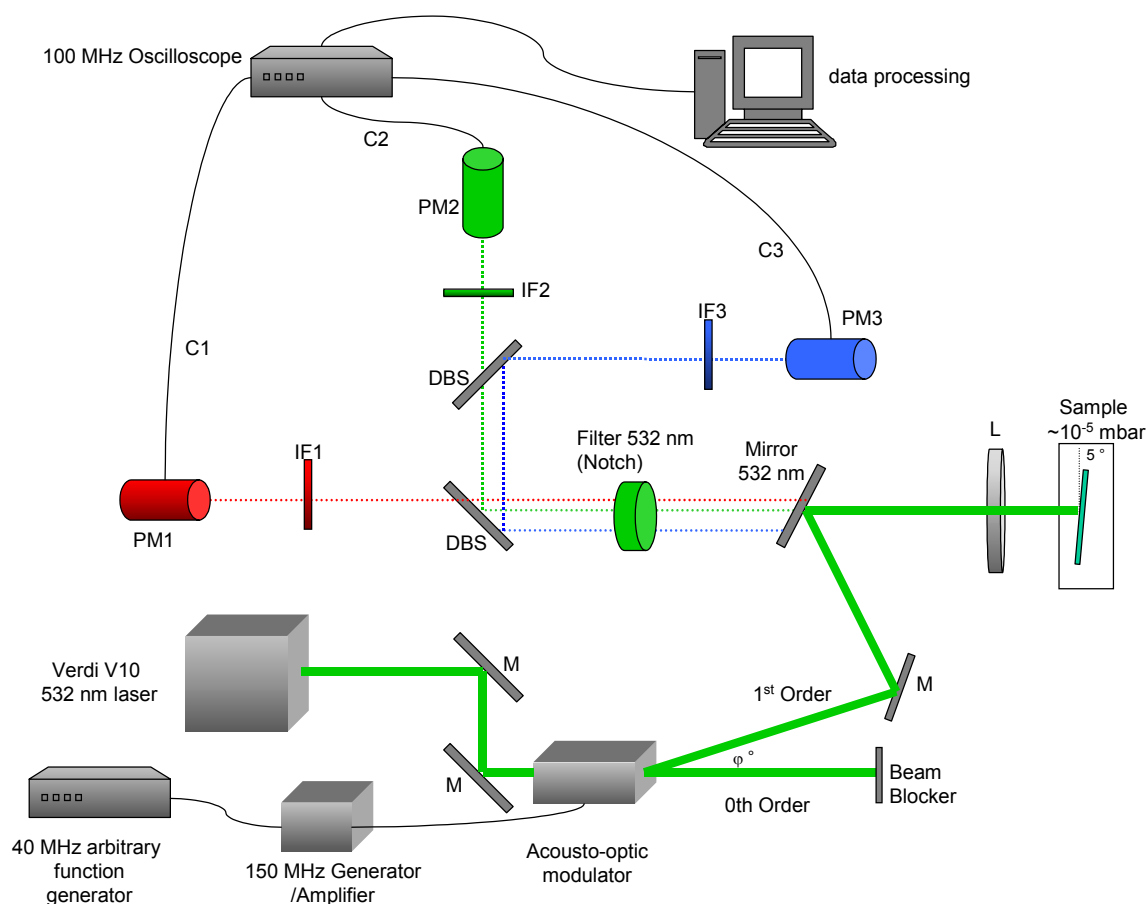
Scheme 4.6: A schematic representation of the set-up that was used for the probing of the up-conversion dynamics (see text).

## 4.5.2 Results

From the discussion presented in paragraph 4.4.5, it is clear that the phosphorescence lifetime of the MeOEP incorporated in the blends of the blue emitting hosts influences substantially the photo kinetic behaviour of the up-converted excited state. Figure 4.19 shows the dependence of PtOEP lifetime on the concentration doping of the films. As a reference, the phosphorescence lifetime of PtOEP dispersed by 10 wt% in an electronically inactive PS matrix is presented.
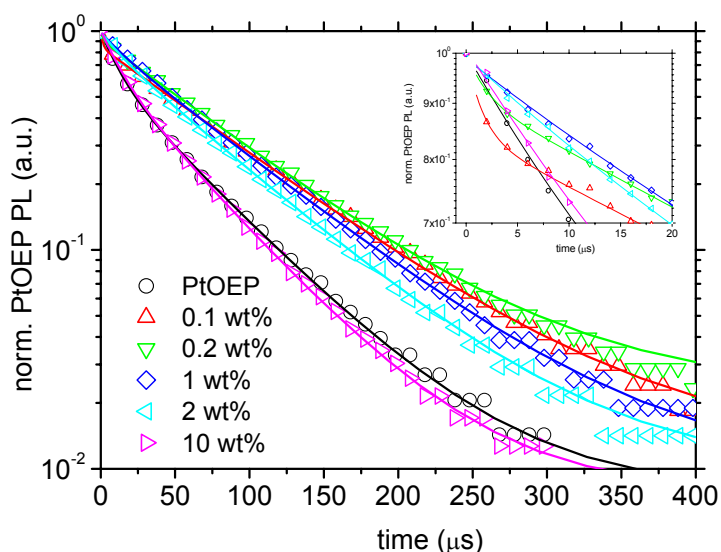
Figure 4.22: Room temperature normalised decay transients monitoring the PtOEP phosphorescence emission of the PtOEP doped PF2/6 films (see text for specification of the monitored spectral area). Excitation was at 532 nm (2.33 eV), at room temperature. The inset is a magnification in the first 20 $\mu s$ of the transients. Pressure was kept at ~$10^{-6}$ mbar. Lines are fits to the data.

The PtOEP phosphorescence decay transients that Figure 4.22 presents are better recovered by a biexponentially decay function. Table 4.10 informs that the lifetime values decrease with increasing doping concentration.

| PF2/6:PtOEP wt % | $A_1$ | $\tau_1$ ($\mu s$) | $A_2$ | $\tau_2$ ($\mu s$) |
|---|---|---|---|---|
| 0.1 | 0.83 | 88 | 0.16 | 2 |
| 0.2 | 0.89 | 84 | 0.09 | 2 |
| 1 | 0.88 | 82 | 0.10 | 17 |
| 2 | 0.85 | 74 | 0.12 | 15 |
| 10 | 0.66 | 58 | 0.34 | 14 |
| PS:PtOEP 10 wt % | 0.63 | 62 | 0.36 | 13 |

Table 4.10: The amplitudes and the corresponding lifetimes as determined from fitting of the data in Figure 4.22.

According to eq. 3.15, the intensity of the delayed fluorescence emission that originates from the interaction of two excited triplet states, should posses an exponential decay transient characterised by a lifetime value that is half of that the phosphorescence decay exhibits.

For the case of up-conversion observed in blends of blue-light-emitting matrices and MeOEPs, if the up-converted photons ideally result in from triplet-triplet annihilation that occurs between the dopant molecules, the decay transient of the up-converted emission should decay twice faster

as the phosphorescence of the metalloporhyrin derivative that is incorporated in the matrix of the host.
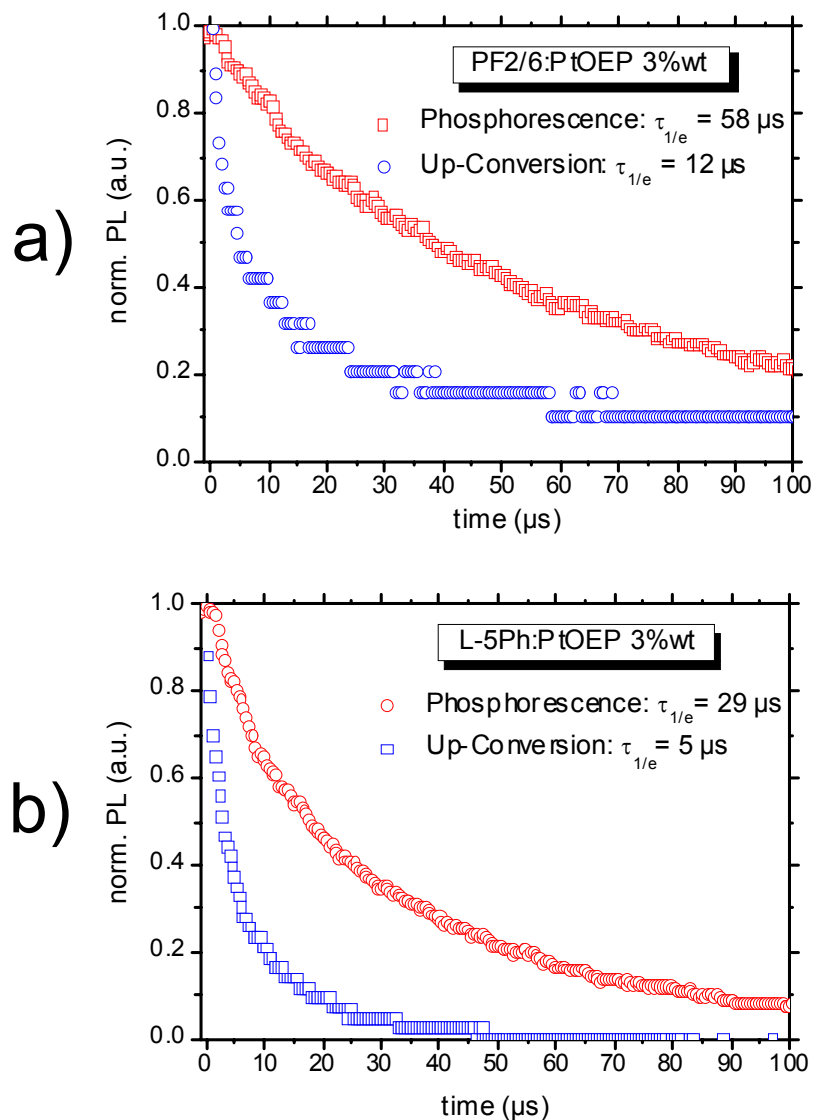


Figure 4.23: Room temperature normalised decay transients monitoring a) the PtOEP phosphorescence emission (squares) of the PtOEP and the up-conversion emission of PF2/6 (circles), b) the PtOEP phosphorescence emission (circles) of the PtOEP and the up-conversion emission of L-5Ph (squares). (see text for specification of the monitored spectral area). Excitation was at 532 nm (2.33 eV), at room temperature. Pressure was kept at ~$10^{-6}$ mbar. Both PF2/6 and L-5Ph were doped with 3 wt% PtOEP.

As figure 4.23 presents, for the case of a two different blue emitting matrices doped by 3 wt% with PtOEP, the $\dfrac{\tau_{Ph}}{\tau_{up-conv}}$ ratio is greater than ideal value that a triplet-triplet fusion would give.

More specifically, $\frac{\tau_{Ph}}{\tau_{up-conv}} \sim 5$ for the PF2/6 matrix whereas for the case of L-5Ph matrix a ratio

of $\frac{\tau_{Ph}}{\tau_{up-conv}} \sim 6$ is determined for a doping concentration of 3 wt %.

The dependence PtOEP phosphorescence and PF2/6 up-conversion lifetime, on the doping concentration of PtOEP in PF2/6 matrix is shown in Figure 4.24.
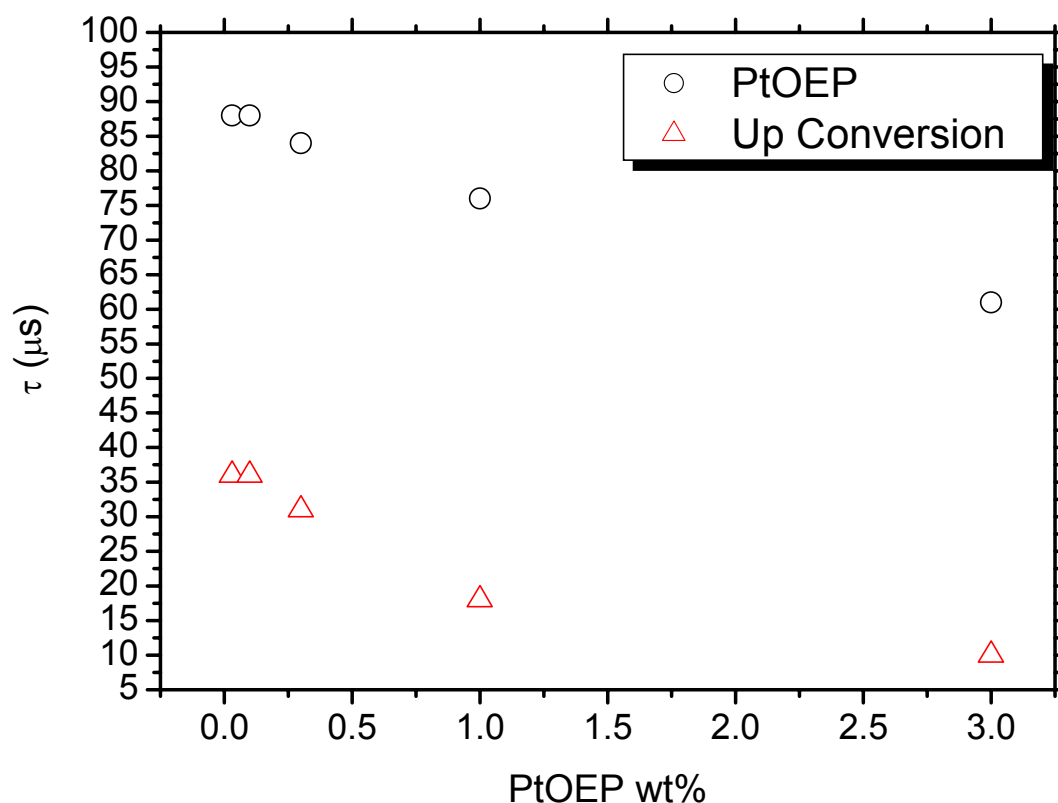


Figure 4.24: The $\tau_{1/e}$ lifetime values of PtOEP phosphorescence (circles) and PF2/6 up-conversion emission (triangles) as a function of PtOEP doping concentration in blends of PF2/6:PtOEP on quartz substrates. Excitation was at 532 nm (2.33 eV) with a pump pulse of 400 $\mu s$ duration and a waiting period of 400 $\mu s$. Room temperature, p~$10^{-6}$ mbar, 250 mW average laser power.

It is found that the up-conversion lifetime follows the decrease of the PtOEP phosphorescence lifetime upon the increased loading of the matrix with PtOEP.

## 4.5.3 Discussion

Our time-resolved phosphorescence studies in blends of PF2/6:PtOEP demonstrate the impact of concentration effects of PtOEP molecules in the observable phosphorescence lifetime of PtOEP. Particularly for the PF2/6:PtOEP 1 % wt we determine a PtOEP triplet lifetime $\tau_{1/e}$ ~ 74 $\mu s$, which is longer than the one previously reported [8].

We consider the data of Figure 4.23 and 4.24 to be of great importance for the elucidation of the up-conversion mechanism in our systems. The fact that the a departure of the PL integral ratio is observed from the expected factor of two, indicates that triplet-triplet annihilation within PtOEP molecules, can only partially be considered as the responsible reason for the occurrence of up-conversion. From earlier studies in mixtures of anthracene and xanthone [34], it has been found that triplet-triplet annihilation may have a heterogeneous character. One excited triplet of anthracene could collide with an excited triplet of xanthone resulting in delayed fluorescence of anthracene. This implies that triplet-triplet fusion may take place between two triplets that belong to molecules of different chemical nature.

In the present case of up-conversion within blends of blue-light-emitting matrices and PtOEP, we cannot exclude the possibility that triplet-triplet annihilation occurs between an excited triplet of the metalloporphyrin and a triplet of the host matrix. The latter could eventually be activated by triplet energy transfer from MeOEP to host (see Scheme 4.5c), presumably by a Dexter type energy transfer mechanism. In this case, the intensity of the temporal dependence the up-converted emission intensity should be expressed as:

$$I_{up-conv} = [T]_G * [T]_H = \left\{ [T_0]_G * \exp(-t/\tau_G) \right\} * \left\{ [T_0]_H * \exp(-t/\tau_H) \right\} =$$

$$([T_0]_G * [T_0]_H) * \exp\left[ -t * (\frac{1}{\tau_H} - \frac{1}{\tau_G}) \right] = ([T_0]_G * [T_0]_H) * \exp\left[ -t * \left( \frac{\tau_G - \tau_H}{\tau_H * \tau_G} \right) \right] \Rightarrow$$

$$I_{up-con} = A_0 * \exp(-t/\tau_{up-conv}), \qquad \text{(eq 4.9)}$$

where $A_0 = [T_0]_G * [T_0]_H$ and $\tau_{up-conv} = \frac{\tau_H * \tau_G}{\tau_G - \tau_H}$, if phosphorescence of host and guest decay monoexponentially in time.

In the above described equations $\tau_H$ represents the phosphorescent lifetime of the host in the absence of the guest, $\tau_G$ corresponds to the phosphorescence life time of the guest at the current doping concentration, $\tau_{up-conv}$ corresponds to the lifetime of the up-converted emission in the

blend, $[T_0]_H$ , $[T]_H$ $[T_0]_G$ and $[T]_G$ correspond to the triplet populations of the host (H) and the guest (G), at time t= 0 and t respectively.

Alternatively the homogeneous triplet-triplet fusion may take place exclusively within the polymer host after triplet-energy transfer from the guest to the host. This would be plausible in the case of room temperature where the energy gap between the triplets of host and guest could be bridged due to thermal effects.

Realistically speaking we cannot exclude that both hetero- and homo- triplet fusion may occur in our system. For the case of PF2/6, the phosphorescence lifetime has been determined to be 0.8 $\mu s$, at 80 K, [54]. We propose that if triplet-triplet annihilation within the host would really be the origin of the observed up-conversion, the half value of host-triplet lifetime should correspond to the determined lifetime of the up-converted blue emission, for a measurement like that of Figure 4.23 at 77 K. This experiment should be performed in order to clarify the branching ratio of hetero- and homogeneous triplet-triplet annihilation in Host:MeOEP blends.

## 4.6  UP-CONVERSION IN SOLUTIONS

In this section experimental results are presented from measurements performed on host/porphyrin solutions. According to the experiments shown below, the up-conversion process is taking place even in the highly diluted regime, albeit weakly. It is concluded that, the process of up-conversion occurs without the existence of an intensity threshold and its detection is limited only from the experimental set up conditions that have been described in detail in 4.3.1.

### 4.6.1 Experimental

A range of dilute solutions was prepared where the concentration of PtOEP was kept constant while a gradual increase of the polymer was taking place. The systems studied with this method were PF3/5:PtOEP and PF1/7:PtOEP. Tables 4.11-4.13 are presenting $M_n$ values of the hosts and the exact details of the doping concentrations used.

| Host | $M_n$ (gr/mole) | D |
|------|------|------|
| PF3/5 | $3.2*10^4$ | 2.04 |
| PF1/7 | $2.03*10^5$ | 2.21 |

Table 4.11: The polymer used as hosts and the $M_n$, D values.

| PtOEP (mg/mL) | PF3/5 (mg/mL) | M PF3/5 (moles/L) | M PtOEP (mmoles/L) |
|---|---|---|---|
| 0.400 | 10 | $3.12*10^{-4}$ | 0.55 |
| 0.402 | 5 | $1.56*10^{-4}$ | 0.55 |
| 0.403 | 3.3 | $1.03*10^{-4}$ | 0.55 |
| 0.403 | 1 | $3.12*10^{-5}$ | 0.55 |
| 0.403 | 0.5 | $1.56*10^{-5}$ | 0.55 |
| 0.403 | 0.33 | $1.03*10^{-5}$ | 0.55 |
| 0.403 | 0.1 | $3.12*10^{-6}$ | 0.55 |
| 0.403 | 0.01 | $3.12*10^{-7}$ | 0.55 |

Table 4.12: The individual concentrations of PtOEP and PF3/5 in the PtOEP:PF3/5:Toluene solutions prepared.

| PtOEP (mg/mL) | PF1/7 (mg/mL) | M PF1/7 (moles/Lt) | mM PtOEP (mmoles/Lt) |
|---|---|---|---|
| 0.420 | 10 | $4.93*10^{-5}$ | 0.58 |
| 0.420 | 5 | $2.46*10^{-5}$ | 0.58 |
| 0.421 | 3.3 | $1.62*10^{-5}$ | 0.58 |
| 0.459 | 1 | $4.93*10^{-6}$ | 0.63 |
| 0.421 | 0.5 | $2.46*10^{-6}$ | 0.58 |
| 0.421 | 0.33 | $1.62*10^{-6}$ | 0.58 |
| 0.421 | 0.23 | $1.13*10^{-6}$ | 0.58 |
| 0.421 | 0.1 | $4.93*10^{-7}$ | 0.58 |
| 0.421 | 0.02 | $9.85*10^{-8}$ | 0.58 |
| 0.411 | 0.01 | $4.93*10^{-8}$ | 0.58 |

Table 4.13: The individual concentrations of PtOEP and PF1/7 in the PtOEP:PF1/7:Toluene solutions prepared.

Excitation power dependence measurements were performed for the above described solutions, in the range of 30-450 mW. For laser induced cw-PL registration, the detector was set up to accumulate the PL signal within 2000 ms, unless otherwise is mentioned in the following. A low band pass optical filter was employed for reducing the PtOEP emission in favour of the monitored up-converted blue emission. In such a way, saturation of the detector was avoided. In all cases, the laser beam was focused on a spot of app. ~ 80 μm diameter.

For the steady state optical measurements of dilute solutions, different polymer hosts were used for preparing the mixtures with PtOEP in degassed toluene. Three of the most representative hosts are presented in the following. Table 4.14 presents the amount of each of the compound that was taken. Degassing of the toluene took place after purging Ar with parallel ultrasonication for 15 min. A spectrofluorometer was used for recording the luminescence of the solutions presented in Table 4.14, after excitation upon 390 nm and registration time of 5000 ms.

| material | $M_n$ (gr/mole) | PS (D) | mg/mL | C (mole/Lt) | $c^*$ (mole/Lt) |
|---|---|---|---|---|---|
| PF2/6 endcapped | $2.0*10^4$ | 2.0 | 0.23 | $11.5*10^{-6}$ | $19.1*10^{-6}$ |
| PF 3/5 | $3.2*10^4$ | 2.04 | 0.26 | $8.1*10^{-6}$ | $19.1*10^{-6}$ |
| L-5Ph | $2.64*10^5$ | 2.79 | 0.28 | $1.1*10^{-6}$ | $1.1*10^{-6}$ |
| PtOEP | 727.87 | - | 0.40 | $0.55*10^{-3}$ | - |

Table 4.14: The polymer used as hosts and the $M_n$, D values. The concentration of the solutions prepared and the $c^*$ overlap concentration for each of the polymer are given.

The chemical structures of PF3/5 and L-5Ph have been shown in Chart 4.2 while these of PF1/7 and PF2/6 endcapped are presented in Chart 4.3.



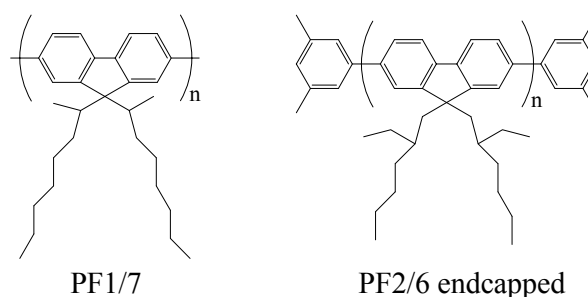PF1/7                    PF2/6 endcapped

Chart 4.3: The chemical structure of the PF derivatives that was studied in solution.

## 4.6.2 Concentration dependence in solutions

Figure 4.25a presents the PL spectrum of a highly diluted solution of PF1/7 derivative after laser excitation in the Q-absorption band of PtOEP at 532 nm. Due to the relatively high concentration of PtOEP molecules in the solution, appropriate optical filters were used in order to reduce the PtOEP emission band and to avoid saturation of the detector. It is clear that the characteristic emission band of PF1/7 is also observed in the region of 420 nm, albeit very weak. Therefore it is concluded that up-conversion may take place even in vanishing amounts of host material.
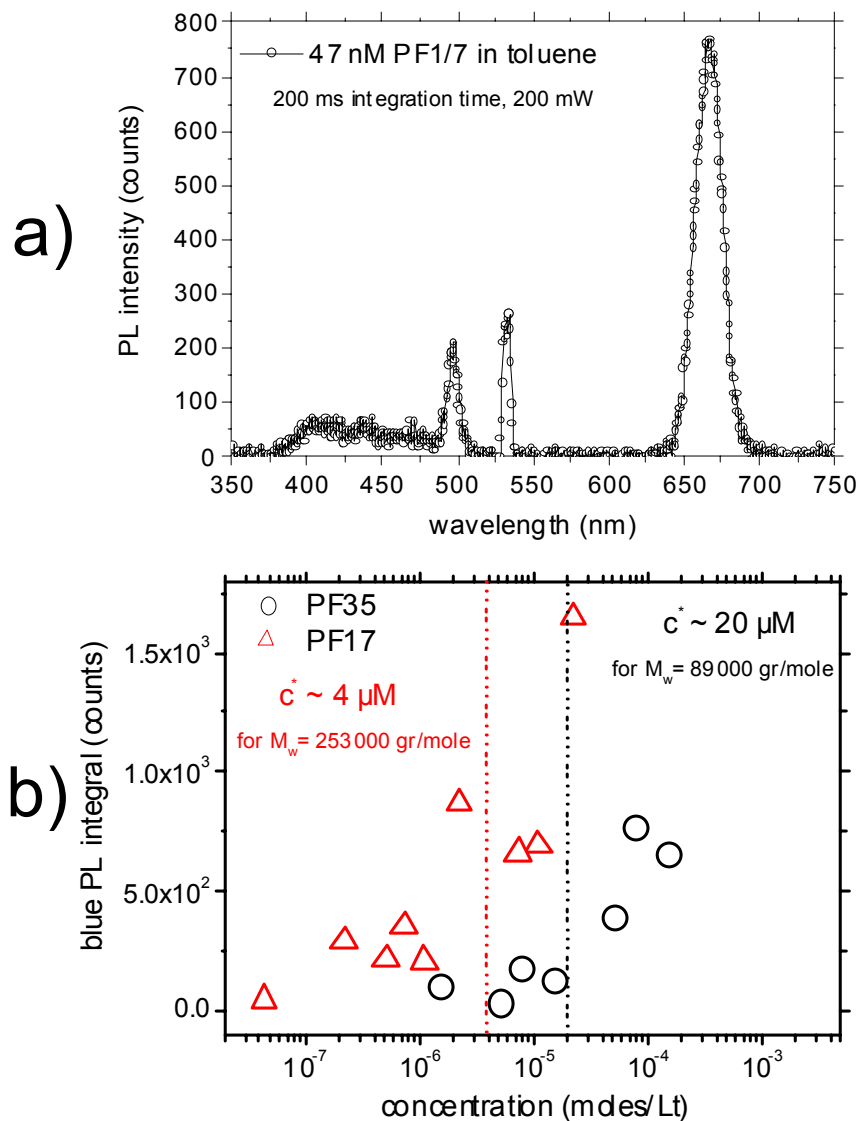
Figure 4.25: a) Up-conversion of PF1/7 in a highly diluted solution (~50 nM) of toluene. In the same solution the concentration of PtOEP is 0.6 M. appropriate filters were used for the reduction of PtOEP emission on the benefit of PF1/7 emission. b) The concentration dependence of the up-conversion of PF3/5 (circles) and PF1/7 (triangles) on the corresponding polymer concentration. For both a) and b), excitation at 532 nm (2.33 eV), at room temperature.

Figure 4.25b presents the concentration dependence of the up-conversion blue PL integral that is observed for the two different PF derivatives in dilute solutions. The values of the studied concentrations are given in Table 4.12 and 4.13.

## 4.6.3 Intensity dependence in dilute solutions

Like in section 4.4.3, excitation power dependence of the up-conversion process was performed for all the solutions that Tables 4.12 and 4.13 present. Figure 4.26 shows the power dependence for a solution of PF1/7:PtOEP. A quasi-quadratic character of the up-converted PL integral arises at ~ 100 mW of excitation power.
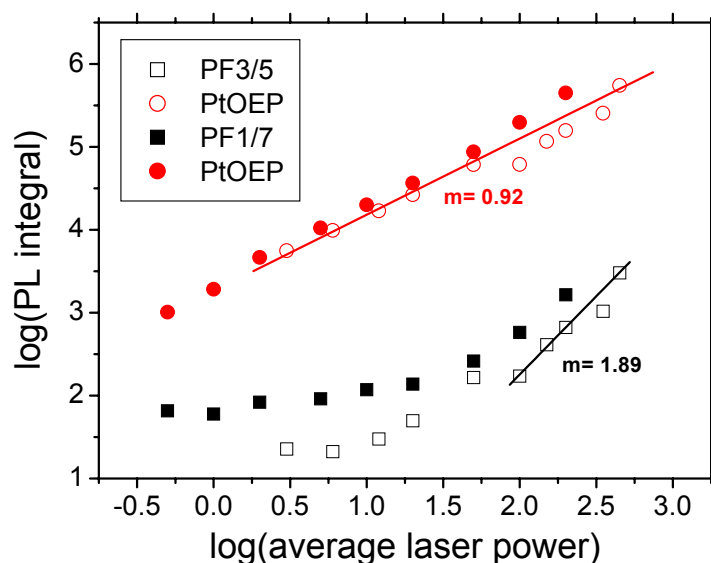


Figure 4.26: The excitation intensity dependence of PtOEP phosphorescence spectral integral (circles) and the up-conversion spectral integrals of the studied polymers (squares) obtained for a solution of PF3/6:PtOEP (open symbols) and PF1/7:PtOEP (filled symbols), in toluene. The doping concentration of PdOEP was at 10 wt%, (see first row of Tables 4.12 and 4.13). The measurement performed at room temperature for excitation at 532 nm (2.33 eV). Excitation power units are in mW and the lines are fits to the data.

## 4.6.4 CW-photoluminescence spectroscopy of solutions

As presented in section 4.4.2 (Figure 4.15), the up-conversion host emission has been found to be stronger in the case of films composed of L-5Ph:PtOEP than in the films of other PF derivatives that were used as active matrices. Since up-conversion is operative also in the case of dilute solutions (Figure 4.25a), a comparison is presented for solutions of L-5Ph and other PF derivatives. Three different polymers have been used for the preparation of dilute solutions of Host:PtOEP systems. In these systems the PtOEP concentration was kept constant. Care was taken as the concentration of the polymers adjusted to be not higher the critical concentration of chain overlap [56]. The three different polymers used and their characteristic details are presented in table 4.14.

As Figure 4.27 shows, for laser excitation of the studied solution at 532 nm, up-conversion is demonstrated for all three systems prepared but the magnitude of the up-converted emission varied considerably dependent on the polymeric structures used. It is evident that similar to the case of thin films, L-5Ph exhibits significantly stronger up-converted blue emission than the PF derivative do.
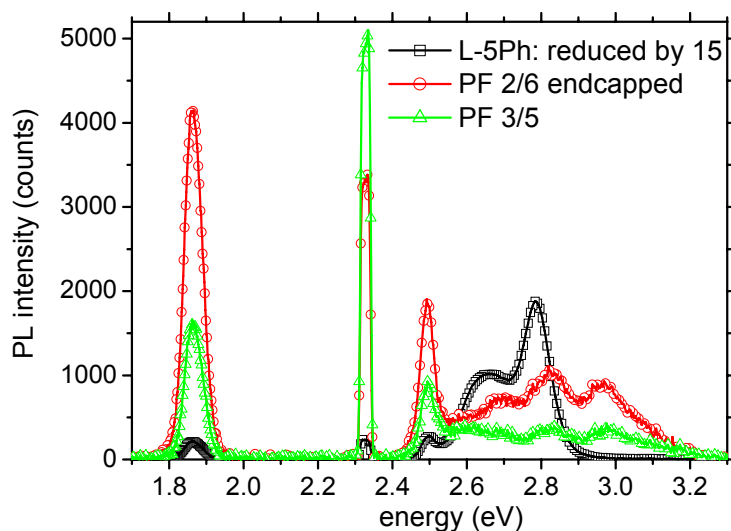


Figure 4.27: Up-conversion of the 532 nm excitation observed for three different polymers in polymer:PtOEP:toluene solutions (see Table 4.14). The concentration of the polymers was not higher than the critical concentration for chain overlap. In the case of L-5Ph a multiplication factor of 0.067 is used. The measurement performed at room temperature.
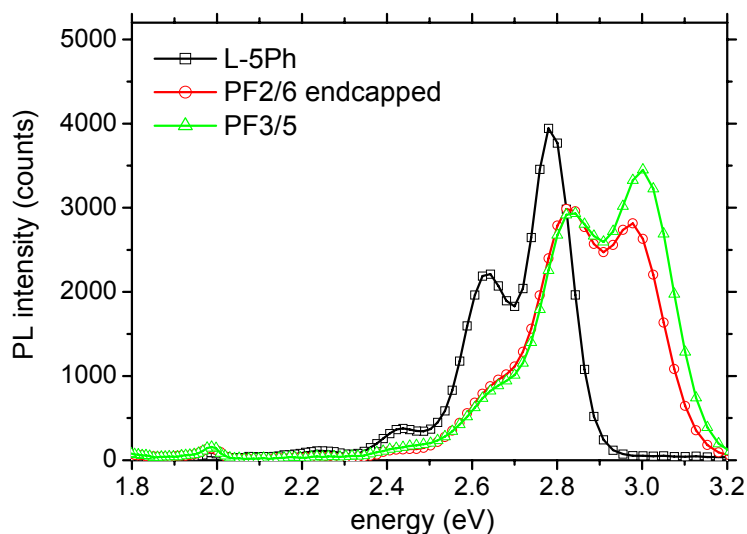
Figure 4.28: cw-PL spectra of the three different polymers in polymer:PtOEP:toluene solutions (see Table 4.14). The concentration of the polymers was not higher than the critical concentration for chain overlap. The measurement performed for excitation at 390 nm (3.18 eV) at room temperature.

In order to exclude the possibility that L-5Ph exhibits stronger up-conversion due to its higher PL quantum efficiency, a comparison is presented between the PL spectra of the three different solutions. Figure 4.28 presents the cw-PL spectra of the three solutions, for excitation at 390 nm with a spectrofluorometer set-up. It seems that at the concentrations used, the PL yield is similar. However, the efficiency of up-conversion PL as deduced from the spectral PL integral of Figure 4.27, seems to change by a factor of 30 upon shifting from PF to L-5Ph polymer hosts.

Figure 4.29 presents the absorption spectra of the three different Host:PtOEP solutions.
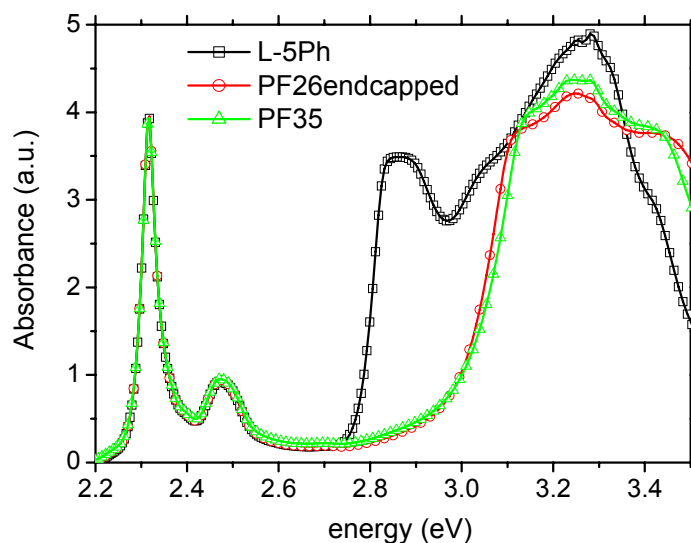
Figure 4.29: Room temperature absorption spectra of the three different polymers in polymer:PtOEP:toluene solutions (see Table 4.14). The concentration of the polymers was not higher than the critical concentration for chain overlap c$^*$.

The absorption spectra of the hosts in toluene solution in the absence of PtOEP molecules are presented in Figure 4.30, together with the absorption spectrum of PtOEP. In comparison with the PtOEP-free host solutions, no additional spectral features are observed in the absorption spectrum of Host:PtOEP, systems. Actually the latter seem to be superpositions of the individual spectra of the components.
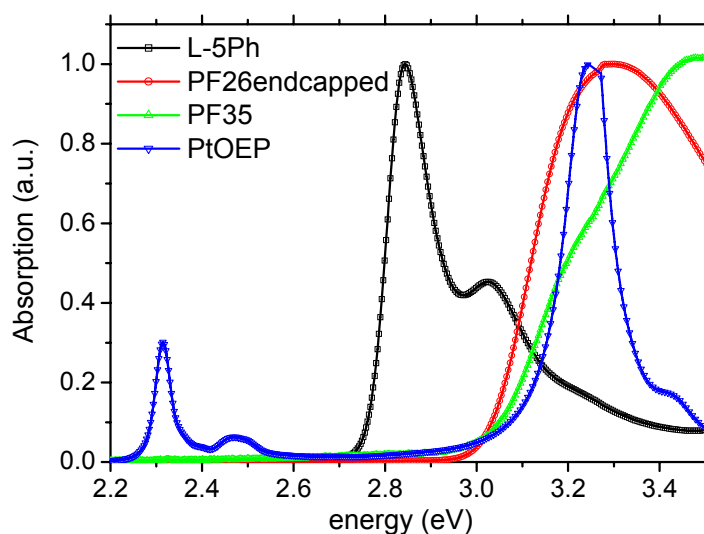


Figure 4.30: Absorption spectra of the three different polymers and for PtOEP in toluene solutions.

## 4.6.5 Excited state absorption of PtOEP

The higher up-conversion efficiency of the L-5Ph-blend in comparison with the PF2/6-blend, observed in Figures 4.15 and 4.20, can be partially attributed to differences on the effect of re-absorption of the host emission fluorescence from the excited dopant molecule. Under cw-excitation of the blends, excited singlet and triplet states of the metallated porphyrin molecules are generated continuously. Therefore, the excited state absorption of the porphyrin molecule is one of the critical parameters defining the up-conversion efficiency.

Figure 4.31 shows the transient absorption spectra of the PtOEP-molecules in toluene solution: The *fs* set-up being the same as reported earlier [57]. The pump beam 800 nJ, 40 *fs* FWHM is provided by a noncollinear optical parametric amplifier (NOPA) [58]. The probe and reference beams, (320-750 nm, 150 *fs*) are generated by focusing a very small part of the Ti:Sapphire commercial laser (Clark-MXR, CPA-2001) beam used to pump the NOPA on a $CaF_2$ crystal. Both the probe and the reference spectra are detected independently and simultaneously by a CCD array.
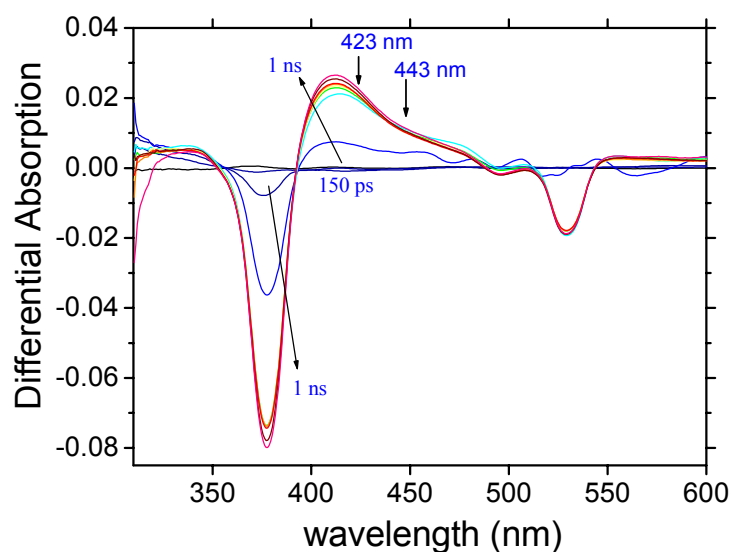


Figure 4.31: Pump-probe excited state absorption spectra of the film of PtOEP 0.15 wt % in toluene. The tilted arrows indicate the trend in the spectra from 150 *ps* to 1 *ns*. The vertical arrows indicate the spectral areas of interest (see text). Pump pulse excitation at 532 nm, probe pulse was supercontinuum (see text).

## 4.6.6 Discussion

It is clear Figure 4.25 that up-conversion in solutions may take place even in vanishing amounts of host material present in excess of PtOEP molecules. Figure 4.26 shows that PtOEP is found to depend linearly on the excitation power used, for the whole range of excitation powers used. This is attributed to the fact that triplet-triplet annihilation is less probable in the high concentration regime of PtOEP solutions due to the decreased phosphorescence lifetime of PtOEP. We attribute this reduction in the lifetime of the triplet-excited state to effects of collisional quenching between the excited PtOEP molecule with other molecules in the ground state. This decrease of triplet-triplet fusion process reduces substantially the bimolecualar factor of eq. 3.10, thus resulting in the dominance of the monomolecular term in the expression of the temporal excited triplet level concentration. However the fact that up-conversion can be observed declares that the extend at which triplet-triplet annihilation occurs is sufficient enough in order to activate the singlet excited state of the host and to exhibit up-conversion host emission.

The replacement of a stepladder-type polymeric host (PF) from a ladder-type polymeric structure (L-5Ph) results in significant increase of the up-conversion efficiency. The measurement of excited state absorption of PtOEP that part 4.6.5 has described, may partially explained this difference. As seen in Figure 4.31, together with the ground-state bleaching around 380 nm (Sorret-band) and 537 nm (Q-band), a strong absorption in the region between 405 and 440 nm is observed with a maximum at 412 nm. This absorption increases when the delay is varied from 150 *ps* to 1 *ns*. Since the peak of the fluorescence emission of PF2/6 is centred around 423 nm, it will be strongly re-absorbed by the excited macrocycle molecules. In contrast, the L-5Ph fluorescence emission has a PL maxima at 445 and 472 nm that overlap weakly with the tail of the excited state absorption spectrum of PtOEP. This spectral shift leads to less re-absorption of the PL emission in L-5Ph than in PF2/6 and therefore to higher up-conversion efficiency (see also Figure 4.32).

It has to be noted that the more planarised and rigid the backbone of the polymer host is, the more intense is the up-converted observed up-conversion emission. In combination with the fact that the PtOEP has also a planar geometry, it is possible that the up-conversion process is favoured under conditions where the interaction of organic macro-ring and the polymer is optimised in a π-stacked arrangement. This type of interactions is reminiscent of a hetero-dimer moiety consisting of two distinct molecules of a polymer segment and a porphyrin ring. Such type of bimolecular interaction of molecules of different nature is known to lead either to charge-transfer or to exciplex complexes [59]. The absorption spectra of Figures 4.29 and 4.30 were

recorded in order to distinguish which of the two cases could be attributed to the here studied systems. Charge-transfer aggregates are result of ground state electronic interaction, therefore the lack of such spectroscopic signature in the absorption spectra of the system suggests the absence of ground state charge-transfer complex of the two components in solution.

The bimolecular interaction of the speculated charge-transfer complex should be created in the excited state of one of the components. The maximum time for the creation of this exciplex should be the lifetime of the triplet state in PtOEP. All hosts used are not absorbing in the region of 532 nm, which is why the excited PtOEP is the only component able to initiate the formation of the exciplex. In principle, exciplexes are formed from the interaction of an excited donor and an acceptor, or from a donor and an excited acceptor. The former case is more plausible as PF is considered to act as an acceptor of the PtOEP excitation energy. The relative positions of the electronic levels of PF2/6, L-5Ph and PtOEP, as determined from PL and PLE spectroscopy of dilute solutions, are depicted below in Figure 4.32. No significant spectroscopic differences exist between PF2/6 and PF3/5, in solution, so the energy levels are representative for both of these poly(fluorene) derivatives.
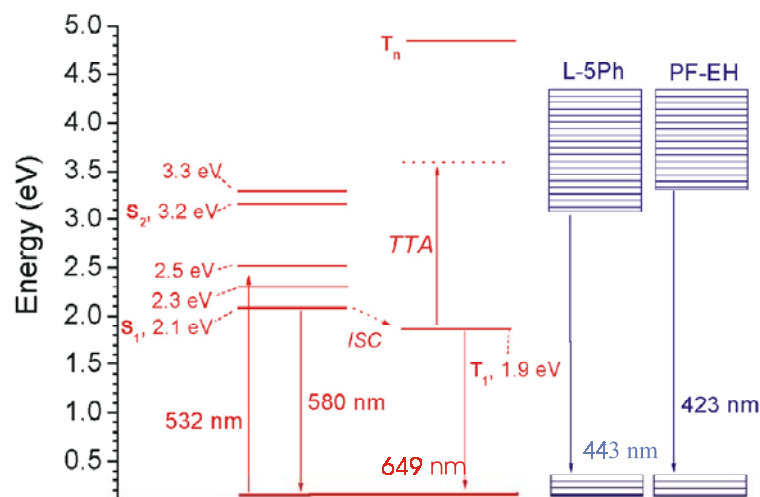


Figure 4.32: A schematic representation of the energy levels of PtOEP, PF2/6 and L-5Ph. The given values are extracted from absorption, PL and PLE spectra of these materials as thin films.

In fact, the formation of an exciplex between the polymer hosts and PtOEP should depend on the redox potential of the components involved in the complex. These issues are addressed by experiments that the next section presents.

# 4.7 ELECTROCHEMISTRY MEASUREMENTS

We employ cyclic voltammetry and differential pulse voltammetry in order to deduce the frontier orbital values (see Chapter 1) of PtOEP and the blue emitting hosts, in solution of $CH_2Cl_2$. The obtained values in combinations with the spectroscopic observations on up-conversion process that have been presented in described in the preceding paragraphs, contribute substantially to the elucidation of the up-conversion mechanism.

## 4.7.1 Introduction

Optical spectroscopy provides information on the optical gap in which a transition is involved after the excitation of a molecule. Especially in the class of conjugated polymers, the optical gap corresponds to an electronic transition within the highest occupied and the lowest unoccupied π-molecular orbitals, HOMO and LUMO respectively. Therefore no direct information is extracted regarding the absolute energy values of these frontier levels in respect with the vacuum level. For the determination of the absolute HOMO and LUMO values, electrochemistry methods are considered as more appropriate since they involve the determination of oxidation and reduction potentials that are indirectly linked to the optical gap of the molecule. Scheme 4.7 depicts the oxidation and reduction processes and their relation to the energy gap $E_g$ of the two states that constitute the system.
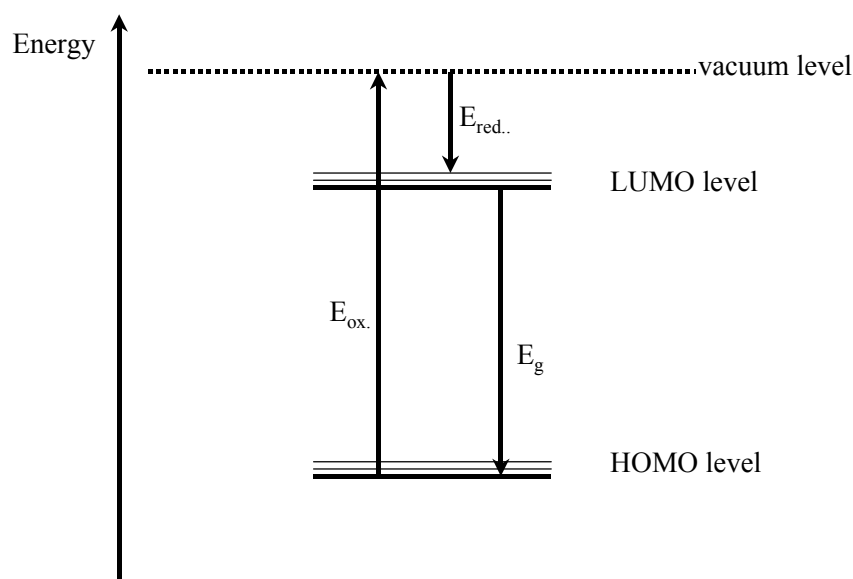


Scheme 4.7: The relative energetic positioning of the HOMO and the LUMO levels of a molecule in respective to the vacuum level. The oxidation ($E_{ox.}$) and the reduction ($E_{red.}$) potentials are depicted together with the energy gap ($E_g$) of the molecule.

## 4.7.2 Experimental

In general, voltammetry describes the experimental methods that monitor the relationship between voltage and current during an electrochemical processes. Voltammetry refers to the observation of current flow through an electrolysis cell as a function of the potential applied on an electrode, the working electrode. If the applied potential is a triangular or saw-tooth wave the resulting experiment is described as cyclic voltammetry.

The set-up of cyclic voltammetry consists of three electrodes. A periodic variation of the potential takes place between the working electrode, and a second electrode with a thermodynamically-defined potential, the reference electrode. Finally, the current flux of the electrochemical process at the working electrode. The circuit is completed with a current-carrying auxiliary electrode, the counter electrode, which supplies the current needed by the working electrode.

Electron flow is observed in the case that the applied electric field exceeds the oxidation or the reduction potential of the substance that is measured. In the first case electrons are flowing from the substance to the counter electrode while in the latter case electrons are flowing from the electrode to the molecules of the substance. By measuring the produced current as a function of the applied field that is periodic in time, a cyclic voltamogram is obtained.

Cyclic voltammetry provides information on the redox behaviour of the compounds measured.

For reversible reactions the values of peak anodic and peak cathodic currents have equal magnitudes and the relationship between them at 298 K can be expressed [60] as:

$$E_{pa} - E_{pc} = \frac{2.22 * R * T}{n * F} = \frac{57}{n}(mV), \qquad \text{(eq 4.10)}$$

where $E_{pa}$ and $E_{pc}$ denote the anodic and cathodic peak of the cyclic volatgram, respectively. F corresponds to the Faraday constant, R is the gas constant and T is the measuring temperature. Based on this relationship the number n of electrons that participate in the half-reaction can be determined.

New techniques have been developed for applying cyclic voltammetry on thin films of redox compounds. However, no important changes have been observed in the redox values of solutions and thin films apart from small differences attributed to intermolecular effects of the electroactive species, in the solid state.

Alternatively, the determination of the half-wave potential $E_{1/2}$ can be deduced without the need for numerical analysis, directly from the differential pulse voltammetry. In the following both methods are applied. Table 4.16 shows the measured quantities of each material measured:

| material | $M_n$ (gr/mole) | PS (D) | m(mg) | mg/mL | C (M) |
|---|---|---|---|---|---|
| PF2/6 endcapped | $2.0*10^4$ | 2.0 | 2.4 | 0.24 | $12*10^{-6}$ |
| PF 3/5 | $3.2*10^4$ | 2.04 | 2.23 | 0.22 | $6.88*10^{-6}$ |
| L-5Ph | $2.64*10^5$ | 2.79 | 15 | 1.5 | $5.68*10^{-6}$ |
| PhLLLP | 11460 | 1.54 | 2.1 | 0.21 | $18.3*10^{-6}$ |
| PtOEP | 727.87 | - | 13.4 | 1.34 | $1.84*10^{-3}$ |
| L-5Ph monomer | 1632 | - | 9 | 0.9 | $0.55*10^{-3}$ |

Table 4.15: The materials that were measured together with their corresponding $M_n$ and polydispersity (D) values. The mass obtained and the corresponding concentration of the solution, for each material are also given.

Calibration of the performed electrochemical measurements took place by using Fc/Fc$^+$ (ferrocene/ferrocenium) as a reference (~0.363 V, 4.8 eV). Tetrabutylammonium tetrafluoroborate (0.1 M) was used as supporting electrolyte. As solvent $CH_2Cl_2$ was used. The electrochemical measurements were performed directly after purging of $N_2$ throughout the prepared solutions, in order to avoid the influence on the electrochemical behaviour of the measured species, from their interaction with dissolved $O_2$. Both of the used electrolyte and the solvent were of high purity in the order of 99 % and 99.8 %, respectively. The temperature of the measurements was at room temperature. The sweep rate for all measurements was kept at 100 mV/sec. A disk Au working electrode was used with an area of 1 mm diameter. As counter electrode, a coiled Pt wire was used, whereas an Ag electrode was used as a reference electrode.

## 4.7.3 Results

Figure 4.33 shows the cyclic voltagram of PtOEP in solution. In the first look the oxidation potential seems to consist of an anodic wave, which is found to be quasi-reversible. By employing pulsed amperometry we deconvolute the two overlapping peaks. In a previous study on the electrochemical properties of metal octabromoporphyrin derivatives in $CH_2Cl_2$, the obtained cyclic voltamograms also exhibited two oxidation and reduction peaks [61].
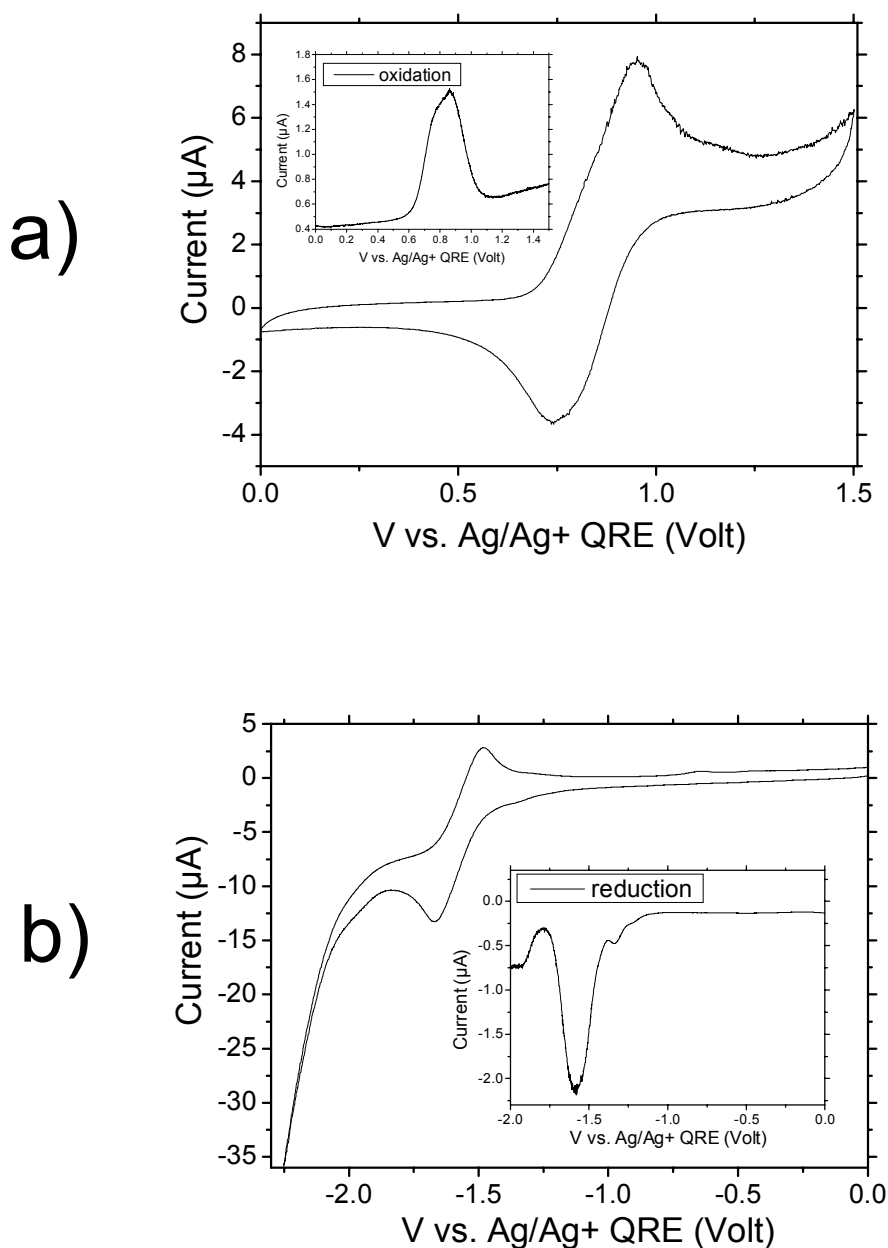
Figure 4.33: Cyclic voltammogram for PtOEP solution of $CH_2Cl_2$ a) for oxidation and b) reduction. The swept rate of the potential was 100 mV/sec and the working Au electrode had a 1 mm diameter. A Pt wire was the counter electrode and Ag was used as a reference electrode. The insets are showing the half-wave potentials $E_{1/2}$ as obtained from differential pulse voltammetry. Tetrabutylammonium tetrafluoroborate was used as the supporting electrolyte (0.1 M).

Figure 4.34 shows the cyclic voltamogram of L-5Ph in solution. For this material, the oxidation potential consist of an anodic wave of quasi-reversible character and exhibits wave peaks that overlap with each other. We resolve the position of the redox waves by utilizing differential pulse voltammetry .
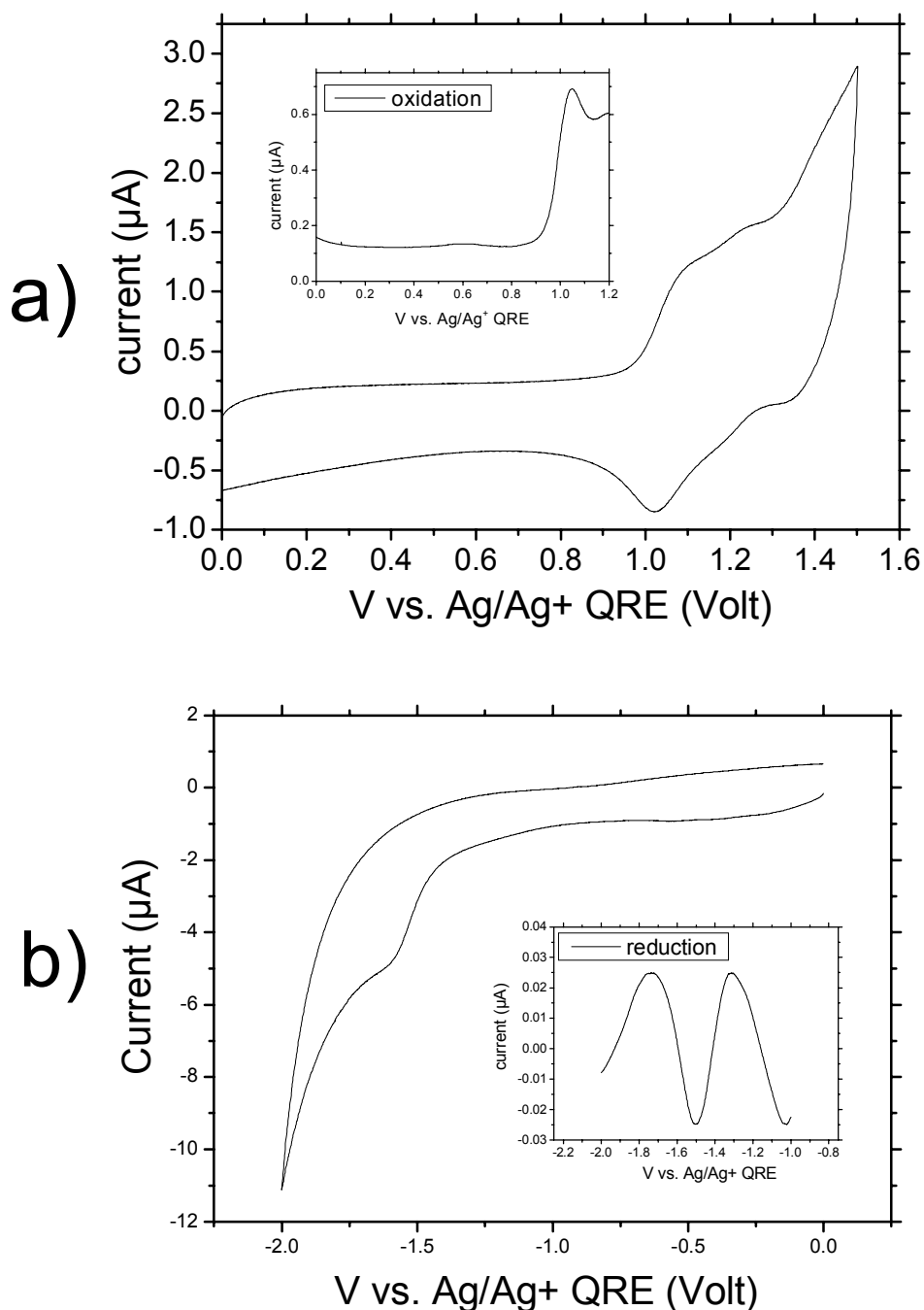
Figure 4.34: Cyclic voltammogram for L-5Ph solution of $CH_2Cl_2$ a) for oxidation and b) reduction. The swept rate of the potential was 100 mV/sec and the working Au electrode had a 1 mm diameter. A Pt wire was the counter electrode and Ag was used as a reference electrode. The insets are showing the half-wave potentials $E_{1/2}$ as obtained from differential pulse voltammetry. Tetrabutylammonium tetrafluoroborate was used as the supporting electrolyte (0.1 M).

The values of the determined half-wave potential for all the materials measured are presented in table 4.16.

| material | Oxidation (Volts) | | Reduction (Volts) | |
|---|---|---|---|---|
| | $E^{I}_{p,a,1}$ | $E^{II}_{p,a,2}$ | $E^{I}_{c,a,1}$ | $E^{II}_{c,a,2}$ |
| **PtOEP** | 0.74 | 0.87 | -1.33 | -1.58 |
| **PF2/6** | 1.26 | 1.47 | - | - |
| **PF 3/5** | 1.35 | - | - | - |
| **PhLLLP** | 1.41 | 1.59 | -1.19 | - |
| **L-5Ph** | 1.05 | - | -1.51 | - |
| **L-5Ph monomer** | 1.14 | 1.55 | -1.54 | - |

Table 4.16: The potential values where the peak of the oxidation and reduction waves was observed for each of the materials studied.

## 4.7.4 Discussion

In the case where determination of the reduction potential was not possible, due to the irreversibility of the redox process, the energy gap of the material, as determined from PL measurements was used for deducing the LUMO values. We have to note that in a previous work [9], the HOMO value of PtOEP has been reported to be 5.3 eV. However no information on the measuring technique that has been used was given. Further more it was it not clear if the reported value corresponded to PtOEP films or solutions.

| material | HOMO (eV) | LUMO (eV) | LUMO$^{a}_{Eg}$ (eV) | Optical gap (eV) |
|---|---|---|---|---|
| **PtOEP** | 5.18 | 3.11 | 3.02 | 2.16 |
| **PF2/6** | 5.70 | - | 2.72 | 2.98 |
| **PF 3/5** | 5.80 | - | 2.80 | 3.00 |
| **PhLLLP** | 5.85 | 3.25 | 3.19 | 2.66 |
| **L-5Ph** | 5.49 | 2.93 | 2.74 | 2.75 |
| **L-5Ph monomer** | 5.58 | 2.90 | 2.66 | 2.92 |

Table 4.17: The HOMO and LUMO values of the materials studied based on the oxidation and reduction potential values as of Table 4.16 together with the corresponding $E_g$ values as determined from cw-PL.$^{a}$: The LUMO values as determined from the combination of HOMO values and the optical gap values. A value of 4.8 eV below the vacuum level was assumed for the ferrocene/ferrocenium redox couple.[✤]

✤ Sheats J. R., Antoniadis H., Hueschen M., Leonard W., Miller J., Moon R., Roitman D., Stocking A. *Organic Electroluminescent devices*. Science, 1996. **273**: p.884
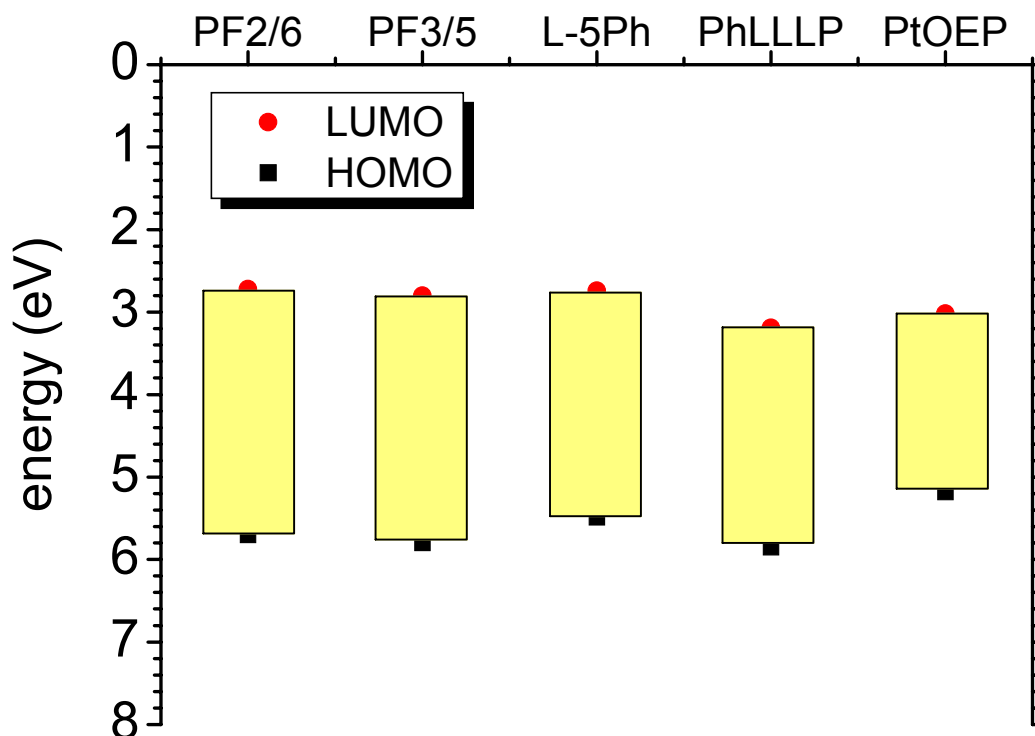
Figure 4.35: A visualisation of the HOMO and LUMO$_{Eg}$ levels of the materials studied based on the values of Table 4.17.

 We exploit the Rehm-Weller equation [20], [23] in order to evaluate the efficiency of a potential electron transfer process between an excited PtOEP molecule and a ground state host molecule. We presume that this electron transfer process is taking place by the time that triplet-triplet annihilation results in efficient population of a PtOEP level that equals the energy of two triplet PtOEP quanta. That is $E_{PtOEP}{}^*=2*E_{T1}=3.8$ eV= 87.6 kcal/mole. According to the Rehm-Weller equation, the free energy change during the electron transfer between a redox pair is:

$$\Delta G_{el} = 23.06*\left[E^0(D^{\cdot+}/D) - E^0(A/A^-)\right] - E, \qquad \text{(eq. 4.11)}$$

where $-E^0(D^{\cdot+}/D)$ and $E^0(A/A^-)$ correspond to the oxidation and reduction potential of the donor and the acceptor neutral molecules, respectively. The term $E$ includes the energy of the excited state from where electron transfer occurs together with a coulombic term, which reflects the stabilisation energy of the created radical ion pair. By using the potential values that Table 4.16 presents, we deduce the free energy values $\Delta G_{el}$ for the materials studied. Table 4.18 presents the determined $\Delta G_{el}$ values.

279

| [PtOEP$^+$...Host$^-$] | $\Delta G_{el}$ (kcal/mole) | $\Delta G_{el}$ (eV) |
|:---:|:---:|:---:|
| **PF2/6** | -66.30 | -2.88 |
| **PF 3/5** | -67.92 | -2.95 |
| **L-5Ph** | -71.14 | -3.09 |
| **PhLLLP** | -78.52 | -3.41 |

Table 4.18: The $\Delta G_{el}$ electrochemical force values for the host-PtOEP redox couples as determined from eq. 4.11, assuming a stabilisation energy coulombic term of 1.3 kcal/mole [20].

By simply applying the electron transfer formalism that eq. 4.11 expresses, it is found that the formation of an excited state charge transfer complex between PtOEP and all the polymers investigated, is energetically favoured. The optical absorption of both the negatively and positively charged radical of a Zn(octabromotetraphenylporphyrin) in solution have been reported [61]. More over previous reports have studied the formation of optically excited charged species in fullerene/MeOEP systems in solution [23].

The lifetime of the formed exciplex should be limited due to the unfavourable conditions in which the polymer hosts accommodate an extra negative charge on their LUMO levels. The pathways for the reformation of neutral species will be the return of this electron from the polymer host to PtOEP. This donation may occur either between the LUMO or the HOMO level of the two partners of the redox couple. In the latter case where an electron is back transferred from the HOMO level of the polymer to the HOMO level of the PtOEP, the result will be the formation of a neutral ground state PtOEP molecule and a neutral excited state polymer molecule. Subsequently the polymer can return to its ground state by emitting a photon of energy corresponding to its optical gap.

Based on the values of Table 4.18, it is concluded that the most stable redox couple of Host:PtOEP in $CH_2Cl_2$ will correspond to PhLLLP:PtOEP. However, according to Table 4.17 and Figure 4.35, from all the conjugated polymeric matrices investigated, only L-5Ph posses the closest HOMO level to the HOMO level of PtOEP molecules. Therefore after the creation of the radical ion-pair with an excited PtOEP molecule, only L-5Ph is more energetically favoured to return an electron from its HOMO levels to the HOMO levels of PtOEP. This implies that the final step for the production of an excited neutral polymer molecule and a ground state neutral PtOEP molecule will be more efficient for L-5Ph than for PhLLLP. We consider that these results may explain the reason why L-5Ph exhibits much more efficient up-conversion process than the rest of the hosts tested (Figure 4.27). The electron transfer energetics of the process that may sensitise the host matrix via an excited PtOEP are presented in *Appendix C*.

# 4.8 CONCLUSIONS: SUGGESTING THE UP-CONVERSION MECHANISM

So far it has been shown that up-conversion may be a result of triplet-triplet fusion process (section 4.2.3.) that exhibits temperature dependent characteristics, in accordance with the notion that a triplet level should be a precursor state (section 4.3). It was concluded that the ability of a dopant to support the process of up-conversion is related to the efficient absorption of the low-energy excitation provided and to the efficiency of triplet level population via an singlet-triplet intersystem crossing process (section 4.2.5).

Eventually, as it is suggested from the dynamics of the up-conversion process, it is not necessary that the two interacting triplets belong to the same molecules (section 4.5.2). The branching ratio of homo- and hetero triplet-triplet annihilation should basically be determined by the energy gap between the triplet of PtOEP and the lowest populated triplet state of the host. So far a variety of blue light-emitting polymeric hosts have been positively tested for exhibiting up-conversion emission (section 4.4). The observed variation of the relative up-conversion process in these hosts was attributed to the different characteristics, e.g. film thickness, that each of the measured samples had. Moreover the chemical purity and the different impact of molecular oxygen were considered to influence the up-conversion process.

The issue that still remains unresolved is the nature of the excited level that is populated after triplet-triplet annihilation has taken place. It can not be excluded that the activation of the up-conversion process consists of more than one sensitisation channel. For the moment we may like to speculate on several alternative processes. There are several channels that could be combined in parallel for resulting in population of a high-energy level from the absorption of two photons of lower energy. For sure, the energy of this level should be isoenergetic to, if not lower than the sum of the two quanta that correspond to the participant triplet levels, in the triplet-triplet annihilation process. If triplet-triplet fusion occurs within the dopant molecules, the populated level after the end of this process can be the second excited singlet state $S_2$ of PtOEP. A non-radiative dipole-dipole interaction can not be excluded. The electronic excitation energy of the excited PtOEP $S_2$ state is isoenergetic with the higher excited levels of the singlet state in PF. Excited state absorption experiments have revealed that the PFO derivative possesses a higher energy electronically excited triplet state in that is lying ~150 meV higher than the sum of two quanta of 532 nm. Although we can not for the moment exclude an intersystem crossing step between these high-energy levels, we propose that the significance of such a step is not determining for the up-conversion process. Our suggestion is based on the temperature

dependence results in 4.3 that excludes the possibility for an activation energy of 150 meV at relatively low temperatures.

The notion for the formation of an excited charge-transfer complex is not excluded from the steady state spectra of absorption spectra of the studied dilute solutions (section 4.6.4). Charge transfer complexes have been identified in blends of PtOEP and $C_{60}$ via laser flash photolysis [23]. After a potential triplet-triplet annihilation process between PtOEP molecules the formation of an exciplex between PtOEP and polymer is plausible. This formation is energetically favourable (Table 4.18). The return of this exciplex to the ground state may be occur via the formation of an excited polymer molecule and a ground state PtOEP. The latter step is determined from the energy barrier between the HOMO levels of polymer and PtOEP molecules.

We can not exclude that the formation of an exciplex may take place from the lowest triplet level of PtOEP. In this case, up-conversion should result in as a consequence of an annihilation process that takes place not between two neutral lower lying excited triplet states but between two exciplexes, presumably of triplet character. We do not find a reason for electron spin flipping upon an electron transfer from PtOEP triplet state to the lowest lying triplet state of PF. Two pairs of charge transfer complexes of (polymer-MeOEP) can result in an efficient population of a higher excited state of the polymer.
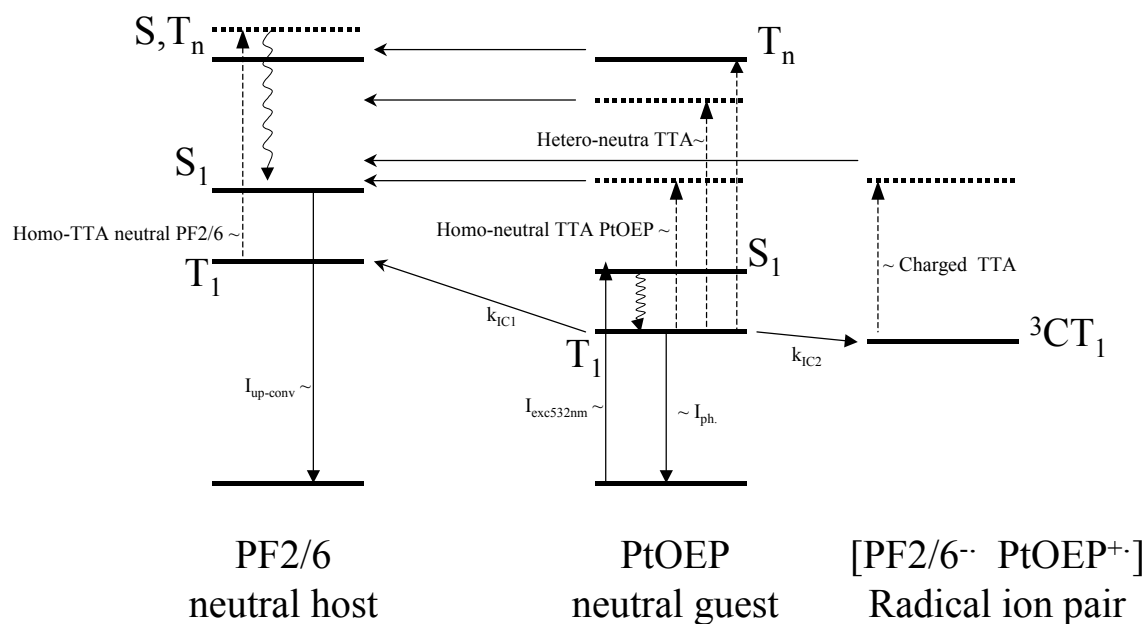
Figure 4.36: A pictorial representation of all the possible mechanisms that may lead to the observation of the 532 nm excitation up-conversion in systems comprised of a polymer host and a porphyrinoid derivative guest. The levels are arbitrary positioned only for a qualitatively visualisation of the processes suggested in this paragraph.

Model compounds should be used with accurately determined triplet energy levels that will allow or forbid the possibility of hetero triplet-triplet annihilation. In this suggested experiment the relative importance of each of the alternative sensitisation channels of PF via up-conversion will be evaluated. From our discussion it is clear that we invoke repeatedly the existence of excited state species that interact with each other in order a higher energy state to be reached. Therefore ultra fast excited state spectroscopy needs to be employed for confirming our hypotheses. By monitoring the excited state absorption of a host-PtOEP system, after exciting it at 532 nm, the new species that are formed can be detected. The following of the transient decay in their formation and extinction rate should inform us for their kinetics. Moreover, the participation of excited states that are charged in nature could be confirmed, at least for the case of thin films, from the dependence of the up-conversion process on the application of an electric field.

From the derived information of our studies, blends of PF2/6:PtOEP seem to be unique system for alternative optoelectronic applications. A variety of potential uses arise starting from the

development of saturated-red-emitting-system for the development of polymeric LED displays, continuing to realisation of optically pumped up-converted blue lasing and finally reaching the sensitisation of PF2/6-based solar cells via PtOEP.

## 4.9 REFERENCES

1.  Cleave V., Yahioglu G., Le Barny P., Friend R.H.,Tessler N., *Harvesting Singlet and Triplet Energy in Polymer LEDs.* Adv. Mater., 1999. **11**(4): p. 285.
2.  Dhoot A.S.,Greenham N.C., *Triplet Formation in Polyfluorene Devices.* Adv. Mater., 2002. **14**(24): p. 1834.
3.  Köhler A.,Wilson J., *Phosphorescence and spin-dependent exciton formation in conjugated polymers.* Organic Electronics, 2003. **4**: p. 179.
4.  Baldo M.A., O'Brien D.F., You Y., Shoustikov A., Sibley S., Thompson M.E.,Forrest S.R., *Highly efficient phosphorescence emission from organic electroluminescent devices.* Nature, 1998. **395**: p. 151.
5.  Lupton J.M., Samuel I.F.D., Frampton M.J., Beavington R.,Burn P.L., *Control of Electrophosphorescence in Conjugated Dendrimer Light-Emitting Diodes.* Adv. Funct. Mater., 2001. **11**(4): p. 287.
6.  Willson J.S., Dhoot A.S., Seeley A.J.A.B., Khan M.S., Köhler A.,Friend R.H., *Spin-Dependent exciton formation in π-conjugated compounds.* Nature, 2001. **413**: p. 828.
7.  O'Brien D.F., Giebeler C., Fletcher R.B., Cadby A.J., Palilis L.C., Lidzey D.G., Lane P.A., Bradley D.D.C.,Blau W., *Electrophosphorescence from a doped polymer light emitting diode.* Synthetic Metals, 2001. **116**: p. 379.
8.  Lane P.A., Palilis L.C., O'Brien D.F., Giebeler C., Cadby A.J., Lidzey D.G., Campbell A.J., Balu W.,Bradley D.D.C, *Origin of electrophosphorescence from a doped polymer light emitting diode.* Phys. Rev. B, 2001. **63**: p. 235206.
9.  Yang X.H., Neher D., Scherf U., Bagnich S.A.,Bässler H., *Polymer electrophosphorescent devices utilizing a ladder-type poly(para-phenylene) host.* J. Appl. Phys., 2003. **93**(8): p. 4413.
10. Laquai F., Im C., Kadashchuk A.,Bässler H., *Sensitized intrinsic phosphorescence from a poly(phenylene-vinylene) derivative.* Chem. Phys. Lett., 2003. **375**: p. 286.
11. Bagnich S.A., Im C., Bässler H., Neher D.,Scherf U., *Energy transfer in a ladder-type methyl-poly(para-phenylene) doped by Pt(II)octaethylporphyrin.* Chem. Phys., 2004. **299**: p. 11.
12. Tsuboi T.,Tanigawa M., *Optical characteristics of PtOEP and Ir(ppy)₃ triplet-exciton materials for organic electroluminescence devices.* Thin Solid Films, 2003. **438-439**: p. 301.
13. McGlynn S.P.& Azumi T. & Kinoshita M., *Molecular Spectroscopy of THE TRIPLET STATE*, Englewood Cliffs, New Jersey: Prentice-Hall, Inc.
14. Bonnett R., Harriman A.,Kozyrev A.N., *Photophysics of Halogenated Porphyrins.* J. Chem. Soc. Faraday Trans., 1992. **88**(6): p. 763.
15. Dolphin D., *The Porphyrins.* Vol. 3. 1978, New York: Academic Press.
16. Gouterman M., *Study of the Effects of Substitution an the Absorption Spectra of Porphin.* J. Chem. Phys., 1959. **30**(5): p. 1139.
17. Ponterini G., Serpone N., Bergkamp M.A.,Netzel T.L., *Comparison of Radiationless Decay Processes in Osmium and Platinum Porphyrins.* J. Am. Chem. Soc., 1983. **105**: p. 4639.
18. Bhyrappa P., Krishnan V.,Nethaji M., *Solvation and Axial Ligation Properties of (2,3,7,8,12,13,-17,18-Octabromo-5,10,15,20-tetraphenylporphyrinato)zinc(II).* J. Chem. Soc. Dalton Trans., 1993: p. 1901.
19. Asano-Someda M.,Kaizu Y., *High-efficient triplet-triplet Intramolecular Energy Transfer and Enhanced Intersystem Crossing in Rigidly Linked Copper(II) Porphyrin-Free Base Porphyrin Hybrid Dimers.* Inorg. Chem., 1999. **38**: p. 2303.
20. Kavarnos G., J., *Fundamentals of Photoinduced Electron Transfer.* 1993, New York, Weinheim, Cambridge: VCH Publishers, Inc.

21.     Drain C.M., Hupp J.T., Kenneth S.S., Wasielewski M.R.,Chen X., *A perspective on four new porphyrin-based functional materials and devices.* J. Porphyrins Phthalocyanines, 2002. **6**: p. 243.

22.     Okura I., *Photosensitization of Porphyrin and Phthalocyanines.* 2000, Tokyo: Kodansa.

23.     El-Khouly M.E., Araki Y., Fujitsuka M.,Ito O., *Photoinduced electron transfer between metal octaethylporphyrins and fullerenes ($C_{60}/C_{70}$) studied by laser flash photolysis: electron-mediating and hole-shifting cycles.* Phys. Chem. Chem. Phys., 2002. **4**: p. 3322.

24.     El-Khouly M.E., Ito O., Smith P.M.,D'Souza F., *Intermolecular and supramolecular photoinduced electron transfer processes of fullerene-porphyrin/phthalocyanine systems.* J. Photochem. PhotoBiol. C: Photochemistry Reviews, 2004. **5**: p. 79.

25.     Guldi D.M., *Fullerene-porphyrin architectures; photosynthetic antenna and reaction center models.* Chem. Soc. Rev., 2002. **31**: p. 22.

26.     Mansour K., Alvarez Jr. D., Perry K.J., Choong I., Marder S.R.,Perry J.W., *Dynamics of Optical Limiting In Heavy-Atom, Substituted Phthalocyanines.* SPIE Organic And Biological Optoelectronics, 1993. **1853**: p. 132.

27.     Perry J.W., Mansour K., Lee I.-Y.S., Wu X.-L., Bedworth P.V., Chen C.-T., Ng D., Marder S.R., Miles P., Wada T., Tian M.,Sasabe H., *Organic Optical Limiter with Strong Nonlinear Absorptive Response.* Science, 1996. **273**: p. 1533.

28.     de la Torre G., Vázquez P., Agulló-López F.,Torres T., *Phthalocyanines and related compounds: organic targets for nonlinear optical applicatiions.* J. Mater. Chem., 1998. **8**(8): p. 1671.

29.     Su W., Cooper T.M.,Brant M.C., *Investigation of Reverse-Saturable Absorption In Brominated Porphyrins.* Chem. Mater., 1998. **10**: p. 1212.

30.     Qureshi F.M., Martin S.J., Long X., Bradley D.D.C., Henari F.Z., Blau W.J., Smith E.C., Wang C.H., Kar A.K.,Anderson H.L., *Optical limiting properties of a zinc porphyrin polymer and its dimer and monomer model compounds.* Chem. Phys., 1998. **231**: p. 87.

31.     Papkovski, D.B., *New oxygen sensors and their applications to biosensing.* Sens. Actuators B, 1995. **29**: p. 213.

32.     Douglas P.,Eaton K., *Response characteristics of thin film oxygen sensors, Pt and Pd octaethylporphyrins in polymer films.* Sens and Actuators B, 2002. **82**: p. 200.

33.     Lupton J.M., *A molecular thermometer based on long-lived emission from platinum octaethyl porphyrin.* Appl. Phys. Lett., 2002. **81**(13): p. 2478.

34.     Klessinger M. & Michl J., *Excited States and Photochemistry of Organic Molecules.* 1995, New York, Weinheim, Cambridge: VCH Publishers, Inc.

35.     Dichtel W.R., Serin J.M., Edder C., Fréchet J.M.J., Matuszewski., Tan L.-S., Ohulchanskyy T.Y.,Prasad P.N., *Singlet Oxygen Generation via Two-Photon Excited FRET.* J. Am. Chem. Soc., 2004. **126**: p. 5380.

36.     Virgili T., Lidzey D.G.,Bradley D.D.C., *Efficient Energy Transfer from Blue To Red in Tetraphenylporphyrin-Doped Poly(9,9-dioctylfluorene) Light-Emitting Diodes.* Adv. Mater., 2000. **12**(1): p. 58.

37.     Lyons B.P., Wong K.S.,Monkman A.P., *Study of the energy transfer processes in polyfluorene doped with tetraphenyl porphyrin.* J. Chem. Phys., 2003. **118**(10): p. 4707.

38.     Li B., Li J.L., Fu Y.,Bo Z., *Porphyrins with Four Monodisperse Oligofluorene Arm as Efficient Red Light-Emitting Materials.* J. Am. Chem. Soc., 2004. **126**: p. 3430.

39.     Wong K.F., Bagchi B.,Rossky P.J., *Distance and Orientation Dependence of Excitation Transfer Rates in Conjugated Systems: Beyond the Förster Theory.* J. Phys. Chem. A, 2004. **108**: p. 5752.

40.    Lakowicz J.R., *Principles of Fluorescence Spectroscopy*. 2nd ed. 1999, New York, Boston, Dordrecht, London, Moscow: Kluwer Academic/Plenum Publishers.

41.    Medinger T.,F., Wilkinson, *Mechanism of Fluorescence Quenching in Solution*. Trans. Faraday Soc., 1965. **61**(508P): p. 620.

42.    Suna A., *Kinematics of Exciton-Exciton Annihilation in Molecular Crystals*. Phys. Rev. B, 1969. **1**(4): p. 1-1716.

43.    Radziszewski J.G., Waluk J., Nepras M.,Michl J., *Fourier Transform Fluorescence and Phosphorescence of Porphine In Rare Gas Matrices*. J. Phys. Chem., 1991. **95**: p. 1963.

44.    Ariu M., Lidzey D.G., Sims M., Cadby A.J., Lane P.A., Bradley D.D.C., *The effect of morphology on the temeprature-dependent photoluminescence quantum efficiency of the conjugated polymer poly(9,9-dioctylfluorene)*. J. Phys.: Condens. Matter, 2002. **14**: p. 9975.

45.    Callis J.B., Gouterman M., Jones Y.M.,Henderson B.H., J. Mol. Spectrosc., 1971. **39**: p. 410.

46.    Schroeder R., Ullrich B., Graupner W.,Scherf U., *Excitation density and photoluminescence studies of polyfluorene excited by two-photon absorption*. J. Phys.: Condens. Matter, 2001. **13**: p. L313.

47.    Gadermaier C., Lanzani G., *Photophysics of conjugated polymers: the contribution of ultrafast spectroscopy*. J. Phys.: Condens. Matter, 2002. **14**: p. 9785.

48.    Samoc A., Samoc M.,Luther-Davies B., *Upconversion of He-Ne Laser Light in Xanthene Dye-Doped Polymer Waveguides*. Polish J. Chem., 2002. **76**: p. 345.

49.    Callis, J.B., Gouterman M., Jones Y.M., Henderson B.H., J. Am. Chem. Soc., 1971. **39**: p. 410.

50.    Drobizhev M., Karotki A., Kruk M., Krivokapic A., Anderson H.L.,Rebane A., *Photon energy upconversion in porphyrins: one-photon hot-band absorption versus two-photon absorption*. Chem. Phys. Lett., 2003. **370**: p. 690.

51.    Jacob J., Sax S., Piok T., List E.J.W., Grimsdale A.C., Müllen K., *Ladder-Type Pentaphenylene and Their Polymers: Efficient Blue-Light Emitters and Electron-Accepting Materials via a Common Intermediate*. J. Am. Chem. Soc., 2004. **126**: p. 6987.

52.    Monkman A.P., Burrows H.D., Hartwell L.J., Horsburgh L.E., Hamblett I.,Navaratnam S., *Triplet Energies of π-Conjugated Polymers*. Phys. Rev. Lett., 2001. **86**(7): p. 1358.

53.    Hertel D., Setayesh S., Nothofer H.-G., Scherf U., Müllen K.,Bässler H., *Phosphorescence in Conjugated Poly(para-phenylene)-Derivatives*. Adv. Mater., 2001. **13**(1): p. 65.

54.    Hertel D., Bässler H., Guentner R.,Scherf U., *Triplet-triplet annihilation in a poly(fluorene)-derivative*. J. Chem. Phys., 2001. **115**(21): p. 10007.

55.    Sinha S., Rothe C., Güntner R., Scherf U.,Monkman A.P., *Electrophosphorescence and Delayed Electroluminecence from Pristine Polyfluorene Thin-Film Devices at Low Temperature*. Phys. Rev. Lett., 2003. **90**(12): p. 127402.

56.    Somma E., Loppinet B., Fytas G., Setayesh S., Jacob J., Grimsdale A.C., Müllen K., *Collective orientation dynamics in semi-rigid polymers*. Colloid. Polym. Sci., 2004. **282**: p. 867.

57.    Tzankov P., Fiebig T.,Buchvarov I., *Tunable fs pulses in the near-ultraviolet from ultrabroadband parametric amplification*. Appl. Phys. Lett., 2003. **82**: p. 517.

58.    Raytchev M., Pandurski E., Buchvarov I., Modrakowski C.,Fiebig T., J. Phys. Chem., 2003. **107**: p. 4592.

59.    Jenekhe S.A.,Osaheni J.A., *Excimers and Exciplexes of Conjugated Polymers*. Science, 1994. **265**: p. 765.

60. Harris D.C., *Quantitative Chemical Analysis*. 4th ed. 1995, New York: W.H. Freeman and Company.

61. Bhyrappa P.,Krishnan V., *Octabromotetraphenylporphyrin and Its Metal Derivatives: Electronic Structure and Electrochemical Properties*. Inorg. Chem., 1991. **30**: p. 239.

# Appendix A: π-secondary interactions

In the general case of π-secondary interactions, π-π stacking is the most common interaction that is normally observed in small aromatic molecules. However other type of π-secondary interactions may be also important in the structural motifs of these molecules. More importantly these π-secondary interactions may also equally determine the optical properties in the bulk. In the case of poly-*p*-phenylene related materials like poly(fluorene)s, the torsional angle between the monomer units of the polymer backbone provides unfavourable conditions for direct π-π stacking interactions. However other type of π-secondary interaction such as edge-to-face interactions might be also the origin of the broadened PL spectra observed in the case of a dendronised PF derivative. This is further evidenced from the X-ray data of the monomer crystal (see inset of Figure 2.4 and Figure 2.5). Two different views are shown in Figure A.1 and Figure A.2.
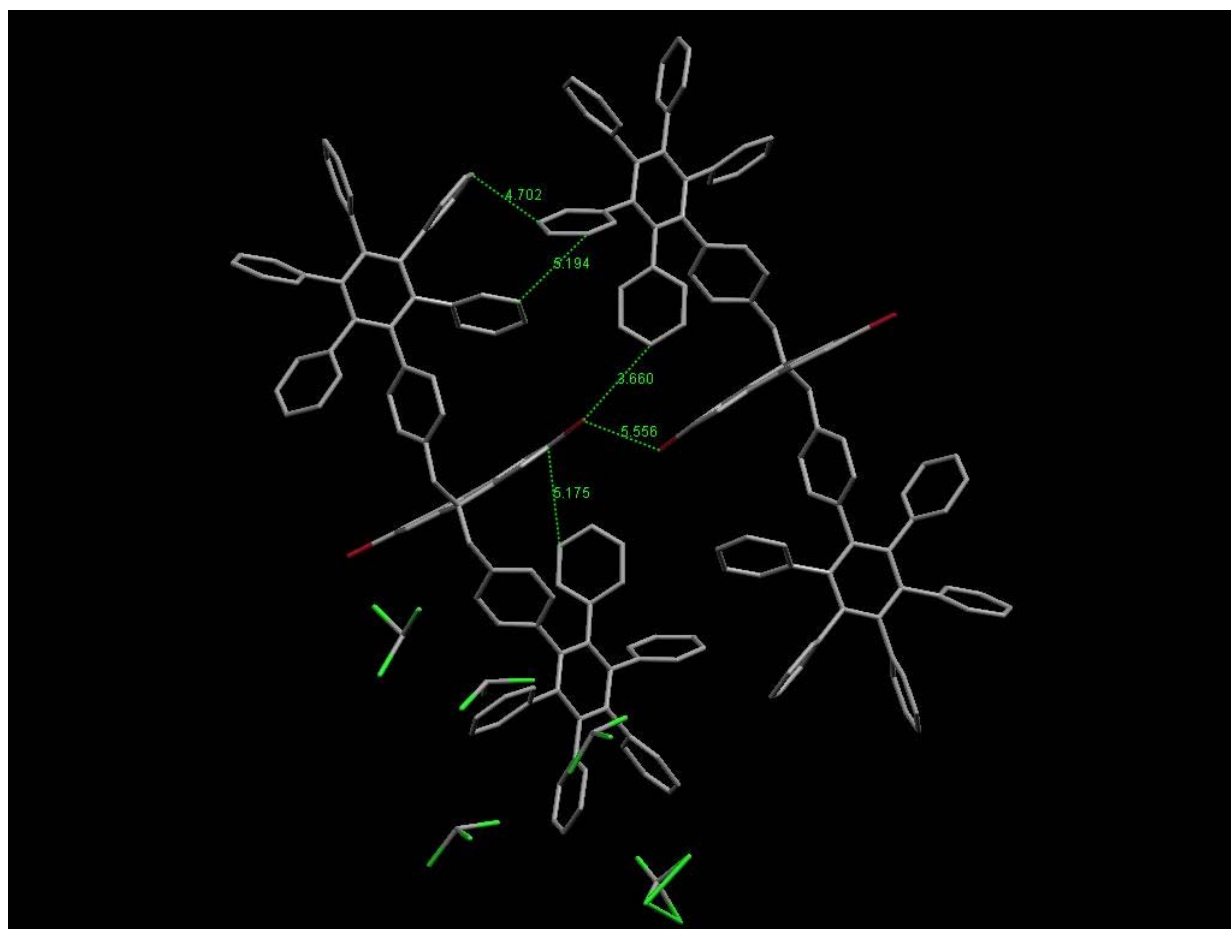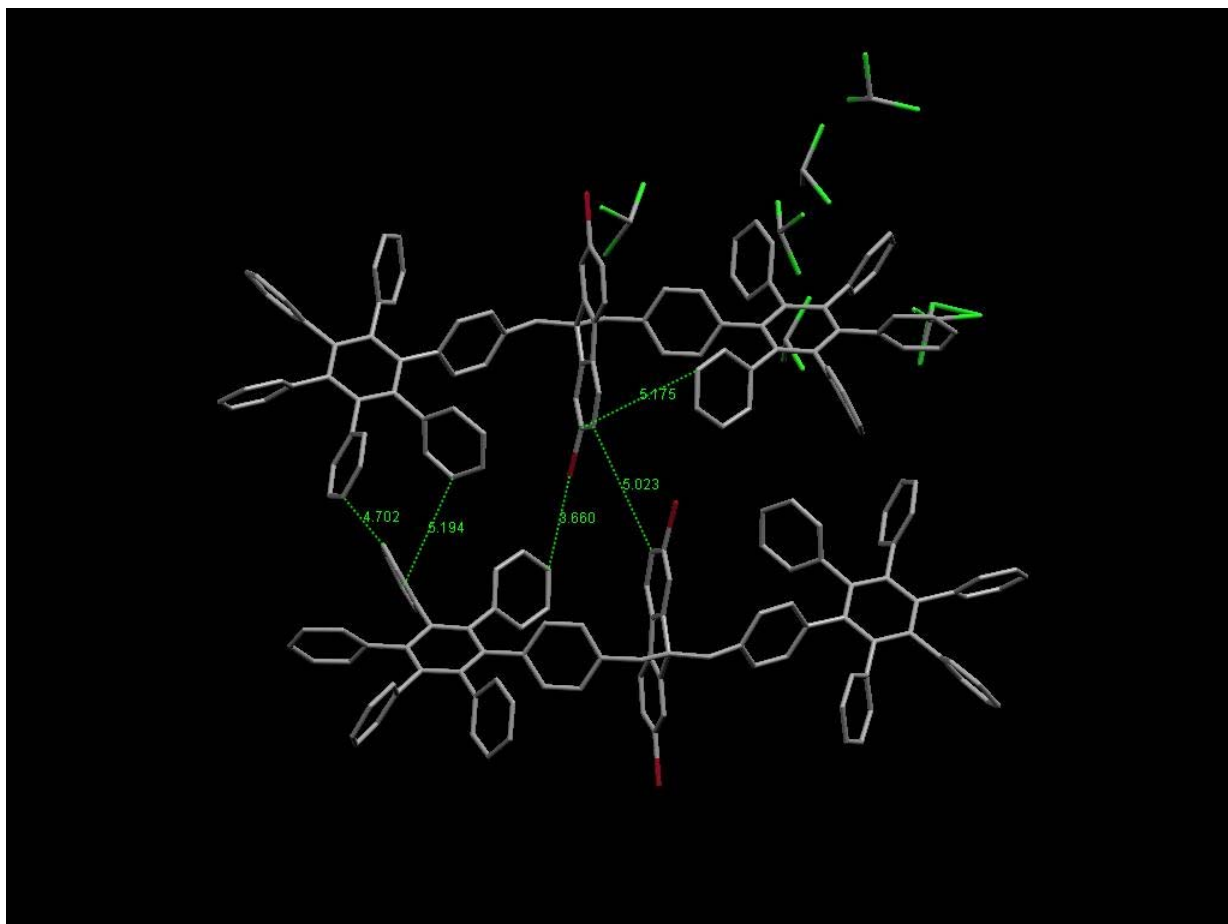


Figure A. 1

Figure A. 2

As Figure A.3 shows, edge-to-face interactions dominate in the crystal structure of benzene.
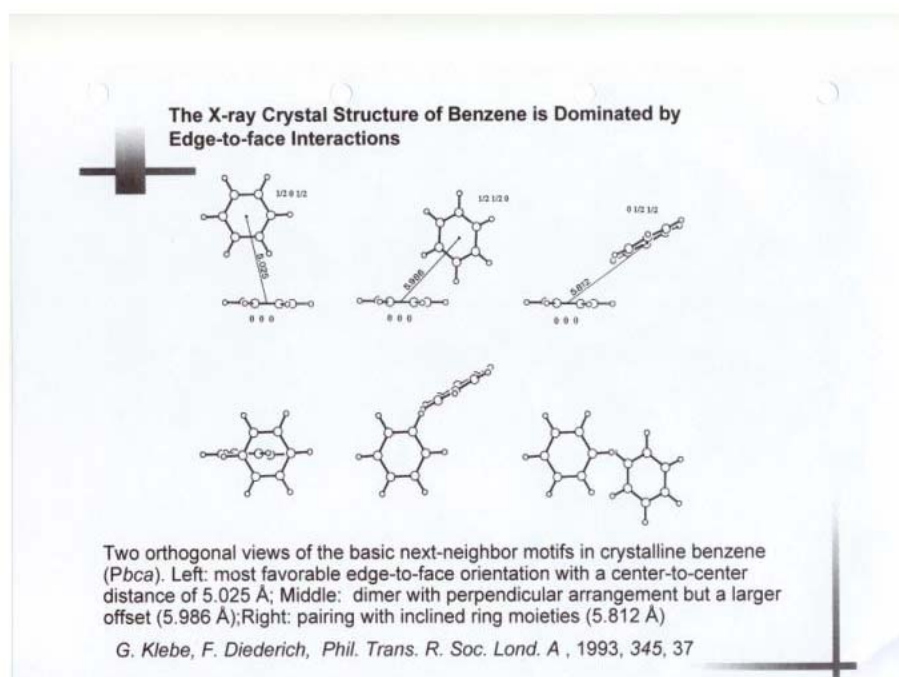


Figure A. 3

# Appendix B: Steady-state conditions

$$\frac{d[A^*]_0}{dt} = I - k_1 * [A^*]_0 \qquad \text{(eq. 4.2)}$$

$$\frac{d[A^*]}{dt} = I - k_1 * [A^*] - k_q * [Q] * [A^*] + \frac{1}{2} * \gamma * [Q^*]^2 \qquad \text{(eq. 4.3)}$$

$$\frac{d[Q^*]}{dt} = -k_2 * [Q^*] + k_q * [Q] * [A^*] - \frac{1}{2} * \gamma * [Q^*]^2 \qquad \text{(eq. 4.4)}$$

With continuous excitation the excited state population $[Q^*]$ of eq. 4.4 is constant:

$$\frac{d[Q^*]}{dt} = 0 \Leftrightarrow -k_2 * [Q^*] + k_q * [Q] * [A^*] - \frac{1}{2} * \gamma * [Q^*]^2 = 0 \text{, then}$$

$$[Q^*]_{1,2} = -\frac{-k_2 \pm \sqrt{(-k_2)^2 - 4 * \left(-\frac{1}{2}\right) * \gamma * k_q * [Q] * [A^*]}}{2 * \left(-\frac{1}{2}\right) * \gamma} =$$

$$\frac{-k_2 \pm \left(k_2^2 + 2 * \gamma * k_q * [Q] * [A^*]\right)^{1/2}}{\gamma} = \frac{-k_2 \pm \left(k_2 + \dfrac{\gamma * k_q * [Q] * [A^*]}{k_2^{1/2}}\right)}{\gamma} =$$

$$\frac{-k_2^{3/2} \pm \left(k_2^{3/2} + \gamma * k_q * [Q] * [A^*]\right)}{\gamma * k_2^{1/2}} \Leftrightarrow [Q^*] = \frac{k_{q\cdot}}{k_2^{1/2}} * [Q] * [A^*]$$

Therefore, eq. 4.3 becomes

$$\frac{d[A^*]}{dt} = I - k_1 * [A^*] - k_q * [Q] * [A^*] + \frac{1}{2} * \gamma * \left(\frac{k_{q\cdot}}{k_2^{1/2}} * [Q] * [A^*]\right)^2 \Leftrightarrow$$

$$\frac{d[A^*]}{dt} = I - k_1 * [A^*] - k_q * [Q] * [A^*] + \frac{1}{2} * \gamma * \frac{k_{q\cdot}^2}{k_2} * [Q]^2 * [A^*]^2 = 0$$

Exploiting the steady-state conditions the derivatives in eq. 4.2 and 4.3 can be eliminated :

$$\frac{d[A^*]_0}{dt} = \frac{d[A^*]}{dt} = 0 \Leftrightarrow$$

$$I - k_1 * [A^*]_0 = I - k_1 * [A^*] - k_q * [Q] * [A^*] + \frac{1}{2} * \gamma * \frac{k_q^2}{k_2} * [Q]^2 * [A^*]^2 \Leftrightarrow$$

$$k_1 * [A^*]_0 = k_1 * [A^*] + k_q * [Q] * [A^*] - \frac{1}{2} * \gamma * \frac{k_q^2}{k_2} * [Q]^2 * [A^*]^2 \Leftrightarrow$$

$$[A^*]_0 = [A^*] + \frac{k_q}{k_1} * [Q] * [A^*] - \frac{1}{2} * \gamma * \frac{k_q^2}{k_1.k_2} * [Q]^2 * [A^*]^2 \Leftrightarrow$$

$$[A^*]_0 = [A^*] * \left( 1 + \frac{k_q}{k_1} * [Q] - \frac{1}{2} * \gamma * \frac{k_q^2}{k_1.k_2} * [Q]^2 * [A^*] \right) \Leftrightarrow$$

$$\frac{[A^*]_0}{[A^*]} = 1 + \frac{k_q}{k_1} * [Q] - \frac{1}{2} * \gamma * \frac{k_q^2}{k_1.k_2} * [Q]^2 * [A^*] \Leftrightarrow$$

$$\frac{[A^*]_0}{[A^*]} = 1 + k_q * \tau_0 * [Q] - \frac{1}{2} * \gamma * k_q^2 * \tau_0 * \tau_{Ph} * [Q]^2 * [A^*] \Leftrightarrow$$

$$\frac{I_0}{I} = 1 + k_q * \tau_0 * [Q] - \frac{1}{2} * \gamma * k_q^2 * \tau_0 * \tau_{Ph} * I * [Q]^2 \qquad \text{(eq. 4.5)}$$

# Appendix C: Photo-induced electron transfer formalism

## Rehm-Weller Formalism

$$\Delta G_{el}(kcal/mol) = 23.06\left[E^0_{(D^+/D)} - E^0_{(A/A^-)}\right] - E - w_p$$

$E^0_{(D^+/D)}, E^0_{(A/A^-)}$     Redox potential of donor and acceptor (Volts)

$E$     Energy of the excited state, where electron transfer occurs

$w_p$     Coulombic stabilisation of the redox couple

Rehm,D.,Weller, A. Isr. J. Chem. **1970**, 8, 259
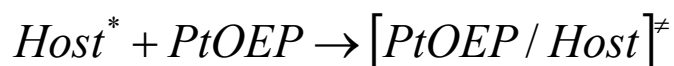G. J. Kavarnos, Fundamentals of Photoinduced Electron Transfer, VCH, 1993

## Energetics of electron transfer

$$PtOEP^{**} + Host \xrightarrow{\Delta G_1} [PtOEP/Host]^{\neq} \xrightarrow{\Delta G_2} PtOEP + Host^*$$

The overal free energy change will be:

$$\Delta G_{el} = \Delta G_1 + \Delta G_2$$

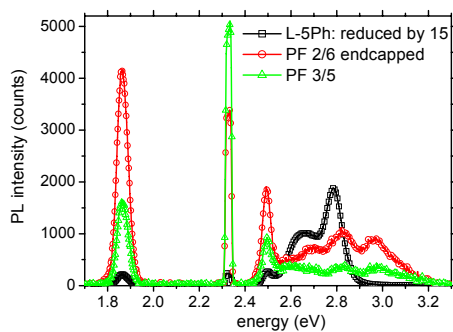$\Delta G_2$   is the negative   $\Delta G$ that Rehn-Weller formula predicts for

$$Host^* + PtOEP \rightarrow [PtOEP/Host]^{\neq}$$

# Results

| PtOEP-HOST | $\Delta G_1$ (eV) | $\Delta G_2$ (eV) | $\Delta G_{el}$ (eV) |
|:---:|:---:|:---:|:---:|
| **PF2/6** | -2.82 | 2.00 | -0.82 |
| **PF 3/5** | 2.89 | 2.09 | -0.80 |
| **PhLLLP** | -3.35 | 2.21 | -1.14 |
| **L-5Ph** | -3.03 | 1.98 | -1.05 |

$$\Delta G_{el}(kcal/mol) = 23.06\left[ E^0_{(D^+/D)} - E^0_{(A/A^-)} \right] - E - w_p$$ , where $E = 2T_1$ of PtOEP for $\Delta G_1$ and $E = E_g$ for $\Delta G_2$

---

L-5Ph is expected to be better sensitized
than PF2/6 by the redox process

---

# Results



DILUTE
SOLUTIONS

THIN FILMS
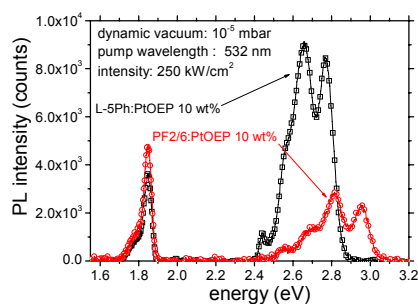
# Appendix D: Optically pumped-induced spectral narrowing in PIF-Aryl-Octyl films

In the recent years π-conjugated polymers have become the subject of intesive research of material scientists that aim for the development of modern electro-active devices. Already conjugated polymers have become important functional units of commercially available light-emitting diodes and considerable attention is now given for the optimisation of polymer-based solar cells. In parallel to those research activities a great interest has been expressed for the realisation of electrically pumped polymer-based solid-state lasers. Due to their high luminescence efficiencies and large cross sections for stimulated emission, conjugated polymers have been identified as appropriate candidate lasing materials[1,2]. The optical gain mechanism in conjugated polymers as bulk materials has been described similarly the one that is known for organic dye lasers; a four-level system has been invoked in which lasing occurs between vibronic levels of two different electronic states, that are not directly involved in the optical pumping process[3].

One of the important parameters that characterise the active lasing media is the gain parameter *g*. For the optical excitation of several conjugated polymers, amplified spontaneous emission (ASE) has been reported both for the case of solutions[4] and films[5,6]. Through these experiments the gain parameter could be deduced from the fitting of the obtained data. Especialy for the case of films, optically pumped-induced ASE has been achieved via waveguiding of the radiative modes of the medium that can effectively couple with the modes of the waveguide structure. A first indication for the occurrence of ASE in planar waveguides is the observation of fluorescence spectral narrowing, after a defindable excitation intensity threshold. For distinguishing[6] wether this spectral narrowing originates from ASE or from another process e.g superradiance or interacting excitons, an appropriate experimental set-up is used. Optical excitation of the polymer film is performed with a stripe of variable length and the dependence of the light intensity that emerges out of the end of the stripe is parameterised both to excitation intensity and stripe length. According to the rough one-dimensional approximation[7] of luminescence intensity propagation witin the waveguide, the output intensity from one end of the stripe should be expresses as:

$$I(\lambda) = \frac{A(\lambda) * I_p}{g(\lambda)} * \left\{ \exp[g(\lambda) * L] - 1 \right\} \quad \text{eq. D.1}$$

where $A(\lambda)$ is related to the cross section for spontaneous emission, $I_p$ is the pumping intensity, *g* is the net gain coefficient and L is the length of the pumped stripe on the film.

For the case of PIF-Aryl-Octyl films on quartz substrates, excitation at 410 nm (3.02 eV) with laser pulses of 10 *ns* duration and a repetition rate of 10 Hz, resulted in spectral narrowing of the registered photoluminescence. The used films were of 120 nm thickness, as determined both from ellipsommetry and surface profiling. The experiment was performed with the set-up that paragraph *3.4.2.1* describes and the excitation of the studied films was within the range of kW/cm$^2$. As Figure D.1 shows, spectral narrowing occurrs in PIF-Aryl-Octyl film in the spectral region of the $S_{0-1} \leftarrow S_{1-0}$ vibronic transition at 465 nm (2.67 eV), after a certain level of excitation intensity. At higer excitation intensities (15 μJ/pulse) a collapse of the $S_{0-1} \leftarrow S_{1-0}$ vibronic transition width was observed (FWHM ~ 5 nm).

Our experimental results were obtained by collecting the PL signal in an angle to the axis of excitation. Moreover, the laser spot was kept with an apperture to a round shape of ~ 2 mm diameter. Therefore the observed spectral narrowing could not be for the moment attributed to the occurrence of ASE in the PIF-Aryl-Octyl film. Up to now, we consider these results as preliminary evidence for the possibility of ASE in PIF-Aryl-Octyl based planar waveguides. From ellipsomerty experiment, the effective refractive index of PIF-Aryl-Octyl was determined to be 1.71. Given that the quartz substrates used have[6] a refractive index of 1.46, waveguiding effects are expected to occur in PIF-Aryl-Octyl that may lead to ASE process.

Excitation of the samples should be performed with a stripe with variable and well-defined dimensions. Subsequently, stripe-edge detection of the output PL with an optical fibre can give further information on the origin of the observed spectral narrowing in PIF-Aryl-Octyl films.
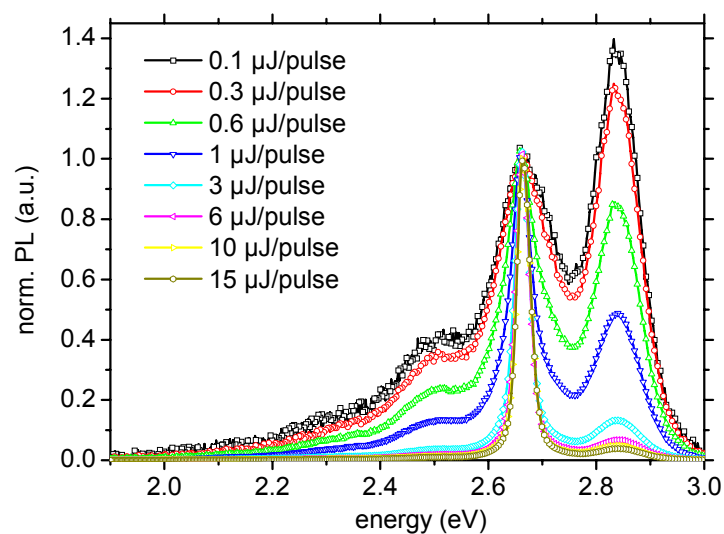
Figure D. 1: Normalised room temperature cw-PL of a PIF-Aryl-Octyl film, on quartz substrate. Excitation was at 3.02 eV (410 nm) in vaccum of $10^{-5}$ mbar. Variation of the excitation intensity was achieved with the use of an appropriate neutral density filter. The spectrum was recorded in a time window of 10 *ms*. Averaging of the registerd PL signal was performed over 100 excitation pulses.
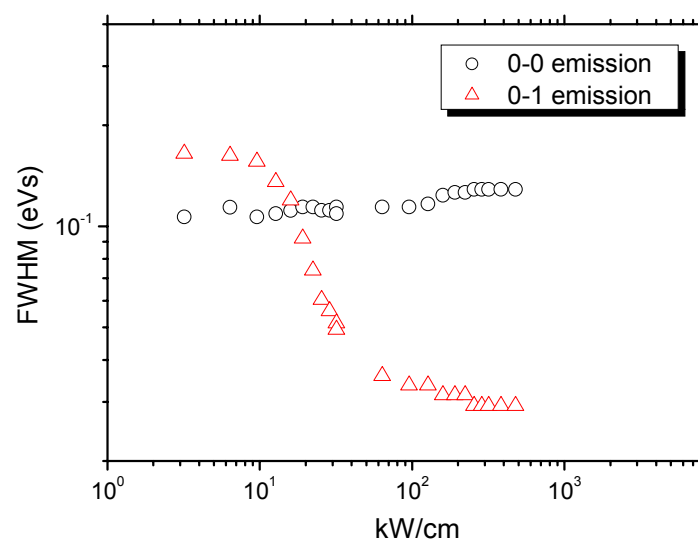


Figure D. 2: Comparison of the FWHM values for two different spectral regions of the cw-PL of a PIF-Aryl-Octyl film, on quartz substrate. Two different spectral regions are monitored that correspond to the $S_{0-0} \leftarrow S_{1-0}$ (circles) and $S_{0-1} \leftarrow S_{1-0}$ (triangles) transition, respectively. Data were obtained after integration of the non-normalised data of Figure D.1.
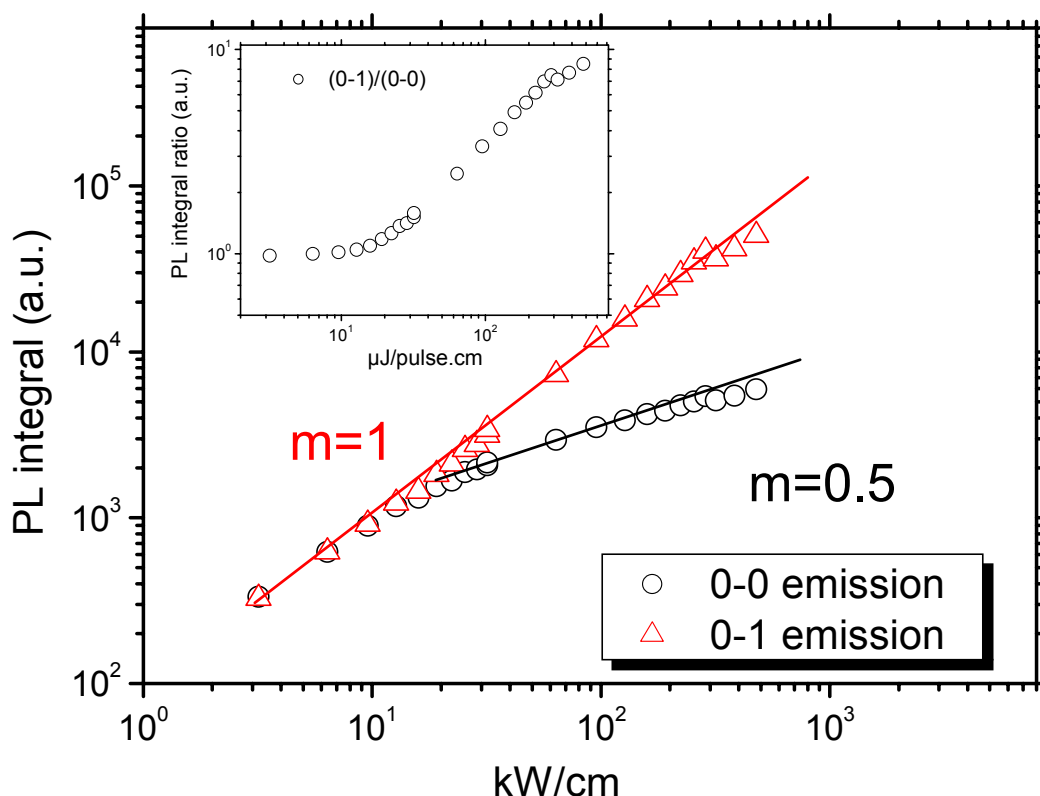
Figure D. 3: Excitation intensity dependence of cw-PL of a PIF-Aryl-Octyl film, on quartz substrate. Excitation was at 3.02 eV (410 nm) in vaccum of $10^{-5}$ mbar. Two different spectral regions are monitored that correspond to the $S_{0-0} \leftarrow S_{1-0}$ (circles) and $S_{0-1} \leftarrow S_{1-0}$ (triangles) transition, respectively. The inset depicts the dependence of the ratio $(S_{0-1} \leftarrow S_{1-0})/(S_{0-0} \leftarrow S_{1-0})$ intensities as a function of the excitation intensity.

[1] F. Hide, M. A. Díaz-García, B. J. Schwartz, M. R. Andersson, Q. Pei, A. J. Heeger, *Science*, **1996**, 273, 1833

[2]  U. Scherf, S. Riechel, U. Lemmer, R. F. Mahrt, *Curr. Op. Sol. Stat. Mater. Sc.*, **2001**, 5, 143

[3] B . Schweitzer, G. Wegmann, H. Giessen, D. Hertel, H. Bässler, R. F. Mahrt, U. Scherf, K. Müllen, *Appl. Phys. Lett.*, **1998**, 72 (23), 2933

[4] M. Fakis, G. Tsigaridas, I. Polyzos, V. Giannetas, P. Persephonis, *Phys. Rev. B*, **2003**, 68, 035203

[5] M. D. McGehee, R. Gupta, S. Veenstra, E. K. Miller, M. A. Díaz-García, A. J. Heeger, *Phys. Rev. B*, **1998**, 70, 35.

[6] G. Helliotis, D. D. C Bradley, G. A. Turnbull, I. D. W. Samuel, *Appl. Phys. Lett.*, **2002**, 81 (3), 415

[7] Y. Sorek, R. Reisfeld, I. Finkelstein, S. Ruschin, *Appl. Phys. Lett.*, **1995**, 66 (10), 1169